Western University
Scholarship@Western

Digitized Theses | Digitized Special Collections

1971

Crustal Seismic Studies In Northern Ontario And Manitoba From Project Early Rise Data

James Alexander Hunter

Follow this and additional works at: https://ir.lib.uwo.ca/digitizedtheses

Recommended Citation
Hunter, James Alexander, "Crustal Seismic Studies In Northern Ontario And Manitoba From Project Early Rise Data" (1971). *Digitized Theses*. 546.
https://ir.lib.uwo.ca/digitizedtheses/546

This Dissertation is brought to you for free and open access by the Digitized Special Collections at Scholarship@Western. It has been accepted for inclusion in Digitized Theses by an authorized administrator of Scholarship@Western. For more information, please contact tadam@uwo.ca, wlswadmin@uwo.ca.

The author of this thesis has granted The University of Western Ontario a non-exclusive license to reproduce and distribute copies of this thesis to users of Western Libraries. Copyright remains with the author.

Electronic theses and dissertations available in The University of Western Ontario's institutional repository (Scholarship@Western) are solely for the purpose of private study and research. They may not be copied or reproduced, except as permitted by copyright laws, without written authority of the copyright owner. Any commercial use or publication is strictly prohibited.

The original copyright license attesting to these terms and signed by the author of this thesis may be found in the original print version of the thesis, held by Western Libraries.

The thesis approval page signed by the examining committee may also be found in the original print version of the thesis held in Western Libraries.

Please contact Western Libraries for further information:
E-mail: libadmin@uwo.ca
Telephone: (519) 661-2111 Ext. 84796
Web site: http://www.lib.uwo.ca/

CRUSTAL SEISMIC STUDIES

IN

NORTHERN ONTARIO AND MANITOBA

FROM

PROJECT EARLY RISE DATA

by

James A. M. Hunter

Department of Geophysics

Submitted in partial fulfillment

of the requirements for the degree of

Doctor of Philosophy

Faculty of Graduate Studies

The University of Western Ontario

London, Canada

Sept. 1971

© James A. M. Hunter 1971

ABSTRACT

The 1966 Project Early Rise crustal seismic experiment considerably increased knowledge of the crust and upper mantle in North America. The 39 explosions comprising the experiment were centrally located in Lake Superior. The data obtained by the University of Western Ontario, and discussed herein, focussed on northern Ontario and Manitoba.

Two radial lines were occupied by U.W.O. having lengths of 600 and 1500 km. First arrival results suggest that a sub-Mohorovicic refractor was present at a depth of about 85 km. As well,crustal thicknesses varied from about 50 km near Lake Superior to about 27 km in the region of the boundary between the Churchill and Superior provinces of the Canadian Shield. The crust of the older Superior Province is 30-35 km thick, whereas that of the Churchill Province is approximately 40 km.

An analysis of first arrival amplitudes for the seismic records gives further evidence for the existence of the sub-Moho refractor. Discontinuities in the amplitude-distance curves correlate well with the first arrival time-distance plot.

The first arrival particle motions from the three component records demonstrate a good correlation between the interpreted upper crustal velocities, the observed gravity anomalies and the regional geology.

A study of the attenuation properties of the first arrival by spectral methods gives wide ranges of values for the specific attenuation factor Q and large statistical error.

Digital filtering methods applied to the seismic records enhance the interpretation of later events. The most promising filter involves the use of three components of ground motion.

Model studies of later arrivals for the crust and upper mantle suggest that converted refracted events should not be prominent on the records. However, reflected events from crustal and upper mantle discontinuities should be observable. The early portions of the Early Rise records show events which can be reasonably well correlated both in arrival time and amplitude, with predicted reflected events. Such events give further evidence for the existence of sub-Moho seismic discontinuities.

The author recommends the adoption of the name 'Hales' to the well-defined sub-Moho refractor discontinuity.

Acknowledgments

The author wishes to express his indebtedness to the members of his supervisory committee, Dr. L. Mansinha and Dr. R. E. White and in particular his chief supervisor Dr. R. F. Mereu for guidance and encouragement in this research. The technical work of Mr. R. M. Gagné is gratefully acknowledged.

This work has been funded by grants from the National Research Council and the Arctic Institute of North America. The author was supported in this work through receipt of Province of Ontario Graduate Fellowships.

TABLE OF CONTENTS

page

Page

LIST OF TABLES

LIST OF FIGURES

FIGURE page

FIGURE page

FIGURE page

CHAPTER I

INTRODUCTION

1.1 Description of Survey and Statement of Thesis

In the summer of 1966 the crustal seismic experiment, Project Early Rise, was conducted in Lake Superior by the United States Geological Survey for the Advanced Research Projects Agency of the U.S. Department of Defense. The experiment used 39 large explosions, each of 10,000 lbs of high velocity explosive, detonated at one location in Lake Superior. Several research groups participated in the experiment, each occupying a series of recording stations radiating outwards up to 4000 km from the shot location (see fig. 1-1). The tabulation of participants, shot and recording positions and travel-times are given in detail by Warren et al. (1967).

The main goal of the experiment was to investigate the variation in the seismic velocity-depth function and attenuation in the upper mantle with azimuth from the shot position. By maintaining the shot in a fixed position in an area which had been seismically well-investigated (Smith et al. (1966); Roller and Jackson (1966)) the uncertainties in crustal delay times and source conditions at the shot point were minimized.

The University of Western Ontario recording team, using three portable stations, occupied recording locations in northern Ontario and Manitoba as shown in fig. 1-2. The line of stations from Lake Superior to Baralzon Lake, N.W.T. (hereafter called the 'Early Rise Line') was occupied by two 3-component stations (one vertical and two horizontal component seismometers) which were moved by aircraft after each night's shooting. Since two shots were fired each night (at 3.00 A.M. and 4.00 A.M.)

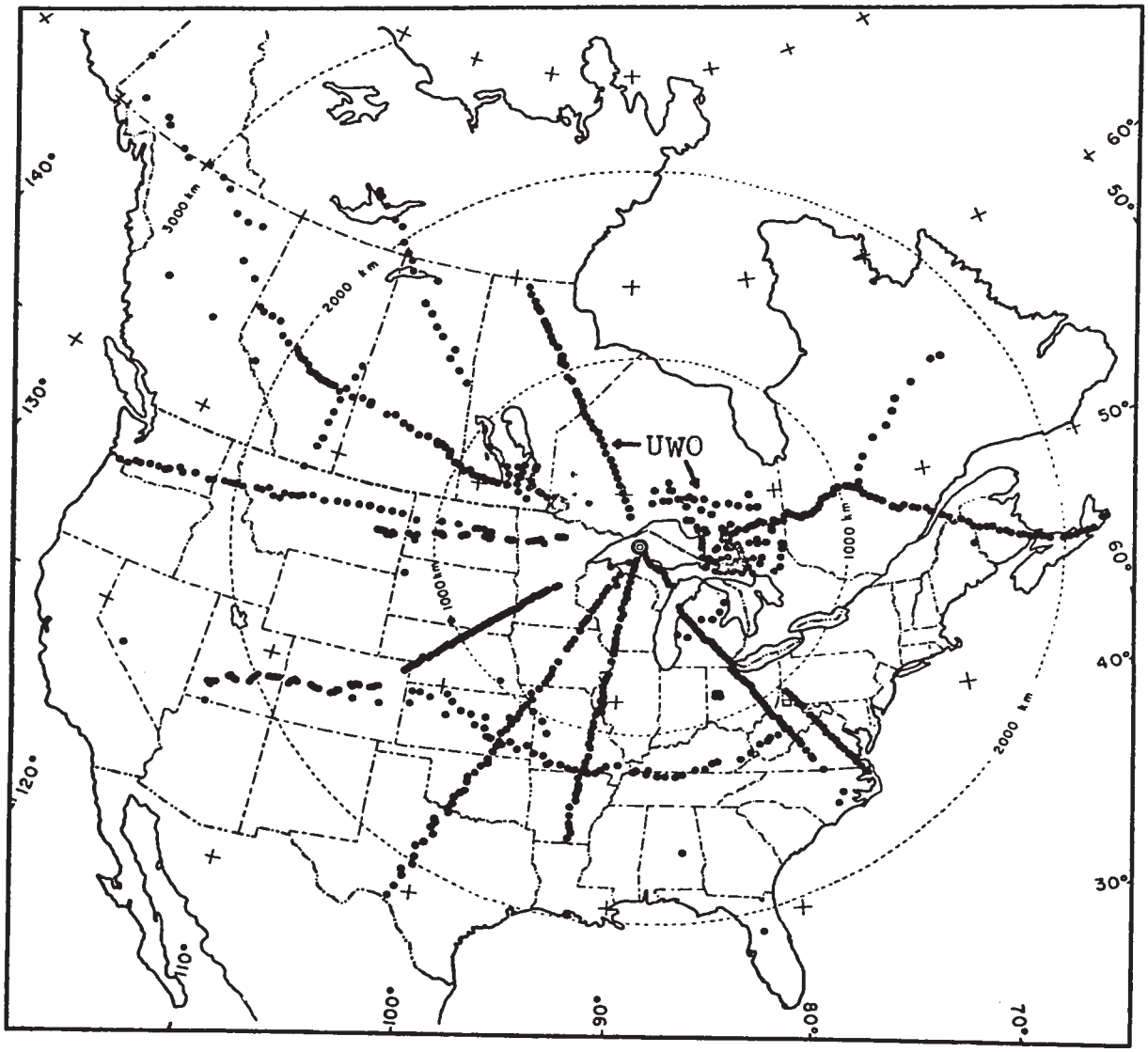

Fig. 1-1 Positions of recording stations for the Early Rise project.

two seismograms were obtained at each station position. One station was operated by remote pre-programmed switching while the other was manned by the recording crew. Both stations recorded three components of ground motion onto FM tape recorders.

The recording positions in Northern Ontario from Lake Nipigon to Smooth Rock Falls (see fig. 1-2) were occupied by a truck-mounted single vertical component station, which recorded two shots at each station. Permanent records were obtained on a hot-wire chart recorder.

Recording stations in both areas were placed on bedrock with the exception of two stations where bedrock was not accessible.

The northern Ontario recording locations as shown in fig. 1-2 as well as those forming the Early Rise Line were positioned so as to bridge the gap between structural information in the Lake Superior region and the Hudson Bay region.

This thesis offers the results of an investigation into the identification of seismic events on the early portions of the Early Rise seismograms as an aid in refining the crustal and upper mantle model derived from first arrival times.

Since the onset of the first arrival on a seismogram is often the most reliably picked event, emphasis was placed on obtaining as much information as possible from this arrival in the form of amplitude, frequency spectrum and particle motion measurements. The interpretation of later events on the seismogram involved:

1) A study of wavelet characteristics as an aid in identification of later events,
2) A model study of amplitudes of events to establish identification guidelines for later events,
3) The application of digital filter techniques for enhancement of seismic events.

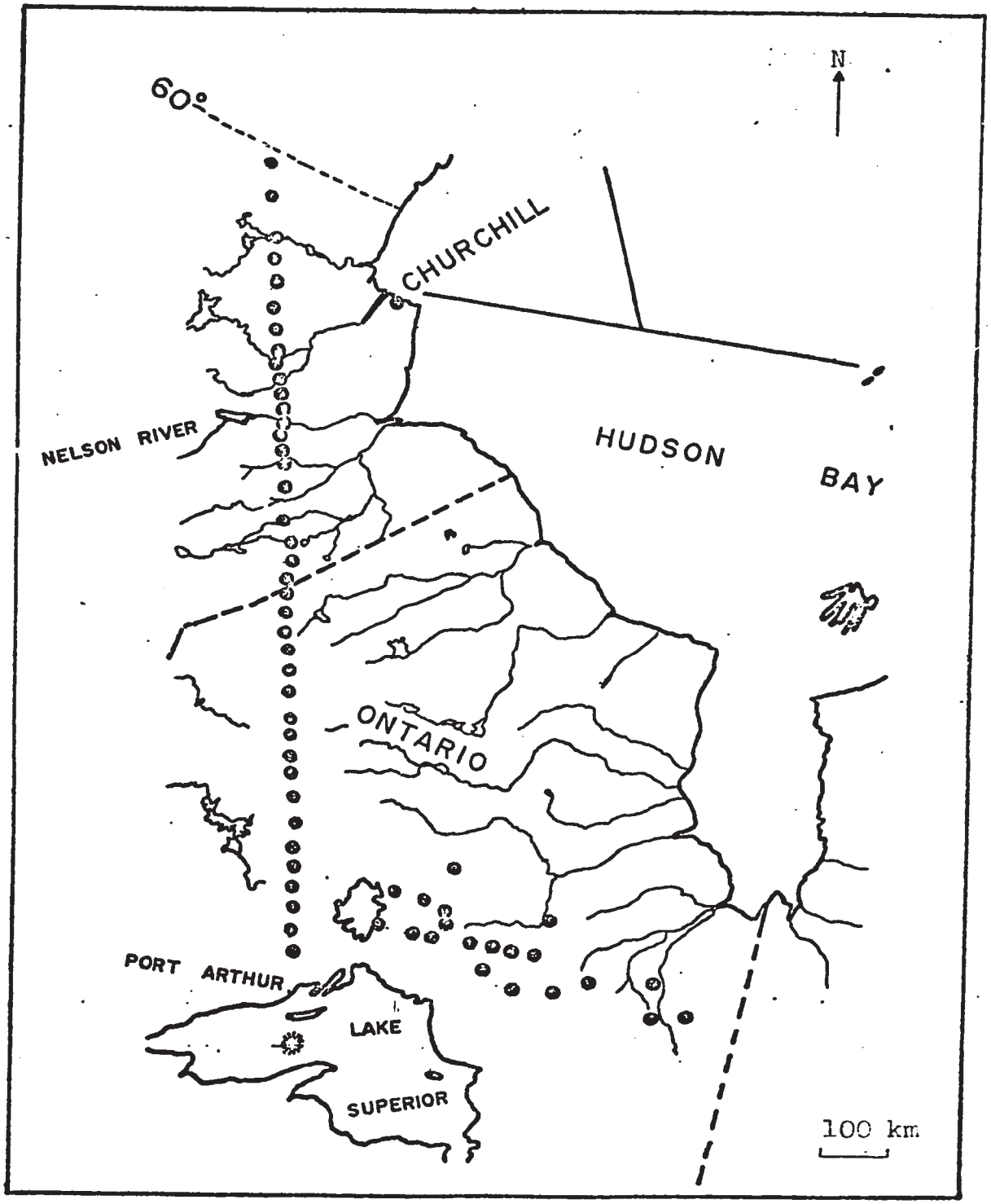

Fig. 1-2 Positions of U.W.O. recording stations in Ontario and Manitoba.

The rock underlying the seismic stations, both on the Early Rise Line and the northern Ontario stations is PreCambrian in age and forms the stable interior shield region of North America.

The Early Rise Line crosses the Quetico, English River and Cross Lake structural belts of the Superior structural province and the Churchill structural province (Stockwell, 1964). The northern Ontario recording stations also encompass the Quetico and English River belts of the Superior province. Rock types in both areas range from granitic to basic in composition.

The geology of Lake Superior in the region under the shot position can be ascertained from Halls (1967) ~~in his~~ review of the geology of Lake Superior. The central portion of the lake is thought to be underlain by a synclinal sequence of gabbros, volcanics and sediments of Animikean and Keeweenawan age (late Proterozoic) which, on the north shore, is in excess of 17 km. thick.

The structural belts of the Superior province have been outlined by Stockwell (1964). They consist of tightly down-folded metavolcanics and metavolcanics with pronounced E-W lineations. The E-W trends of the Superior province are terminated by the north-south structural trends in the James Bay region, and by the Churchill Superior boundary zone in the west.

The geology of the boundary zone between the Churchill and the Superior structural province has been summarized by Gibb (1968). Fig. 1-3 shows a generalized regional geology map of Northern Ontario and Manitoba. In the vicinity of the Nelson River a further division called the Pikwitonei subprovince has been outlined (Bell, 1966). This area consists mainly of rocks of the granulite facies and lies directly south of the mafic zone

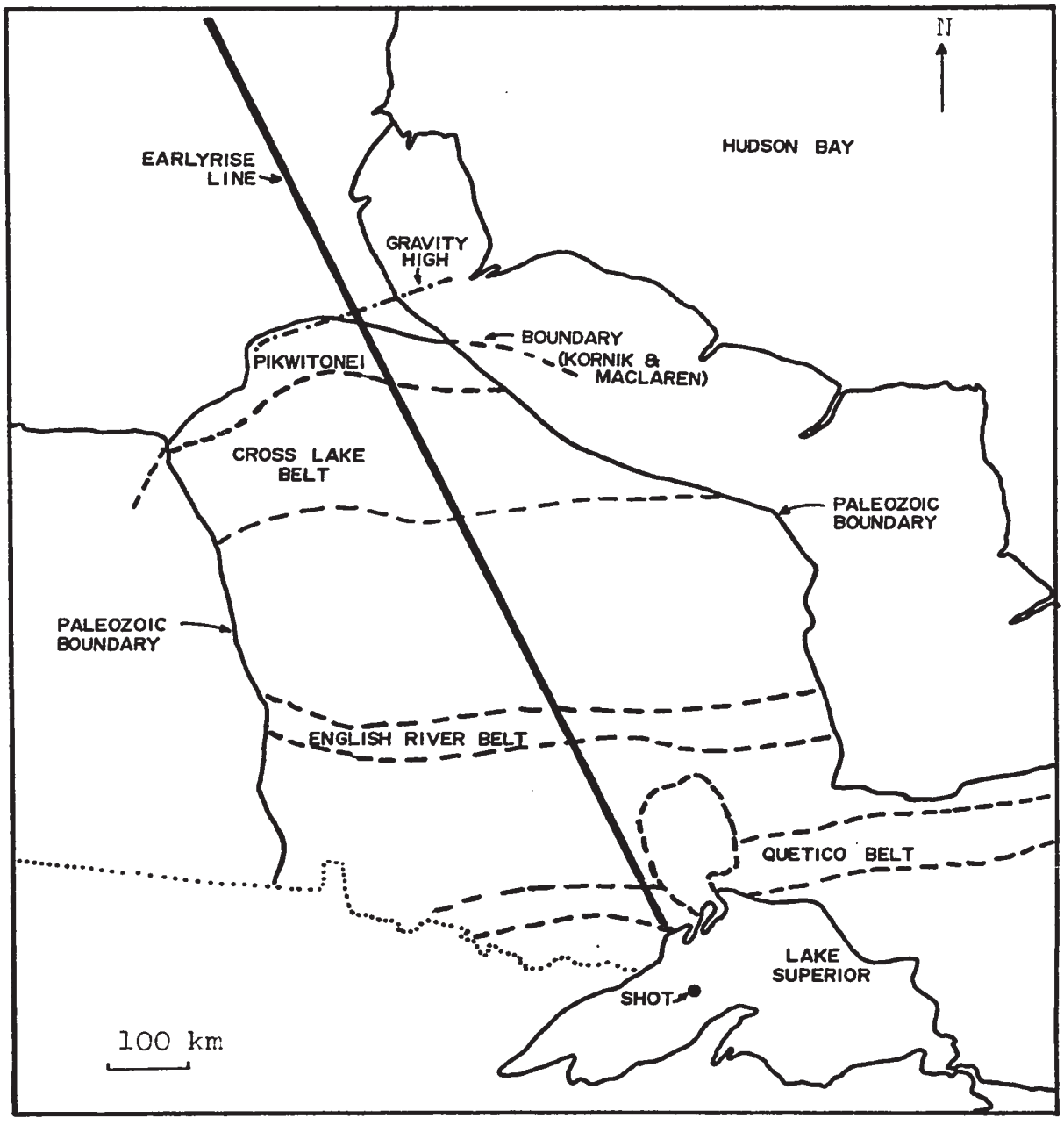

Fig. 1-3 Generalized structural geology map of the survey area showing the position of the Early Rise recording line.

considered by many to be the boundary between the Churchill and Superior provinces. North of this zone, the rock consists of granite gneisses of the Churchill province. Differences of opinion exist amongst workers as to the positioning of the boundary in the region east of the Early Rise Line. Innes (1960) and Wilson and Brisbin (1962) suggest that the boundary trends northeast across Hudson Bay to link up with the Cape Smith-Wakeham Bay fold belt of the Ungava Peninsula. However, Kornik and MacLaren (1966) and Bell (1966) suggest that the boundary zone runs easterly, to the south of Hudson Bay.

1.3 Regional Geophysics

Large scale Bouguer gravity anomalies were first outlined in Northern Ontario and Manitoba by Innes (1960). An elongate positive anomaly, 60 miles wide striking northeast adjacent to the Nelson River, was interpreted as being due to deep-seated crustal effects and near surface density increases associated with basic intrusive rocks. Throughout Northern Ontario positive Bouguer anomalies have been correlated with the greenstone zones within the structural belts.

Shimazu (1962) has investigated the gravity data for this area of the Shield and interpreted the mean crustal thickness to be approximately 36 km. From examining the anomalous zone of the Nelson River high he concludes that crustal thinning in the order of 3 kilometers has occurred in the Superior Province.

Gibb (1968) has accounted for most of the local gravity anomalies in the boundary zone between the two provinces in terms of density contrasts of near-surface rock types.

Gravity surveying in the Lake Superior region has been done in a reconnaissance manner by Weber and Goodacre (1966). Their interpretation suggests that the crust under the Lake is composed of high density rock whose thickness is greater than 40 kilometres. This anomalous crustal density profile is thought to be confined to the area around the Lake and normal crustal densities and thicknesses are thought to prevail north of the Lake.

Kornik and MacLaren (1966) have examined the magnetic expression of the boundary zone between the Churchill and Superior Provinces. The prominent magnetic lineation in the Nelson River region has been interpreted as defining the boundary zone. A narrow magnetic low chosen as the boundary lineation can be followed in a NE direction from the southern limit of the Shield area to the Early Rise Line where the strike changes to an easterly direction (see fig. 1-3).

Several seismic surveys have been performed in Shield areas adjacent to the present survey area. One of the first refraction surveys in the Shield was performed by Hodgson (1953). From mine rockbursts and timed explosions, he found an average crustal velocity of 6.23 km/sec and an average crustal thickness of 35 km in the Kirkland Lake district. His results favoured a single layered crustal model with an upper mantle velocity of 8.18 km/sec.

The results of a time-term analysis of the 1963 Lake Superior crustal experiment are given by Smith et al. (1966). They suggest that the best fitting model is one consisting of a two-layer crust having velocities 5.5 and 6.68 km/sec and thicknesses of 9 km and 20-50 km respectively. The P_n velocity was determined to be 8.07 km/sec. Also they suggest that the Lake Superior basin has been formed by the isostatic adjustment of the crust to loading by high density material which may form part of a rift

zone in the PreCambrian Shield.

Berry and West (1966) reached similar conclusions to those given above in analysing the Lake Superior seismic data. They correlate the upper crustal seismic layer with a thick sequence of late Proterozoic sedimentary rock and the lower crustal seismic layer with mafic volcanics.

A re-interpretation of the Lake Superior data by O'Brien (1968) suggests a slightly lower crustal refractor velocity (6.75 km/sec) and slightly higher upper mantle velocity (8.16 km/sec), with much lower structural relief on the Moho. Crustal thicknesses range from 38 km in the western end of the Lake to 55 km in the central portion of the Lake and thinning to 45 km at Foleyet, Ontario.

Roller and Jackson (1966) give the results of the second seismic survey in Lake Superior in 1964 and have shown the crust SW of Lake Superior to be composed of two layers, one 15 km thick with a velocity of 5.5 km/sec and the lower 35 km thick with a velocity of 7.2 km/sec. The upper mantle velocity was determined to be 8.2 km/sec. A deeper horizon occurring at a depth of 105 km gave a velocity of 8.5 km/sec.

Brune and Dorman (1963) have measured velocities of Raleigh and Love waves from various path directions across the Canadian Shield and have obtained an average crustal thickness of 35 km. In their best-fitting model the crust has been divided into three layers with estimated P wave velocities of 5.64, 6.15, and 6.60 km/sec and thicknesses of 6.0, 10.5 and 18.7 km respectively. Their model for the upper mantle consists of layering with estimated compressional velocities of 8.1, 8.2, 8.3 and 8.7 km/sec and thicknesses of 80, 100 and 100 km respectively.

Hall and Brisbin (1965) have conducted a seismic refraction survey across the southern extension of the Nelson River high from Flin Flon to Mafeking. Their model, being an interpretation based on the observation of converted refracted events, consists of a two layered crust of velocities 6.15 and 6.65 km/sec and thicknesses of approximately 15 and 19 km respectively. The Moho velocity was determined to be 7.90 km/sec. They suggest a crustal thinning across the structural boundary from 34 km at Flin Flon to 31 km at Mafeking. This correlates well with Shimazu's (1962) gravity analysis and suggests that erosion and uplift has occurred in the older Superior Province.

Structural interpretations for the crust under Hudson Bay from the 1965 Hudson Bay crustal seismic experiment have been made by several people including Ruffman and Keen (1967), Hunter and Mereu (1967), Hobson, Overton, Clay and Thatcher (1967), Overton (1969), Ruffman (1969), Hajnal (1969), and others. The basic structure consists of a crust (possibly two seismic layers) with an average velocity of 6.3 km/sec and thicknesses ranging from about 45 km near Churchill to 27 km in the centre of the Bay. The upper mantle velocity is approximately 8.25 km/sec, a value slightly higher than that found for the Lake Superior region.

CHAPTER II

Instrumentation

2.1. Field Stations

The three mobile seismic stations used in the Early Rise experiment were composed of detection, amplification and recording units as given by fig. 2-1.

The remote-controlled station was operated by means of a pre-programmed clock-switch. On and off contacts with 15 minutes between switch cycles were set for the scheduled shot times and alternate times. Contact closures powered the amplifiers, tape recorder and time-signal receiver. The complete remote station was operated from two 2' x 2' field cases. Power for the instruments was supplied by two 6 volt heavy-duty truck batteries. The station was covered with plastic sheeting weighted with rocks to effect waterproofing.

The manned three-component station was housed in a manner similar to that described above and was operated from a tent.

The single component station was contained within one case and was operated from a truck. With all stations it was found that sufficient protection against shock damage was obtained by packing each individual instrument in the case with foam-rubber padding. A loose packing of instruments in this manner meant that they could easily be removed from their cases and used separately in other systems.

The Electrotech EV-17 and EV-17-H seismometers used for the survey were mounted on metal plate supports with three levelling legs. Hence, despite uneveness and slope encountered on rock outcrop the seismometers could be successfully levelled. To orient the horizontal seismometers in a NS and EW direction a survey chain was first laid out using a

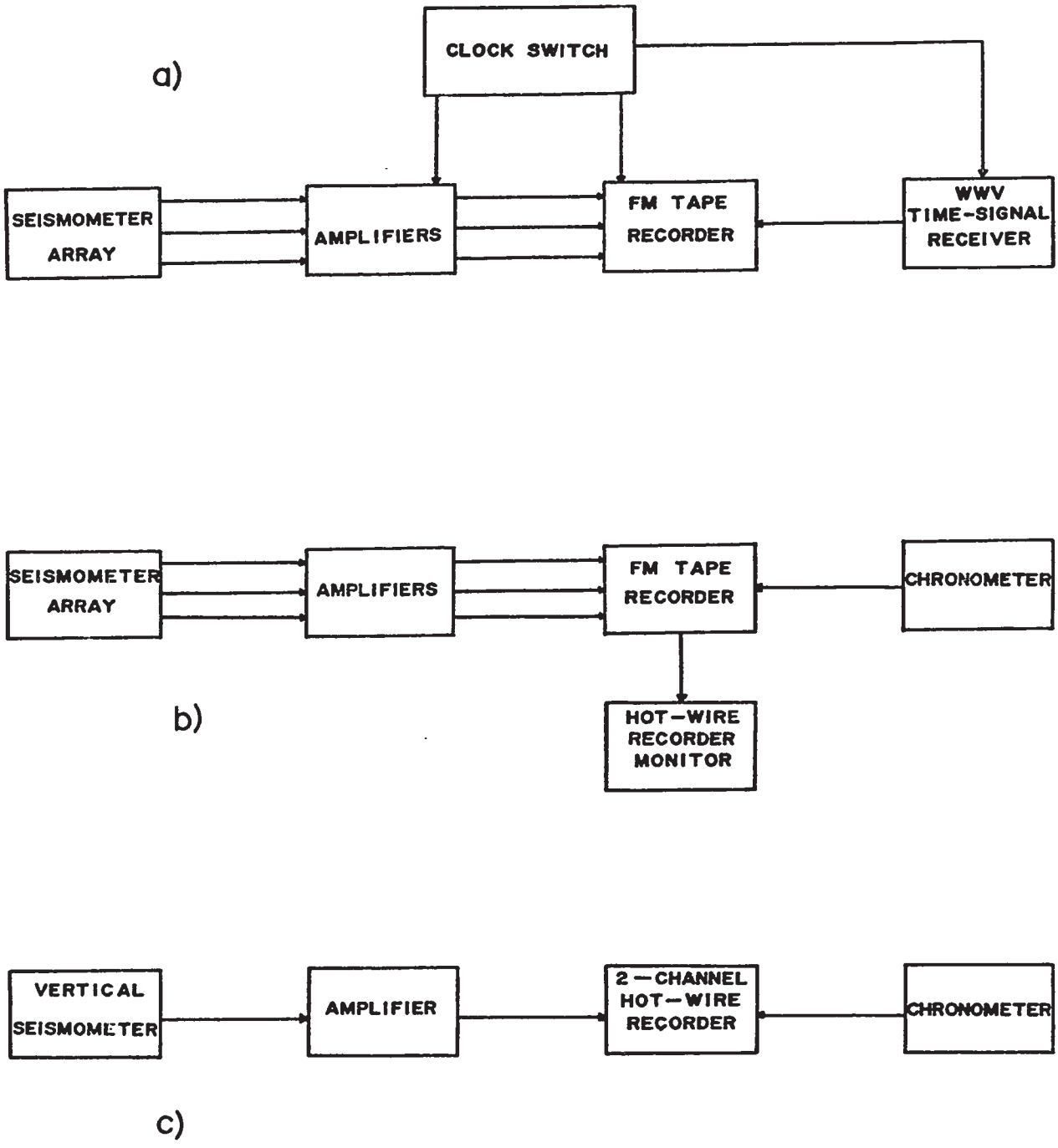

Fig. 2-1 Block diagrams of the field recording systems, a) three-component 'remote' station, b) three-component manned station, c) single component station.

Brunton compass. The seismometers were then positioned such that the direction arrows on the casings were parallel to the chain. It was felt that the seismometers could be successfully positioned to within ±2°. The presence of strong magnetic anomalies in the Earth's magnetic field are often found in the survey area, and it is possible that positioning errors could result.

To calibrate each channel of recorded seismic trace, a 1 hertz oscillator signal of known voltage was introduced at the input to the amplifiers and was subsequently recorded on tape prior to each shot seismogram. To test whether each station was operational, after set-up on the outcrop, the magnetic tape input was monitored for each channel as an operator/s assistant performed "knee-bends" by each seismometer. This test was extremely valuable since the seismometers often jammed during transport.

The stations along the Early Rise line were moved in leap-frog fashion along the seismic line by a float-mounted DeHavilland Beaver Aircraft. The relatively short summer night at these latitudes facilitated the search for outcrop on which to place the stations. Two of the stations were not placed on bedrock since exhaustive air searches could reveal no rock in the immediate area.

The single-component (vertical) station was operated from a three-ton truck fitted with a cab containing instrument room and living quarters. Recording was done at night, while during the day the truck was moved to each new recording position. To obtain a good spacing between recording stations, highways, secondary roads, logging roads and abandoned trails were utilized throughout northern Ontario.

2.2 Specifications

The specifications of each of the component instruments in the systems are described in detail in Appendix A. The extremely low frequency ground response expected on the seismograms made FM tape recording a necessity. The tape recorder input voltages in the range of 0.001-1.0 volts dictated that the amplifier gain be as high as 10^6. The seismometer, amplifier and combined frequency responses are given in fig. 2-2. The response of the seismometer (operated about 70% damped) was relatively flat in the frequency range down to about 1 hertz.

As a check on the low frequency response of the system a simple experiment was devised to measure the combined responses. The geophone and amplifier were connected as in field use, with the geophone resting on a low-noise decoupled cement pillar in the U.W.O. seismic laboratory. The case of the seismometer was removed and a small weight was placed on the boom. The weight was quickly knocked off with a pencil using upward motion. The resultant simulated ground acceleration is that of a step function and the ground velocity spectral response can be computed. The system response from the amplifier output was recorded on an oscilloscope and photographed. The photographed response was then digitized and Fourier-analysed by computer to obtain the spectral response. The measured system responses in the time and frequency domains are given in fig. 2-3. The oscillating nature of the frequency response curve for high frequencies is interpreted to be the effect of pillar noise, downward aliased instrumental noise and increased spectral measurement un certainty as one approaches the Nyquist frequency (limit of resolution, f_n = 22.5 hertz). However, the low frequency response measured by this method compares well with the combined responses as given by the manufacturers (see fig. 2-2).

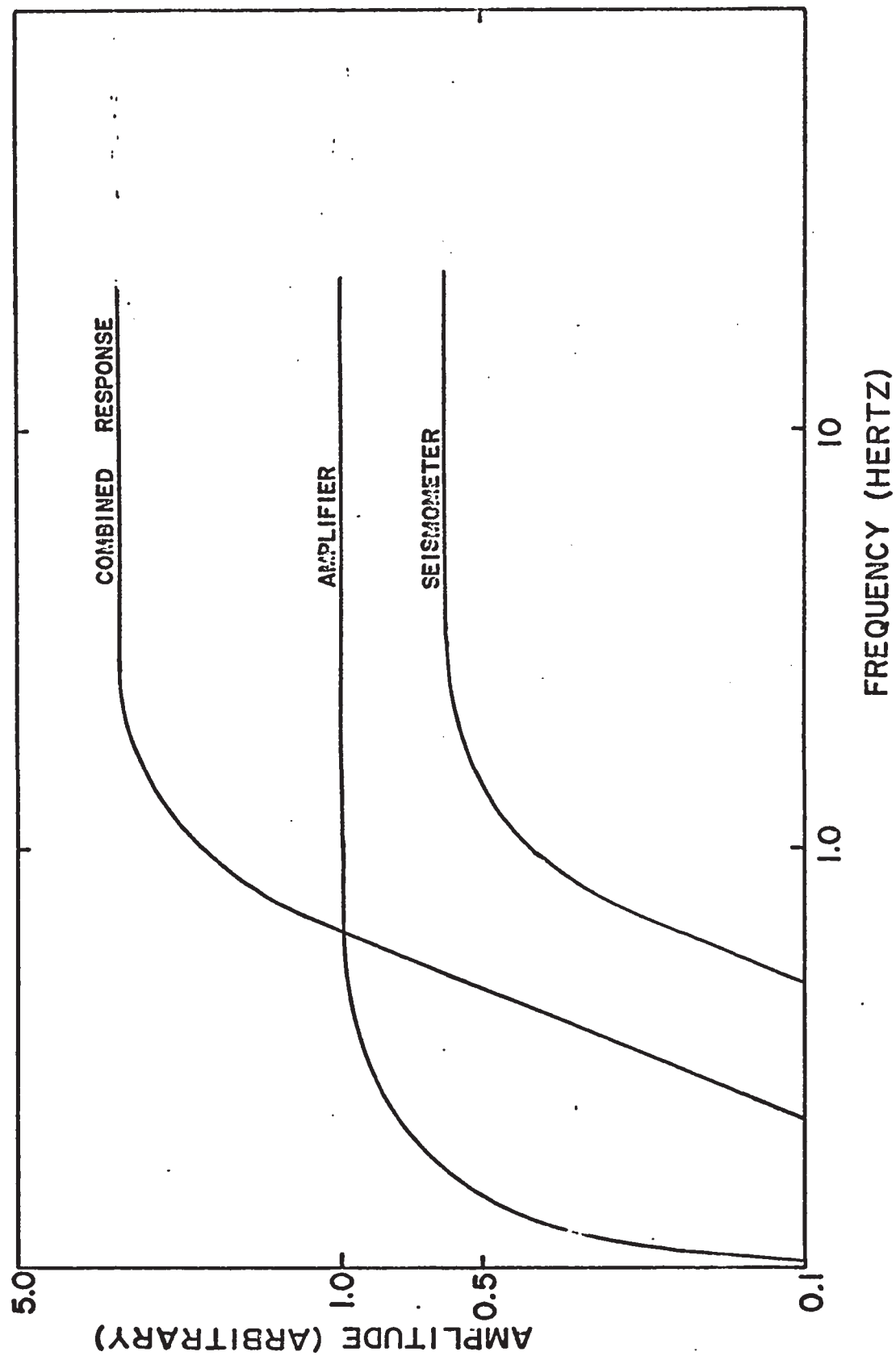

Fig. 2-2 Manufacturer's response curves for the seismic systems

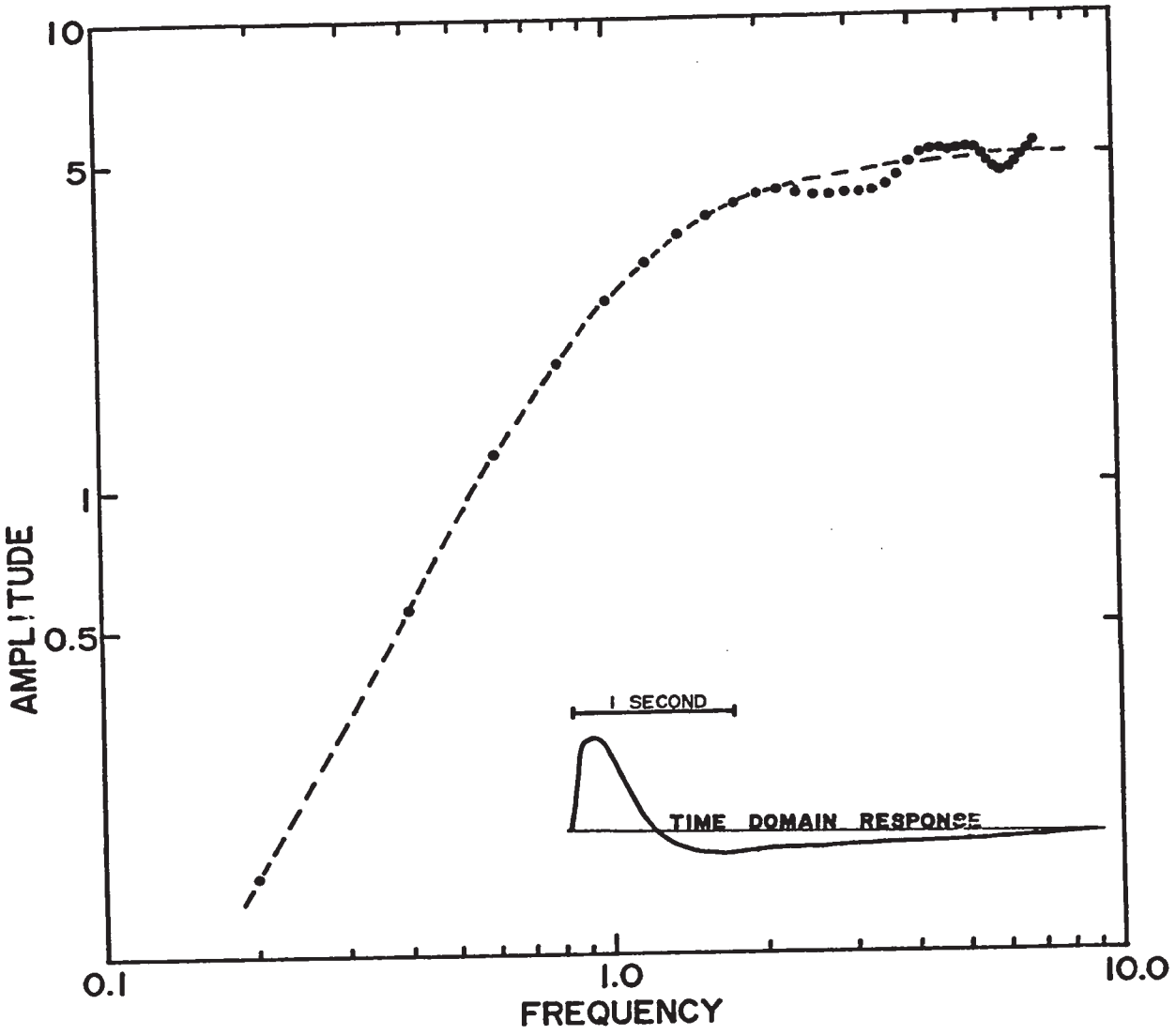

Fig. 2-3 (a) Measured amplitude response curves for the smic systems.

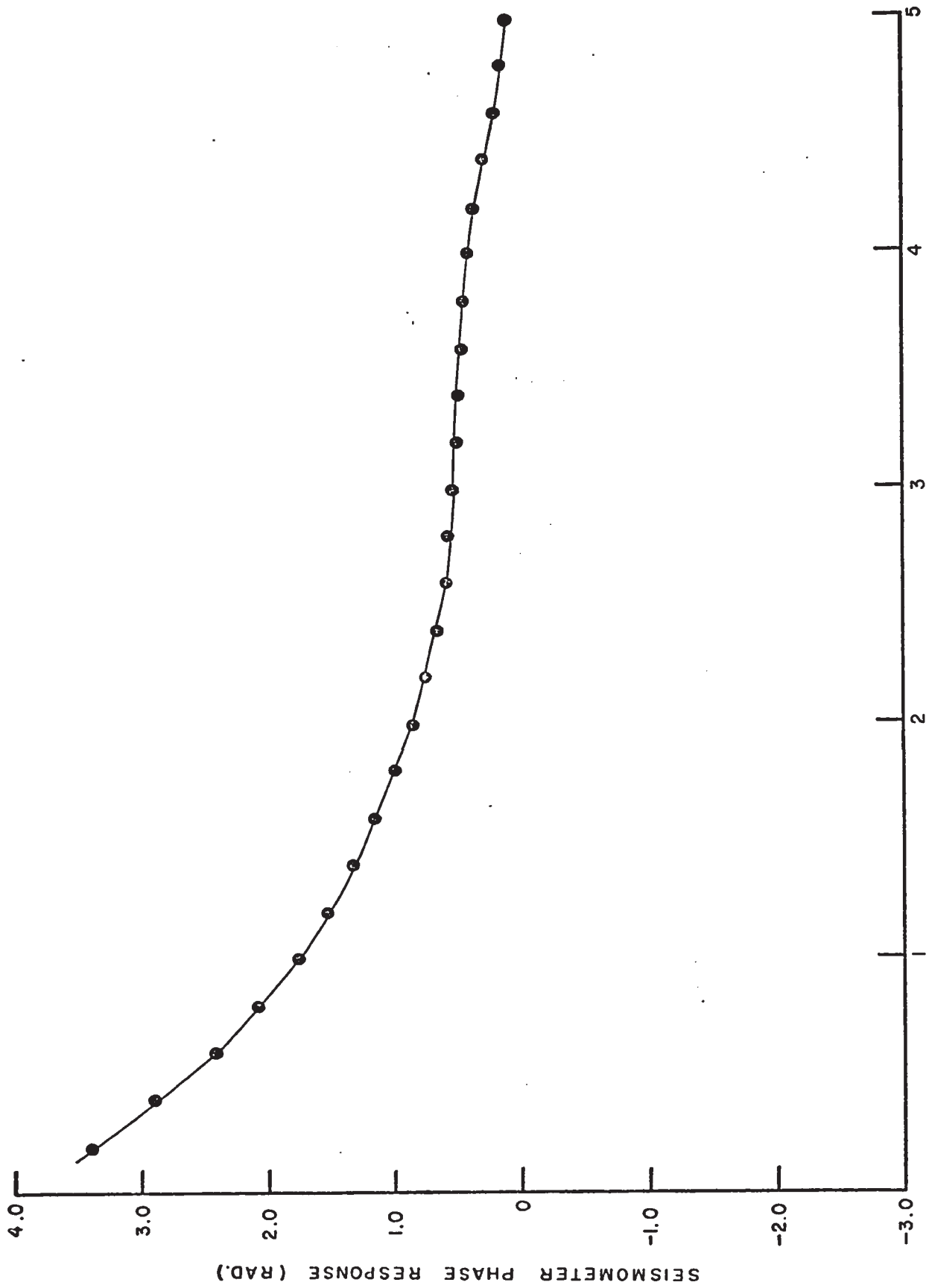

Fig. 2-3 (b) Measured phase response curve for the seismic systems.

2.3 Digitizing of Seismic Records

The transfer of the Early Rise records from FM analog magnetic tape to computer-compatible binary format digital tape was accomplished in several steps. These involved primarily the transfer of analog data from the P.I. ¼" tape recorder to a digital magnetic tape using a Hewlett-Packard Data Acquisition System (digitizer). Since the seismograms from the manned three-component station were recorded on ¼" magnetic tape the seismograms could be played directly into the digitizer. However, since the "remote" station recordings were made on ½" magnetic tape an auxilary analog transfer was required. With the aid of the U.W.O. Medical Department's ½" tape recorder, the "remote station" recordings were re-recorded onto the P.I. ¼" tape recorder at twice real speed. Further, with the help of the U.W.O. Dept. of Physics Nematron tape recorder, these records were re-recorded onto the P.I. ¼" tape recorder at real speed. The resultant "remote station" recordings sometimes demonstrated a loss of quality by the addition of 60-cycle noise and overload from high amplitudes incurred in the intermediate recording stages.

The Hewlett-Packard digitizing system sequentially samples an array of input channels and records the resultant voltages in digital form on ½" magnetic tape. Although up to 300 channels may be sampled only 4 were used in this experiment (3 seismic channels and 1 time-code).

The digital system in block diagram form is shown in fig. 2-4. The scanner control operates an electro-mechanical scanner which samples the input channels. The input voltage is introduced from the scanner into the integrating digital voltmeter. The channel identifier from the scanner control and the sampled voltage are written in Binary Coded Decimal form on either the Kennedy incremental tape recorder at 512 bits/inch or in printed

Leaf 19 missing in page numbering.

decimal form on paper tape. The timing involved in initiating writing and sampling is shown in fig. 2-5. The sample rate for the system with tape recordings alone is fixed at 18 measurements per second whereas with the addition of paper tape the sample rate is reduced to 17.5 measurements/sec. Because of the slight decrease in sample rate, paper punch monitoring was not used during digital recording.

The sampling rate of the digital system governed the range of digital accuracy obtainable. By playing the P.I. tape back at one tenth of recording speed (0.375 inch/sec) and digitizing at a rate of 4.5 measurements/sec/channel, a sampling rate of 45 measurements/sec/channel was achieved for the seismogram. This rate gave a Nyquist frequency of 22.5 hertz (well above the seismic band). Hence no appreciable seismic energy should be folded back or "aliased" from high frequencies above the Nyquist frequency. Care was taken to shield external leads between instruments to reduce contributions of 60 hertz noise.

The analog tape input to the digital system was monitored by a Sanborn 4-channel hot-wire amplifier and recorder system. Approximate starting points for digitizing shot recordings were noted on the analog monitor record and were used for estimating approximate first arrival positions in digital analysis. As well, input calibration signals were recorded on tape and monitored for channel calibration.

The low density (512 bits/inch) B.C.D. digital tape produced by the digital system is not directly compatible with the U.W.O. computer system when standard programming modes are used. The U.W.O. computer system on a Fortran read command accepts tape input into buffer storage in the form of 750-bite blocks separated by inter-record gaps. The BCD digital tape output is designed to minimize the number of inter-record gaps since in the digitizing sequence the seismic information is low (not

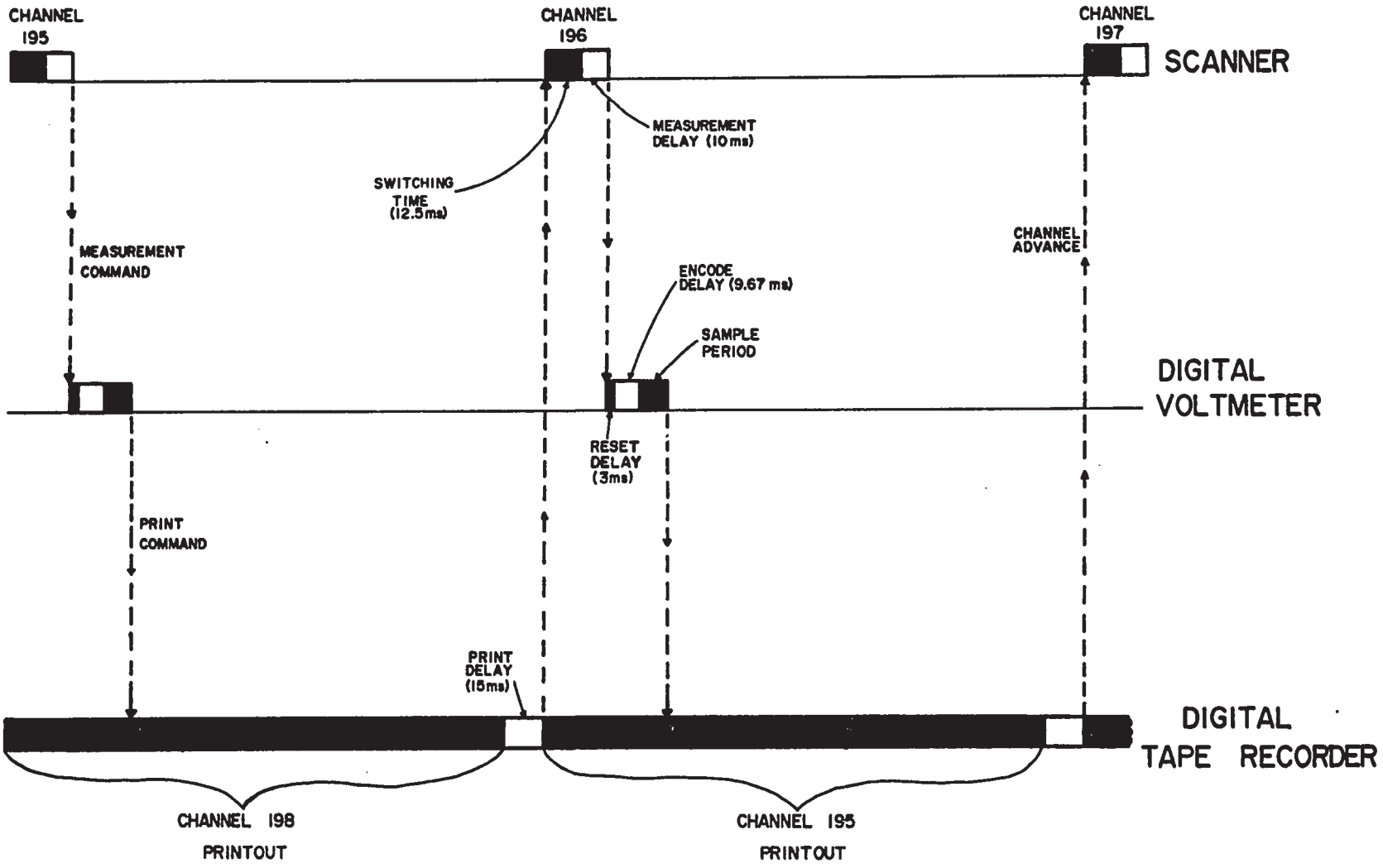

Fig. 2-5 Diagrammatic representation of the sampling and recording time sequences of the Hewlett-Packard system.

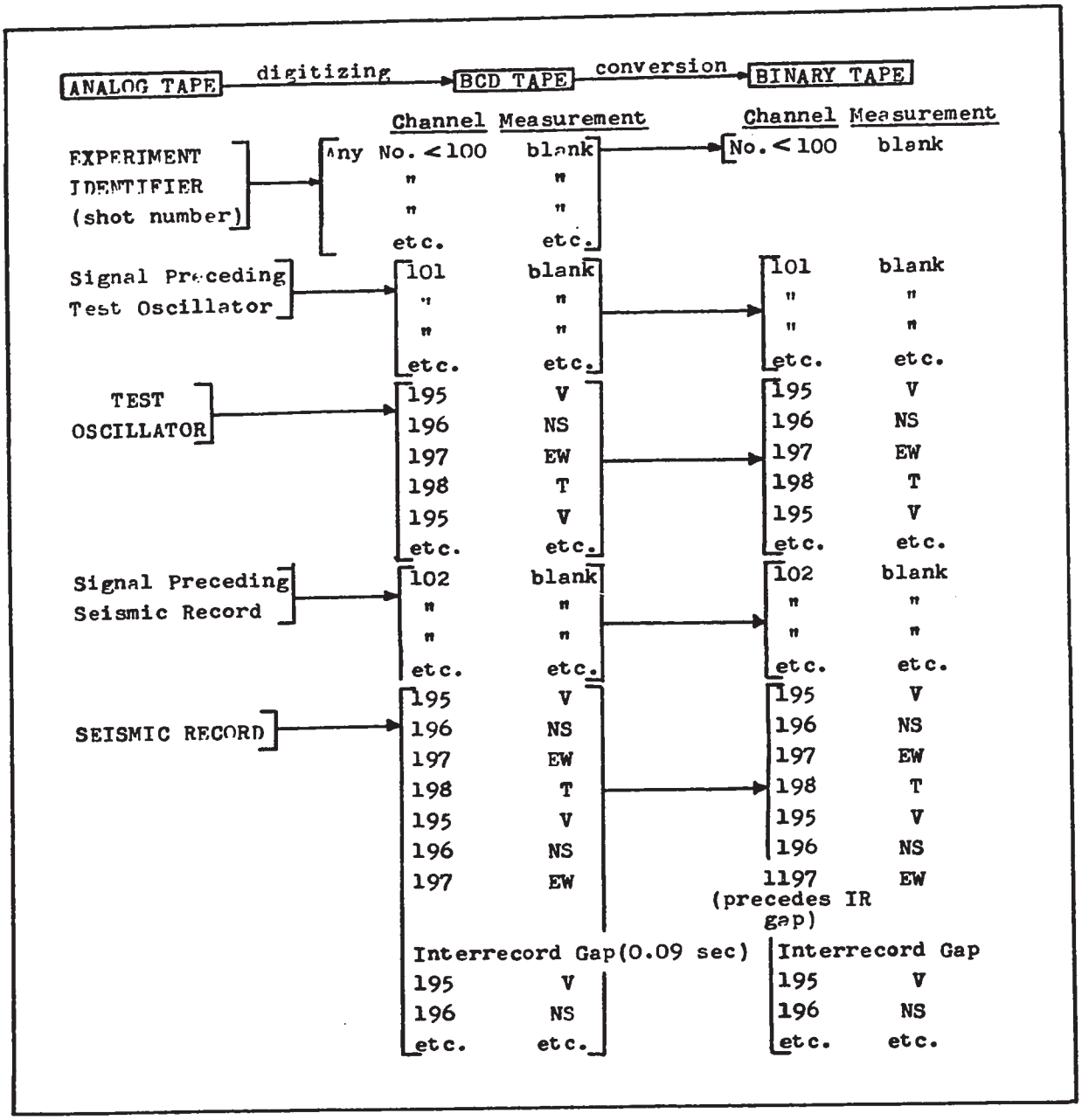

Fig. 2-6 Tape formats used to produce the binary tapes.

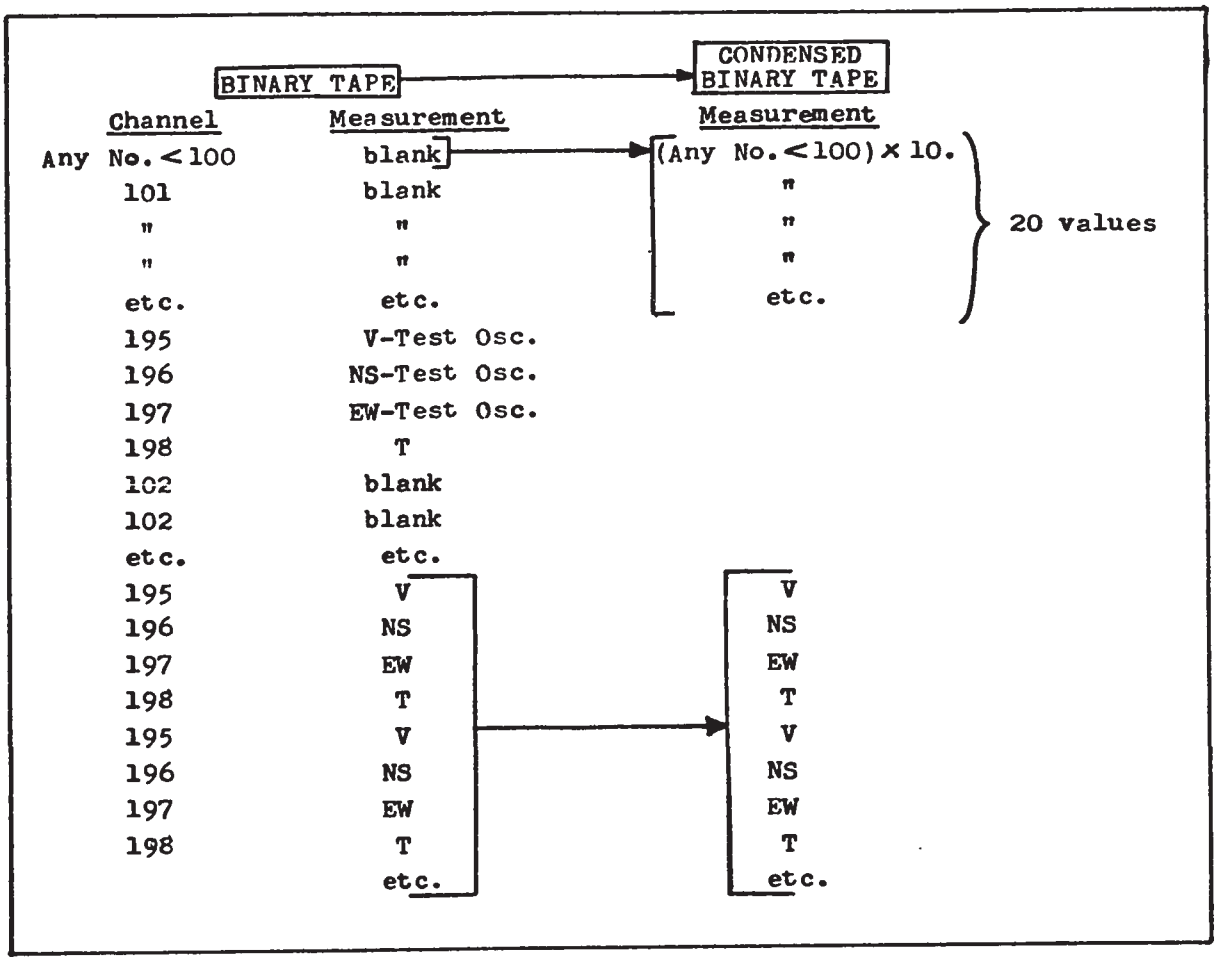

Fig. 2-7 Tape transfer procedures used to produce a 'condensed' binary tape.

recorded digitally) during the time the IR gap is being written. For this reason, and also to reduce tape read formating, an additional transfer step from BCD low-density tape to Binary high-density (880 BPI) was introduced in the record processing. A computer program designed by the U.W.O. computing centre is used to transfer the BCD records to computer-compatible Binary tapes. A standard coding has been adopted for digitizing and tape transfer and is given in fig. 2-6. Within this format any experiment with a large number of channels may be processed.

A further editing step was made with the binary digital tapes. Since each channel contained a separate identification word it was decided to remove them and reduce the tape storage by 50% per seismogram. As well further editing removed the test oscillator signal and retained the first 30 seconds of record without IR gap notation. Thus a new set of condensed binary tapes were produced as given by fig. 2-7. This resulted in condensing the necessary portions of all the Early Rise records into six 200 ft. digital tapes.

A description of the steps involved in digitizing the seismic records and the computer program involved are given in Appendix A. Many problems were experienced in transferring records from analog to digital form. The "write" heads of the digital tape recorder are extremely sensitive to magnetic pick-up. It was discovered that a magnetic mineral separator operated in an adjoining room was the cause of many tape errors which had resulted in many hours of re-digitizing. Subsequently, the digital system was operated only after regular working hours when the magnetic separator was not in use.

Tape "drop-outs" or imperfections in the analog tapes often produced voltage spikes which were recorded as a voltage overload on the digitizing system. This resulted in an unusually high number written in

the data channel. Although these events were infrequent it was thought necessary to write in a testing and removal subroutine within data retrieval programs.

In order to retain much of the seismic information unaltered, the I.R. gap rate set for the B.C.D. tapes was maintained low. Often 700 measurements/channel were made between I.R. gaps which taxed the computer buffer storage limit in transferring to Binary tape. Failure to write an I.R. gap was responsible for failure of some of the tape transfer procedures. This failure rate was small, however, compared to operator error in pre-selecting the tape densities on the tape units prior to tape transfer.

CHAPTER III

A CRUST AND UPPER MANTLE MODEL FROM FIRST ARRIVAL TRAVEL TIMES

3.1 First arrival Model for the U.W.O. Survey Area

A first arrival-time earth model has been given by Mereu and Hunter (1969) for the Early Rise Line and the Nipigon-Smooth Rock Falls records. For continuity of exposition a brief description of the observations and results are repeated here.

A tabulation of recording positions, distances and first arrival times for all U.W.O. stations is given in Appendix B. The positioning of stations are estimated to be correct to 0.1 km. The arrival times are estimated to be correct to 0.1 to 0.2 seconds.

Fig. 3-1 shows a first arrival-time distance plot for the Early Rise Line. An interpreted break in the travel-time slope occurs at approximately 630 km. distance suggesting that first arrivals beyond this point are from a horizon deeper than the Moho. The events from this horizon are designated as 'P' events to distinguish them from P_n Moho refractions. A least squares line fitted to P_n events from 300 to 640 km gave an apparent velocity of 8.12 ± 0.02 km/sec. This compares well to P_n velocities determined from the Lake Superior experiment (see Table III-I, a tabulation of crustal results from adjoining areas). A fit of a least squares line to the data between 700 and 1500 km yielded an apparent P velocity of 8.44 ± 0.02 km/sec, whereas fitting only points in the region of 700 to 1000 km yielded an apparent velocity of 8.52 ± 0.03 km/sec.

Fig. 3-2 shows first and later arrivals interpreted as P_g events plotted against distance. A line passing through the first two points

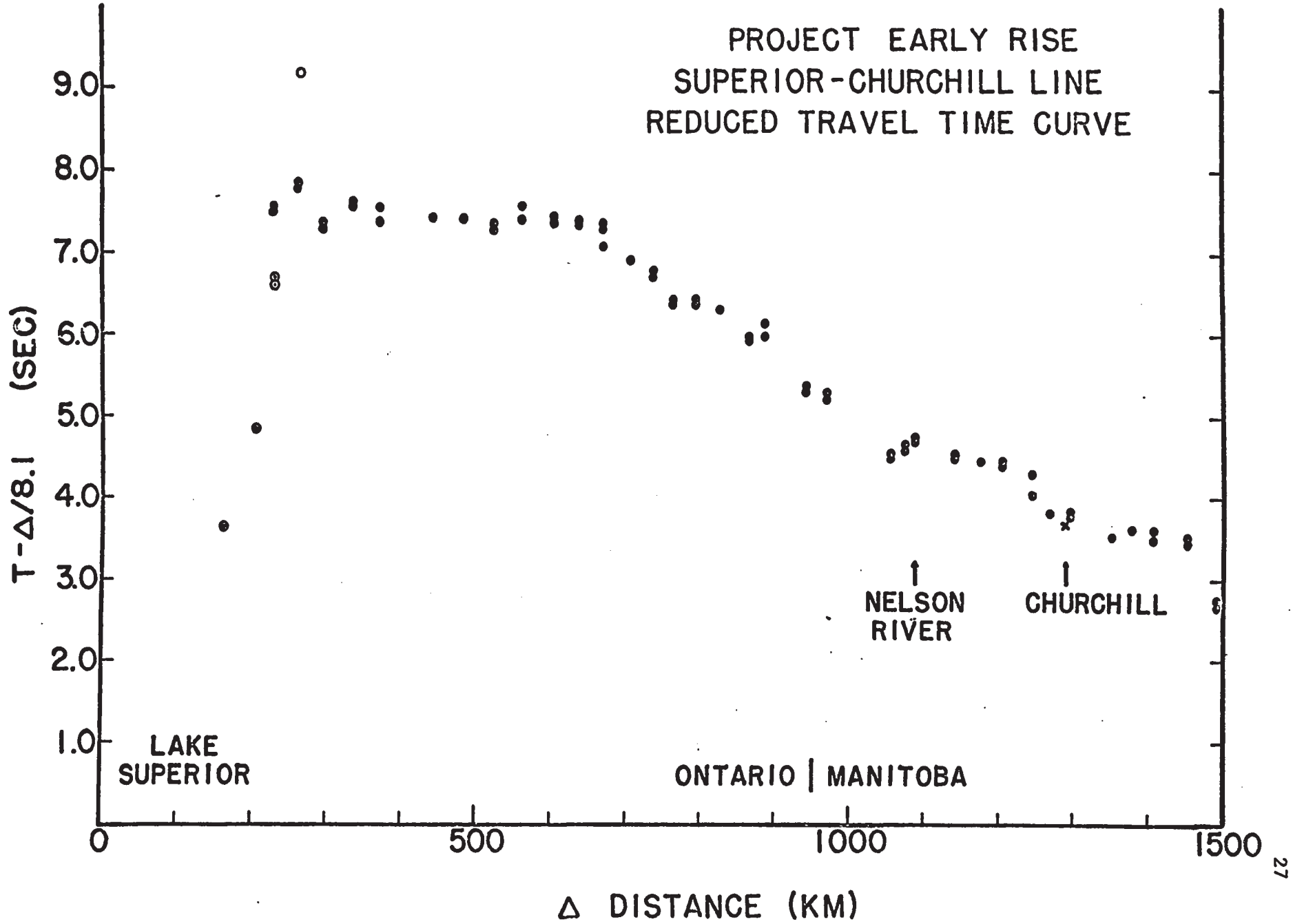

Fig. 3-1 Reduced travel-time curve for first arrivals from the Early Rise line.

only, has an apparent velocity of 6.65 km/sec however, a least squares line from all P_g data gave an apparent velocity of 6.23 ± 0.20 km/sec. This suggests that a high crustal velocity may exist in the region of Lake Superior, whereas normal crustal velocities prevail north of the Lake. The crustal velocities observed in the area of the Lake and in adjacent areas (see Table III-I) substantiate the interpretation of the anomalous high velocity crust.

It was felt that the velocity decrease at the far end of the Early Rise line may be due to structure on the Moho. Knowing the Moho time-term under the shot point (Mereu & Hunter, 1969) and the Moho time-term under Churchill station from the Hudson Bay experiment, three travel-time equations were formed from:

1) the P_n ray arriving at the break-over point to the P layer near 630 km (station 14)
2) the P ray arriving at Churchill (Early Rise Line station 40, see fig. 3-1)
3) the P ray arriving at the breakover point,

of the type:

$$T = \Delta/V + a + b$$

where, a, b, are the shot and station time-term respectively and

V = the apparent refractor velocity.

Solving this set of three equations by iterative methods and taking into consideration curvature corrections given by Mereu (1968), the apparent velocity of P waves was determined to be 8.54 ± 0.03 km/sec while the depth to the P interface was computed to be 84.3 ± 3 km. The curvature-corrected velocities for P_n and P are 8.05 and 8.43 km/sec. respectively.

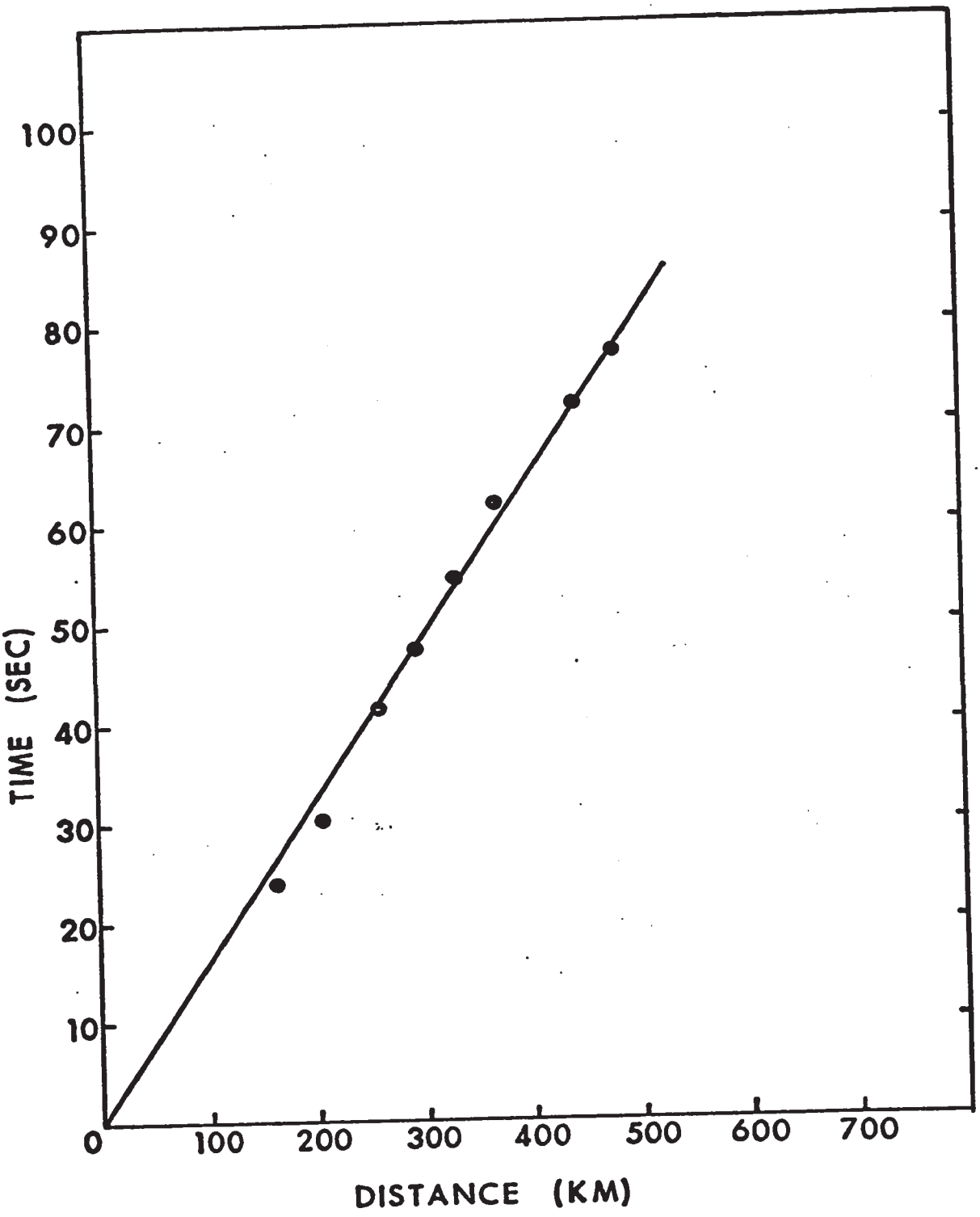

Fig. 3-2 Picked events for the P_g wave.

Under the assumption that the P interface is flat and all arrival time delays are due to Moho topography, the Moho time-terms and depths from both P and P_n arrivals were computed iteratively, as given in Appendix B. A mean P_g velocity of 6.30 km/sec was used to convert the time-terms to depths. A plot of the results for the Early Rise Line are given in fig. 3-3; the points with open circles are the results taken from the Gambler line of the 1963 Lake Superior experiment. The point plotted as an X is the Churchill station from the Hudson Bay experiment (Hunter and Mereu (1967). The Moho depths given along the Early Rise Line indicate that normal crustal thickness (34 km average) exists immediately north of Lake Superior. Crustal thinning (to 28 km) occurs in the vicinity of the Superior-Churchill structural boundary. To the north of this boundary the crust thickens to a depth of about 55 km in the Churchill province.

Fig. 3-4 is a contoured map of the time-terms in the Lake Superior region employing the results of the 1963 experiment and the Nipigon-Smooth Rock Falls data (Mereu, 1966). The contours are extended south of Kapuskasing based on data of the University of Toronto (Warren et al., 1961). An approximate conversion of time-terms to depths can be made by multiplying the time-terms by 10. The large time terms of the Lake Superior region return to normal values within the Superior province suggesting that the Moho is a basin-shaped depression centred under the northern part of the Lake.

The exact values of the Moho time-terms computed for the stations are strongly dependent on the value of the shot time-term. The value used (4.3 ± 0.2 sec) was taken from a time-term solution of the 1963 Lake Superior data by Mereu (1966). The estimated uncertainty in time-terms, as a result of uncertainties in the shot time-term and refractor and crustal velocities under the shot travel time and distance errors, is 0.4 seconds.

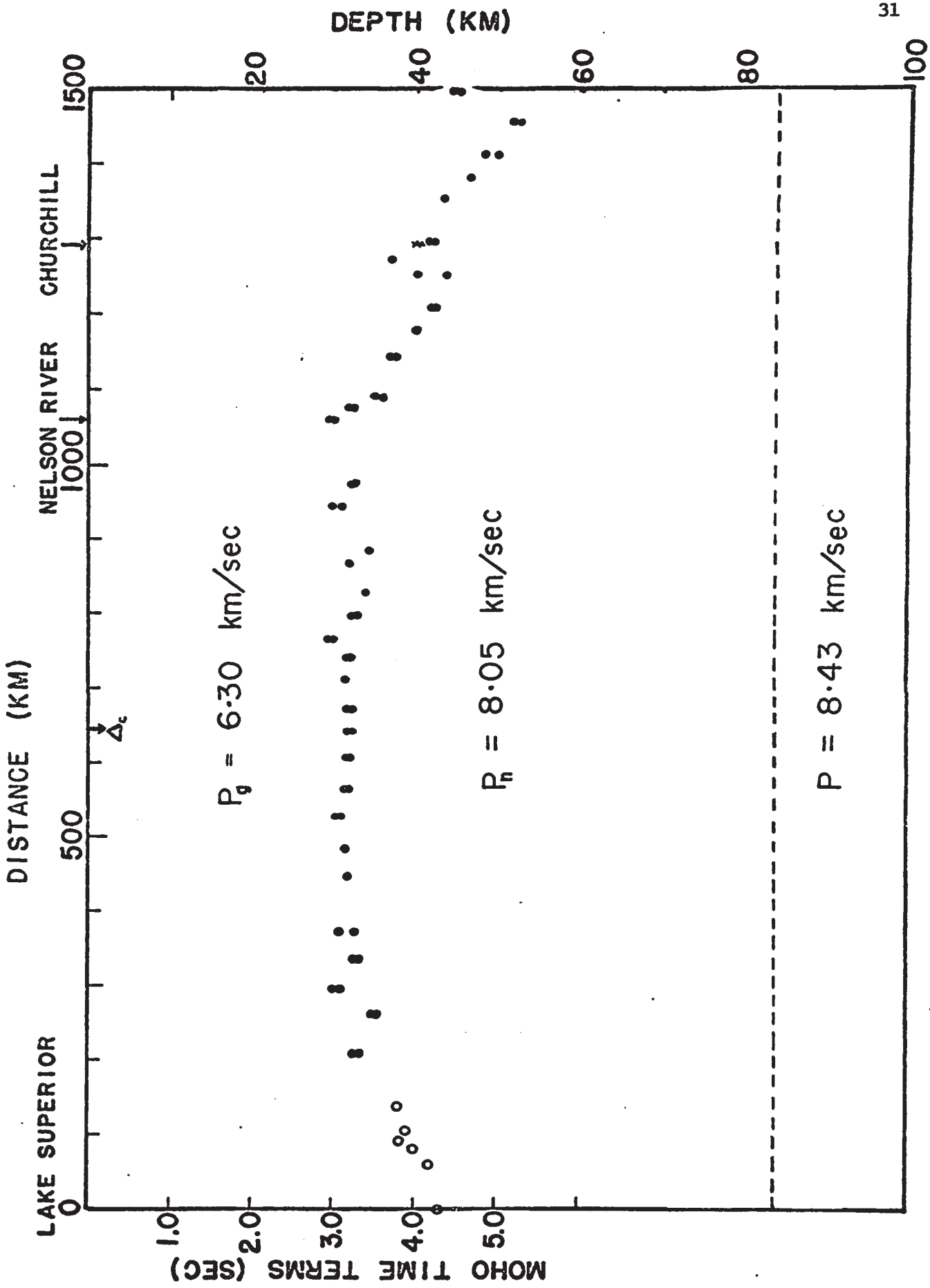

Fig. 3-3 MOHO TIME TERMS AND DEPTHS
SUPERIOR-CHURCHILL LINE

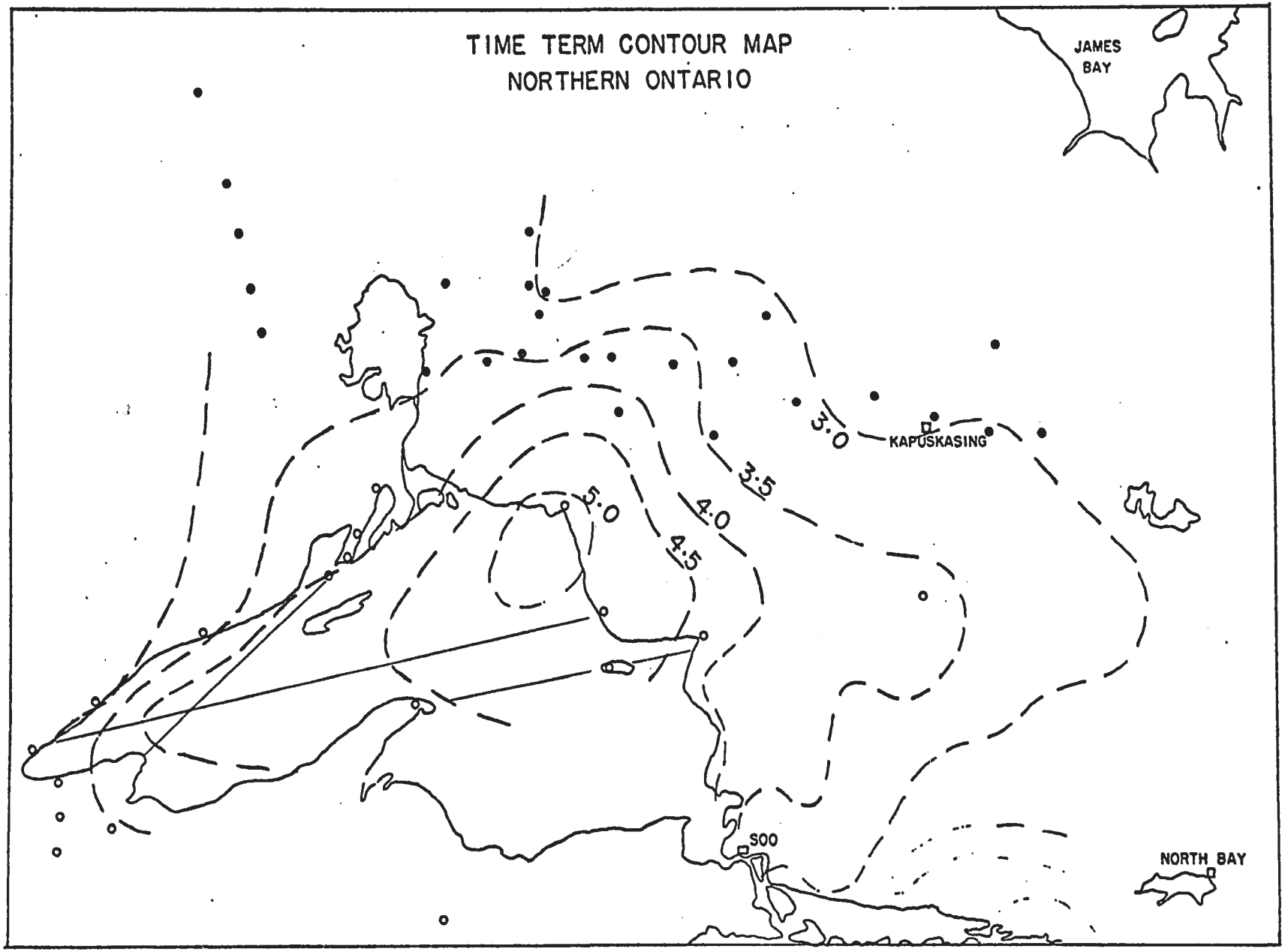

Fig. 3-4 Time-term contour map of northern Ontario based on U.W.O. results and previous surveys.

TABLE III-I

SUMMARY OF CANADIAN SHIELD SEISMIC STUDIES

Investigator	Region Studied	Apparent P_g km/sec	Apparent P_n km/sec
Hodgson (1953)	Northern Ontario	6.19, 6.29	8.17 ± .013
Brune and Dorman (1963)	Canadian Shield, (Surface Wave Study)		
Hall and Brisbin (1965)	Northern Manitoba	6.15, 6.65	8.17 (2 layer crust)
Hunter and Mereu (1967)	Hudson Bay	6.32 ± .06	8.23 ± .03
Ruffman and Keen (1967)	Hudson Bay	6.33	8.27
Hobson (1967)	Hudson Bay	6.28	8.25
Barr (1967)	Hudson Bay	6.50	8.23
Berry and West (1965)	Lake Superior	6.63	8.10
Smith et al (1966)	Lake Superior	6.69 ± .02	8.07 ± .03
Mereu (1966)	Lake Superior	6.68 ± .01	8.10 ± .02
Steinhart and Meyer (1961)	North Central Wisconsin	6.28	8.01
	Keewanaw North Wisconsin	6.42	8.08
Slieter (1961)	Wisconsin-Upper Michigan	6.21	8.17
Mereu (1968)	Early Rise Superior-Churchill line	6.23 ± .20	8.12 ± .02
O'Brien (1968)	Lake Superior	6.75	8.16

One of the major assumptions made is that seismic boundaries become much more regular with depth, hence all structure indicated by travel-time variations is due to topography on the Moho. This assumption is reasonable if one accepts the hypothesis that Moho topography is related to fine scale geological processes occurring on the surface of the earth.

3.2 Comparisons With Other Early Rise Models

The velocity model produced by first-arrival analyses of the Early Rise data for the various radial recording lines showed many similarities [see Barr (1967), Green and Hales (1968), Lewis and Meyer (1968), Mereu and Hunter (1969), and Iyer et al. (1969)]. Each analysis observed upper mantle velocities of about 8.10 - 8.20 directly beneath the Moho. A higher velocity of 8.35 - 8.45 km/sec was observed at depths between 80 and 130 km. No evidence for low velocity layering for P waves in the upper mantle could be found for profiles in eastern North America in contrast to the results obtained in the Western United States [Lehmann (1964)]. Lewis and Meyer (1968) have detected from the Early Rise western seismic profile a low velocity layer for shear waves in the upper mantle. However, the layer is not well enough defined to be detected as a P wave velocity decrease.

Green and Hales (1968), Lewis and Meyer (1968), Barr (1967) and Mereu and Hunter (1969) have interpreted the velocity increase from the P_n velocity to the 8.4 km/sec velocity to be rapid enough to be considered a velocity discontinuity, giving rise to reflected events.

Iyer et al. (1969) considered all first arrival events from all stations and have produced a velocity depth function for North America. They favour, as an average model, a slowly increasing velocity in the upper mantle from P_n to P velocities.

From the published results of first arrival analyses a regional velocity model for North America can be developed. A well-formed low velocity layer in the upper mantle at a depth of 80-100 km in western North America is seen to decrease in thickness easterly until it is undetectable in central portions of the continent. A well-defined horizon corresponding to a velocity discontinuity between 8.2 and 8.4 km/sec (denoted here as the 'Hales' discontinuity) is present throughout most of North America. Further substantiation of this horizon awaits the identification of converted reflections and refractions formed by it.

CHAPTER IV

Amplitude Studies of First Arrivals

4.1 Results of Past Surveys

Amplitude measurements from earthquake seismograms have been used in past surveys in an attempt to refine earth models. One of the great weaknesses of the technique was the large error involved in estimating the source strength. With the advent of controlled explosive sources for crustal studies, this uncertainty has been removed, to be replaced by uncertainties from poor signal to noise ratios.

Romney (1959) was one of the first to report amplitude results from nuclear blasts for a series of recording stations from Nevada to Maine. He found that the first arrival amplitude (P_n measured as the maximum of the first few cycles) varied inversely as the cube of the distance in the region of 200 to 1100 km shot distance. Beyond this point the P_n wave amplitude became very small and a P event of slightly lower frequency became dominant, having a maximum amplitude at 2000 km distance. A travel-time break-over point for first arrivals correlating with the amplitude results, was interpreted to be at 1500 km distance.

Pakiser and Hill (1963) measured first break amplitudes of nuclear blast seismograms recorded in the western states from Nevada to Idaho. Their measurements confirmed that P_n amplitudes vary inversely as the cube of the distance out to 500 km.

Healy's (1963) results for first break peak-to-peak measurements for a survey along the California coast gave values of the decay rates of between $r^{-3.84}$ and $r^{-2.68}$ for P_n. The two sets of data obtained showed large scatter.

Ryall and Stuart (1963) give amplitude results from nuclear blasts recorded on a line between Nevada and Colorado. They suggest that P_n amplitudes fall off with distance according to the head wave theory of Heelan (1953), with an attenuation given by Q = 520. They found the amplitude of P_g (the direct wave) falls off rapidly with distance and is replaced by $\overline{P}$ (the Moho reflection) as a later event at greater distance. Amplitude measurements of $\overline{P}$ suggested a Q of 200 for the crust.

Eaton (1963), Roller and Healy (1963), Hill and Pakiser (1966) and Roller (1965) have utilized amplitude measurements to interpret events on seismograms in the western United States. They have shown that the low decay rate is characteristic of crustal P_g and Moho reflected waves in that region.

A comparison between measured and computed amplitudes for head and reflected waves at near distances is given by Berry and West (1966). The good agreement in decay rates between theoretical results and Roller's (1965) observed results suggest that simple crustal models may be adequate to explain amplitude measurements.

Amplitude measurements of first arrivals from the 1964 Lake Superior experiment have been reported by Mansfield and Evernden (1966) and Roller and Jackson (1966). At distances between 200 and 1300 km

they found that the amplitudes of first arrivals did not fit a simple inverse cube law but rather an r^{-1} variation. An amplitude discontinuity could be interpreted in the region of 1000-1300 km distance which correlated well with a change in slope in the travel-time distance plot.

The first arrival amplitude measurements from Project Early Rise for the southern radial profiles are given by Green and Hales (1968)(see fig. 4-1). The total data fit an r^{-1} decay law, whereas amplitudes at recording distances greater than 800 km obeyed an r^{-2} decay law.

Lewis and Meyer (1968) have measured amplitudes along the Early Rise western profile. Their measurements are based on the amplitude spectra of arrivals, using a 10 second sampling window. Reasonable correlation (see fig. 4-2) was obtained between measurements and theoretical amplitudes of reflections based on the travel-time model. Their work strongly supports the argument that reflections following closely after the first event may be responsible for large errors in first arrival measurements. For a further example of later arrival interference in amplitude measurements, the reader is referred to Vanek's (1968) work on body waves in southeast Europe and Asia Minor.

A compilation of measured amplitudes of compressional waves for North America from earthquakes and large explosions is given by Kaila (1970). Fig. 4-3 is a plot of average attenuation with distance after Kaila. It is interesting to note that the two segments of the amplitude curves, corresponding to the two given average upper mantle ray velocities overlap in the region of 500-800 km. Depending upon layer thicknesses either ray (7.9 km/sec or 8.5 km/sec) may become the first arrival in this region.

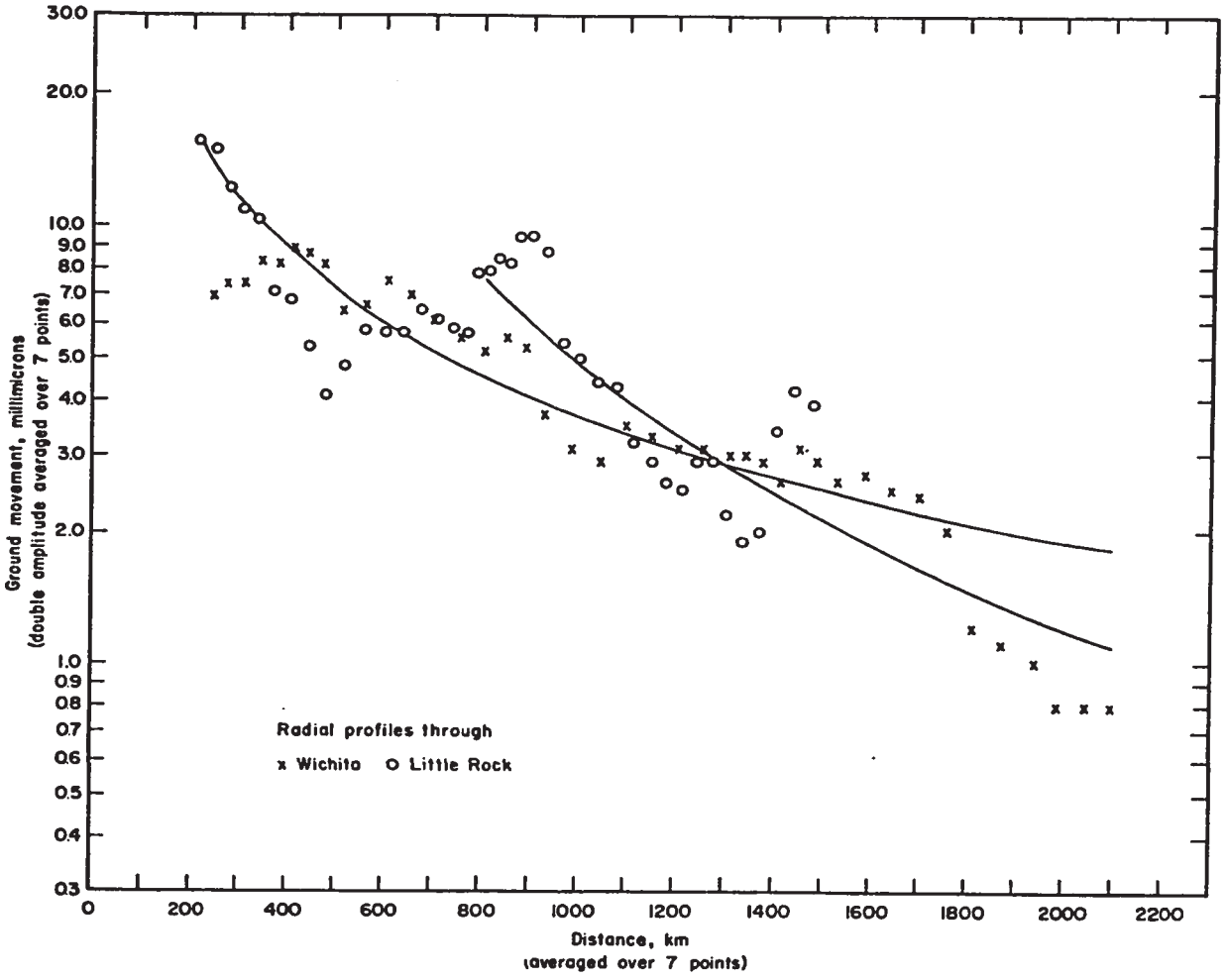

Fig. 4-1 Amplitudes of first arrival ground movement from Early Rise southern profiles from Green and Hales (1968).

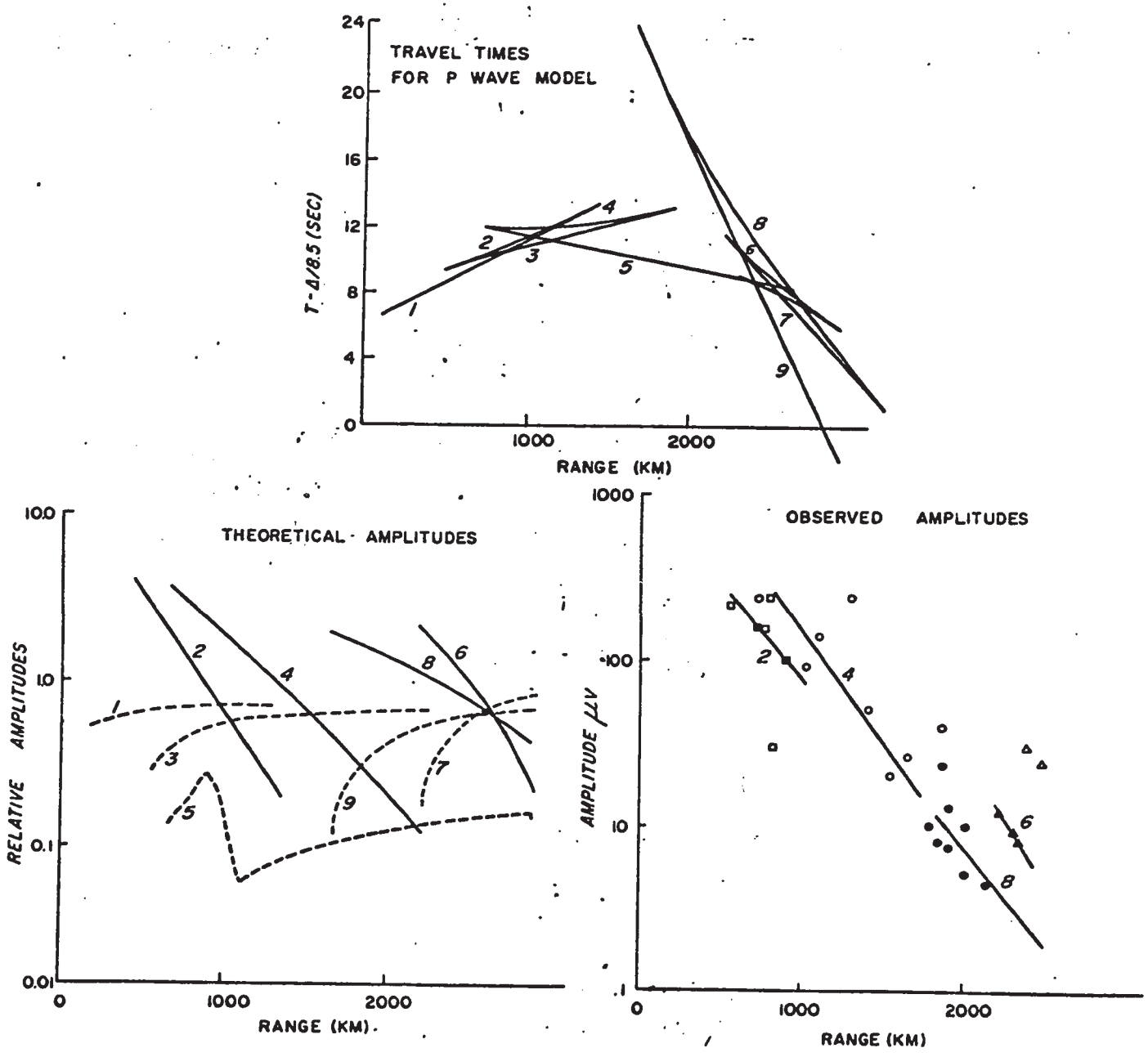

Fig. 4-2 Amplitudes of first arrivals for the Early Rise western profile from Lewis and Meyer (1968).

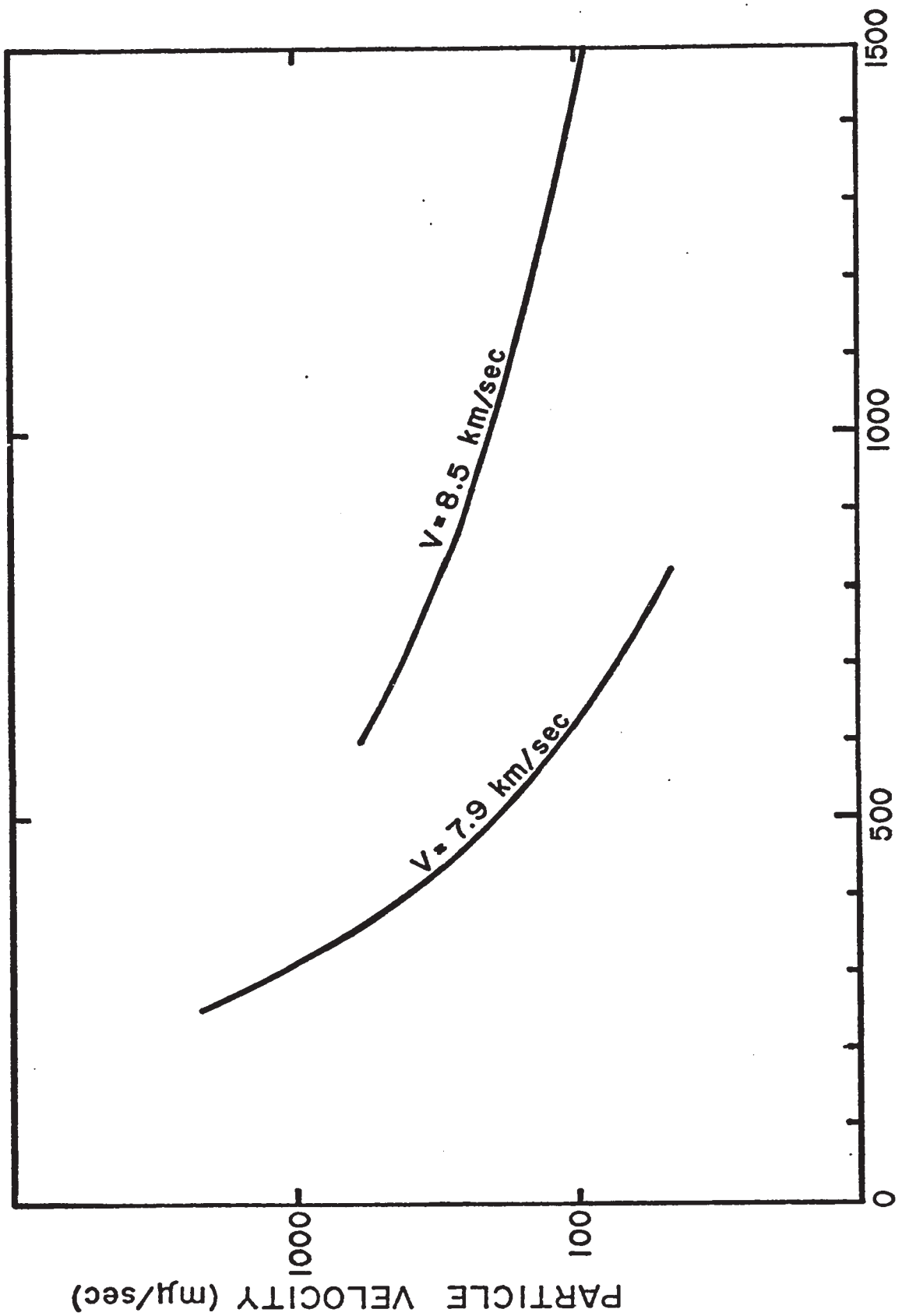

Fig. 4-3 Curve of first arrival amplitude decrease with distance from a compilation of North American earthquakes and large explosions by Kaila (1970).

4.2 Measurement of First Arrival Amplitudes

Preliminary measurements of amplitudes for the U.W.O. survey area were made by Mereu and are given by Warren et al.(1967) based on the peak amplitude of the first few cycles of motion on the analog records. To obtain a more accurate measurement of first arrival amplitudes, the traces of each of the digitized records were printed out by computer for 10 seconds of record beginning a few seconds before the onset. The digitized time trace in conjunction with the analog records and the printer plot of the traces were used to accurately orient the first arrival onset. Two measurements were made on each record, the first peak and the first peak-to-peak motion. Later cycles were not considered (although they often exhibited higher amplitudes) due to the possible interference from later events.

The amplitude measurements (in mμ/sec seismometer output) are tabulated in Appendix C and are plotted against distance in fig. 4-4 for the first break and the peak-to-peak measurements. Both plots give similar results suggesting that the first cycle of motion is largely unaffected by overlapping wavelets with a delay of 1/2 cycle or greater. The logarithm of the amplitudes falls off in a linear way with distance out to approximately 600 km. From 600 km to the end of the seismic line at 1500 km the rate of decay is much less, with several deviations from a linear fit. Amplitude peaks in this portion of the plot occur at 700, 1025, and 1400 km.

The amplitude results for the peak-to-peak measurements of first arrivals from the Nipigon-Smooth Rock Falls seismograms are shown in fig. 4-5 and are tabulated in Appendix C. Onset wave motion is weak

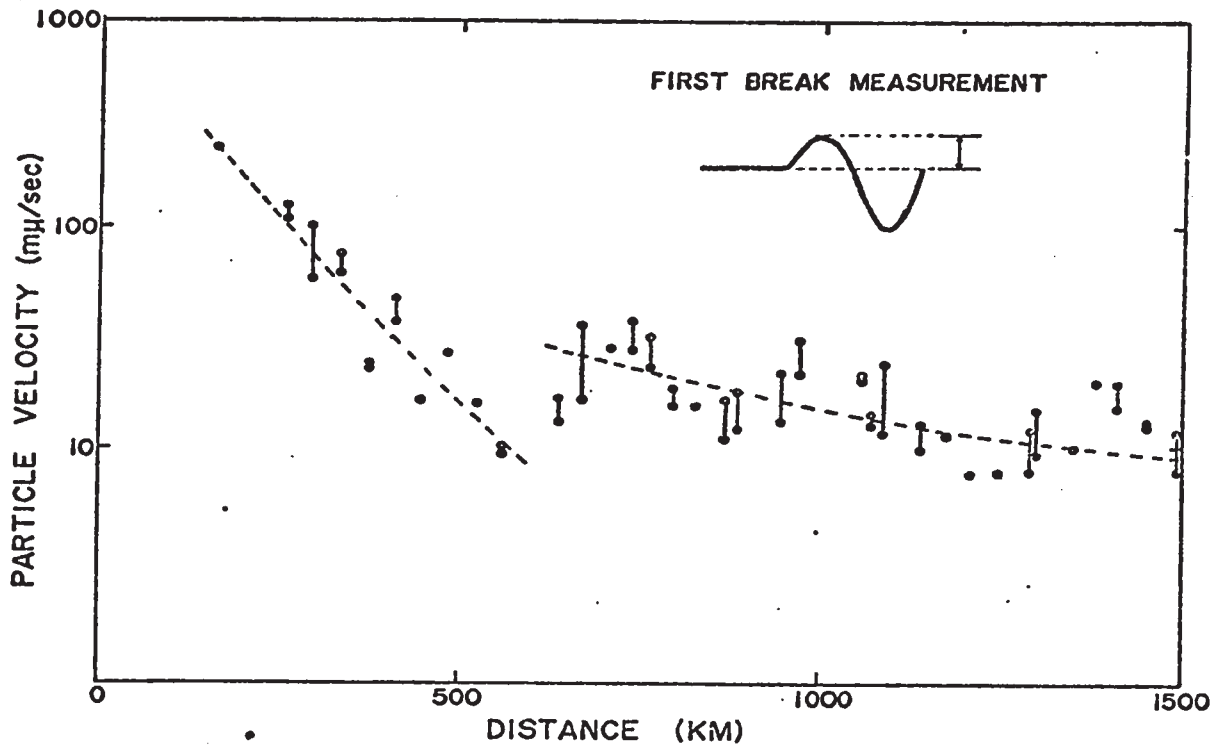

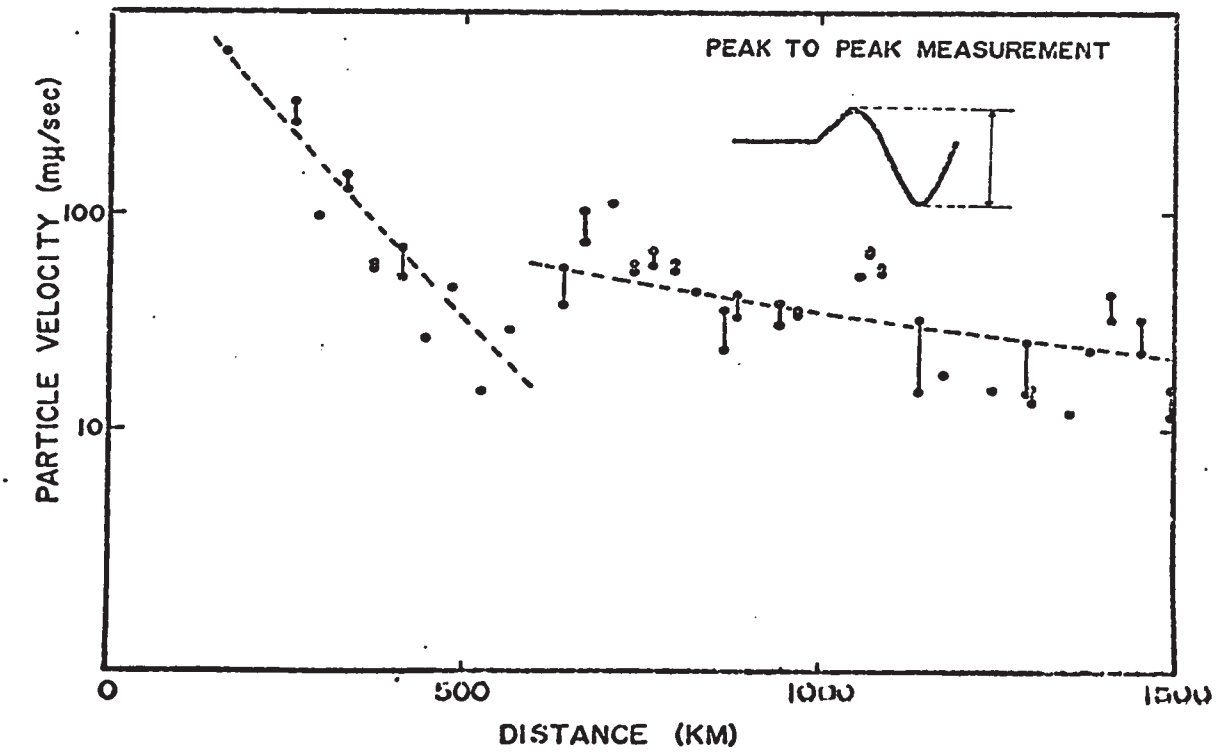

Fig. 4-4 First arrival amplitudes for the U.W.O. Early Rise line.

in many cases and measurement errors are very large. Since accurate digitized measurements were not available for these records, the measurements cannot be considered as reliable as those made for the Early Rise Line.

4.3 Discussion of Results

The amplitudes shown by the Early Rise Line clearly indicate the presence of an amplitude discontinuity in the region of 600 km. This correlates well with the sharp break indicated by the travel-time graph (see Chapter III). The amplitude plot also corresponds well with the average curves as given by Kaila (1970)(see fig. 4-3). The amplitude plot given by the composite Nipigon-Smooth Rock Falls record section, although scattered, suggests the decreasing amplitudes from 350 to 600 km.

The second order oscillatory nature of the amplitude curves beyond 600 km may be the result of two phenomena. Mereu (1969) has shown that large amplitude variations can occur as a result of topographic focussing of refracted events by curvature on a seismic interface. This suggests that amplitude maxima could occur from small depressions in any discontinuity in the crust or upper mantle at distances of 700, 1050, and 1400 km along the seismic line.

A second possible explanation for the amplitude variations is the effect of interfering wave trains from fine velocity structure immediately beneath the sub-Moho high velocity discontinuity (Vanek and Radu, 1964). Amplitude contributions from waves on portions of travel-time cusps

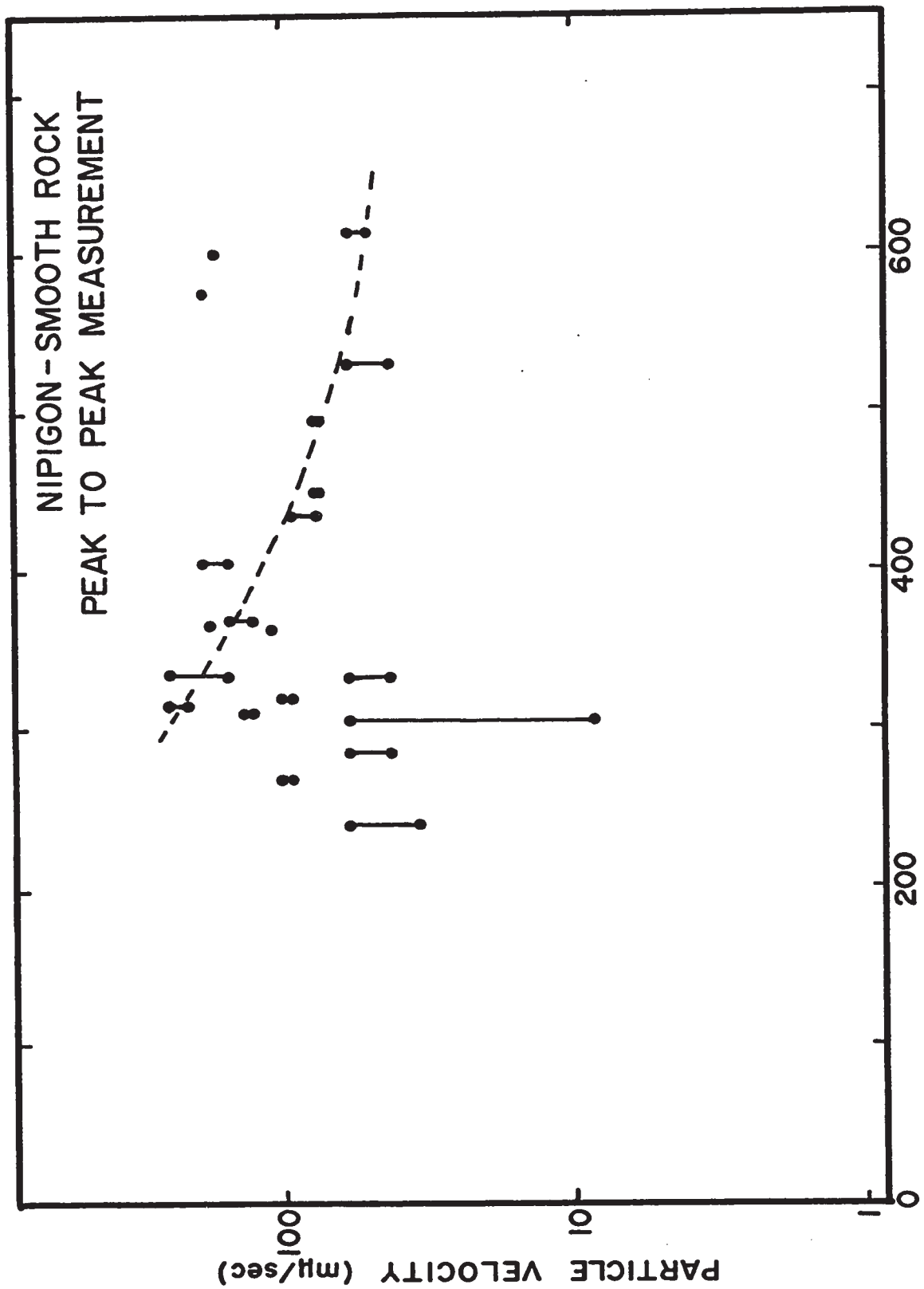

Fig. 4-5 First arrival peak-to-peak amplitudes for the U.W.O. Nipigon-Smooth Rock Falls records.

arriving within about 0.25 seconds of the first arrival with a dominant period of 0.5 sec may cause appreciable destructive interference. Following this argument, destructive interference would affect measurements made in the vicinity of the travel-time cusps, for both the first break and peak-to-peak measurements. From the amplitude plot these would occur at approximately 600, 850, and 1200 km.

From first arrival amplitude measurements alone however, it is not possible to determine which of the two phenomena given above is responsible for the small-scale amplitude variations.

CHAPTER V

ATTENUATION IN THE CRUST AND UPPER MANTLE

5.1 Introduction

The departure of the crust and upper mantle from perfect elasticity can be expressed seismically by attenuation of body and surface waves, following the law $e^{-\alpha t}$ where α is the attenuation coefficient governing energy losses to the transmitting medium and t is the travel-time of the wave. The result of a model with energy losses of this type is to change the shape of the pulse with distance by preferential attenuation of high frequencies.

The attenuation factor has been found to be approximately proportional to frequency (Knopoff, 1969) giving the form:

$$\alpha = w/2Q \qquad \ldots\ldots (1)$$

where, w = circular frequency = $2\pi f$

Q = the specific attenuation factor (a dimensionless quantity).

5.2 Previous Work

Most work on the measurement of Q has been performed by examining shear and surface waves (Knopoff, 1969). The advantages of these methods lie in the high amplitudes observed and, in the case of surface waves, the variability of penetration. Short period waves effectively sample a small portion of the transmitting medium, whereas, very low frequency surface waves give average Q values for greater depths (down to the lower mantle). Even free oscillations of the earth may be used (Alsop et al., 1961) to obtain average values of Q over most of the earth.

Lommitz (1962) gives a summary of measured values of Q to that date, as given in fig. 5-1, and has fitted a logarithmic function to the variation of Q with frequency. The data, although somewhat scattered, suggest that Q measured by surface waves in the range of 10^{-1} to 10^{-2} hertz differs somewhat from that measured by body waves in the range 10^{-1} to 5 hertz.

Anderson and Archambeau (1964), working with surface waves and free oscillations, give a model of the earth with a Q of 80 for S waves in the upper mantle, a Q of 2000 in the lower mantle, and the transition region between the two zones at approximately 400 km depth. They suggest that Q may be frequency-independent in the range of 10^{-1} to 10^{-3} hertz.

Knopoff (1964) in a review paper on Q has summarized laboratory and field results, to that date, as well as current hypotheses for loss mechanisms. He concludes that Q in shear is 110 for the upper mantle and that Q of compression should be somewhat less.

Short period body wave measurements of Q have been made in situ by DeBraemaker et al. (1966) on lava outcrops giving Q's in the range of 4 to 472.

Press (1964), using P_g measurements, gives values of Q for the crust in the range of 180 to 410.

Sutton et al. (1967) have made a study of Q of the crust of the United States by studying P_g and L_g phases. By studying the energy ratio of frequency bands, values of Q ranging between 200 and 1000 have been obtained. They correlate regional changes of Q with large scale tectonic and structural changes in the crust. For the Lake Superior region crustal Q values in the range 210-250 were obtained.

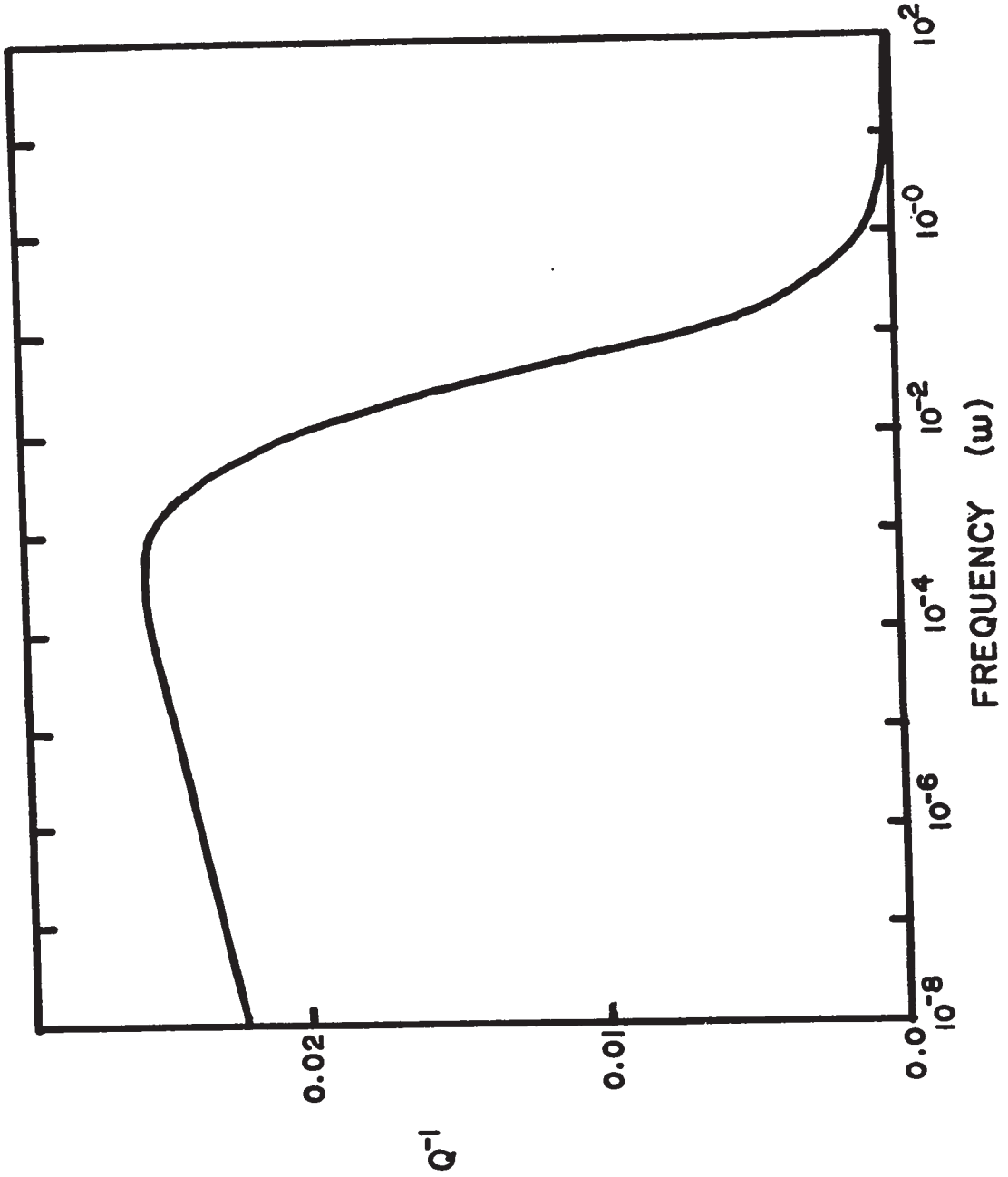

Fig. 5-1 Attenuation vs. frequency relationship for the earth after Lommitz (1962).

Dorman (1968) has investigated the effective Q for body waves in the Lake Superior region using data from the 1963 Lake Superior experiment. His technique, analogous to that used in crustal time-term studies, does not use absolute amplitudes and does not involve focusing or geometrical spreading effects. The average effective Q he obtains is 475 over a range of shot-station distances up to 2700 km. The paths of these body waves are assumed to penetrate to a depth of 125 km, hence the value of effective Q given is that of the upper mantle. Dorman compares this result with that given by Anderson (1967) (approx. Q = 300, from mainly oceanic work) and suggests that the Q of the upper mantle under continents may be much higher than that under oceans.

Long and Berg (1969) have used spectral measurements of first arrivals from nuclear events to determine the effective Q in the upper mantle of Nevada and New Mexico. They obtained values of Q in the range 116-169 with a geometrical spreading factor of $r^{-0.5}$, suggesting direct wave propagation. All measurements were made from spectra of first arrivals with time-windows of approximately 0.5 seconds duration and over a frequency range of 2 to 6 hertz.

Howell (1966) has studied the spectra from first arrivals of events from the Lake Superior 1963 Experiment out to a distance of 250 km. He finds that the spectra can be divided into two ranges, the near range giving a negative absorption coefficient suggesting a large scatter of the data, and the far range from 158-252 km, having a near zero absorption coefficient. The absorption coefficients for both ranges are dependent upon frequency. He suggests that large errors may be introduced by noise in the spectra. As well, he suggests that by measuring the first 0.5 seconds of record, more than one arrival is recorded.

Willis and DeNoyer (1966), using data from the Lake Superior 1963 Experiment, as well as later experiments, have analysed the first arrival spectra for short distances out to 440 km. For the near range out to 160 km, they obtain a value of effective Q of 630-10000 and for longer profiles the effective Q becomes 1570. The spectral measurements were obtained from the first four cycles of the first arrival after the onset, for frequencies between 1 and 20 hertz. They suggest that the spectra are affected strongly by multiple reflection conditions under the shot positions.

5.3 Theory

The form of equation (1) for the attenuation factor α comes from the assumption that any harmonic component of a body wave may be written as (Anderson, 1967):

$$A(w) = (A_o\ (w)\ /r^N)e^{-k_o x}\ e^{i(wt-kx)} \qquad \ldots\ldots\ (2)$$

where,

$A(w)$ = the amplitude of the frequency component

$A_o(w)$ = source amplitude of the frequency component

r^{-N} = a geometrical spreading factor depending on the mode of transmission of the wave.

t = travel time of the wave

and k_o and k are the imaginary and real parts of the complex wave number respectively.

The relation between the specific attenuation factor Q and k_o for compressional body waves is taken to be (Anderson, 1967):

$$k_o = \pi/QCT \qquad \ldots\ldots\ (3)$$

where,

C = velocity of the compressional wave

T = period of the wave

The portion of equation (2) governing the amplitude of the wave may then be considered as:

$$A(w) = (A_o(w)/r^N) \exp(-wt/2Q) \quad \ldots\ldots (4)$$

The ratio of two frequency components of a compressional arrival recorded at the same station is:

$$R_{1,2} = A(w_1)/A(w_2) = (A_o(w_1)/A_o(w_2)) \exp(t(w_2-w_1)/2Q) \quad \ldots\ldots (5)$$

Equation (5) gives a form of the attenuation characteristics with distance which is independent of the measurement of absolute amplitude and the geometrical spreading factor. In terms of a linear equation in Q^{-1}, equation (5) may be expressed as:

$$\ln(R_{1,2}) = \ln(A_o(w_1)/A_o(w_2)) + t(w_2-w_1)/2Q \quad \ldots\ldots (6)$$

Equation (6) is, then, a linear expression whose slope is a function of Q and whose intercept defines the ratio of the amplitude components at the source. Under the assumption that the source spectral component ratios are unchanged for the survey, a least-squares value of Q may be obtained for all stations on the Early Rise Line without the added problem of possible changing absolute amplitudes and geometrical factors along the line.

The least-squares Q given above is, in reality, an effective Q, or the average specific attenuation factor along the length of the travel-path of the wave. The effective Q is given by Long and Berg (1969) to be:

$$Q = t/\int_c \frac{ds}{Q_s} \quad \ldots\ldots (7)$$

integrated along the path s from shot to receiver,

where,

Q_s = the specific attenuation factor at a point s along the line,

c = non-dispersive phase velocity.

Thus an effective Q for the upper mantle may be composed of a crustal Q and an upper mantle Q. Considering first arrivals from a model of a horizontal crustal layer of specific attenuation Q_c overlying a mantle of specific attenuation Q_n, the effective Q may be expressed as:

$$t/Q = (t-2t_g)/Q_n + 2\ t_g/Q_c \quad \ldots\ldots (8)$$

for arrivals from the upper mantle refractor,

where,

t = total travel time

$2t_g$ = total travel time in crust

$t-2t_g$ = travel time in upper mantle

Combining equations (6) and (8) in terms of Q_n one obtains:

$$\ln(R_{1,2}) = \ln(A_o(w_1)/A_o(w_2)) + t_g(w_2-w_1)(1/Q_c-1/Q_n) + t(w_2-w_1)/2Qn \quad \ldots (9)$$

The first two terms of the above expression form the intercept of a straight line whose slope is a function of Q_n. Equation (9) shows that a least-square determination of effective Q assuming a single horizontal crustal layer overlying the mantle, will give the average Q_n of the upper mantle for all first arrivals from the Moho refractor. The crustal travel time t_g is related to the layer thickness (h) and velocities by:

$$t_g = h\ P_n/(P_g \sqrt{P_n^2 - P_g^2}) \quad \ldots\ldots (10)$$

where P_n = upper mantle velocity.

Equation (9) may be extended to encompass refractions from several layers each of which will give a line whose slope is a function of the Q of the layer.

DeBremaecker (1968) cautions that the least-squares best fitting line of an equation of the type of (9) is not the best-fitting least-squares line in the non-linear version of the relation as given in equation (6). In other words, a least-squares analysis of (9) is weighted in favour of points of low t. Such a weighted analysis has merit however, in that the data from large t often contain a higher noise contribution for both components of the ratio, and, since the ratio R is much higher at large t, large error may result from the lower of the two amplitude components being immersed in noise.

5.4 The Data

Spectral analyses over a three second window from the onset of the first arrival, were performed for the vertical components of all digitized records. A detailed description of the spectral analysis and the tape-search program is given in Appendix D. Such a wide time-window was felt to be necessary to insure adequate detail (0.333 hertz resolution) in the regions of spectral peaks. This was done, however, at the expense of isolating the first arrival since possible later arrivals following closely after the first arrival may have been included. It is felt that the inclusion of later events in the sample interval would not seriously alter the observations since such events arriving within three seconds of the first arrival should travel similar paths and show similar attenuation properties. This assumption may be invalid in the regions of the break-over points on the time-distance plots of first

arrivals, where the time-window may sample refractions from two media having different attenuation characteristics.

The plots of all spectra of the recordings used in the analysis are given in the Appendix D. The majority of the spectra show a large spectral peak with steep slopes in the vicinity of 2 hertz. Some spectra show a smaller peak in the vicinity of 4-7 hertz as well.

The assumption has been made that source characteristics were unchanged for all recordings. This assumption has some justification, as shown in Appendix D , since measurements of peak amplitudes of different shots recorded at the same station show little change in character or peak amplitudes. From inspection of the amplitude spectra it was felt that measurements made in the vicinity of the prominent two hertz spectral peak would give representative attenuation observations which would be least affected by frequency-dependent scattering under the station and uncompensated time-window effects. Absolute amplitude component comparisons between two shots recorded at the same station often showed some variation. As well as the seismic noise contribution, this effect could have been caused by small amplitude spikes introduced by instrumental recording equipment, although attempts were made to maintain records noise free in the region of the first arrival. Any noise contribution to the spectral components, whether regular or irregular with frequency, tends to cause variations when comparing absolute amplitudes and may cause large variations in the amplitude ratios of components from shot to shot at the same station. The noise contribution then may be considered a major cause of the scatter of data.

A major cause of variation of absolute amplitudes from station to station can be attributed to conditions in the crust under the stations.

Although the effect of low velocity layering immediately under the stations can be ruled out because of the choice of sites (see introductory chapter), large scale scattering and focusing effects should not. The topography of the Mohorovicic discontinuity beneath each station may cause focusing (gain-changing) effects (Mereu, 1969). When topography on the Moho and crustal layering are of the same dimension as the seismic wavelengths, scattering effects are frequency dependent (Asano, 1966). This effect could cause variations in amplitude ratios at the stations leading to scatter of the data.

5.5 Experimental Technique and Results

The frequency components selected for this analysis lay in the region of the spectral peak at about 2 hertz. Amplitude ratios at 1:2, 1.33:2, 1.33:2.67, 2:2.67, 2:3 hertz were computed for all stations. The natural logarithms of these ratios vs. travel-time are shown in fig. 5-2. Least-squares analyses of these ratios following the linear equation given by (9) were performed. Removal of data with low probabilities of occurrence in the set was done using Chauvenet's rejection criterion as given by Worthing and Geffner (1943) (see Appendix D). The least squares slopes computed and the effective Q's are given in Table V-I.

The negative slopes associated with ratios at the low frequency end of the spectral peak suggest that errors contributed by all forms of noise mask the attenuation effect. The larger attenuation effect of higher frequencies is demonstrated by the somewhat smaller scatter of data and the acceptable (although large) Q values given by the 2.00:2.67 and the 2.00:3.00 hertz amplitude ratio results.

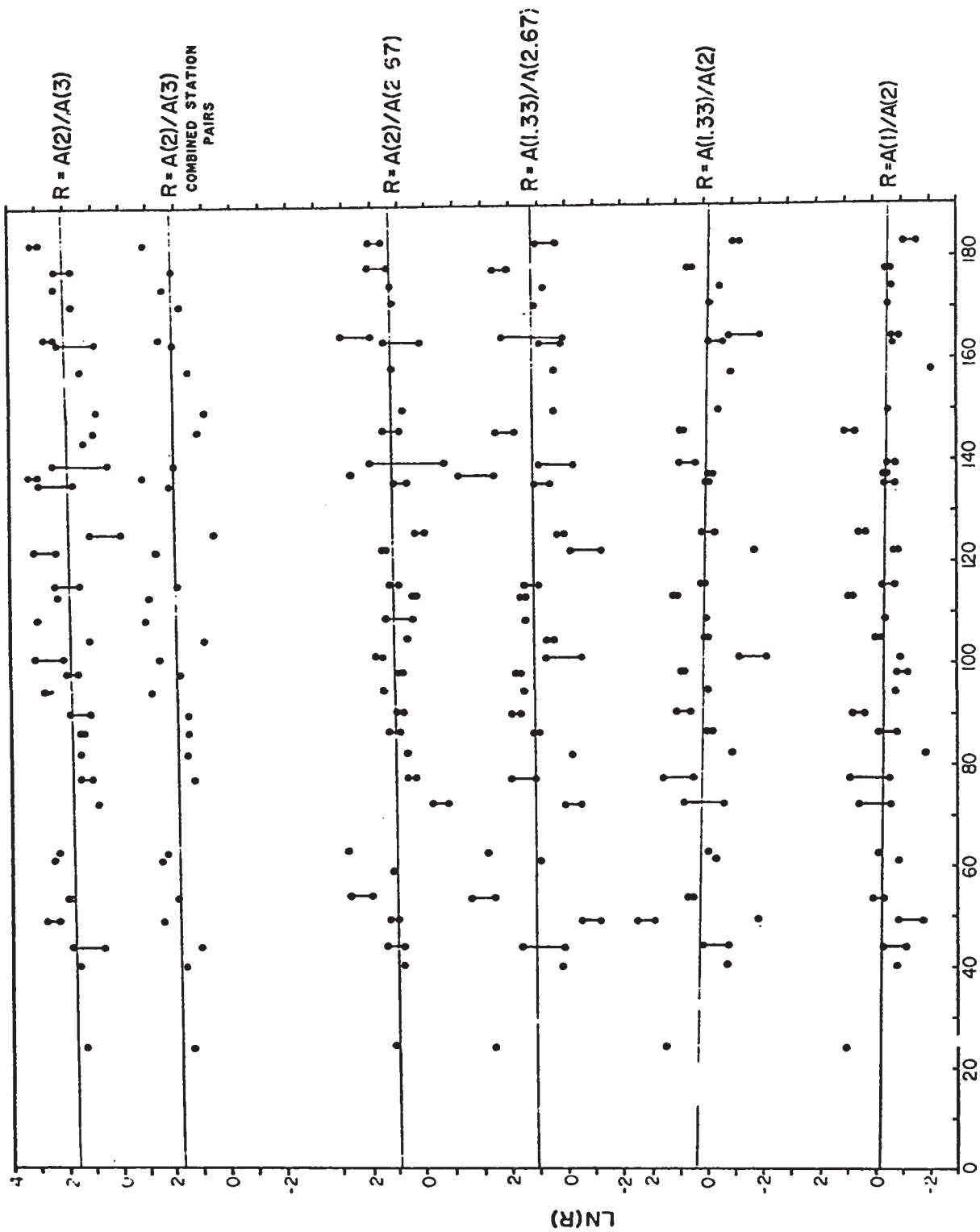

Fig. 5-2 Natural logarithms of amplitude ratios vs. first arrival travel time for selected pairs of spectral components.

An inspection of the plots of ln R vs. T for the 2.00:2.67 2.00:3.00 and 2.00:3.00 station pair ratios indicated that Q may not be constant over the length of the Early Rise line and that the large scatter of data may result from contributions from portions of the plots having three different values of Q. Accordingly, the ln R vs. t plots were divided into three sections, from travel-times 0-65 sec, 65-140 sec. and 140-183 seconds. Least-squares analyses of each of the three sections for each set of amplitude ratio were again carried out following equation (9). Chauvenet's rejection criterion was again employed to reject data points with a low probability of belonging to the set. The results of these analyses are plotted in figs. 5-3, 5-4, and 5-5 and are summarized in Table 5-III.

The division of the data into three groups with respect to travel time results in a large change in the slopes of the line Q^{-1}. The standard errors of the slopes of the line segments however are large as well. The arithmetic mean values of Q for the three sets of amplitude ratios are given in Table along with the standard error limits set by the mean standard error of each set.

Since the limits set by the standard error overlap between data sets, the Q's computed for each cannot be considered to differ statistically. At best, the mean Q's computed for each set can be considered as suggesting a trend in the measurement of Q from first arrivals coming from media of low, high, and low Q's respectively along the seismic line.

TABLE V-I

LEAST-SQUARES RESULTS FOR ALL DATA

FREQUENCY RATIO	NO. OF OBSERVATIONS	SLOPE Q^{-1} ($\times 10^{-3}$)	STANDARD ERROR OF SLOPE ($\times 10^{-3}$)	Q
1.0:2.0	53	-0.79	0.75	------
1.33:2.00	53	-1.89	1.24	------
1.33:2.67	55	0.22	0.85	4550
2.00:2.67	54	1.42	1.18	708
2.00:3.00	52	1.12	0.80	896
2.00:3.00 (combined station pairs)	33	1.00	0.88	1010

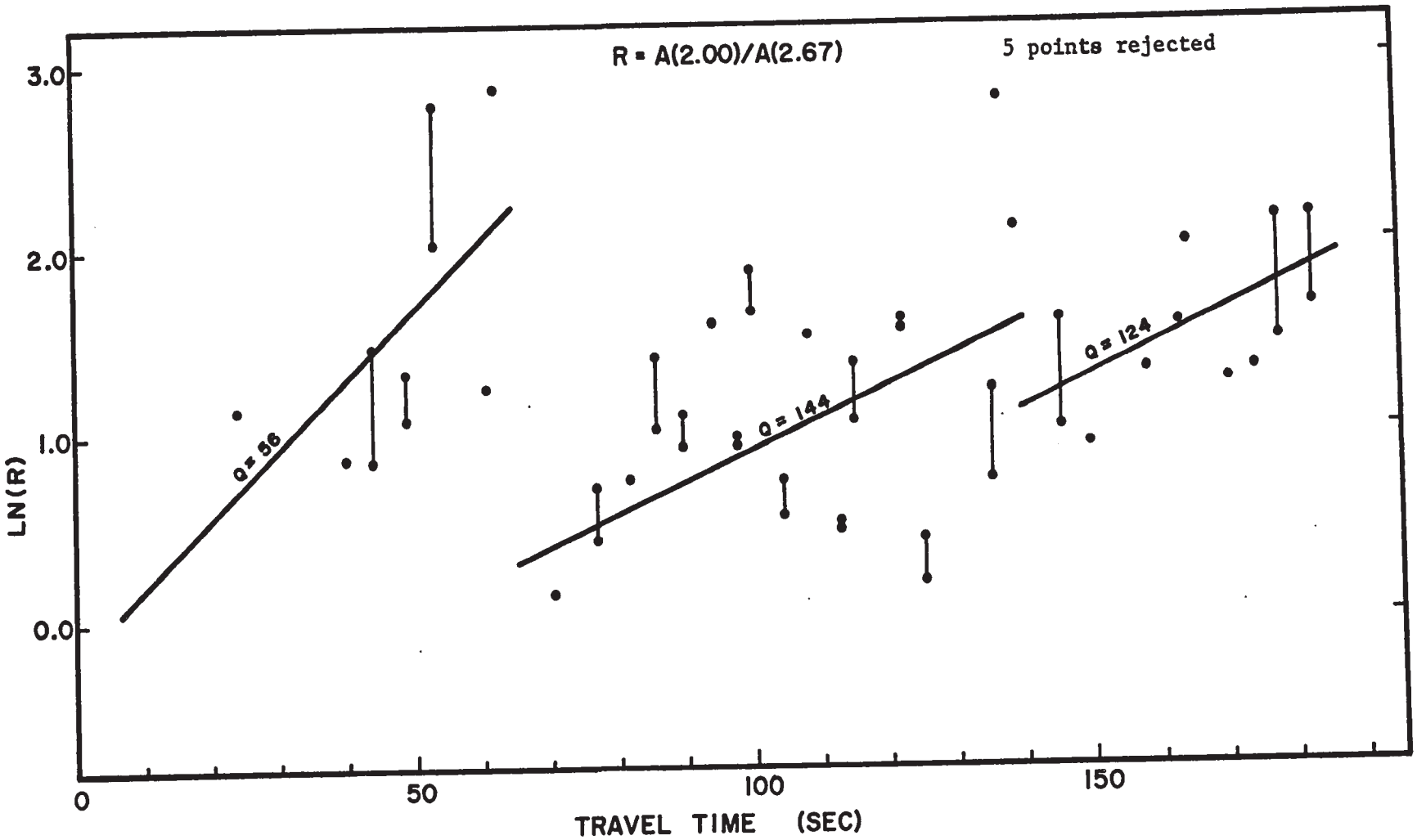

Fig. 5-3 Logarithmic amplitude ratio vs. travel time for the 2:2.67 hertz frequency ratio after the Chauvenet rejection criterion has been applied.

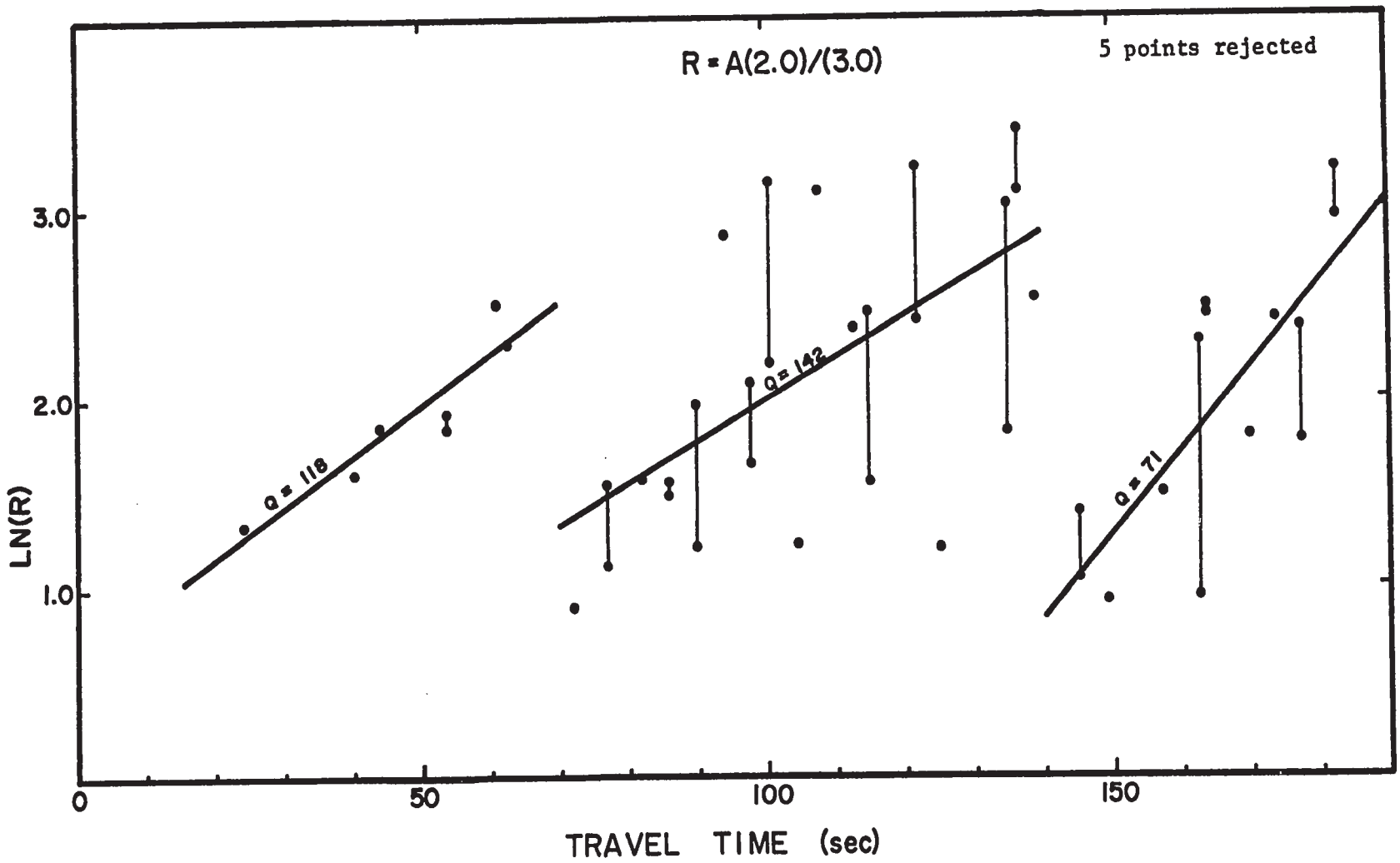

Fig. 5-4 Logarithmic amplitude ratio vs. travel time for the 2:3 hertz frequency ratio after the Chauvenet rejection criterion has been applied.

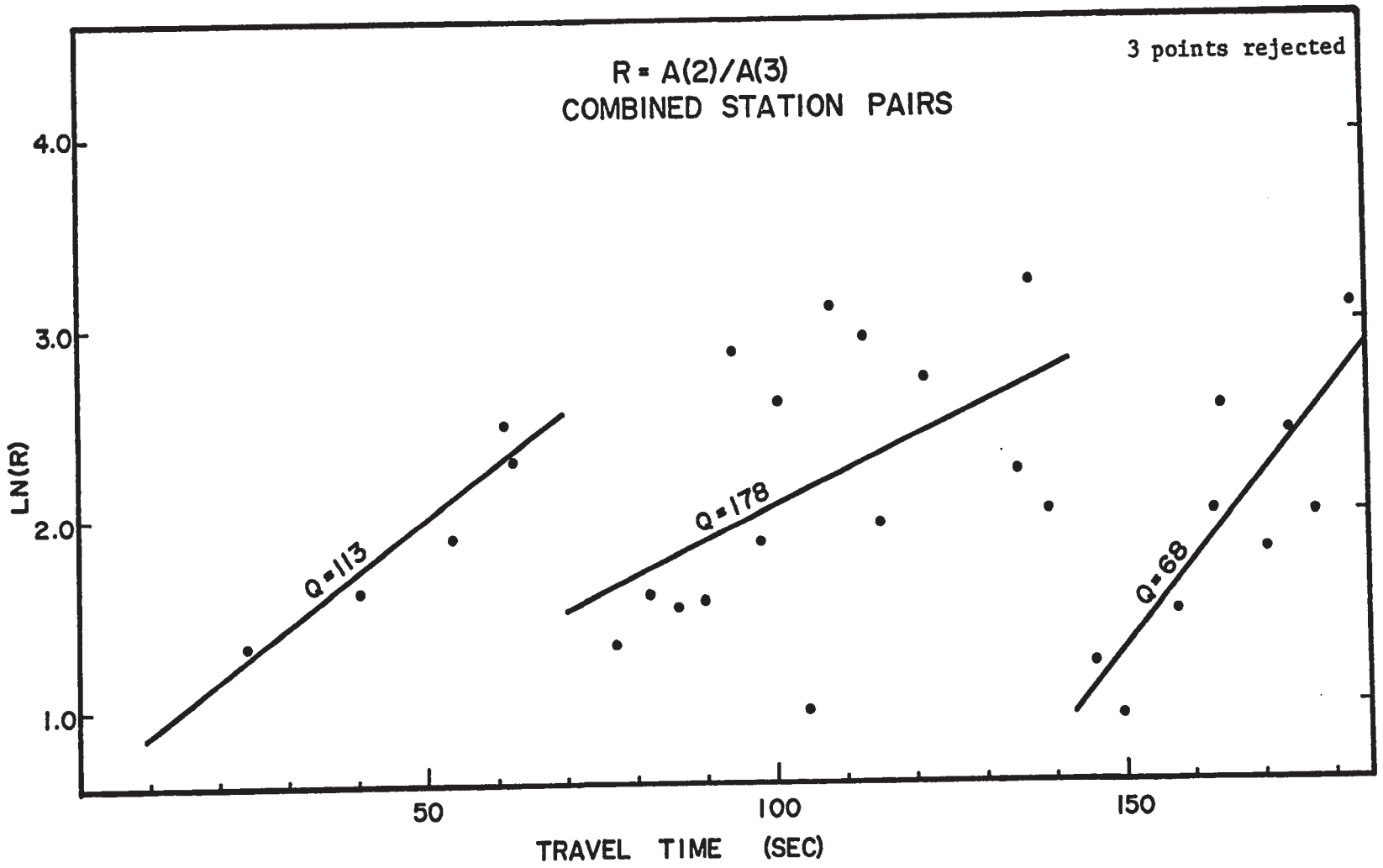

Fig. 5-5 Logarithmic amplitude ratio vs. travel time for the 2:3 hertz frequency ratio combined station pairs after the Chauvenet rejection criterion has been applied.

TABLE V-II

LEAST-SQUARES RESULTS OF AMPLITUDE RATIO SETS

AMPLITUDE RATIO	RANGE OF t	SLOPE $Q^{-1}(x10^{-3})$	STANDARD ERROR OF SLOPE $(x10^{-3})$	Q	NO.OF OBSERVATIONS
2.00:2.67	0 - 65	17.90	9.18	56	10
	65- 140	7.49	2.80	144	29
	140- 183	8.06	3.62	124	12
2.00:3.00	0- 65	8.51	1.54	118	7
	65- 140	7.07	1.89	142	26
	140- 183	14.18	3.62	71	14
2.00:3.00 (station pairs)	0- 65	8.84	1.74	113	5
	65- 140	5.92	2.71	178	15
	140- 183	14.67	3.47	68	9

TABLE V-III

MEAN VALUES OF Q

RANGE OF t (sec)	MEAN Q	STANDARD ERROR
0 - 65	96	+64
		-27
65 - 140	155	+99
		-43
140 - 183	89	+42
		-21
0 - 183	850	+3580
		-392

5.6 Discussion of Results

The values of effective Q computed for the total range of travel-time (0-183 sec) are acceptable but rather high. The effective Q's computed for the three ranges of travel-time are lower and more in line with results in adjacent areas (see section on Previous Work). The three travel-time sets imply three different attenuation conditions to produce the offsets of the three lines on the ln R vs. travel-time plots. Since all arrivals at the base of the crust beneath the stations come from upper mantle refractors travelling similar paths under the shot, they should be subjected to similar attenuation conditions. This suggests that much of the offsets of the data sets may come from a variation of attenuation conditions in the crust under the stations. Under this assumption the crust under the stations has decreasing attenuation with increasing distance along the line. Since attenuation conditions under the shot are not known, it is not possible to compute values of crustal attenuation.

A comparison of points of discontinuity between the sets of data and the first arrival time-distance plot (given in Chapter III) shows no direct correlation. The break between the first two sets of data at 65 sec travel-time may be associated with the break-over time of 85 sec between the 8.05 km/sec and the 8.44 km/sec layers on the travel-time distance plot if one recalls that the three second time sampling window of the spectral analysis may detect the presence of the lower refractor as a second arrival. This interpretation does not explain, however, the attenuation offset of the lines of the two sets of data beyond 65 sec. travel time. There is no correlation between the first discontinuity and any structural delineation in the Superior structural province. There is a good correlation between the second

discontinuity (145 sec travel time or 1100 km shot distance) and the Superior-Churchill structural boundary. This suggests that the crustal rock of the Churchill province may have lower attenuation than that of the Superior province.

The first two data sets suggest that the effective Q increases with depth (i.e. with increasing travel-time). The third data set suggests that arrivals which sample deeper into the mantle (approximately 90 km depth) are attenuated slightly more, perhaps indicating the onset of arrivals from a medium of higher attenuation (the low velocity layer?). To reiterate, however, the standard error limits associated with the effective Q determinations of the sets overlap indicating that the effective Q's computed for each data set may not differ.

CHAPTER VI

EMERGENT ANGLE PARTICLE-MOTION STUDIES

6.1 Introduction

The apparent angle of emergence of the first arrival compressional refraction from the upper mantle, as given by the ratio of vertical to horizontal components of ground velocity, can be used as an indicator of velocity variation within the upper portion of the crust under conditions where low velocity near-surface layering is absent.

6.2 Results of Previous Workers

One of the earlier attempts to use particle-motions of the first compressional waves is described by Nuttli and Whitmore (1961). Using P arrivals from earthquakes having periods between 3 and 7 seconds, they found that the velocity of P waves is 8 km/sec at the surface, suggesting that waves of these periods did not detect a low-velocity crust. The scatter of their data ranges between 7 and 9 km/sec; as well, they suggest that their results may contain fluctuating magnification errors.

Papazachos (1964), however, has shown, that the crust can be detected by compressional arrivals with periods of 7 to 15 seconds. By studying particle motions of P and PP for 29 earthquakes, he gives an average velocity of 6.4 km/sec for the crust in the central U.S. under the assumption that $\sigma = 0.25$. Unlike previous work, Papazachos chose to work with longer periods where the instrumental magnification errors were small. He concludes that the crust may be considered a refractor of compressional waves of long period (7-15 sec).

Mereu (1965), using 3-component records from explosions from the 1963 Lake Superior crustal experiment, found that it was possible to distinguish first arrivals from different refractors. By digitizing

the first second of the first arrival for each record he was able to apply statistical techniques to obtain a best straight-line fit to the data, hence the best apparent angle of emergence. The refractor velocities gave average values of 6.6 and 8.2 km/sec indicating first arrivals from the lower crustal layer and the Mohorovicic discontinuity. The difference between the observed angles of emergence for the two refractors was approximately 12°.

The utility of the particle motion display technique in the detection of converted refraction events on seismograms has been demonstrated by Hall and Brisbin (1965). They show that compressional and shear events may be separated by the apparent angle of emergence as given by the major axis of the particle motion ellipse in the V-H plane. Due to amplitude and phase shift differences between vertical and horizontal detectors, they do not give quantitative results, but rather, use the technique as a qualitative indicator.

Ellis and Basham (1968), and Basham and Ellis (1969) have used particle motion studies to examine crustal structure in Alberta from first arrivals of several earthquakes. They found anomalous shear motion occurring within one second of the compressional wave onset giving rise to elliptical and otherwise distorted particle motion of the first arrival. They suggest that interfering converted SV waves are being generated at the base of the sedimentary layering under the stations. As well, they suggest that the rough unconformable sediment-basement contact may produce scattered SH waves which give rise to non-rectilinear first motions. Thus, the presence of near-surface non-plane boundaries may severely restrict the use of particle motion studies.

6.3 Theory

The angle of emergence of a P wave refracted at depth in the earth is a function of the velocity contrast and angle of incidence at the refractor interface. When considering small shot-station distances (such as in this experiment) the differences between grazing and non-grazing angles of incidence at upper mantle discontinuities are small; hence a horizontally layered earth model can be assumed and the angle of emergence with respect to the horizontal is:

$$\cos e = v_0/v_1 \qquad 6\text{-}1$$

where v_0 = velocity in upper layer

v_1 = refractor velocity

For a refracted P wave the observed motion recorded at the surface is a result of the addition of three waves, the incident P, the reflected P, and the reflected SV waves. The angle of emergence is related to the apparent angle of emergence by the Weichert relation (Ewing et. al., 1957), and, under the assumption that Poisson's ratio = 0.25, is given by:

$$2\cos^2 e = 3(1-\sin \bar{e}) \qquad 6\text{-}2$$

where $\bar{e}$ = the apparent angle of emergence.

Thus the velocity of the upper layer of the earth model may be determined by measuring the apparent angle of emergence under the assumption that P_n is known.

6.4 Analytical Technique

To examine the particle motions of the first arrivals for the Early Rise Line, a computer program (see Appendix E), utilizing the UWO Calcomp plotter system, was written to produce vertical versus horizontal plots for the first

few seconds of record after the onset of the first arrival. The records were sharply filtered with a 5 cps digital low-pass filter prior to plotting; also, the program performed zero-trace adjustment, and gain equalization between vertical and horizontal traces (see Appendix E). Based on ease of computer manipulation of data, the sampling window per plot was chosen to be 0.8 seconds, thus assuring that at least one cycle of motion is present per plot for most records. The P-M plots begin at a point several seconds before the onset of the first arrival and are plotted from 0.8 second intervals after that point.

A further description of the program and a compilation of the P-M plots for all records amenable to this technique is shown in Appendix E. Most records show particle motion being elliptical in nature. Some records show a degree of signal-generated noise both in the presence of background noise and with little background noise, suggesting the production of near surface SH and other converted waves tending to reduce the linearity of the particle motion.

A close examination of the first cycle of particle motion shows in general, a large variation of amplitude from one peak to the next. Thus any sample of any arbitrary time length within the first cycle when analysed statistically for the best-fitting line (some form of least squares fit), would be extremely susceptible to a sample window bias. The only way to overcome such a bias would be to perform the statistical fit on the isolated arrival pulse over a time interval set to include all of the pulse. The angle of the best-fitting line of the particle motion of such a pulse would then approximate the apparent angle of emergence. Such an isolated first arrival pulse is seldom met.

The most important points in the particle motion plot thus become the positions of the maximum amplitudes (both +ve and -ve) since the noise contribution at these points is small and since these points should lie on the major axis of the particle motion ellipse. Thus the eye has been assumed to be the best interpreter of the axis of elliptical particle motion. This technique is somewhat subjective, but not entirely so, since the interpreter is constrained to use the position of successive amplitude maxima as guides. Thus the best-fitting line for the first cycle of particle motion was drawn as shown on the plots (Appendix E). Most lines were drawn through the maximum amplitude points (unless those points showed distortion due to amplifier overload), or parallel to a line through these points in cases where transient zero-offsets were present. To ensure that the first arrival alone was being measured, most analyses were done on the first cycle of the wave.

6.5 Results

The resultant measured apparent angles of emergence are given in Table VI-I for all shots analysed. Due to dead traces or excessively noisy traces, some records were omitted from the analysis. The actual angles of emergence along with the derived crustal velocities are also given in Table VI-I. For those shots where the first arrival had been interpreted as being refracted from the Moho, a basal refractor velocity of 8.05 km/sec was used in the velocity derivations; whereas, a basal refractor velocity of 8.44 km/sec was used for first arrival refractions interpreted to be from the lower mantle layer. The breakover point (critical distance) for refractions from the lower mantle refractor was

TABLE VI-I

RECORD	DISTANCE (km)	APP.ANGLE	REAL ANGLE	CRUSTAL VELOCITY (Km/Sec
33	163.22	36°	38°	------
3	261.00	44°	47°	5.45
36	295.14	42°	45°	5.70
37	295.04	43°	46°	5.55
4	336.01	43°	46°	5.55
5	335.95	40°	43°	5.90
38	373.93	43°	46°	5.55
39	374.04	43°	46°	5.55
7	412.20	43°	46°	5.55
40	446.11	44°	47°	5.45
10	564.22	44°	47°	5.45
44	639.37	47°	51°	5.35
45	639.50	51°	51°	5.35
46	668.96	47°	51°	5.35
47	669.67	40°	43°	6.20 ?
12	708.42	45°	48°	5.60
48	738.44	46°	49°	5.50
13	764.97	42°	45°	5.95
14	765.33	42°	45°	5.95
50	795.22	53°	57°	4.65 ?
15	827.57	42°	45°	5.95
52	866.83	41°	44°	6.05
53	867.18	43°	46°	5.85
16	884.69	41°	44°	6.05
54	944.56	45°	48°	5.60
55	944.63	43°	46°	5.85

TABLE VI-I (Continued)

RECORD	DISTANCE (km)	APP.ANGLE	REAL ANGLE	CRUSTAL VELOCITY (Km/Sec)
18	972.85	36°	38°	6.65
19	972.92	34°	35°	6.85
20	1058.40	38°	41°	6.40
21	1058.34	34°	35°	6.85
56	1071.32	37°	39°	6.50
57	1071.31	39°	42°	6.30
23	1088.16	38°	41°	6.40
58	1142.30	47°	51°	6.35
25	1244.64	45°	48°	5.60
31	1290.10	41°	44°	6.05
32	1290.37	47°	51°	5.35
63	1352.66	40°	43°	6.20
28	1379.34	42°	45°	5.95
64	1408.39	42°	45°	5.95
65	1408.68	41°	44°	6.05
29	1451.57	41°	44°	6.05
30	1451.87	44°	47°	5.70

Note: Error on all angles is $\pm$ 2°, error on velocities is $\pm$0.2 km/sec.

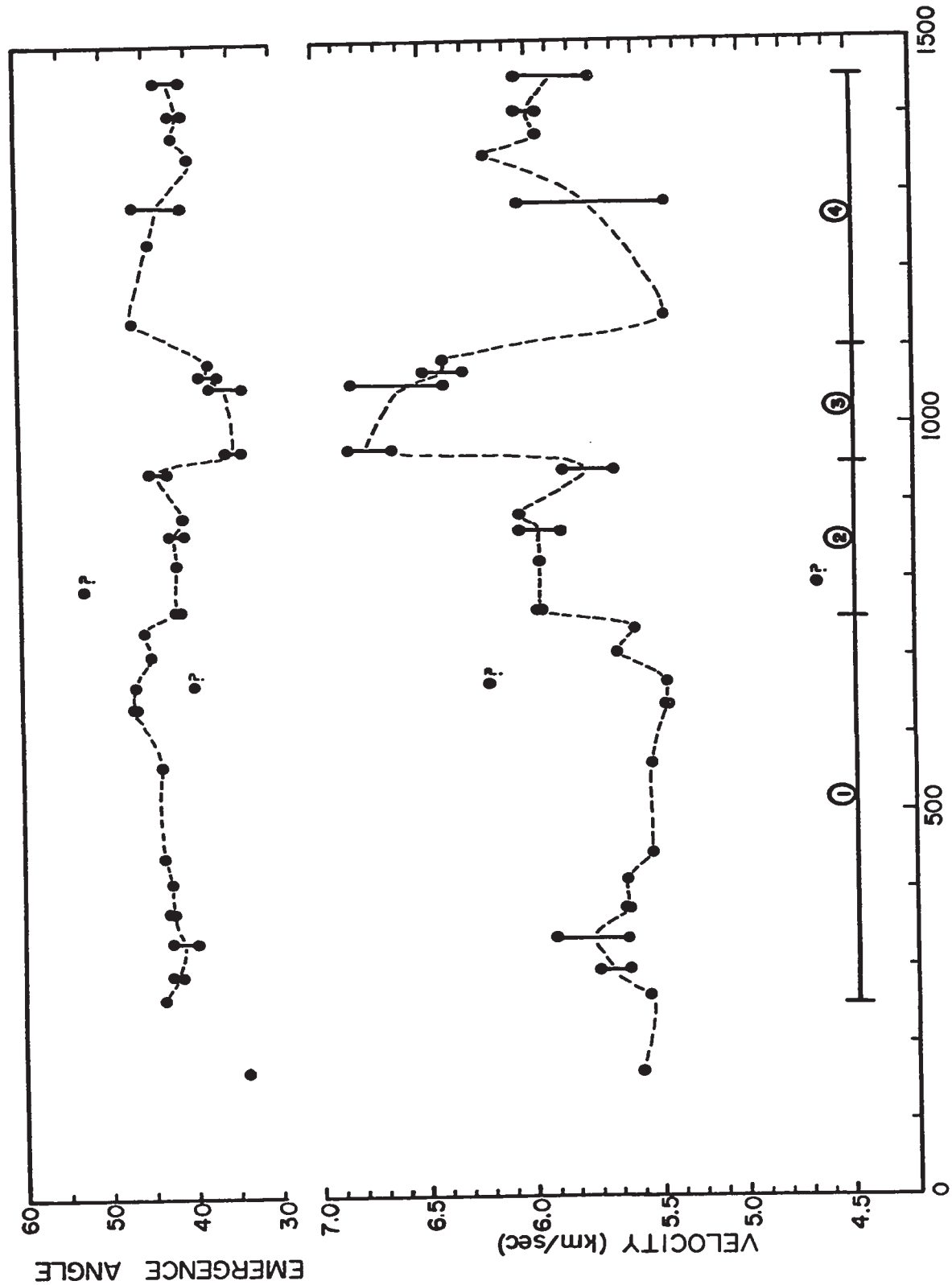

Fig. 6-1 Measured angles of emergence and interpreted upper crustal velocities for the Early Rise line.

interpreted previously to be approximately 600 km. Since no break in the trend of the derived crustal velocities occurs near this point it is suggested that the choice of refractor velocities used in computation may be considered as reasonable approximations.

The apparent angles of emergence and the derived velocities are plotted versus distance in fig. 6-1. As an aid in tracing the variation of emergence angles and velocities, straight lines are drawn between measurements. Where two values were obtained at the same location, the trend line has been drawn to the mean values of the readings. There are two measurements which apparently deviate strongly from adjacent stations: they are, shot 47 at 670 km and shot 50 at 800 km. On inspection of the analog and digitized records for these two shots, it was found that, in the case of shot 47 there was no apparent explanation for the measurement other than the unusual appearance of the particle motion plot; in the case of shot 50, the vertical and horizontal traces showed evidence of high frequency and high amplitudes, perhaps from near-surface scattering.

Most measurements, however, show small scatter when two measurements are made at each station. The far end of the Early Rise Line demonstrated slightly more scattering of results, showing the effects of a decreased signal to noise ratio.

The first measurement on the line is interpreted to be from a supra-Moho refractor because of the exceptional value of its apparent angle of emergence and its proximity to the source. If one assumes a velocity of the crust for this station to be that of the upper crust under the shot (5.5 km/sec) the velocity of the lower crustal refractor as determined from the apparent angle of emergence is 6.76 km/sec, a value not far removed from the accepted value of 6.68 km/sec under the shot position.

The measured velocity distribution of fig. 6-1 may be divided into four segments. The first segment between 200 and 750 km gives an average crustal velocity of 5.5 km/sec. The second segment between 750 and 950 km gives a slightly higher average velocity of 5.91 km/sec. The third segment between 950 and 1100 km gives an average velocity of 6.66 km/sec; and the fourth segment between 1100 and 1450 km gives an average crustal velocity of 5.83 km/sec.

6.6 Discussion of Results

The velocity values measured by the apparent angle of emergence can be considered as the average velocities for the upper portion of the crust.

Since in most instances, the velocity variation is small within one defined segment, it is suggested that the measured crustal velocities are indicative of regional changes in rock type.

One of the major assumptions of the first arrival model computed previously for the Early Rise line (Mereu and Hunter, 1969) is that the average velocity of the crust is 6.3 km/sec, a value which is assumed constant for the line. This assumption was based on a preliminary measurement of available P arrival times on the records as well as several other studies in the adjacent areas to the north and to the east of the Early Rise line (Hunter and Mereu, 1967; Ruffman and Keen, 1967; Hobson et al., 1967; Hall and Brisbin, 1965). In many locations on the North American continent the crust has been interpreted to be sub-divided into layers having velocities in the range of 5.9 - 6.2 km/sec for the upper layer and 6.6 - 7.1 km/sec for the lower crustal layer, as given by Healy and Warren (1969). From previous work in Lake Superior (Smith et al, 1966; O'Brien, 1968) the velocity layering under the shot has been determined

to be 5.5 km/sec for the upper layer and 6.7 km/sec for the lower layer yielding a thickness weighted mean of 6.3 km/sec. It is interesting to note that the velocities obtained from these particle motion studies give strong evidence for an upper crustal velocity slightly below the limits defined by Healy and Warren but however, close to that velocity obtained for the upper layer in Lake Superior. The velocities suggest a sialic composition and correlate well with the granite gneisses outcropping in the area. The slightly higher average velocity associated with the second and fourth segments may be indicative of a more basic rock type or a higher grade of metamorphism within the granite gneisses.

The surface velocities given by the third segment along the line give no evidence for a low velocity upper crustal layer. The average velocity for this segment is that of mafic rock of high density, and is identical to that determined for the lower crustal layer under Lake Superior. It is suggested that in this segment of the line, the sialic crustal layer is missing resulting from possible upwarping and erosion of the crust. Depths to the Moho have been recalculated from the published time-terms using a single layered 6.68 crustal velocity for this segment. The minimum depth computed was 30 km as compared to 27 km determined by Mereu and Hunter (1969).

From the velocity analysis done here it is not possible to determine whether or not a well-developed Conrad discontinuity exists under the Early Rise line. However there is some evidence that in the adjacent Hudson Bay area, reflections occur from a lower crustal layer (Hajnal, 1968).

The only major modification of Moho depth structure as given by Mereu and Hunter (1969) from particle motion studies occurs in the boundary zone area. The topographic Moho high is replaced by a north-dipping undulating boundary.

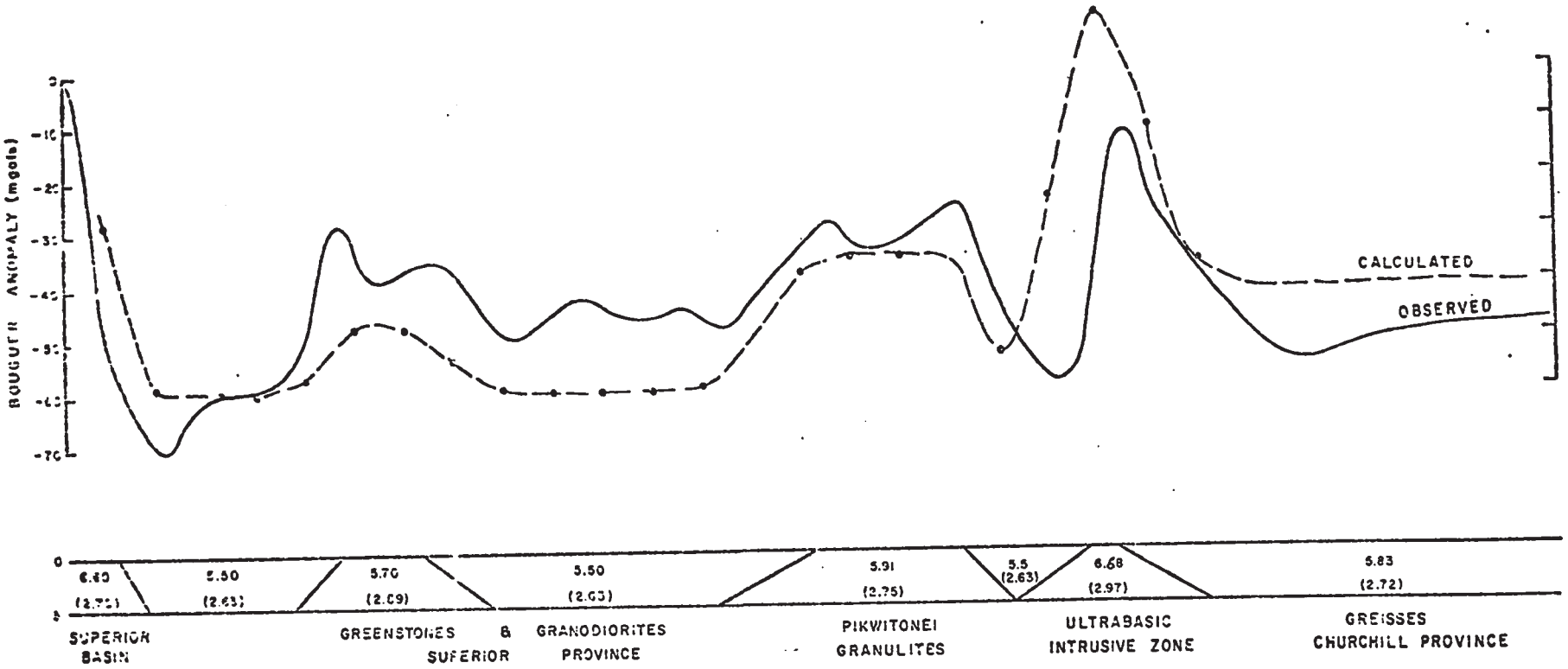

Fig. 6-2 Comparison of observed and calculated bouguer anomalies based on upper crustal velocity results along the Early Rise line.

Although a detailed description of the regional geology and geophysical results is given in Chapter I, it is interesting to compare here the crustal velocity model with general geology and gravity as shown in fig. 6-2 . Density variations due to velocity changes in the upper 5 km of the crust more than account for observed gravity anomalies as shown by the derived gravity model. Angular contacts between adjacent crustal blocks in the model represent gradational velocity variations. Good correlation exists between crustal velocities and the regional geology (after Gibb, 1968) in the boundary area between the structural provinces, where the high velocities are associated with the ultrabasic intrusive zone and the Pikwitonei sub-province anorthosites.

In general, the difference between the two structural provinces is denoted seismically by regional changes in upper crustal velocities as well as change in crustal thickness. The crustal thickening at both ends of the Early Rise line may be correlated with the younger Churchill province to the north and the Lake Superior basin to the south.

CHAPTER VII

AMPLITUDES OF SEISMIC BODY WAVES

7.1 Introduction

The amplitude of a refracted or refracted-reflected wave from an explosive source at teleseimic distances on the earth's surface is a function of the initial amplitude of the wave at the source, attenuation along the travel path, spreading of the wave front, and amplitude losses at interfaces along the travel path.

Comparison of model studies and observed records may be difficult since the variables given above are not easily estimated. For example, Mereu (1969) has shown that comparatively small departures of a seismic boundary from plane at depth may result in a large variation in refracted wave amplitudes because of focusing effects. These effects depend upon the curvature of the refracting boundary, the angle of incidence of the wave, and the velocity and density contrasts across the boundary. As well, near surface irregularities such as local layering and second order changes in velocity gradient may also result in amplitude anomalies. If such variations exist under the Early Rise seismic stations, then plane-layer model studies, at best, may only serve as a guide to the detectability of later events.

The attenuation of a body wave with distance has been discussed in Chapter V. The effect of attenuation with distance may be effectively eliminated if amplitude comparisons between events are confined to the same record (assuming similar path lengths for later events at great distances). Since there is a lack of definite evidence for a discontinuity

in average Q between crust and upper mantle, the effect has not been included in the study of body wave amplitude models.

7.2 Theory of Body Wave Amplitudes

For an earth model having spherical symmetry, the energy per unit area of a body wave front is given by Bullen (1963, p. 126, eq. 1) as:

$$E(\Delta) = (I \cos e_1 \ (de_1/d\Delta)/(r_o^2 \sin \Delta \sin e_o) \quad \ldots\ldots 7\text{-}1$$

where,

I = initial energy per unit solid angle

r_o = radius of the earth

e_o = angle of emergence under station

e_1 = angle of emergence under shot

The variables included in equation 7-1 are illustrated in fig. 7-1.

Since the ray parameter is defined as:

$$p = r_1 \cos e_1/v_1 \quad \ldots\ldots 7\text{-}2$$

then, the rate of change of e_1 with Δ can be found from 7-2 as:

$$de_1/d\Delta = (-dp/d\Delta)\ V_1/(r_1 \sin e_1) \quad \ldots\ldots 7\text{-}3$$

Hence the energy equation becomes:

$$E(\Delta) = I\ v_1 \cos e_1 \ (dp/d\Delta)/(r_o^2 \sin \Delta \sin e_o \sin e_1) \quad \ldots\ldots 7\text{-}4$$

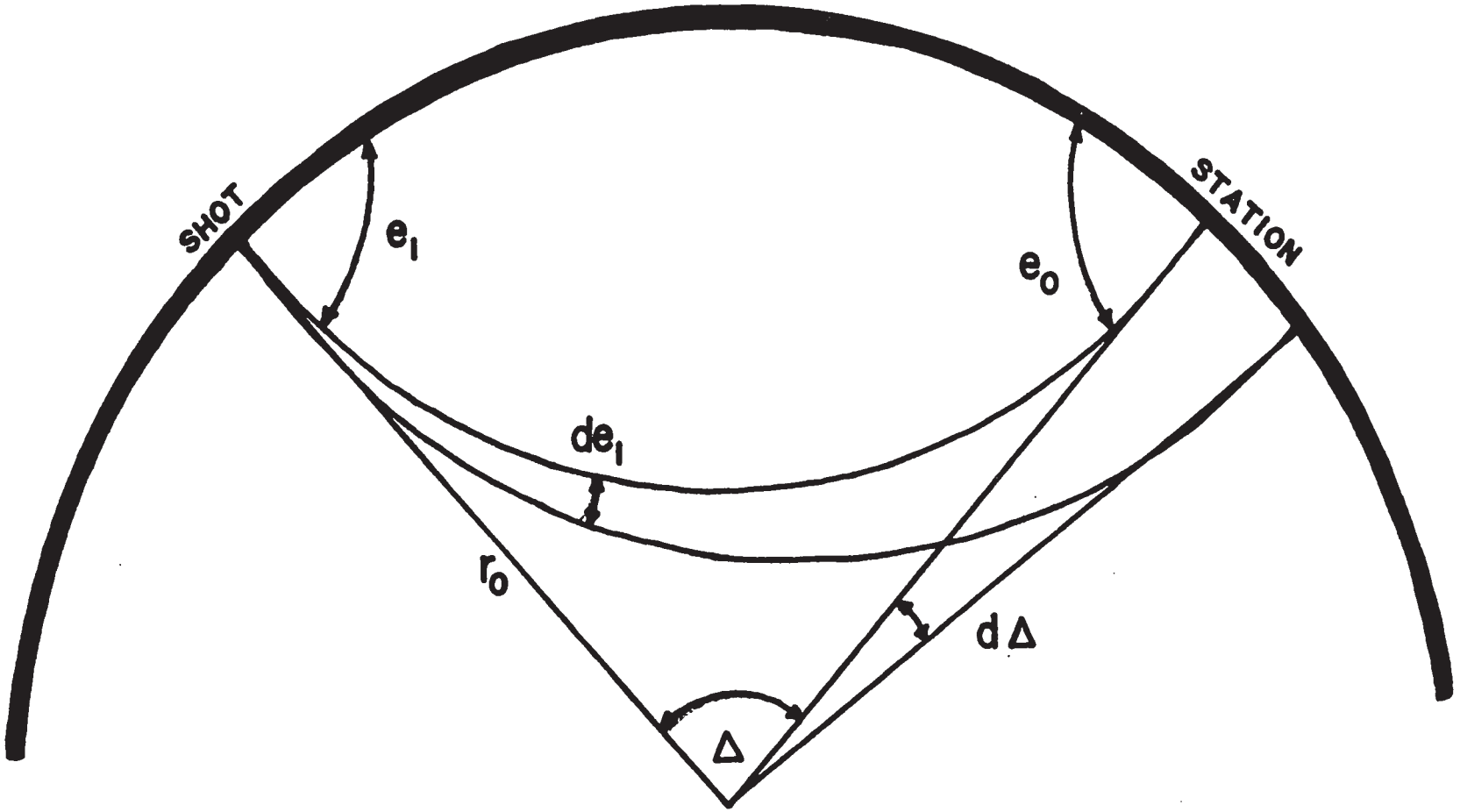

Fig. 7-1 Model variables for curved earth ray path calculations.

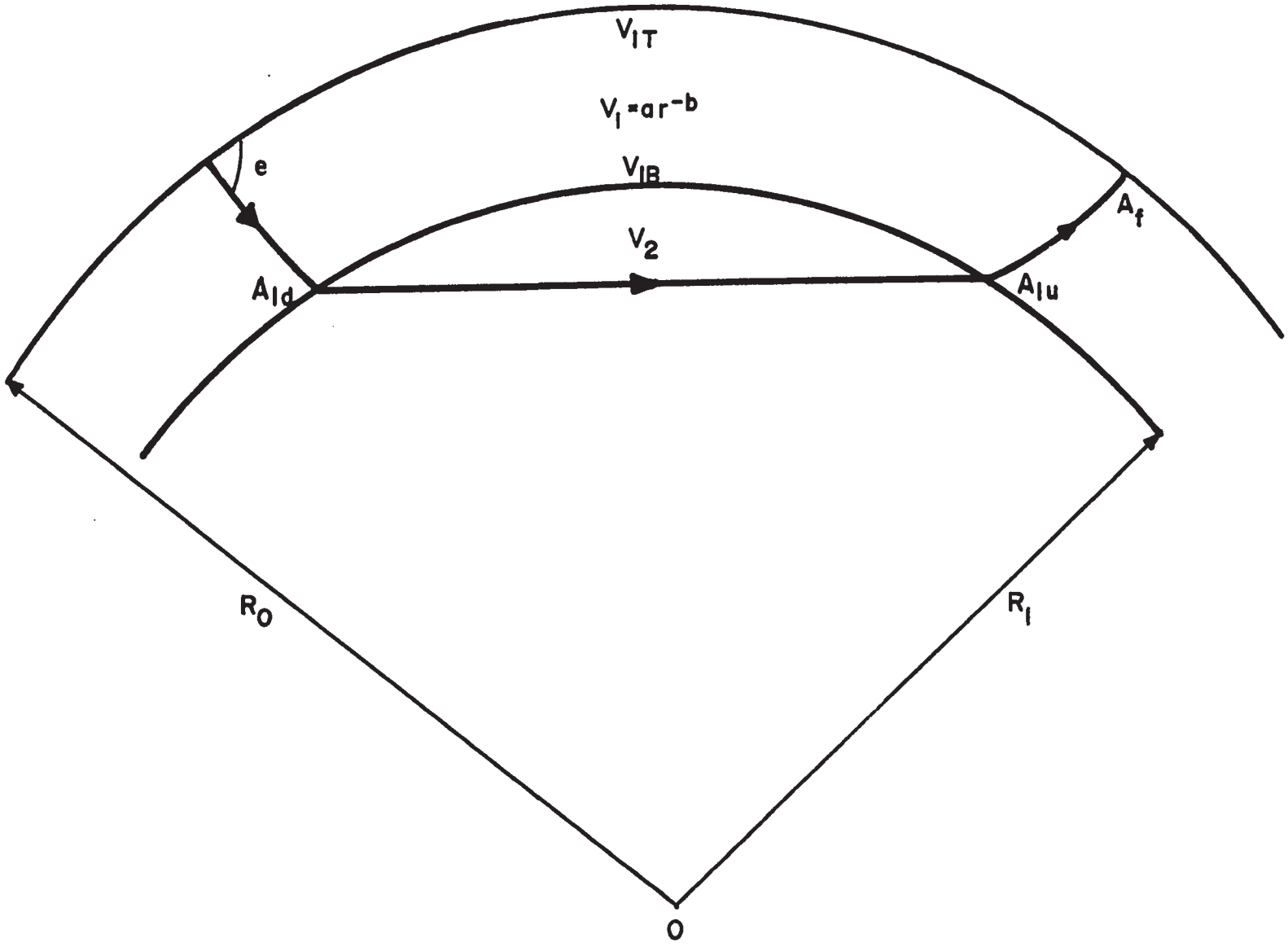

Fig. 7-2 (a) Model variables for the layered earth amplitude analysis.

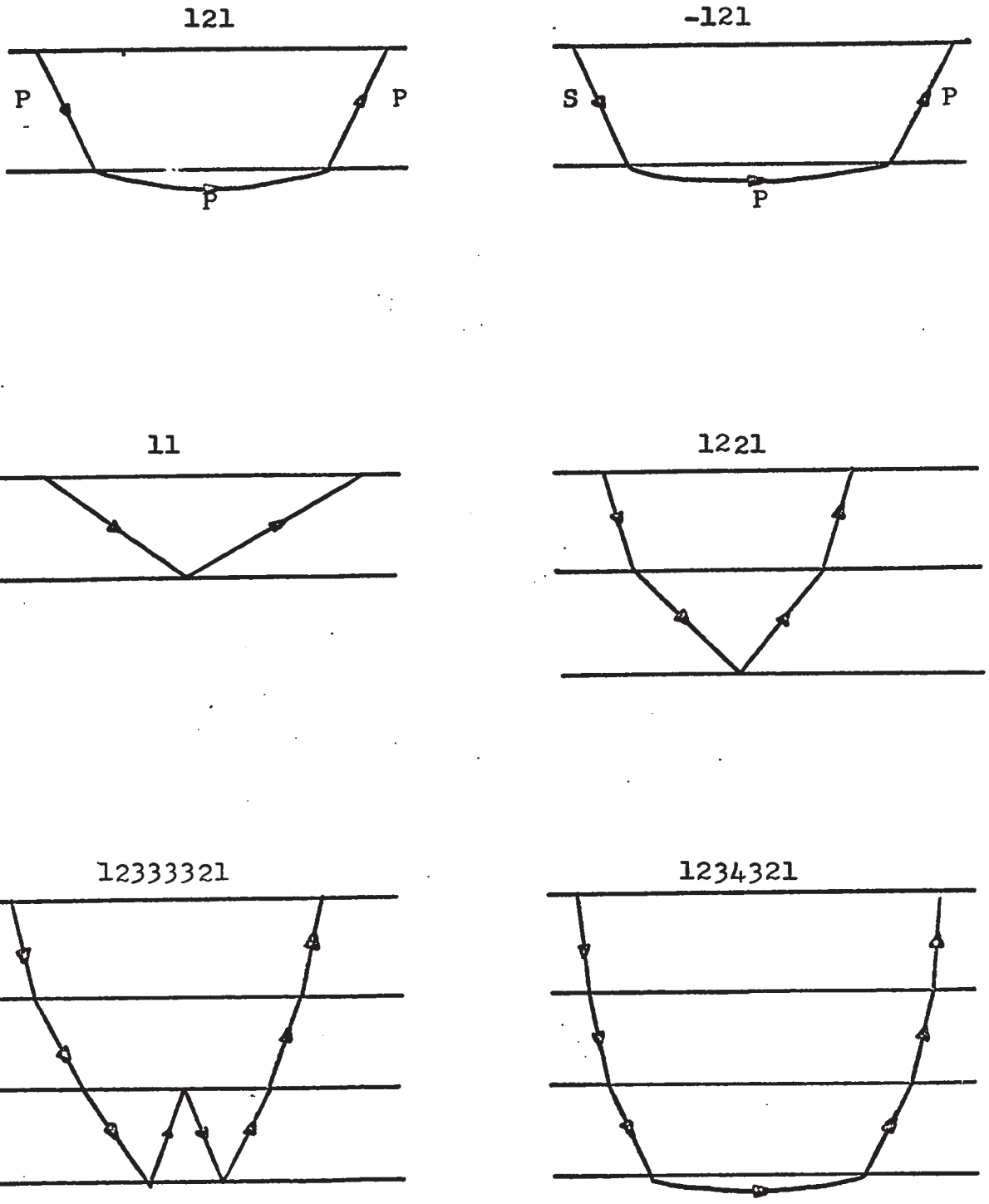

Figure 7 - 2(b) : Diagrammatic representation of the wave coding.

To obtain an expression for dp/d Δ, consider Bullen (1963, p. 111, eq. 8):

$$\Delta = 2p \int_{r_p}^{r_o} r^{-1} (\eta^2 - p^2)^{-\frac{1}{2}} dr \qquad \ldots. 7\text{-}5$$

where,

$\eta = r/v$

$p = r \sin i/v$

i = angle of incidence at any point on the ray

r = distance between the centre of the earth and any point on the ray

r_p = distance between earth's centre and point where ray bottoms.

For any segment of Δ, such as the segment of the ray travelling through one layer in the earth with a velocity distribution of $v = ar^{-b}$, the expression 7-5 becomes:

$$\Delta r_n - \Delta r_{n+1} = (1/(1 + b))(\sin^{-1}(pv_{n+1}/r_{n+1}) - \sin^{-1}(pv_n/r_n)) \qquad \ldots. 7\text{-}6$$

where, v_n, r_n = velocity and earth radius at the top of the layer

v_{n+1}, r_{n+1} = velocity and earth radius at the bottom of the layer

The total Δ would be the sum of the segments on the down-going and up-going portions of the ray. For wave travel in s layers including the one where the ray bottoms:

$$\Delta = 2 \sum_{i=1}^{s} \Delta_i \qquad \text{(source at surface)} \qquad \ldots. 7\text{-}7$$

The distance segment describing the layer in which the ray bottoms is:

$$\Delta_s = (1/1+b_s)(-\sin^{-1}(pv_n/r_n)) \qquad \ldots. 7\text{-}8$$

The derivative of any distance segment with respect to the ray parameter is:

$$d(\Delta_{r_n} - \Delta_{r_{n+1}})/dp = (1/1+b)(1/(\eta^2_{n+1} - p^2)^{\frac{1}{2}}) - (1/(\eta^2_n - p^2)^{\frac{1}{2}})$$

hence the expression required for 7-2 is:

$$dp/d\Delta = 1/\sum_{i=1}^{s} d\Delta_i/dp \qquad \ldots\ 7\text{-}9$$

The expression (7-4) for $E(\Delta)$ does not consider the effect of energy partitioning at seismic interfaces or the effect of reflection at the free surface of the earth at the recording point. Bullen (1963, p. 128) shows that the amplitude squared of the wave motion is proportional to the energy per unit area of the wave. Hence an amplitude expression governing body wave motion, including interface partitioning would be:

$$A_v = K\, A_f \sqrt{A_1 A_2 A_3 \ldots\ldots A_L E^2(\Delta)} \qquad \ldots\ 7\text{-}10$$

where,

K = a constant

A_f = vertical amplitude coefficient at the free surface due to incident and reflected waves (Ewing et al, 1957)

$A_1 \ldots\ldots A_L$ = energy ratio coefficients obtained from solving the Zoeppritz Equations (Steinhart et al. 1961; McCamy et al., 1962: Costain et al., 1963).

Equation 7-10 describes the vertical component amplitude recorded on surface for a body wave which has been refracted and reflected at interfaces at depth in a layered earth. A similar expression can be obtained for the horizontal component by replacing the vertical component free-surface coefficient with the horizontal coefficient. Transformed wave types as well as multiple reflections can also be described by 7-10.

The one remaining unknown variable implicit in the amplitude expression is the ray parameter. A solution for p for each wave type may be obtained by iterating equations 7-7 and 7-9 using an initial value for the ray parameter as given by the critical angle ray at the lowest interface. For most wave types an iterative solution can be obtained rapidly using computer methods.

As an example of the expanded form of 7-10 consider the case of the vertical surface amplitude of a wave refracted in a two layered earth. The variables used are shown in fig. 7-2. The amplitude at distance Δ from the source would be:

$$A_v = K\ A_f\sqrt{A_{1d}A_{1u}}\left(\left(\cos e_s/R_o^3\ \sin\Delta \sin^2 e_s\right)\left(1/\left(2/1+b_1\right)\left(1/\left(\frac{R_1^2}{v_{1B}^2}-p^2\right)^{\frac{1}{2}}\right.\right.\right.$$

$$\left.\left.\left.-1/\left(\frac{R_Q^2}{v_T^2}-p^2\right)^{\frac{1}{2}}\right)-\left(2/1+b_2\right)\left(1/\left(\frac{R_1^2}{v_2}-p^2\right)^{\frac{1}{2}}\right)\right)\right)^{\frac{1}{2}} \qquad \ldots\ 7\text{-}11$$

where K = constant including the initial source intensity of the wave

A_{1d}, A_{1u} = energy ratio transmission coefficients at the interfaces

A_f = vertical component free surface coefficient.

It can be seen that equation 7-10 can be expanded into any form for the description of any wave path by the addition of Zoeppritz coefficients and terms describing each layer in the dp/d Δ segment.

The travel-time of any wave in a form similar to (Bullen, 1963, p. 112):

$$T = P\Delta + 2\int_{r_p}^{r_o} r^{-1}(\eta^2 - p^2)^{\frac{1}{2}}\, dr \qquad \ldots\ldots 7\text{-}12$$

Equation 7-12 can be expanded to describe the travel time in any layer of velocity districution $v = ar^{-b}$ in a manner similar to that of the expansion of the distance equation.

Implicit in the derivation of 7-10 is the assumption of plane wave incidence on any seismic boundary. This assumption is valid in crustal work where curvature of wave-fronts impinging on boundaries at large distances from the source is small.

A Fortran IV program was developed to compute the amplitudes and travel-times of any body wave for typical recording distances used in crustal studies. A detailed description of the program is given in Appendix F.

The computer program was used in the amplitude model studies outlined in the following sections. The wave types chosen for computation were coded in numeric form for computer input. Each layer of the earth model was coded beginning with the numeral 1 at the earth's surface and increasing downwards. The portion of the wave travelling in each layer was then coded with respect to the layer number. In addition, if the travel mode in the layer was shear wave motion, the layer number was negative . For example for a two layered earth (crust and mantle) the refracted P_n wave would be denoted 121 whereas a converted shear refraction (on the upgoing portion)would be 12-1 and the crustal reflection would be denoted as 11. The notation is easily extended to multilayered cases (fig. 7-2b)

7.3 Comparison of Head Wave and Body Wave Amplitudes for a Simple Crustal Model

The amplitudes of head waves for various crustal models has been investigated by Cerveny (1967). To obtain an estimate of crustal models from amplitude studies of the first arrival it is necessary to compare the relative importance of body and head wave amplitudes.

Cerveny states that the amplitude of a head wave depends on the existence of a well defined refractor velocity discontinuity. He suggests that if curvature of the refractor or velocity gradient exists the body wave effect may predominate over that of the head wave. Cerveny (1966) has computed the relative amplitudes of head and body waves for a flat-earth model consisting of of a 6.30 km/sec crust of 30 km thickness, and a P_n velocity of 8.00 km/sec with a positive gradient of 0.00283 sec^{-1}. Fig. 7-3 (after Cerveny, 1966) shows the relative amplitudes of the two refracted wave types in comparison with the reflected wave.

As a guide to the relative importance of the amplitudes of the two refracted wave types in the absence of velocity gradients, a one layer crustal model corresponding to Cerveny's (1967) model M5-1 was examined. The model consisted of a 30 km thick 6.4 km/sec crustal layer overlying the mantle with a velocity of 8.00 km/sec. The vertical components of Moho refraction and reflection amplitudes were computed for various detector distances using the body wave theory as outlined in the previous section. The peak amplitude of the Moho reflection computed by the body wave theory was normalized to that given by Cerveny's model M5-1 (from Cerveny's (1967) fig 12d).

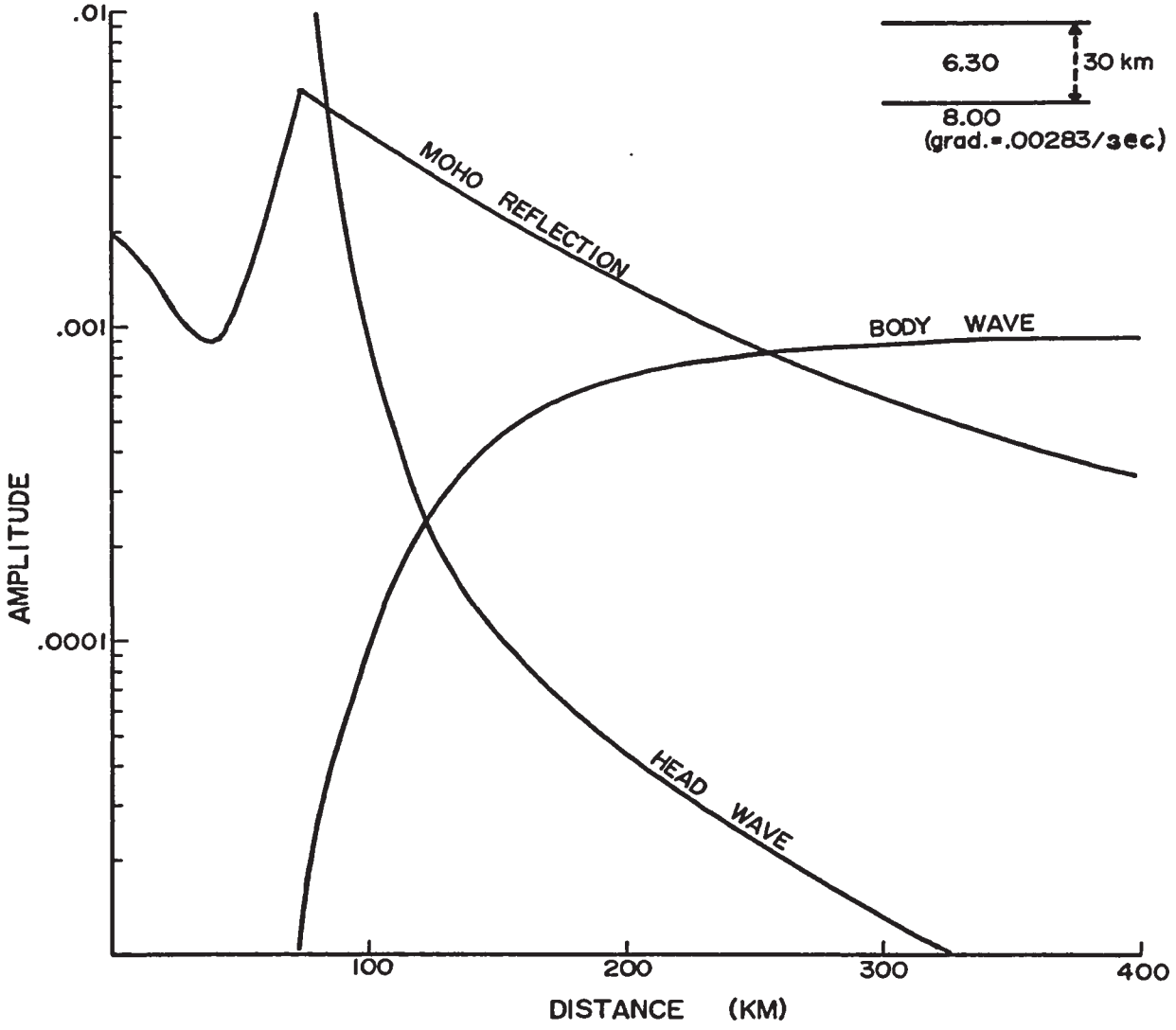

Fig. 7-3 Amplitude comparison of Moho reflection, body wave refraction, and head wave after Cerveny (1966).

A comparison of refraction amplitudes computed for the body and head wave transmission as well as reflection amplitudes are given in fig. 7-4. The head and body-wave amplitudes, assuming no frequency attenuation, are given by the solid lines. For this model, the head wave amplitude dominates in the near range with the body wave becoming dominant beyond 200 km. Cerveny notes that for models having greater crustal thicknesses, the head wave amplitude fall-off is greater with distance. Introducing frequency attenuation has the effect of decreasing amplitudes at large distances as given by fig. 7-4. The dotted and dashed models are for Q = 50 and Q = 100 respectively (Q = specific attenuation factor), assuming a wavelet frequency of 2 hertz.

The results of this model study with both curvature and velocity gradients suggest that first arrival P_n events on typical teleseismic crustal records are body wave events. As well, the presence of a velocity gradient in the upper mantle tends to increase the ratio of body wave to Moho reflection amplitudes.

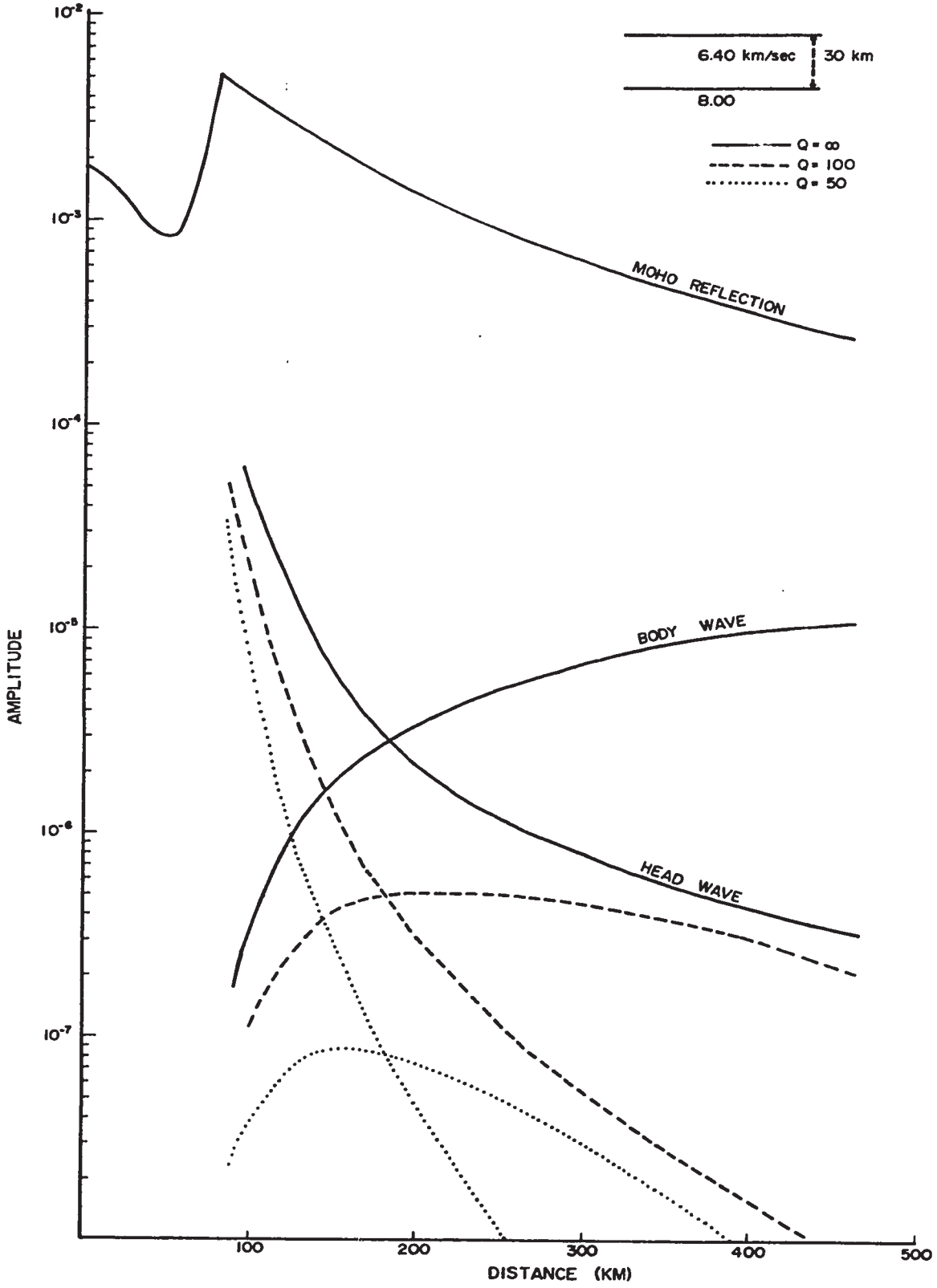

Fig. 7-4 Comparison of Moho reflection, body, and head wave amplitudes showing the effect of attenuation for a single layered crustal model.

7.4 Converted Refracted Body Wave Amplitude Study

Converted refracted body waves from the Moho have arrival times predicted to be within a few seconds of the first arrival, for most continental crustal models. To examine the possibility of observing these waves, several simple mathematical crustal models were assumed. The basic model is a two layered earth consisting of a crustal layer of thickness z and an upper mantle layer of infinite thickness. The amplitude of the waves 121, -121, 12-1, -12-1, and -1-2-1 for S waves were computed using body wave theory (as given in section 2) for various combinations of crustal layer thickness and layer velocities. Most variations in parameter were taken about a standard model consisting of a 30 km thick crust with a velocity of 6.3 km/sec and an upper mantle velocity of 8.1 km/sec. The models have been tabulated in Table VII-I.

The vertical component amplitudes computed for some of the more interesting models are shown in fig. 7-5. All amplitudes shown on the plots are based on an initial common source amplitude and are scaled by a common factor. The amplitude of the -1-2-1 wave was found to be close to that of 121 and that of -121 close to that of 12-1; hence, the two amplitudes -1-2-1 and 12-1 were not plotted in the diagrams. For all models, the amplitudes of converted waves suffering one mode change are approximately one order of magnitude less than the 121 refracted wave. Waves suffering two mode changes are even further attenuated. The effect of crustal thickening is to reduce the amplitudes of all refracted events in the 100-400 km range. It is interesting to note that the amplitudes of all events increase with distance, an effect which results from an increase in the incident angle at the base of the crust with distance. Because of attenuation losses the effect is seldom observed in nature.

Most models show little variation in amplitudes from those given by model (a). Relatively small amplitude variations result from substantial changes in crustal thickness, crustal velocity, or upper mantle velocity. The converted refracted waves for all of these models remain at much lower amplitudes than the refracted compressional wave (121). The exceptional cases (as shown in fig. 7-5) occur when velocity gradients (following the $v=ar^{-b}$ law for these models) exist in the crust or mantle. These effects cause large increases in amplitudes of all refracted waves but little enhancement of the converted types with respect to the compressional event. Rapidly decreasing amplitudes at large distances result from geometrical spreading. In none of the models studied did the amplitude of any converted refracted wave approach that of the compressional refractor. This suggests that converted refracted waves may be 'second order' events on a crustal refraction seismogram being only observed with considerable difficulty.

7.5 Model Studies of Sub-Moho Reflections

In order to study the effects of layering beneath the Moho horizon, several models were devised, with reasonable velocity variations, and the amplitudes and arrival times of the prominent later events were computed. The basic crustal model used throughout was a 30 km thick crust having a compressional velocity of 6.30 km/sec.

The first set of models (a,b, and c) dealt with the positioning of a seismic interface similar to that of the 'Hales' discontinuity. The seismic models are listed in Table VII-II. Amplitudes and travel-times were

TABLE VII - I

CONVERTED BODYWAVE AMPLITUDE MODELS

Model	P_g	Z_g	P_n
a)	6.30	20.	8.1
b)	6.30	30.	8.1
c)	6.30	40.	8.1
d)	6.00	30.	8.1
h)	6.50	30.	8.1
i)	6.30	30.	8.00
k)	6.30	30.	8.15
n)	6.30	30.	8.30
o)	4.80 - 7.80	30.	8.10
r)	5.40 - 7.20	30.	8.10
v)	6.20 - 6.40	30.	8.10
w)	6.30	30.	8.05 - 8.43 (20 km)
x)	6.30	30.	8.05 - 8.43 (40 km)
y)	6.30	30.	8.05 - 8.43 (60 km)
jj)	5.40 - 7.20	20.	8.05 - 8.43 (40 km)
kk)	5.40 - 7.20	30.	8.05 - 8.43 (40 km)
ll)	5.40 - 7.20	40.	8.05 - 8.43 (40 km)
aa)	4.80 - 7.80	30.	8.05 - 8.43 (20 km)
bb)	4.80 - 7.80	30.	8.05 - 8.43 (40 km)
cc)	4.80 - 7.80	30.	8.05 - 8.43 (60 km)
dd)	5.40 - 7.20	30.	8.05 - 8.43 (20 km)
ee)	5.40 - 7.20	30.	8.05 - 8.43 (40 km)
ff)	5.40 - 7.20	30.	8.05 - 8.43 (60 km)
gg)	6.20 - 6.40	30.	8.05 - 8.43 (20 km)
hh)	6.20 - 6.40	30.	8.05 - 8.43 (40 km)
ii)	6.20 - 6.40	30.	8.05 - 8.43 (60 km)

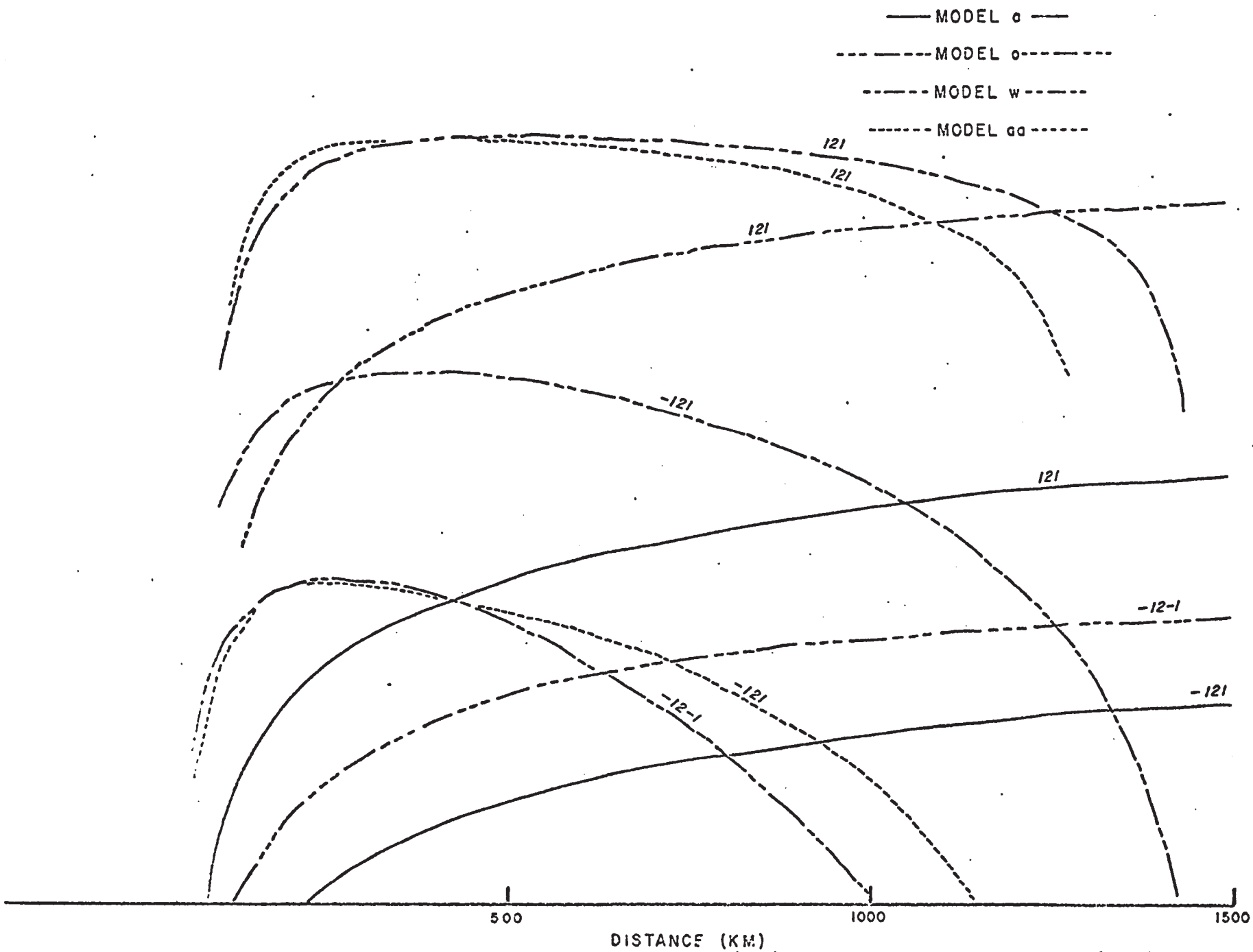

Fig. 7-5 Comparison of the Moho body wave refraction (121) to converted body waves SPP (-121) and SPS (-12-1) for various single layered crustal models studied. (see table VII-1)

computed for the following reflections:
1221, 122221, 12211221, -1221, 12-2-1, which constitute the major reflections from this horizon. Amplitudes for each of the wave types for some of the models, are shown in figs. 7-6. In general, all waves considered have well-defined amplitude maxima. Increasing the depth of the Hales discontinuity has the effect of shifting this amplitude maximum towards greater distances. This variation is quite sensitive to depth changes and should be a prominent diagnostic feature. A velocity gradient between the Moho and the Hales discontinuity has the effect of decreasing the wave amplitudes at distances beyond the peak amplitude. Hence, if an appreciable gradient existed one would expect to identify the event in a restricted portion of the record section. The events 1221, 122221, 12211221 should be identifiable since they retain large amplitudes over large distances. The converted reflection -1221 and 12-2-1 appear at close distances (out to 500 km) and have very low amplitudes at greater distances.

The travel-time for the reflected events examined, demonstrate the effect of change of layer thickness. Differences of up to 10 seconds for thickness changes of 30 km are possible in the observable ranges of some events. The greatest variation is obtainable from the 122221 event. Arrival times of models show changes of up to 2 seconds with the introduction of velocity gradients. However the error of estimate of arrival times on the seismic section may mask some of the more subtle changes due to the presence of velocity gradients.

TABLE VII -II

"HALES" DISCONTINUITY MODELS

Model	P_g	Z_g	P_n	Z_n	P
a	6.3	30	8.05	20	8.43
b	6.3	30	8.05	50	8.43
c	6.3	30	8.05	80	8.43
d	6.3	30	8.00 - 8.20	20	8.43
e	6.3	30	8.00 - 8.20	50	8.43
f	6.3	30	8.00 - 8.20	80	8.43
g	6.3	30	8.00 - 8.30	20	8.43
h	6.3	30	8.00 - 8.30	50	8.43
i	6.3	30	8.00 - 8.30	80	8.43

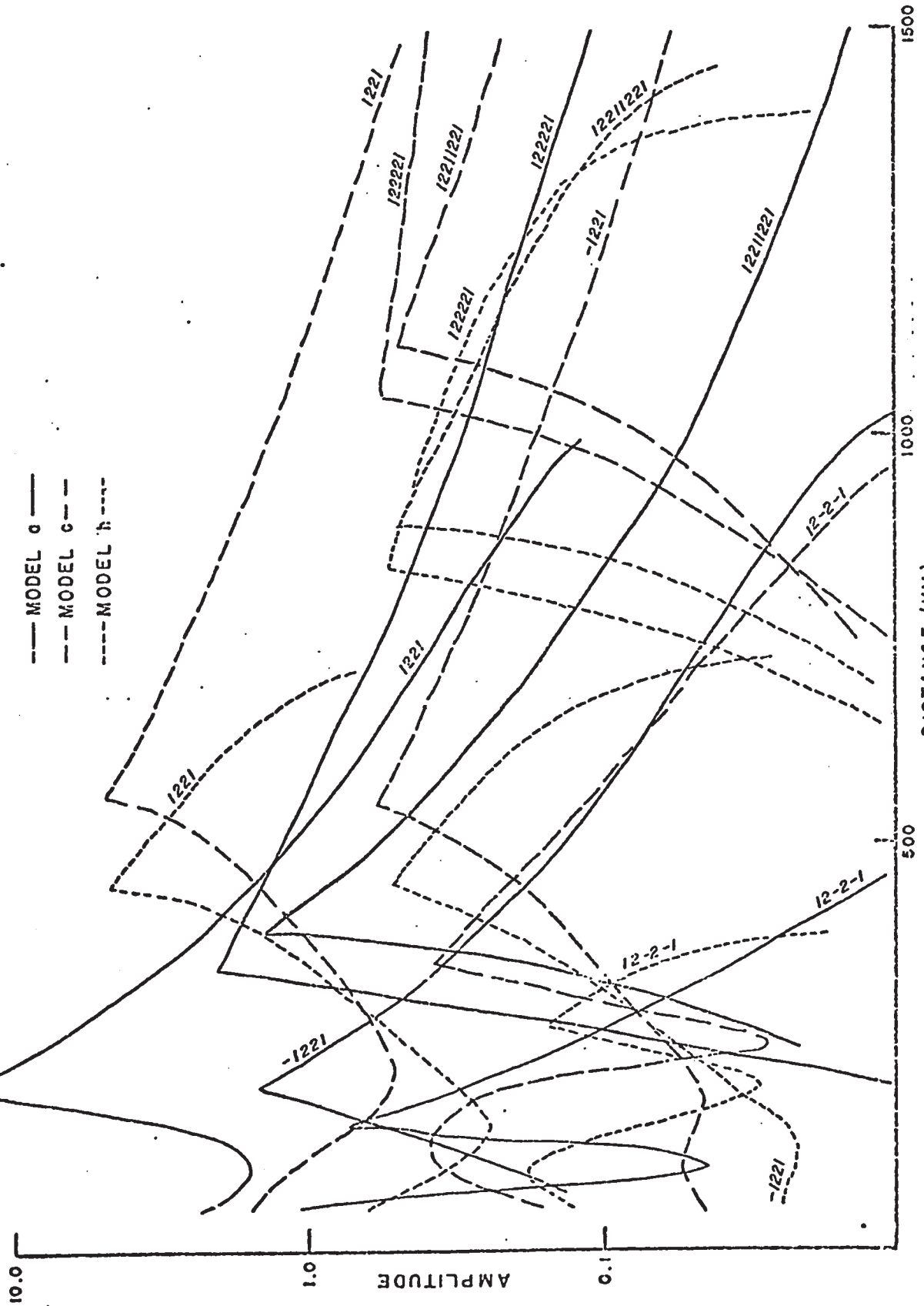

Fig. 7-6 Comparison of amplitudes of major sub-Moho (Hales discontinuity) reflected events for various models studied as given in Table VII-II.

TABLE VII -III

HIGH VELOCITY LAYER MODELS

Model	P_g	Z_g	P_n	Z_n	P_b	Z_b	p
a	6.30	30	8.05	50	8.43	20	8.60
b	6.30	30	8.05	50	8.43	40	8.60
c	6.30	30	8.05	50	8.43	60	8.60
d	6.30	30	8.05	50	8.40- 8.50	20	8.60
e	6.30	30	8.05	50	8.40 -8.50	40	8.60
f	6.30	30	8.05	50	8.40 -8.50	60	8.60
g	6.30	30	8.05	50	8.35 -8.55	20	8.60
h	6.30	30	8.05	50	8.35 -8.55	40	8.60
i	6.30	30	8.05	50	8.35 -8.55	60	8.60

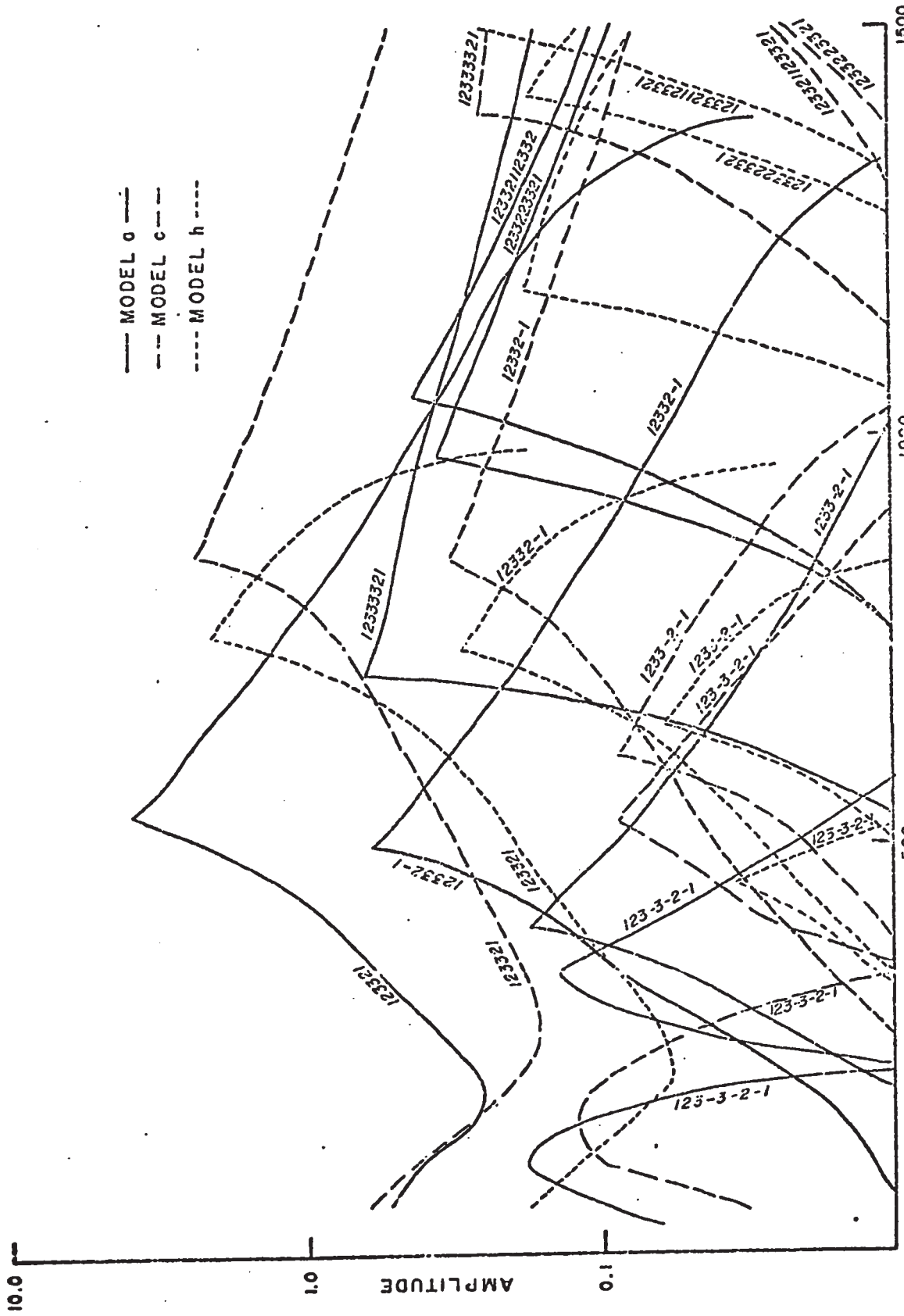

Fig. 7-7 Comparison of amplitudes of major sub-Hales reflected events for valous models given in Table VII-III.

TABLE VII -IV

LOW VELOCITY LAYER MODELS

Model	P_g	Z	P_n	Z_n	P	Z	P_L
a	6.30	30	8.05	50	8.43	20	8.30
b	6.30	30	8.05	50	8.43	40	8.30
c	6.30	30	8.05	50	8.43	60	8.30

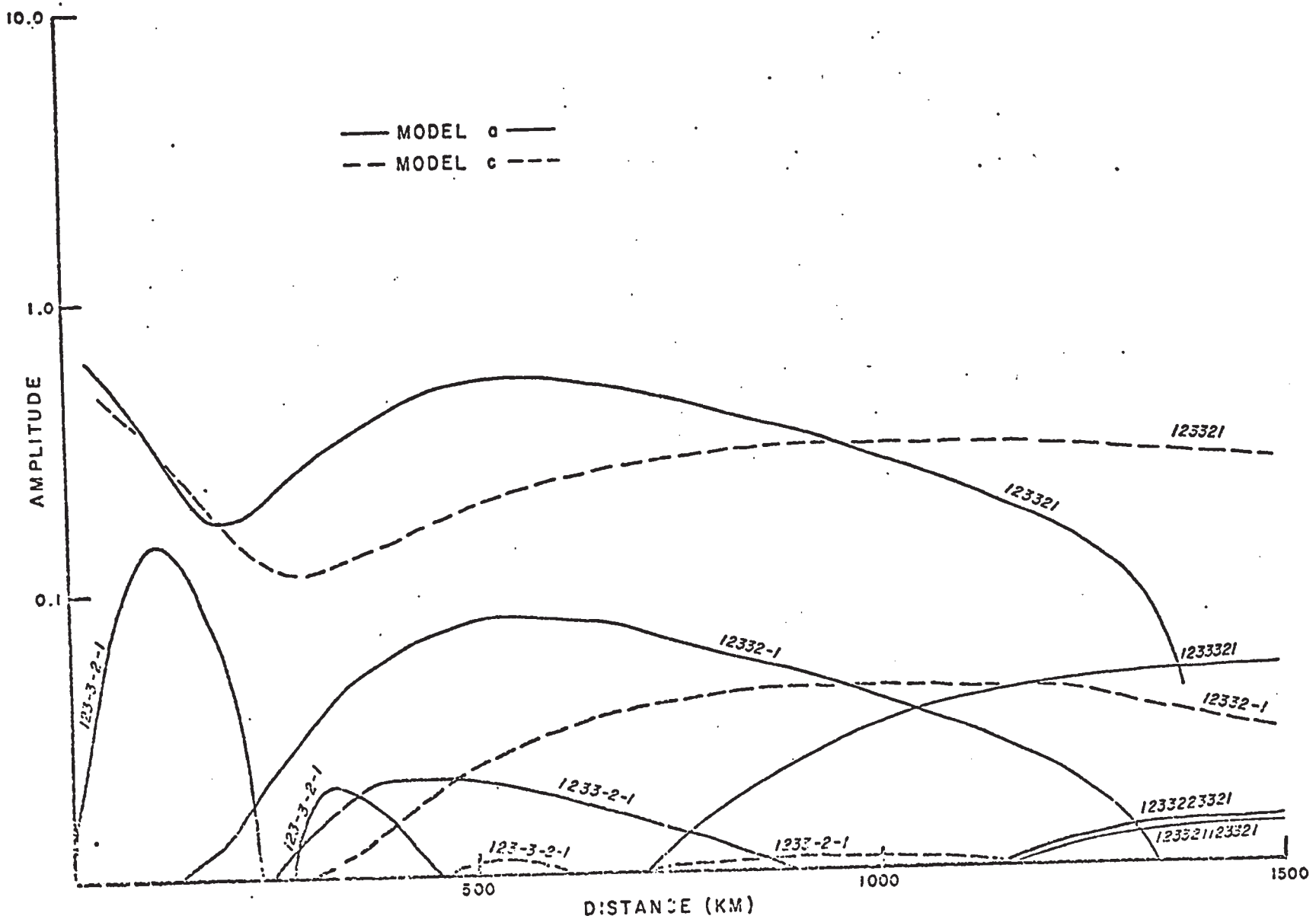

Fig. 7-8 Comparison of amplitudes of major sub-Hales reflected events for low velocity layer models given in Table VII-IV.

In order to test the detectability of later reflected events from a horizon deeper than the Hales discontinuity, a series of models were computed for a layer of 8.60 km/sec velocity at various depths. The models examined are given in Table VIII-III. The reflected events determined in the study were the following: 123321, 12333321, 1233223322, 123321123321, 12332-1, 1233-2-1, 123-3-2-1.

The amplitude plots for some models are shown in fig. 7-7. The events examined show pronounced amplitude maxima, similar in many respects to the reflection results for the Hales discontinuity. The positions of the maxima are strongly dependent on the layer thicknesses and the extent to which the high amplitudes persist beyond the maxima depends on the gradient above the high velocity interface. The 123321 reflection should be observable over the large portion of the record section. The event 123-3-2-1 may be difficult to observe on a travel-time section since the high amplitude portion is restricted to a narrow region in the early portion of the section and may be in the zone of interference from other later events.

A set of models were computed to study the effect of a low velocity layer at depth beneath the Hales discontinuity. The effect of layer thickness variation was examined for the models given in Table VII-IV. The waves studied were the most prominent ones consisting of 123321, 12333321, 1233223321, 123321123321, 12332-1, 1233-2-1, 123-3-2-1. The amplitude results for some models are shown in fig. 7-8. The amplitudes of these events differ from those computed for the Hales and the high velocity layer cases. No sharp amplitude maxima exist except in the case of the 123-3-2-1 event. The events are characterized by smoothly increasing amplitudes in the near range and slowly decreasing amplitudes in the far range. The 123321 event should be a prominent event across the record section.

The multiple reflections are somewhat attenuated with respect to this event, and the 123321123321 event may not be observable at all. The converted reflected event 123-3-2-1 is a prominent event in the near range and may be a diagnostic event in reflection survey techniques.

The major difference between observable events from a high velocity layer and a low velocity layer is the distance variation of amplitudes associated with the 123321 event. In both cases this event may however be within the zone of interference of reflections from the Hales discontinuity and may not be easily identifiable.

7.6 Amplitude and Travel-Time Studies of Early Rise Models

As a guide to the relative importance of seismic events on the Early Rise records, crustal models, based on published first arrival analyses, were studied and compared. The models studied are outlined in fig. 7-9, a cross-sectional representation. Model I is based on the first arrival analysis of Mereu and Hunter (1969), and constitutes an average crustal structure for the Northern Manitoba region. Model II is the average crustal structure under Lake Superior from Smith et al., (1966), consisting of a two layered crust, with a Hales discontinuity added from the Early Rise results. Model III is a variation of Model I under assumption of a single layered crust with a velocity increase with depth.

The wave studied consisted of events which had been assumed to be prominent on the early portions of a crustal seismic record and consisted of the major refracted events from the model interfaces and their converted wave equivalents, as well as reflected events, multiple reflections and converted reflections. The amplitude and travel-time results of the model studies are given in fig. 7-10 to fig. 7-11.

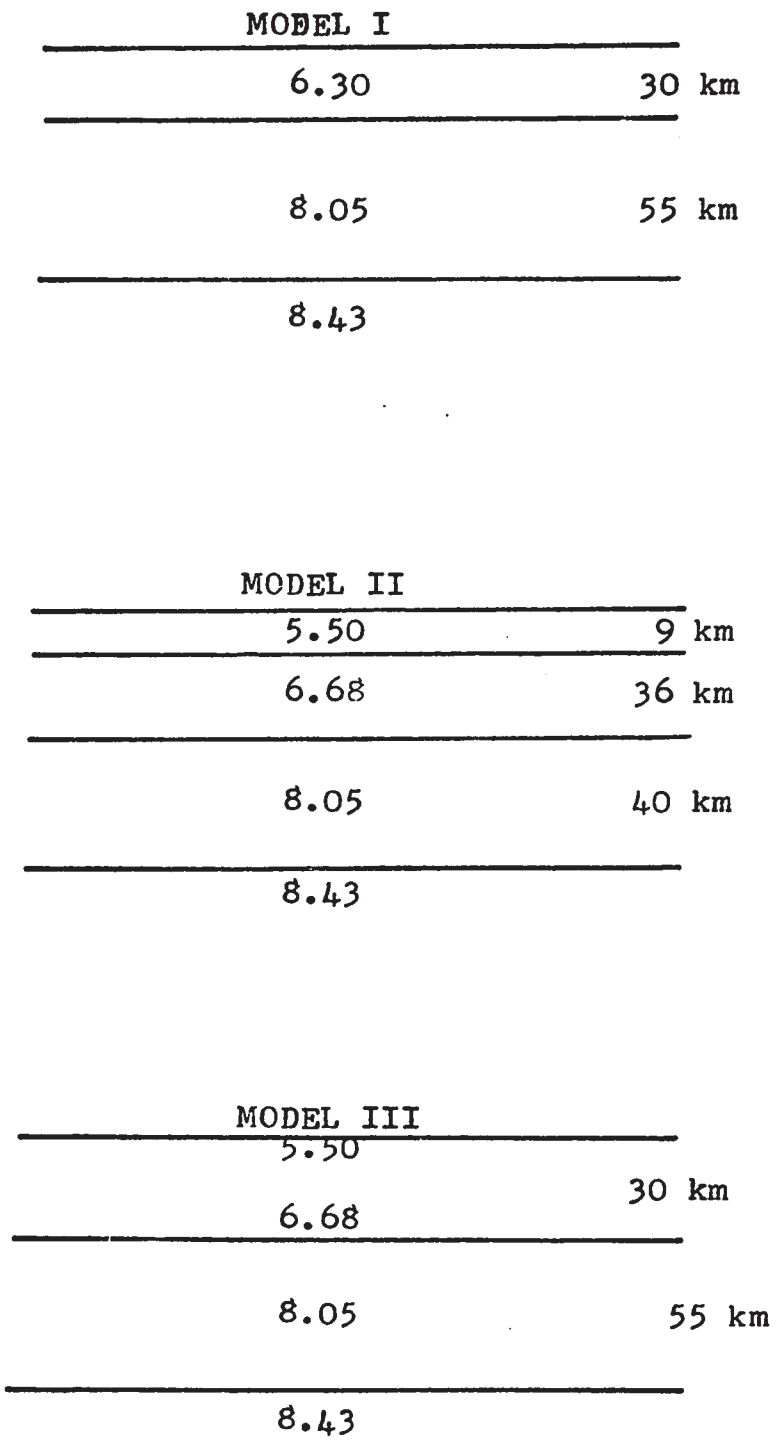

Figure 7 - 9 Diagrammatic representation of the three Early Rise models studied.

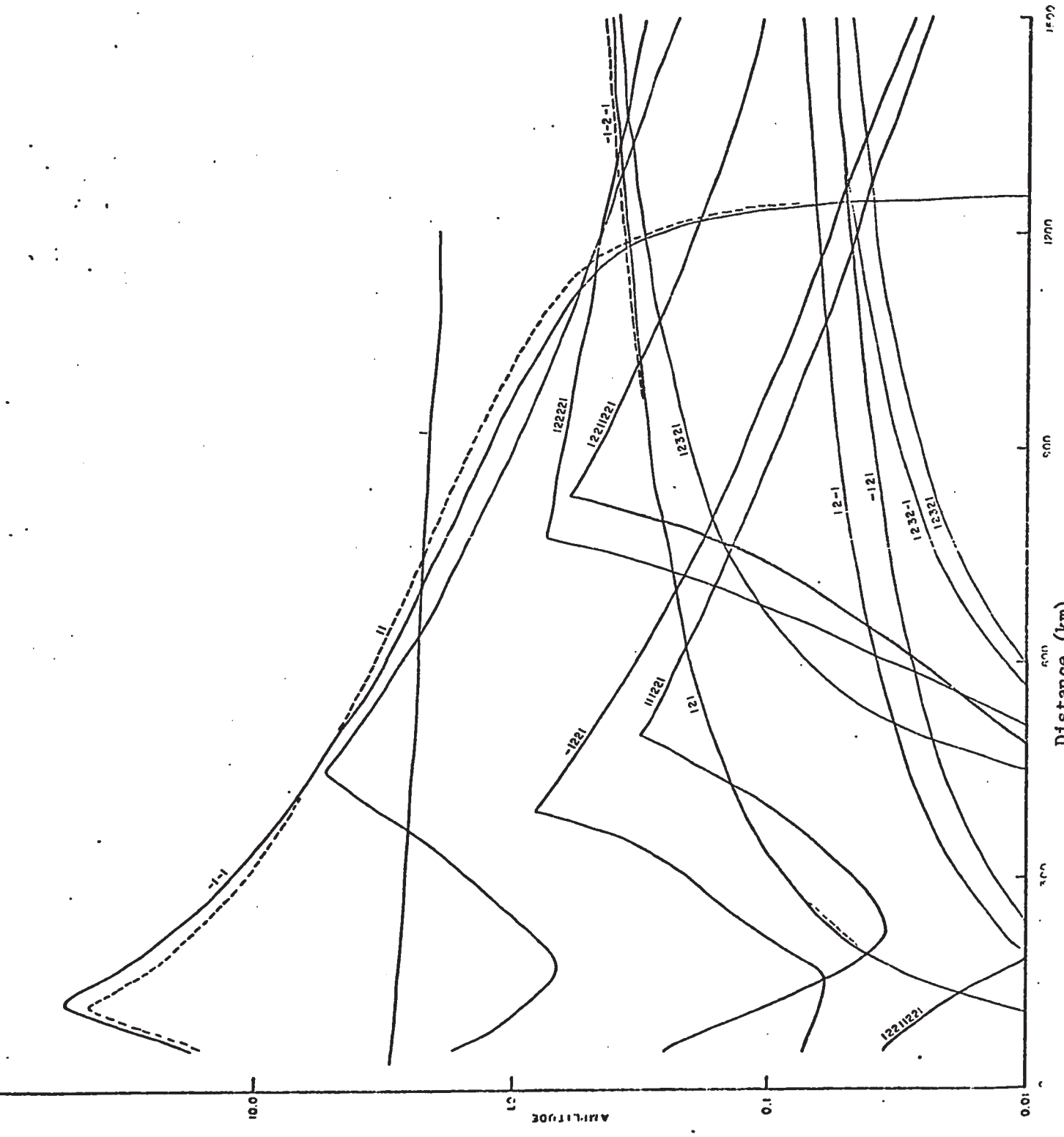

Fig. 7-10 (a) Amplitudes of major events for the crustal model given by Mereu and Hunter (1969).

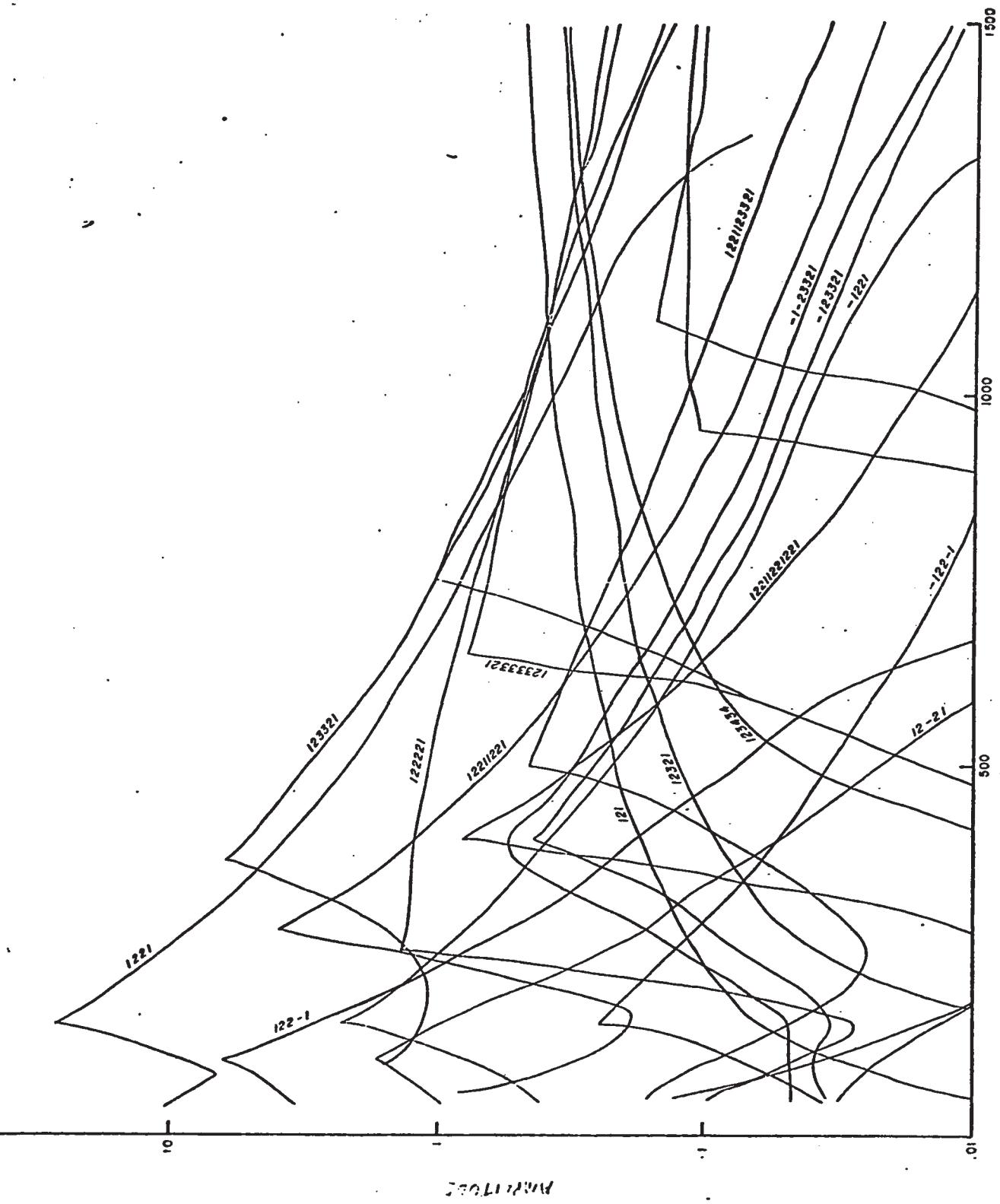

Fig. 7-10 (b) Amplitudes of major events for the crustal model given by Smith et al. (1966).

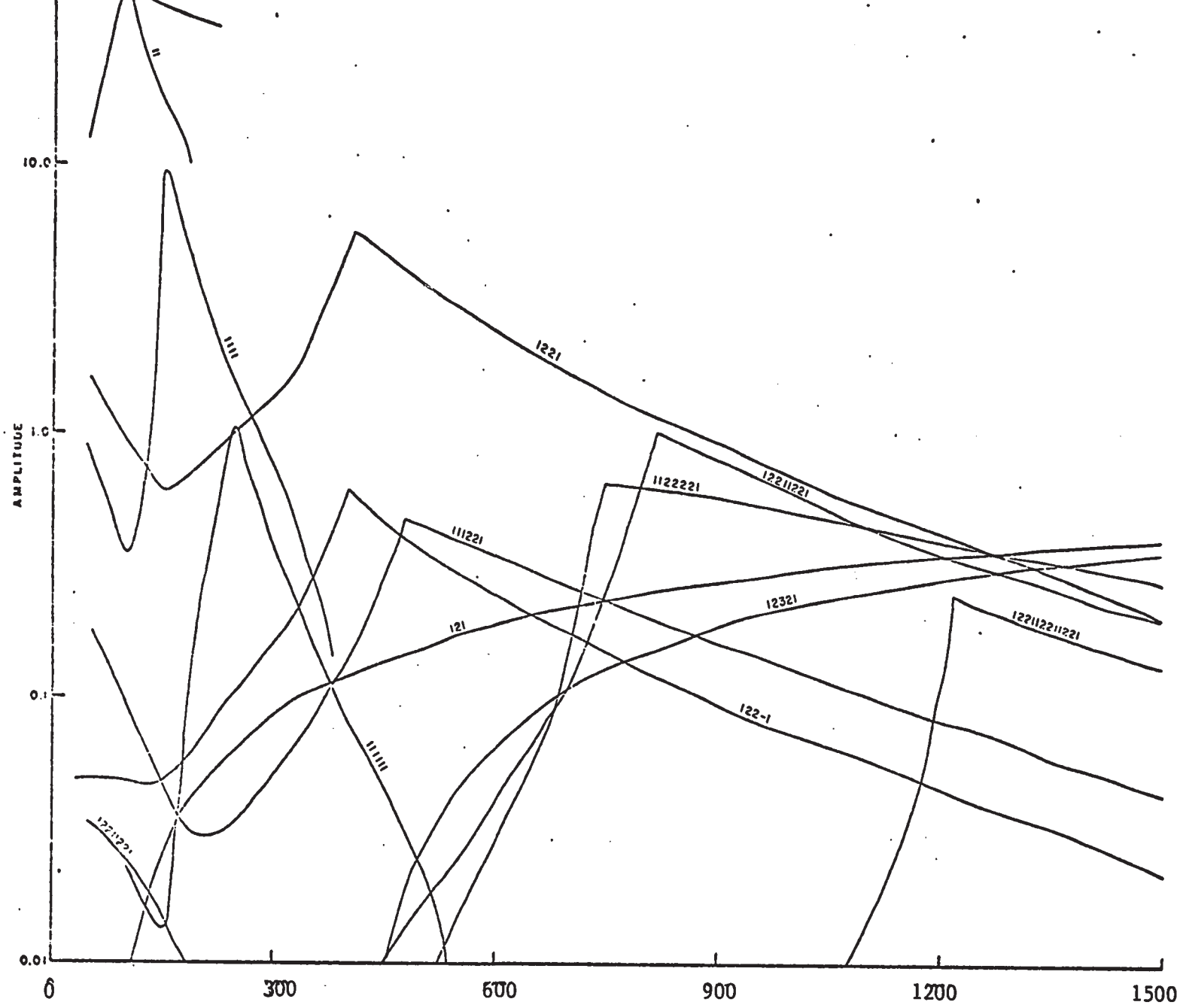

Fig. 7-10 (c) Amplitudes of major events for a variation of the crustal model given by Mereu and Hunter (1969) (see text).

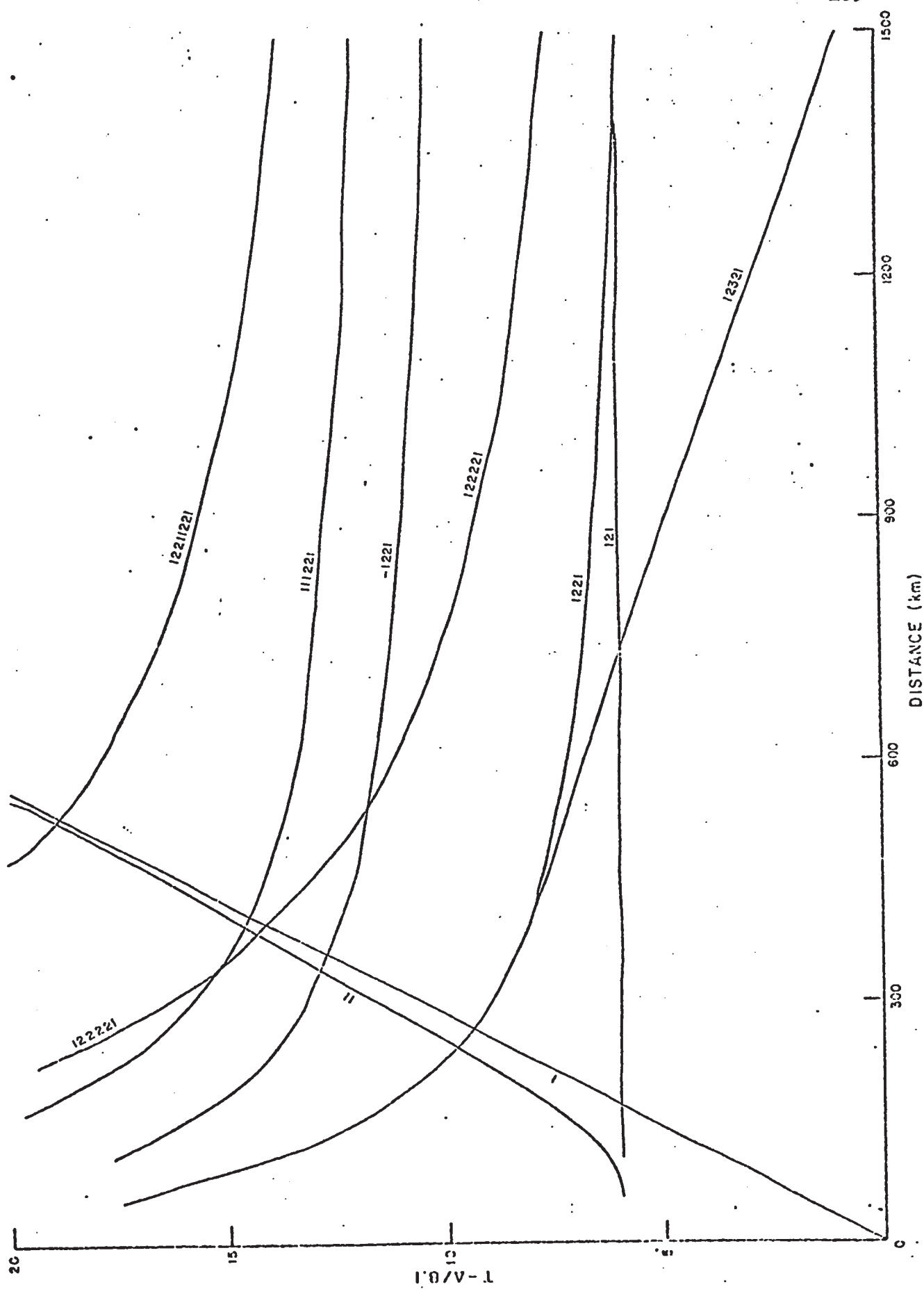

Fig. 7-11 (a) Travel times of major events for the crustal model given by Mereu and Hunter (1969).

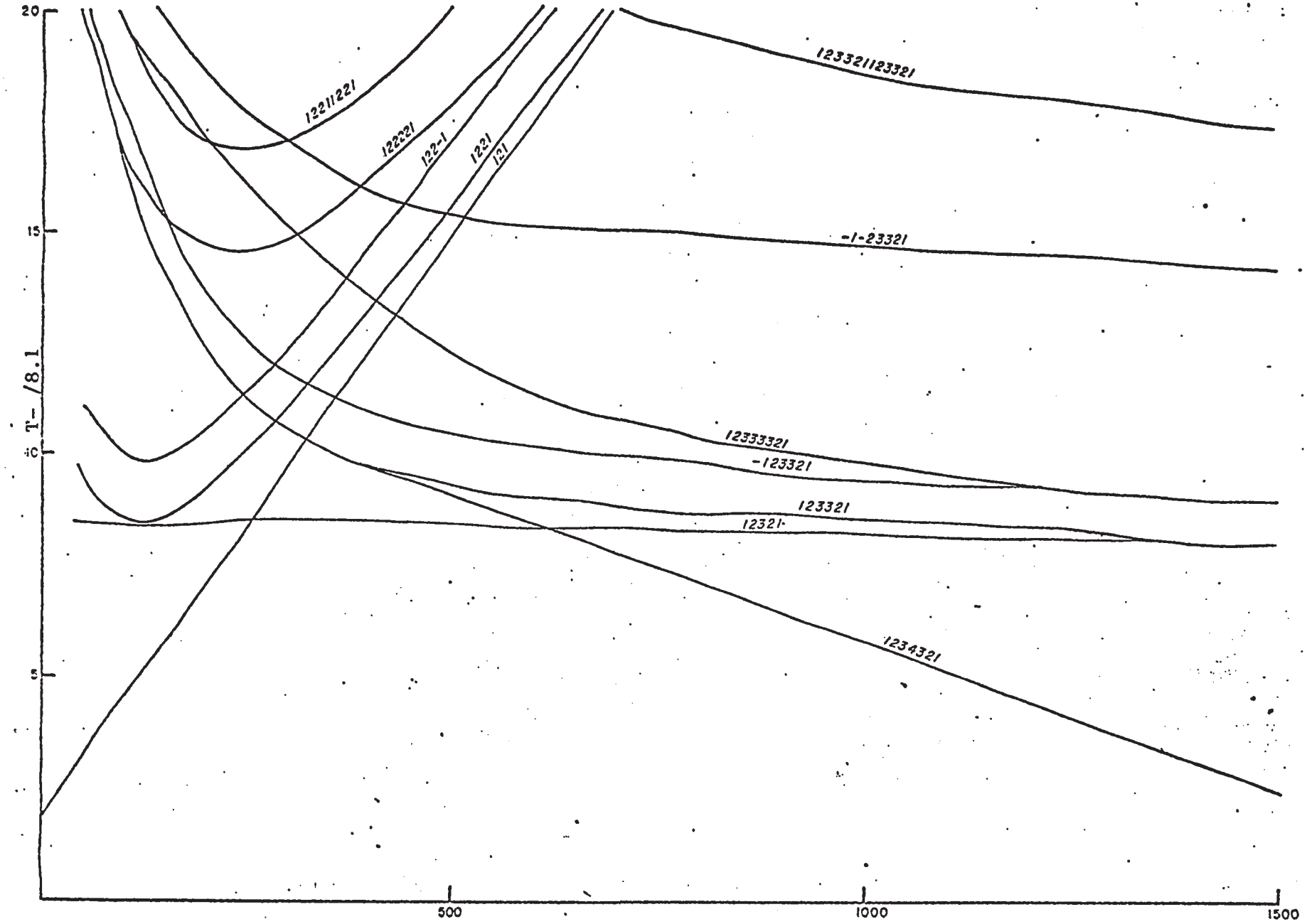

Fig. 7-11 (b) Travel times for major events for the crustal model given by Smith et al. (1966).

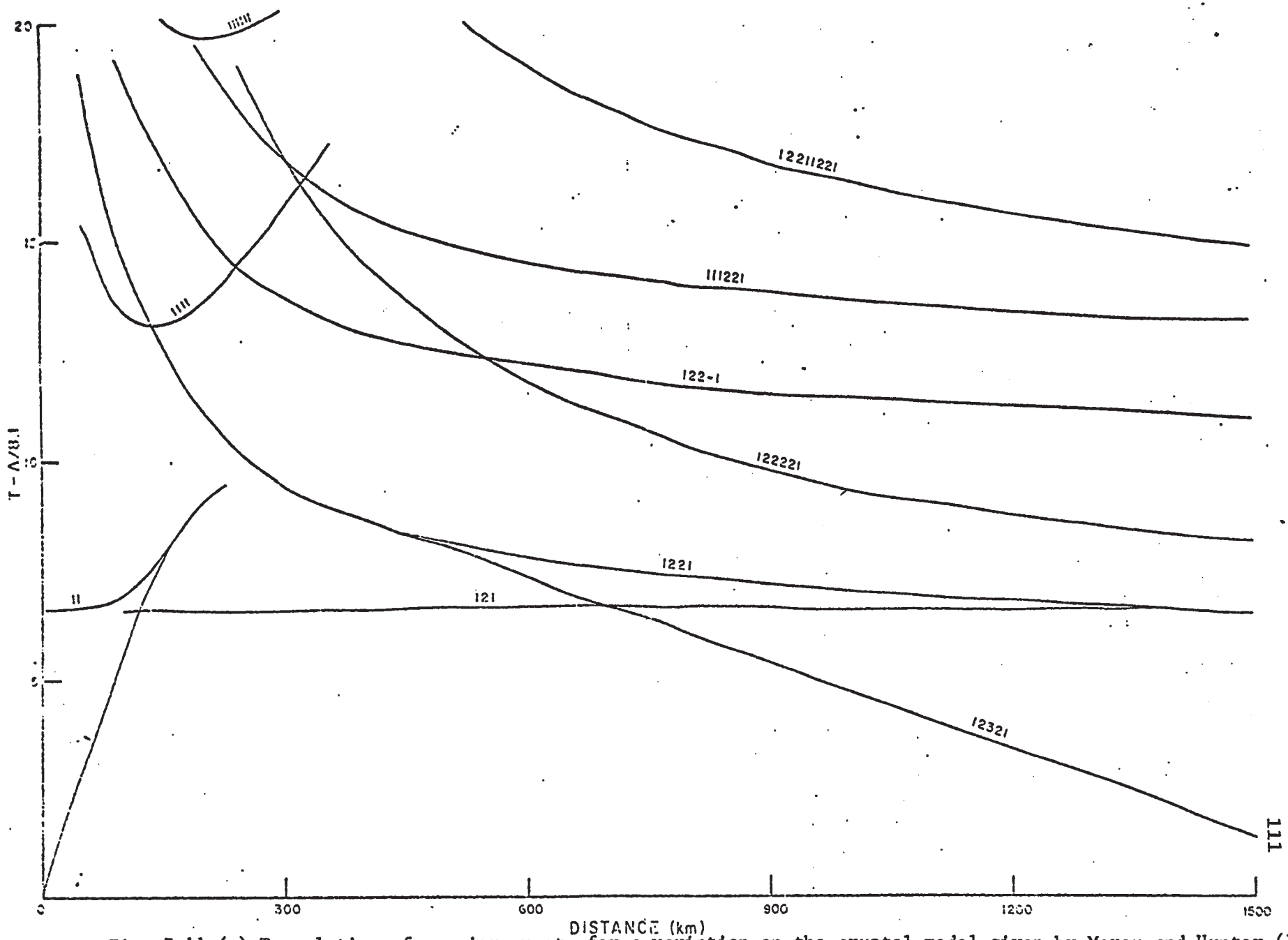

Fig. 7-11 (c) Travel times for major events for a variation on the crustal model given by Mereu and Hunter (1969)

The amplitudes and travel-times of similar events varied from model to model. A close study of these models along with the amplitude studies of the preceding sections have revealed several characteristics from which the following rules of thumb for interpretation have evolved:

1. Refracted P wave amplitudes are enhanced by the presence of a positive velocity gradient in the refractor.
2. Converted refracted wave amplitudes are very small compared to the P refraction. In no crustal model studied were the amplitudes sufficiently high enough to be observed as prominent events in a seismogram, and hence may be very difficult to detect.
3. Reflected P waves have high amplitudes, both for Moho and sub-Moho reflections. Amplitudes decrease if velocity gradients are present in the horizons above the reflector. Hence it is possible to have a reflector amplitude of the same magnitude as the refractor amplitude in the near range.
4. Over restricted portions of a record section multiple reflected P waves have high amplitudes and should be observable as prominent events. The position on the section where these events become observable may be a diagnostic feature; that is, the position of the peak amplitude of these events varies with the layer thickness.
5. The amplitudes of reflected P waves and multiples (including 'peg-leg' or 'trapped' multiples) are sharply curtailed at distances greater than the maximum amplitude positions, if velocity gradients exist in the layer. As well, velocity gradients tend to decrease the sharpness of the maximum amplitude peak.

6. Converted reflected events may be observed on a record section. If a reflected event suffers one mode change in transit the amplitudes may become prominent only in a restricted portion of the section. For a deep horizon, such as the Hales discontinuity, this may be in the range of 300-500 km.
7. Many reflections of high amplitudes exist in the near portions of a seismic section (out to 200 km) with travel times within a few seconds of one another. This suggests that the early portions of a seismic section may be difficult to interpret because of overlapping events.
8. Amplitudes of reflection events from a sub-Hales low velocity layer differ from those of a high velocity layer only in the position of maxima. Hence, although reflected events from a sub-Hales discontinuity may be observable, the velocity structure may not be.

CHAPTER VIII

THE APPLICATION OF DIGITAL FILTERING METHODS TO EARLY RISE RECORDS

8.1 Introduction

With the advent of high speed electronic computers with large immediate-access storage capacity, digital techniques have become increasingly popular in the seismic exploration for oil. Such techniques as phaseless band-pass filtering, deghosting, and multiple-trace correlation methods, have led to the enhancement of reflection events on exploration seismograms. Some of these routine techniques are applicable to crustal seismic work; however, the recording techniques peculiar to crustal refraction shooting lead to some specialized digital processing.

The following sections describe some digital filtering techniques which were performed on the Early Rise records in an attempt to enhance later events on the seismogram.

In order that an assessment of the success of a particular digital filter could be made, the unfiltered Early Rise line records as recorded digitally were produced in the form of a section for comparison with filtered results. A section of the vertical components is shown in Fig. 8-1. Gain adjustments, as shown, have been made regularly along the section so that later events could be maintained observable.

8.2 Low Pass Filter

A low pass filter can be considered a form of band pass filter wherein the band of frequencies passed is between 0 and a cut-off frequency f. All other frequencies are removed by the filter. The major advantages of a digital filter over an analog one are that digital

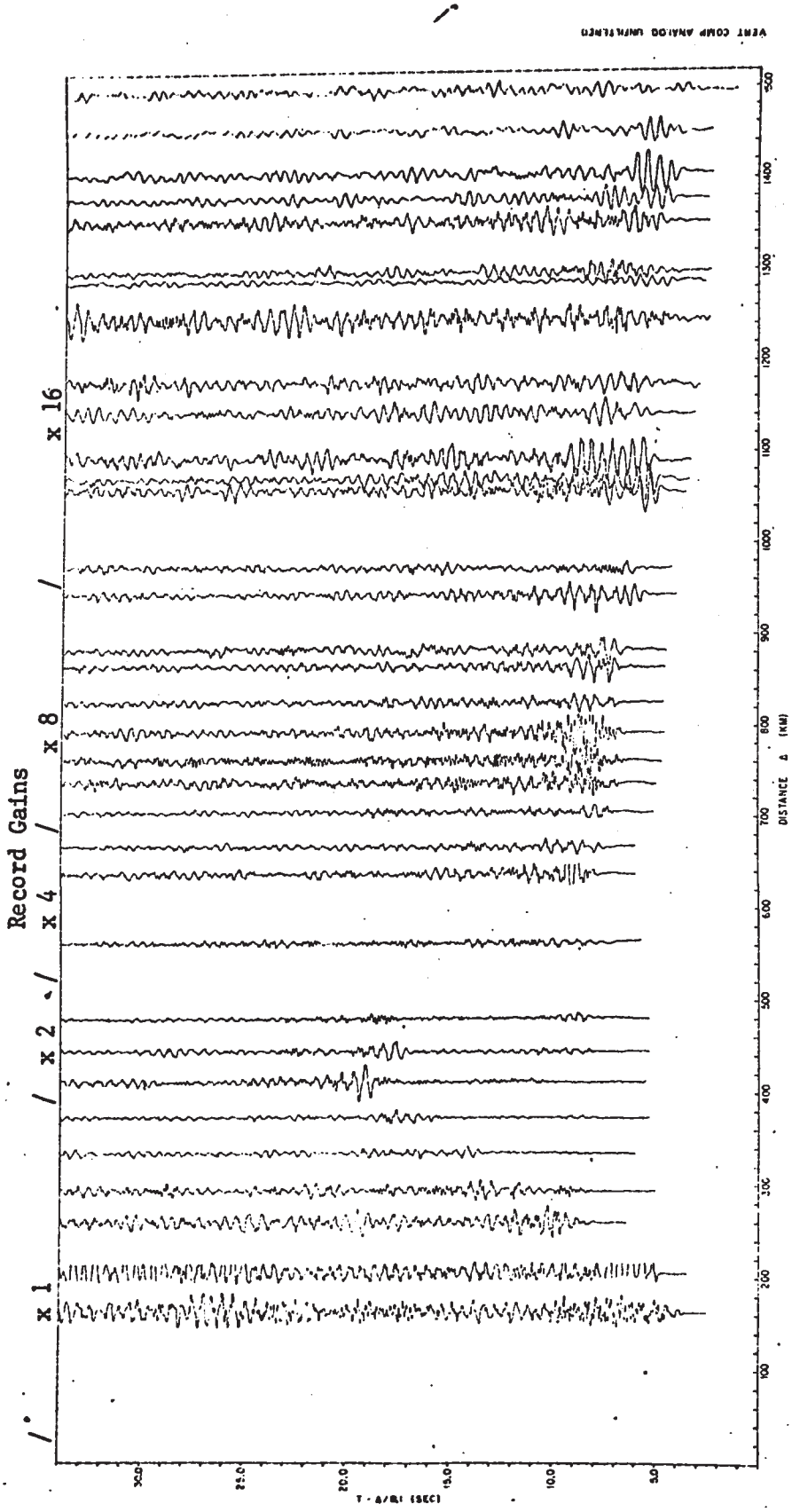

Fig. 8-1 Analog vertical component record section for the Early Rise line.

filters result in no phase distortion of the passed frequencies and, as well, sharp cutoff is possible at the band edges.

The design aspects of a lowpass filter are discussed by Blackman and Tukey (1958) and Robinson (1967).

In the design for the Early Rise records two aspects of the amplitude spectra were considered. The spectra for the early portions of the seismograms as given in Chapter V showed that most of the seismic energy was contained in the low frequency band below 5 hertz. As well, from the theory of aliasing, the uncertainty in the amplitude contributions of each frequency is greatest at the Nyquist frequency (22.5 hertz for Early Rise records). Hence it is determined that removal of the high frequencies from the records should improve the quality. Estimates of noise spectra for the seismic traces prior to the first arrival onsets suggest that the noise is broad-band but, however, for many records, is low in amplitude.

The filter function designed for the 5 hertz low pass filter is given in fig. 8-2. The length of the window used was 1.20 sec. consisting of 53 sample points. Truncation effects of the filter in the frequency domain were considered small and the cutoff slope was relatively steep. A computer program was designed to apply this filter to the Early Rise records. A comparison of a filtered and an unfiltered record is given in fig. 8-3. The loss of the high frequency components is clearly demonstrated; the events appear as overlapping sinusoidal wave trains with a dominant low frequency character (2 hertz).

The 5 hertz low pass filter was applied to the digital records of the Early Rise line. For ease in plotting the output by digital plotter, the maximum amplitude on each record was normalized to a pre-set

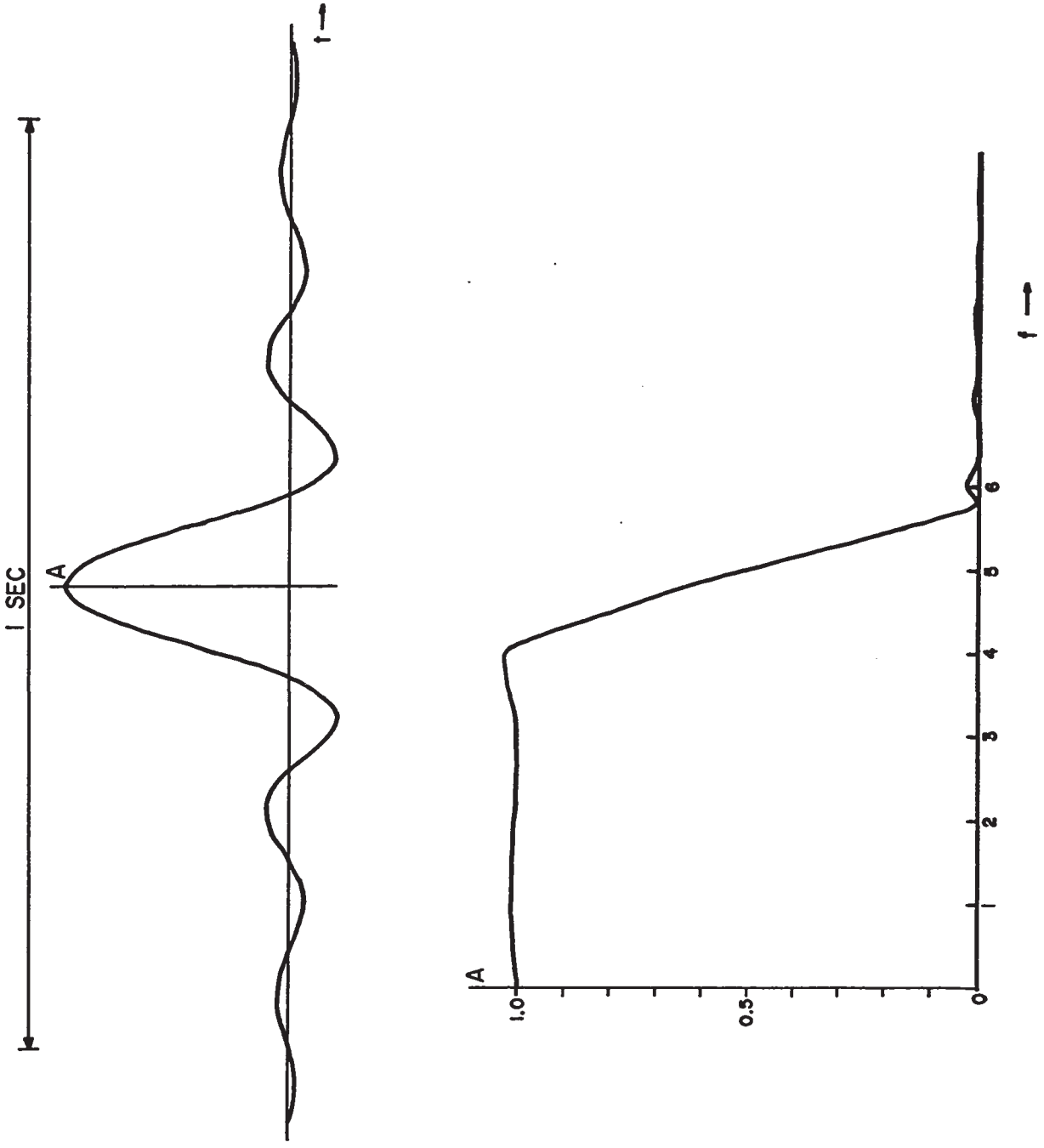

Fig. 8-2 Low pass digital filter design for the Early Rise records.

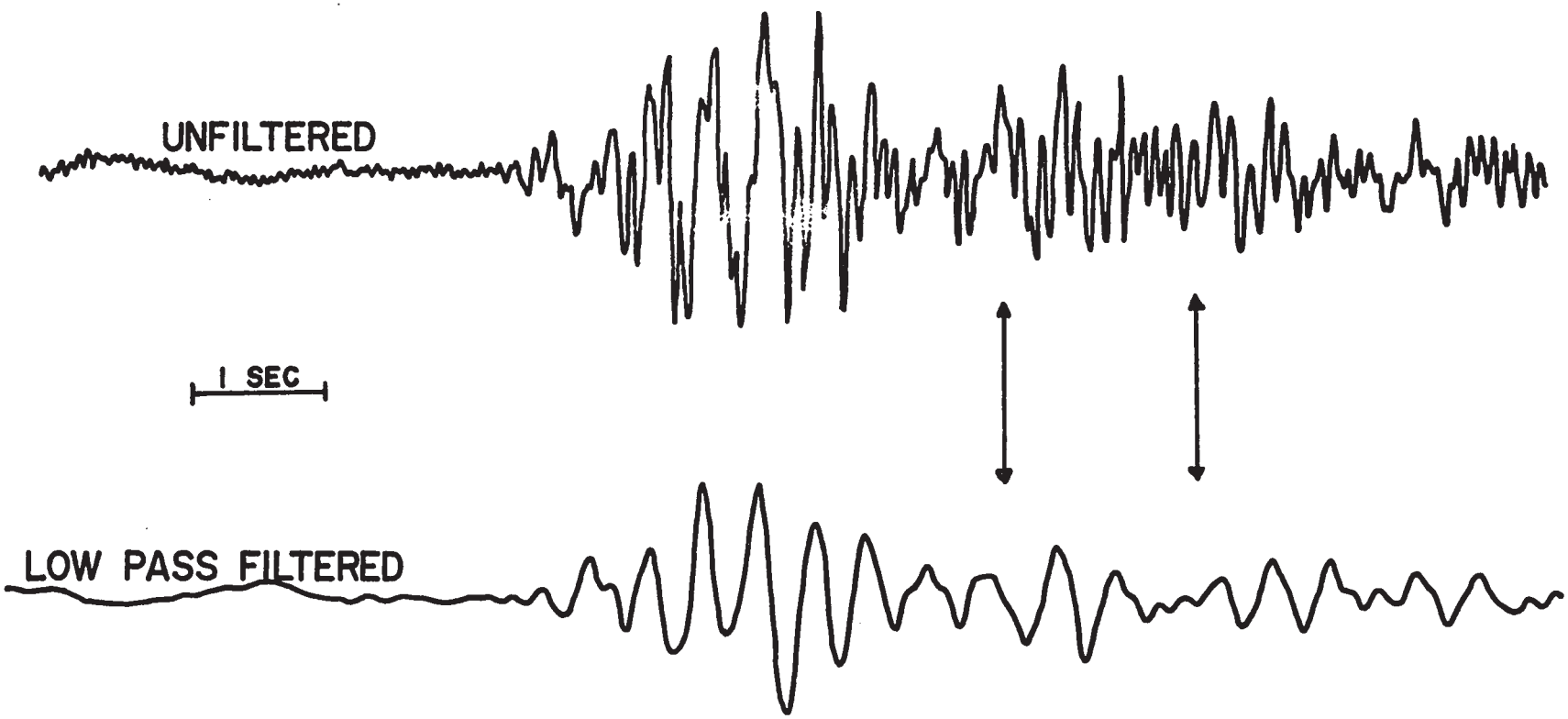

Fig. 8-3 Comparison of unfiltered and low pass filtered records. Arrows denote areas of improved signal detection.

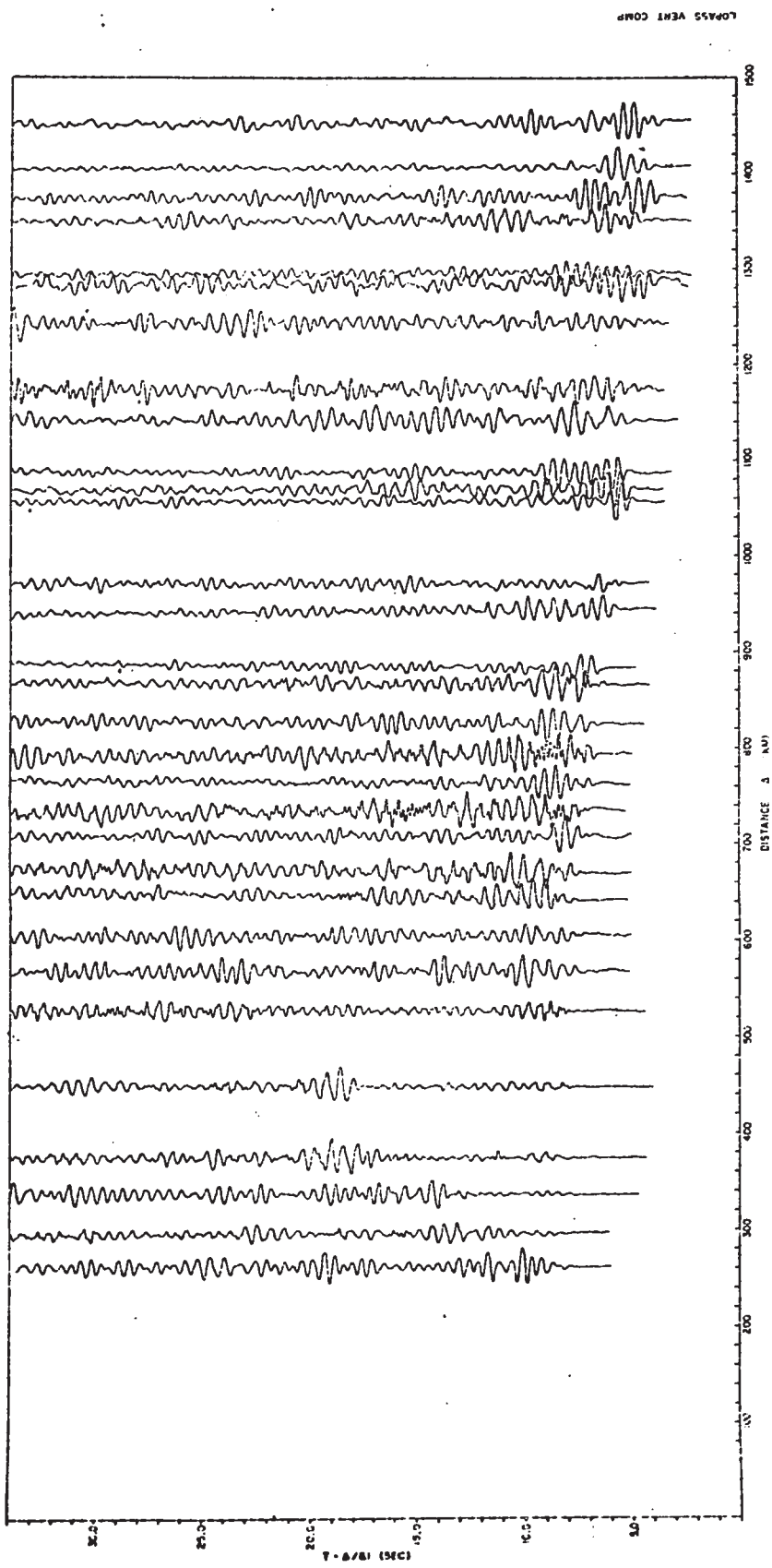

Fig. 8-4 Low pass filtered vertical component record section for the Early Rise line. Note: at locations 512 km and 605 km horizontal components have been substituted for 'dead' vertical traces.

maximum gain; a section composed of a selection of filtered records is shown in fig. 8-4 for the vertical component. In comparing this section with the unfiltered section, changes in the shapes of pulses are observed. Overlapping low frequency wave packets are observable throughout the section. The onset of the first arrival on the filtered section was found to be easily picked for most records, suggesting that the accuracy of picking of the first break does not diminish with low pass filtering. Clearly defined onsets of later events on the seismogram section are not often seen. This is reasonable in lieu of the large number of possible later events with long pulse durations.

8.3 Narrow-Band Filtering of Early Rise Records

From the measurement of the spectra of the Early Rise records, the energy has been shown to be sharply peaked about 2 hertz. In an attempt to enhance this energy peak, a narrow band filter was designed. In constructing the filter, the operator length and the slope of cut-off in the frequency domain determined the parameters. The time and frequency domain functions for the filter operator are given by Grant and West (1965) (p. 32). The shape of the filter operator chosen for the Early Rise records is given in fig. 8-5. The filter operator was applied to (convolved with) the vertical component of the digitized records. A comparison of a filtered and unfiltered trace is given in fig. 8-5. The effect of such narrow band filtering is seen in the almost monochromatic wavelets. Sufficient energy is retained in the low frequency range to produce wave shaping hence distinct packets may still be observed.

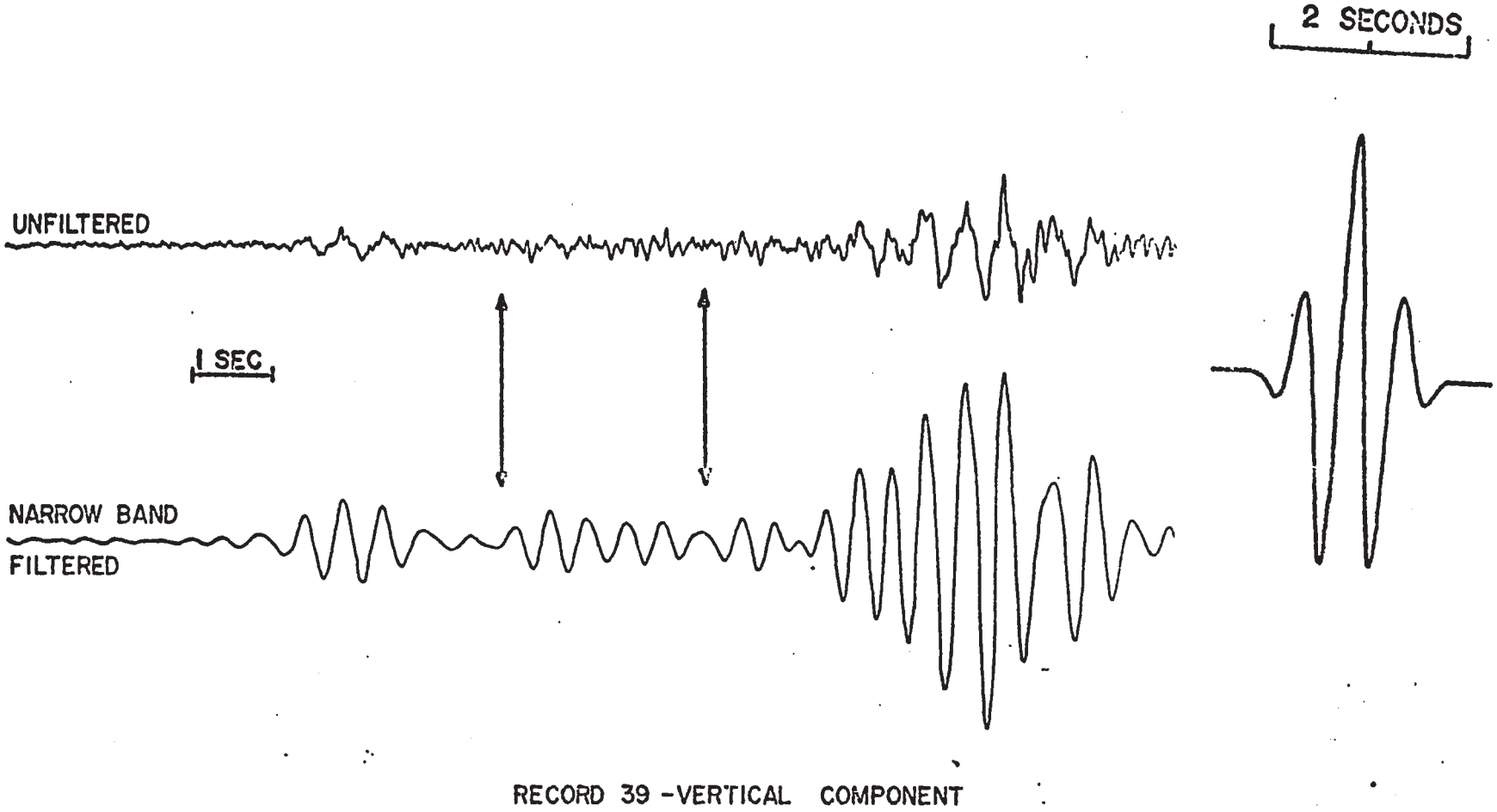

Fig. 8-5 Comparison of unfiltered and narrow-band filtered records. Arrows denote areas of improved signal detection.

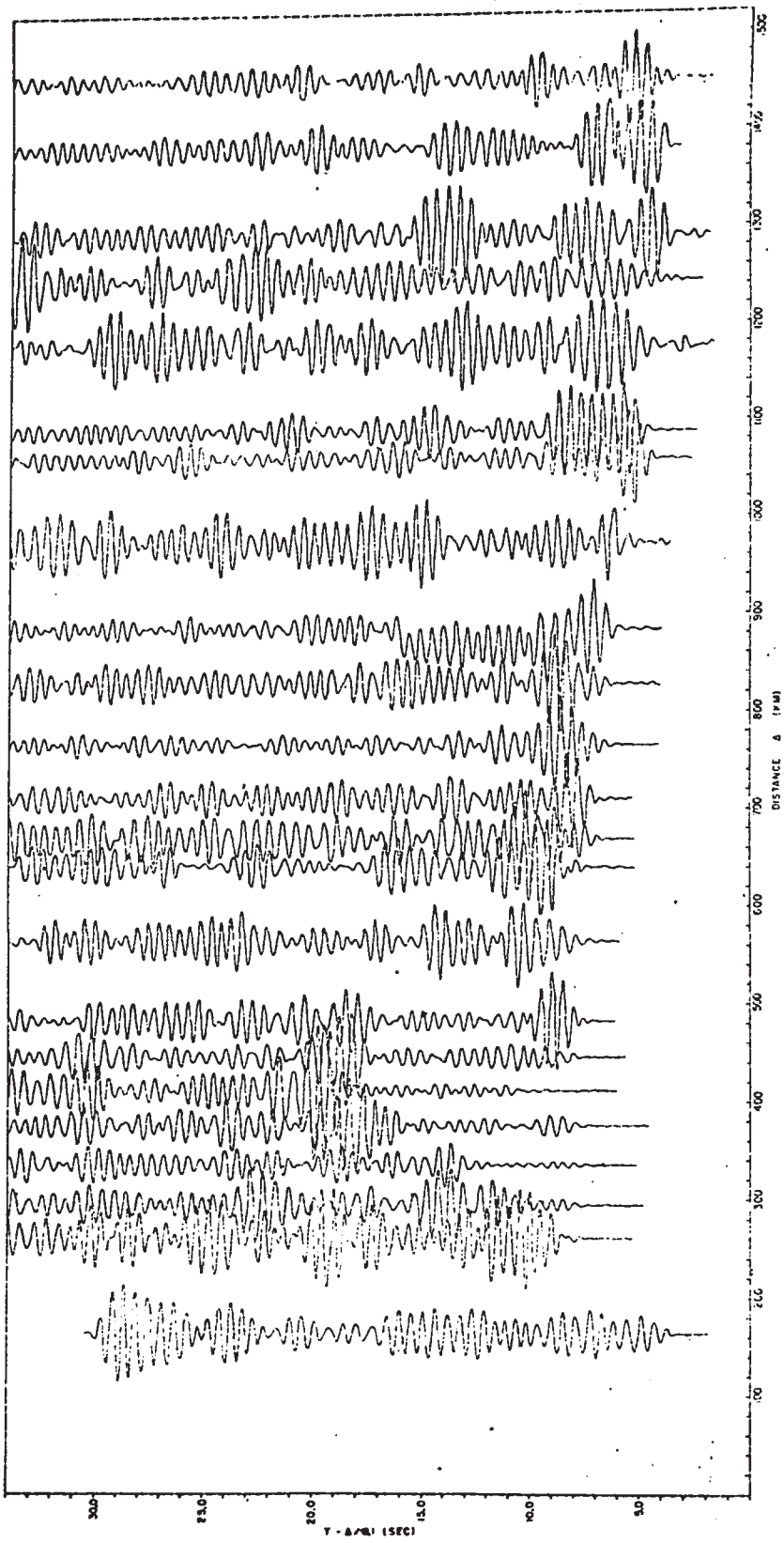

Fig. 8-6 Narrow-band filtered partial section of vertical component records for the Early Rise line.

A seismic section of a selection of narrow band filtered records is shown in fig. 8-6. In general, the filter tends to enhance weak later events at the expense of wavelet resolution.

8.4 Rectilinearity Filter

The relative amplitudes of vertical and horizontal ground motion, when sampled continuously on a seismogram, can be an indicator of wave type and of the amount of wavelet interference.

A compressional wave incident at the surface of the earth produces rectilinear motion acting approximately in the direction of the ray-path. Shear waves on the other hand, cause rectilinear particle motion in the direction perpendicular to the direction of propagation. Interference of either shear or compressional wave types causes motion which may be random or circular, having no particular orientation. Hence a measure of the rectilinearity and phase relationship between vertical and horizontal can be an indicator of later events.

A measure of rectilinearity of vertical and horizontal digitized components of ground motion can be obtained from the correlation coefficient defined as (Spiegel, 1961):

$$R(t) = \frac{n\sum_{i=1}^{n} V_i H_i - \sum_{i=1}^{n} V_i \sum_{i=1}^{n} H_i}{\left[\left(n\sum_{i=1}^{n} V_i^2 - \left(\sum_{i=1}^{n} V_i\right)^2\right)\left(n\sum_{i=1}^{n} H_i^2 - \left(\sum_{i=1}^{n} H_i\right)^2\right)\right]^{1/2}} \quad \ldots 8\text{-}1$$

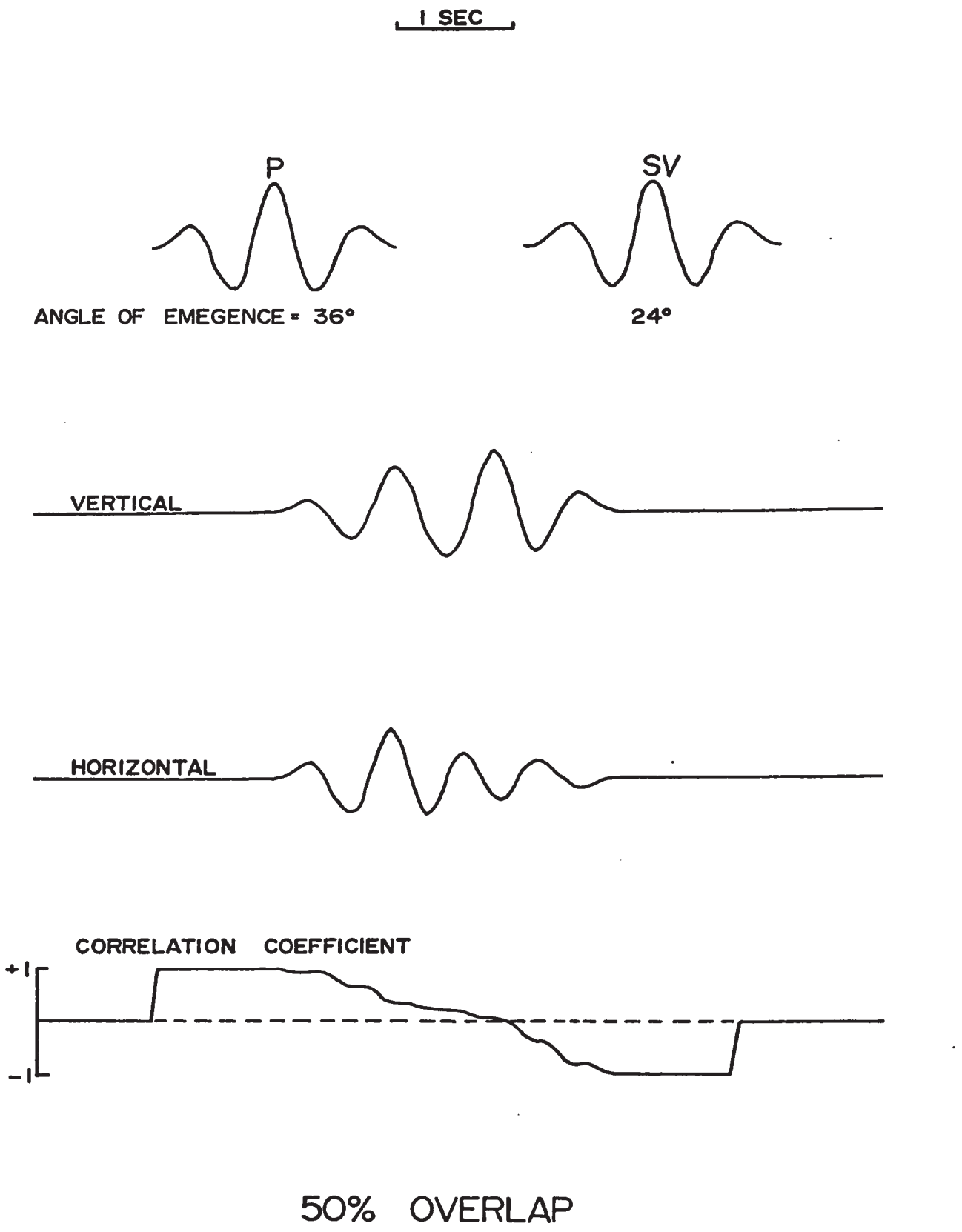

Fig. 8-7 The effect of wavelet interference on the correlation coefficient for the case of 50% overlap of compressional and shear events.

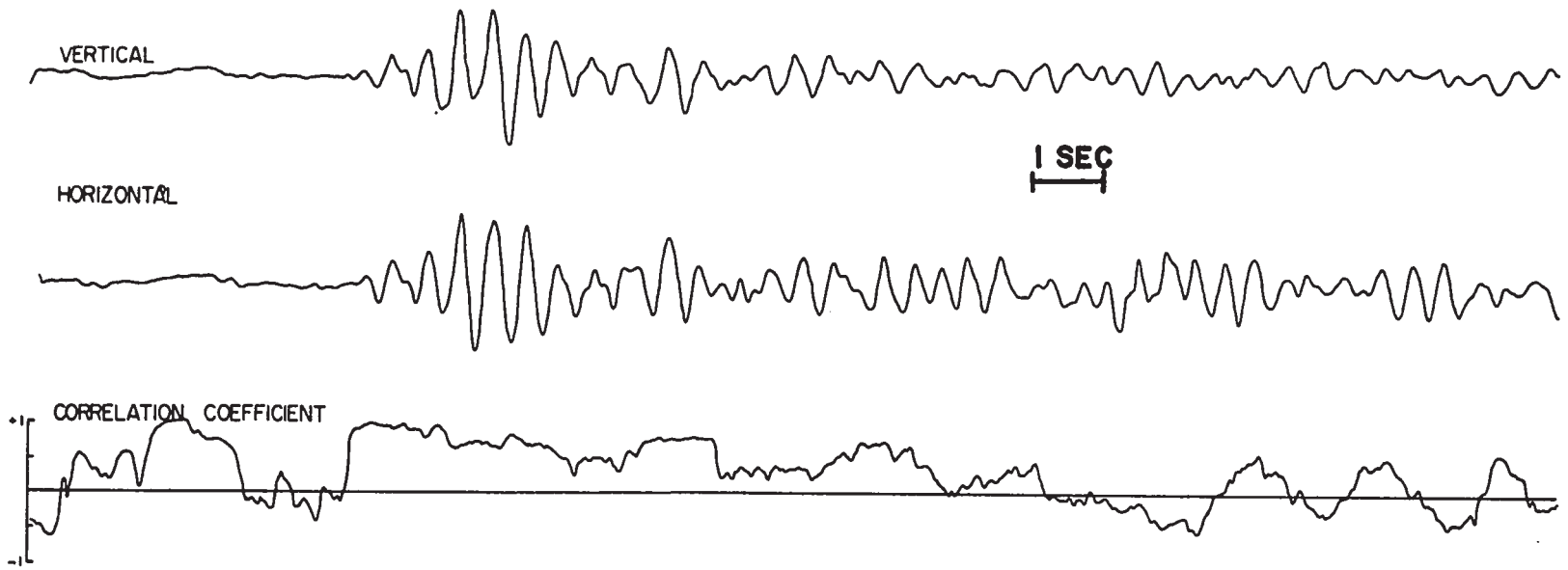

Fig. 8-8 A comparison of the correlation coefficient with the vertical and horizontal traces of an Early Rise record showing a good first arrival definition and the predominance of compressional events on the early portions of the seismogram.

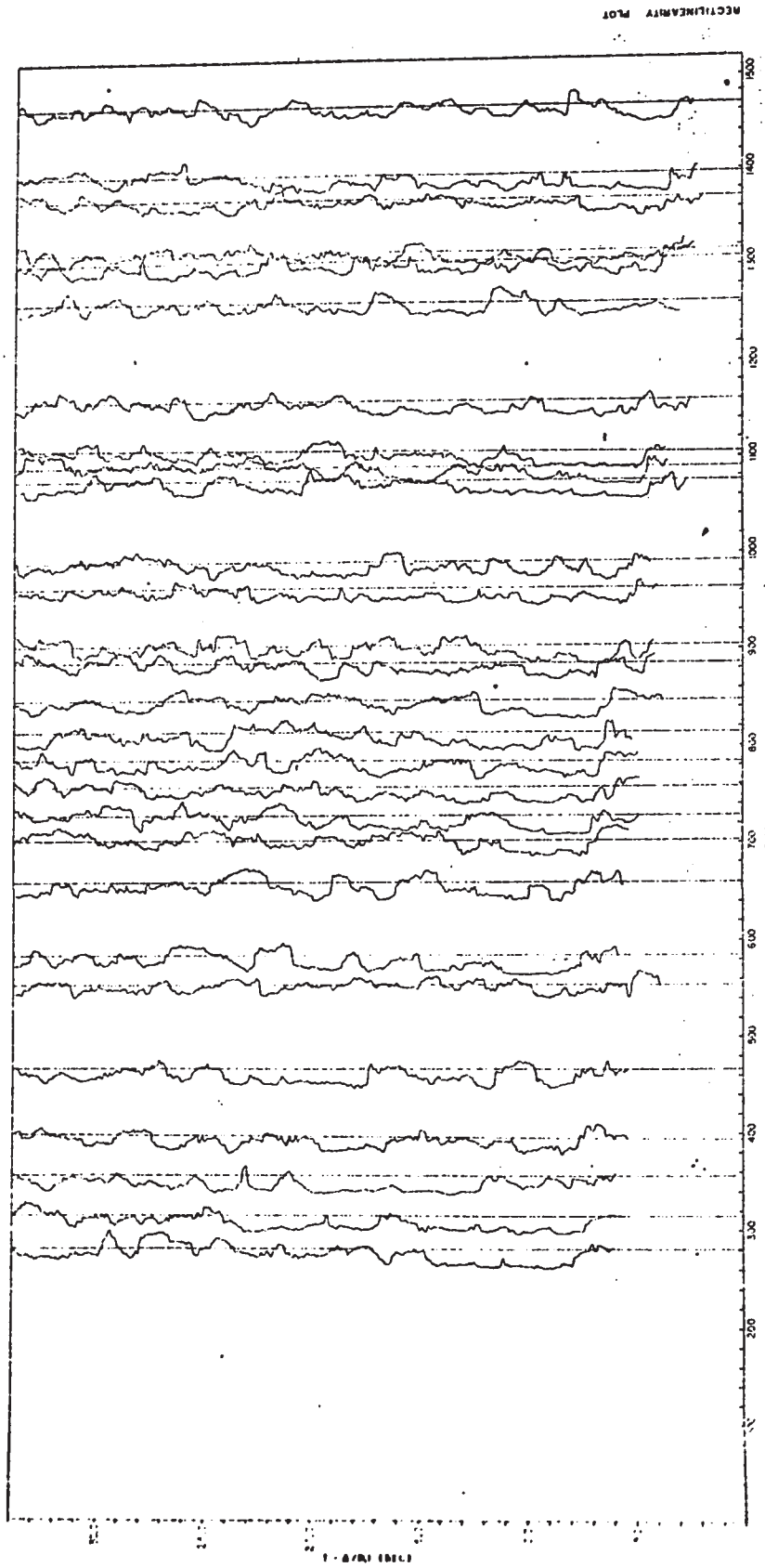

Fig. 8-9 Correlation coeficient section for the Early Rise line.

For a time window n measurements long, the correlation coefficient is +1 if the wave motion is entirely compressional and -1 if the wave motion is entirely shear. The coefficient approaches zero if the particle motion is random or circular indicating an interference effect as demonstrated in fig. 8-7.

A computer program was written to produce rectilinearity plots of the Early Rise records; the window chosen was 0.8 sec. long, a value assumed to be close to that of an individual wavelet and greater than one cycle of wave motion. A comparison between the correlation coefficient and low pass filtered interfering wavelets is shown in fig. 8-8 as an example of the technique. Not only zero crossings, but also abrupt changes in coefficient amplitude signal the onset of a new wavelet.

The results of the rectilinearity plots for the Early Rise seismic section are shown in fig. 8-9. Most records show an onset of the first arrival. Very little purely shear motion is observed. This suggests that shear motion is absent or at least is low in amplitude in the early portions of the seismograms. Degredation of the compressional motion by interfering P wave trains appears throughout the records. The onset of interfering wave trains often is sharply defined.

8.5 Mode Discrimination Filter

As a further attempt to utilize the three-component seismogram information, a filter was designed to discriminate compressional and shear events from the examination of the spectral components. The filter is based on the REMODE filter first described by Archambeau and Flinn (1965).

For a time window of a portion of a three-component seismogram, a filter in the frequency domain passing rectilinear motion can be described by:

$$F(f) = \left[\frac{Vr(f)\ Hr(f) + Hi(f)\ Vi(f)}{ABS(Vr(f)\ Hr(f) + Hi(f)\ Vi(f) + i(Vi(f)\ Hr(f) - Hi(f)\ Vr(f))}\right]^{n} \quad \ldots 8\text{-}2$$

where, $Vr(f)$, $Vi(f)$ = real and imaginary parts of the vertical component transform

$Hr(f)$, $Hi(f)$ = real and imaginary parts of the horizontal component transform

n = an integer determining the sensitivity of the filter.

The filter function F(f) varies between 1 for SV motion and 0 for $\pi/2$ phase shifts between vertical and horizontal, for each frequency component. An integer value n=7 was found to be sufficiently sensitive for the records (see also Lewis and Meyer, 1968).

To obtain filtered components, the filter transform is multiplied by the vertical and horizontal time window transforms respectively; the filtered transforms are converted back into the time domain. The time windows are shifted by discrete intervals down the seismic trace with a new filter function computed for each window. With the advent of fast Fourier transformation methods, filtering in the frequency domain is practical.

A further filter function was computed to discriminate separately between P and SV waves as given by:

$$F_p(f) = \text{SIN}\left(\tan^{-1}\left(\frac{Vr(f)}{Vi(f)}\right) - \tan^{-1}\left(\frac{Hr(f)}{Hi(f)}\right)\right) \quad \ldots\ 8\text{-}3$$

$$F_s(f) = \cos\left(\tan^{-1}\left(\frac{Vr(f)}{Vi(f)}\right) - \tan^{-1}\left(\frac{Hr(f)}{Hi(f)}\right)\right) \quad \ldots . \; 8\text{-}4$$

One of these filter functions was multiplied with the Remode filter to produce a wave discrimination filter. The time window selected for the filter technique was 1.42 sec, a length governed by the assumed pulse width, digital interval and window requirements for the fast Fourier transform method.

A comparison of the original unfiltered record and the P and SV filtered records for two components of an Early Rise record is given in fig. 8-10. The gain adjustments made to the filtered records suggest that the majority of the events on the record are compressional. On the SV discrimination records events have been relatively enhanced, but overall amplitudes are very low.

A section composed of a selection of filtered records is given in fig. 8-11 for the vertical component. The later arrivals corresponding to isolated compressional events appear to be enhanced by the technique. The occurrence of both low and high frequency oscillation can be seen on some of the records. The sporadic enhancement of these frequency components must be tolerated for increased filter sensitivity.

8.6 Discussion of Filter Results

From a comparison of the filtered sections with the unfiltered section the relative values of the filter techniques can be judged. The removal of high frequencies above 5 hertz tends to enhance the identification of later events. This suggests that the high frequency contribution to the seismogram appearing after the onset of the first arrival may in part be signal generated noise in the vicinity of the recording station.

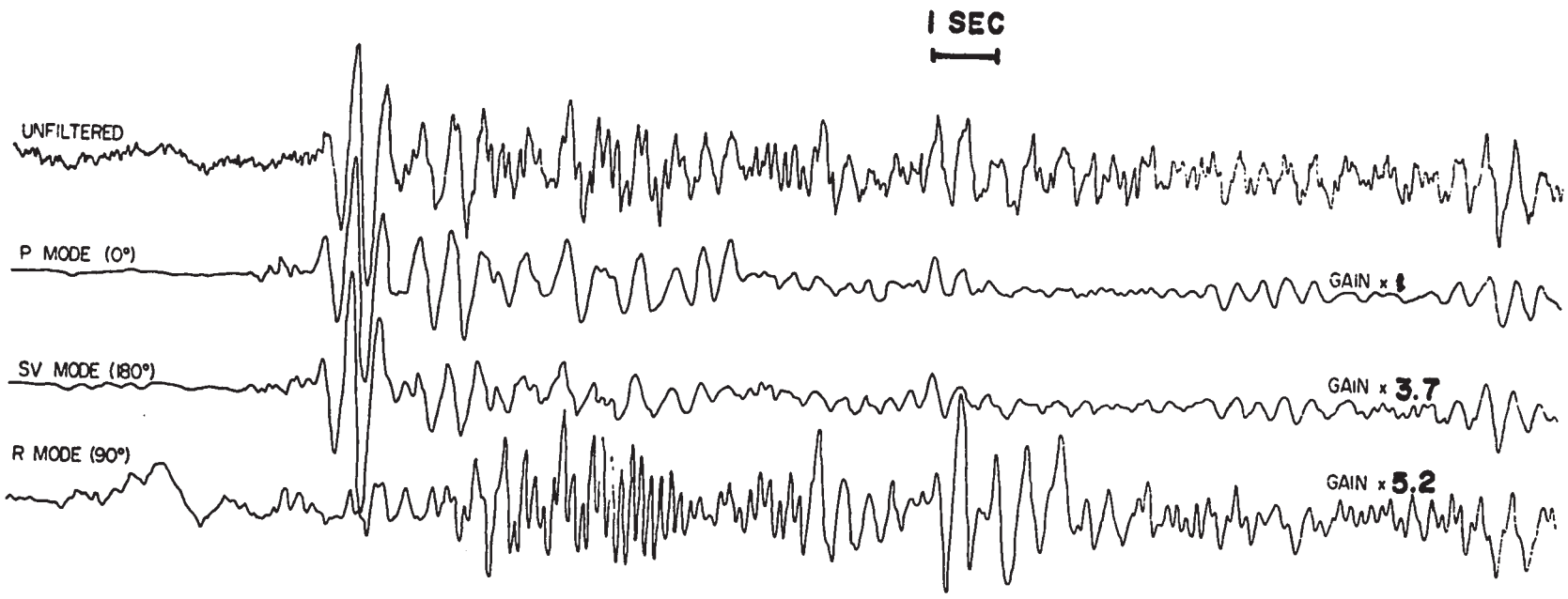

Fig. 8-10 Comparison of the mode discrimination filter for P, SV, and Rayleigh modes for an Early Rise record. Note the differences in gains between traces.

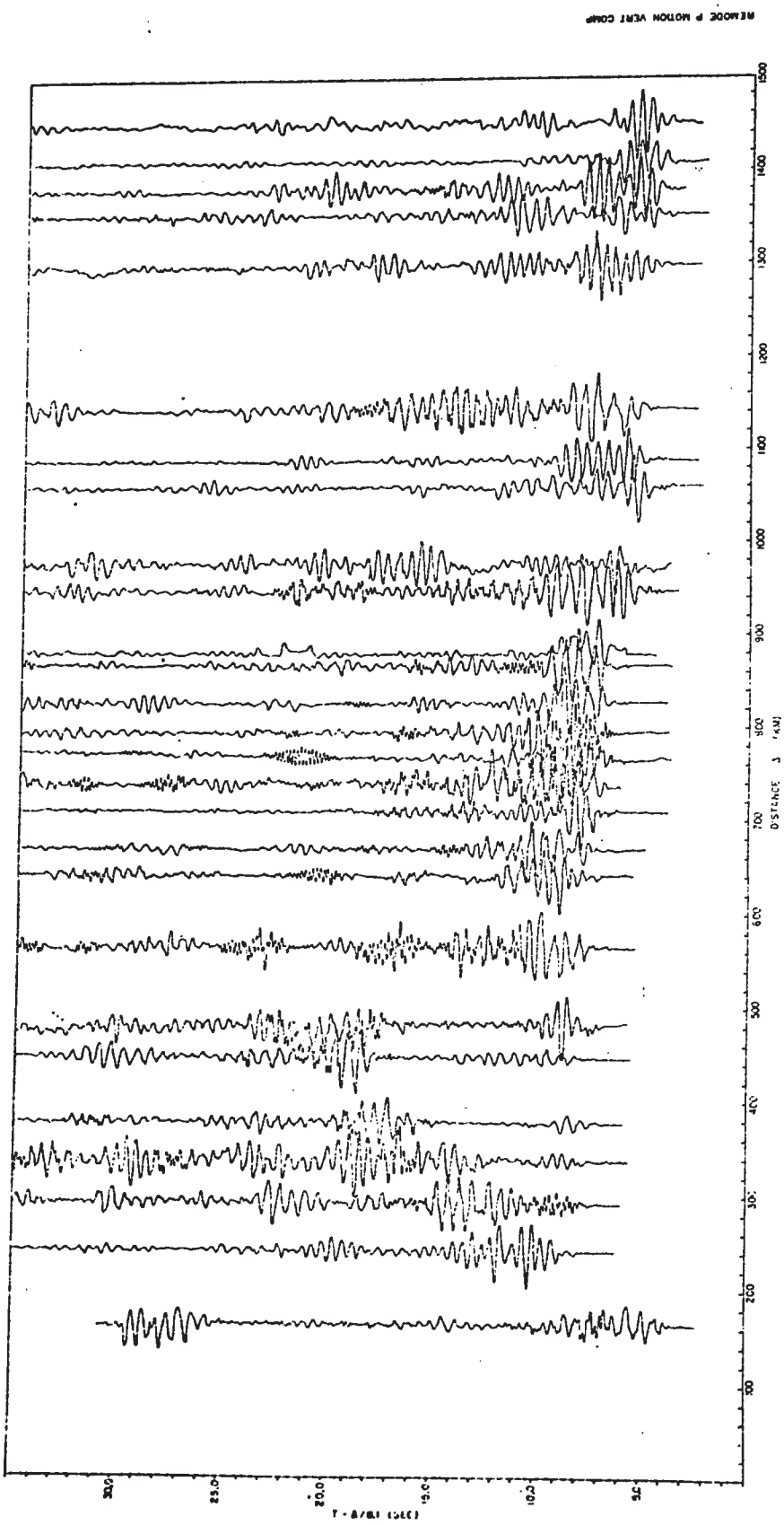

Fig. 8-11 Section of P mode filtered records for the Early Rise line.

Narrow band filtering of the Early Rise records tends to shape events in the form of well-defined packets consisting of several cycles. Definite improvement in the detectability of events is noted in some portions of the section, especially on the records from distant stations. However, in portions of the section where multiple events occur (500 - 1000 km) the separation of events is suppressed and 'ringing' occurs.

The results of the rectilinearity plots in the form of a section cannot be considered to be independently interpretable. Broad outlines of the wave types and onsets are interpretable but trace to trace correlation can be done only with reference to a 'wiggle' trace section. On several records the rectilinearity plot has been found to be an accurate indicator of the onset of the first arrival. The arrival onset is correlated with the mid-point of the first-indicated compressional step discontinuity. The order of accuracy of picking the onset with this technique is similar to that using the seismic trace, and can be used as an alternative method for picking first arrival onsets.

The most promising of the digital filters is the Mode Discrimination filter. The results of this filter when compared to the unfiltered section and other filtered sections show the most enhancement of events of the seismograms. Most of the filtered pulses demonstrate a large amount of low frequency content similar to predicted models, suggesting that much of the high frequency content on the seismograms may be 'noise', of either the ambient or signal-generated type.

Comparing the various filtered sections to the unfiltered one, it can be concluded that the filters described above have each contributed to the enhancement of later events on the seismogram.

CHAPTER IX

IDENTIFICATION OF LATER EVENTS

9.1 Character of Seismic Events

a) Theoretical Impulse Response

The basic properties of an underwater explosion are given by Cole (1948 Arons (1954), Weston (1960), and O'Brien (1960). An explosion, detonated on the bottom of a lake, radiates energy downwards into the bottom as well as upwards as a hemispherical supersonic shock wave. The amount of energy radiated downwards depends upon the type of bottom. For a hard-packed sandy mud bottom, Cole (1948) found that approximately 36% of the initial impulse was transmitted downwards. The impulse imparted to the water is approximately that generated by 1.85 times the weight of explosive used in an infinite depth of water (since the impulse varies with the 1/3 power of charge weight). Thus a rather strong water wave is set up which is supersonic only in the vicinity of the explosion point. When reaching the air-water surface, the wave reflects as a rarefaction. Cole (1948) states that negative pressures reflected downwards with values greater than one atmosphere are probably not realized. Much of the energy instead goes into the cavitation phenomenon: that is, into the development of cavitation bubbles at the surface of the lake. Thus if the peak pressure of the explosion is greater than one atmosphere (14.5 lb/in^2) at the air-water interface, the reflected wave will probably be severely attenuated. For explosive weights and water depths used in crustal refraction surveys, surface pressures above those required for the cavitation phenomenon are often reached. For the 1966 Lake Superior experiment, all shots were 10,000 lbs exploded on bottom

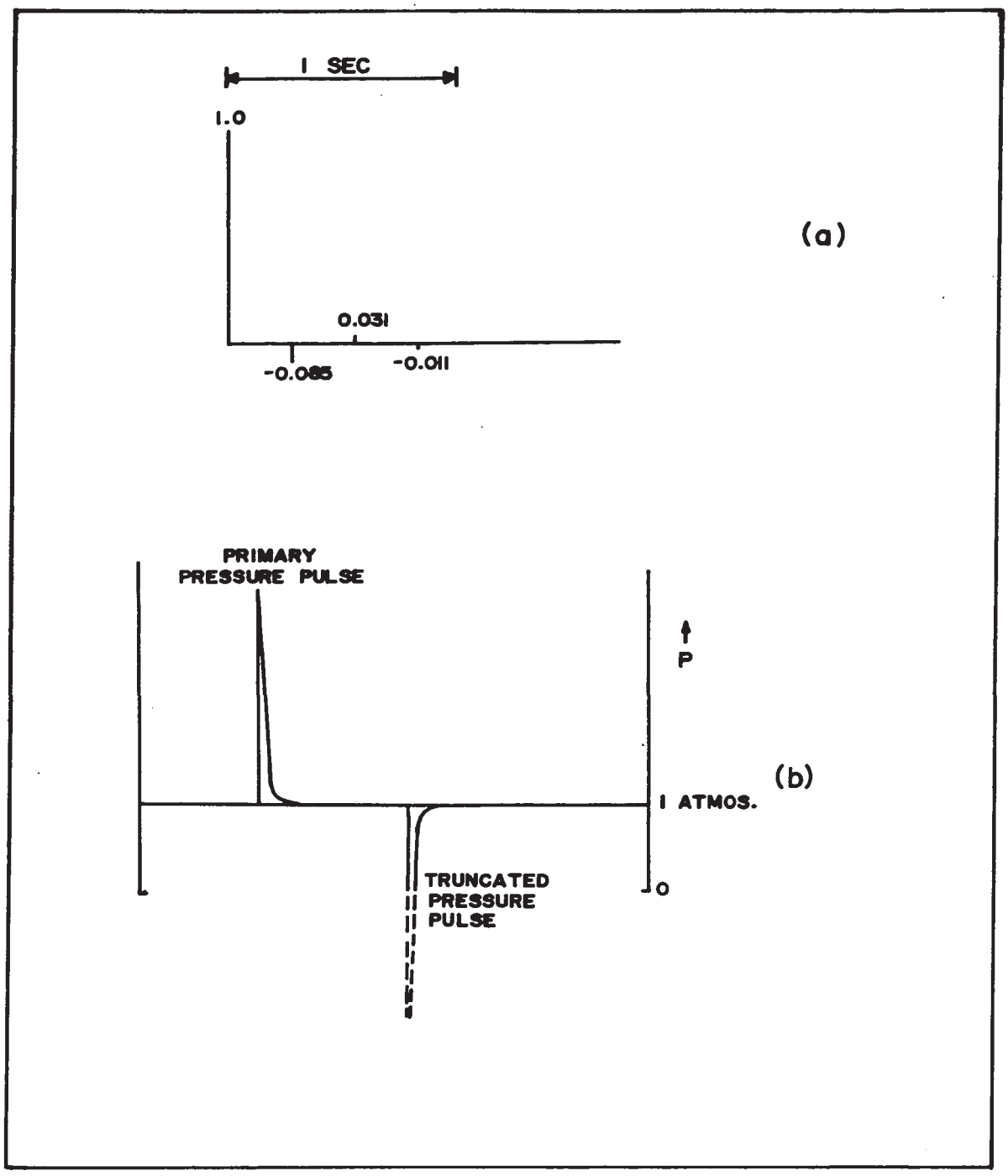

Fig . 9-1 (a) Stickogram of input pulses for the Lake Superior shots,
(b) the truncation effect on the impulse due to cavitation.

at a depth of 600 ft giving rise to a peak pressure at the water-air interface of approximately 40 lb/in^2 (from curves given by Arons, 1954). Thus it must be assumed that some energy was lost to cavitation. The reflected rarefaction impulse, having a peak pressure of 14.5 lb/in^2, gives the appearance of being reduced to a value of 0.13 of the primary positive impulse when viewed from a large distance. If one considers the partition of energy on the lake bottom for multiple reflections as that given above for the positive impulse, the impulse response of the Lake Superior 1966 shots would be as given in fig. 9-1 (a).

The above model impulse response from multiple reflections has been deduced entirely from observational results mainly based on the work of Cole (1948). Since the impulse is the time integral of the exponential pressure pulse form, the values of the impulses assumed to be due to later reflections of truncated pulses may be considered as lower boundary values to impulse models; that is, the model given above assumes the pressure pulses to be spike pulses of finite amplitude. For the Lake Superior 10,000 lb shots, this assumption is valid, since the time constant (effective pulse width) of the pressure pulse for the first surface reflection is approximately 4 milliseconds (Arons, 1954). A qualitative explanatory diagram of the deviation of peak pressure for the surface reflection is shown in fig. 9-1 (b).

Following the initial shock wave from an explosion in open water, is the secondary pulse produced from the oscillation of the gas bubble. The theory of bubble oscillation is given by Cole (1948) and Weston (1960). For the Lake Superior 1966 shots, the positive impulse from the first oscillation of the bubble after the initial shock wave

has been computed to be approximately 0.083 times that of the primary impulse (Weston, 1960, eq. 7) which occurs at a time of 2.0 seconds after the primary pulse. The second bubble impulse is approximately 0.02 times that of the primary and is generated 3.44 seconds after the primary pulse. The small bubble pulses are reflected as well by the air-water interface and the bottom to produce very low amplitude multiple impulses as previously described.

Attenuation and Dispersion Response

A theory of attenuation and dispersion of body waves in an imperfectly elastic medium has recently been given by Futterman (1962). Following his notation, the amplitude of a monochromatic displacement wave of frequency w is:

$$A(w,t) = A_o(w,0)\ e^{i[wt - K(w)R]}$$

where $K(w) = k(w) + i\alpha(w)$

Futterman shows that the real and imaginary parts of K(w) can be related by:

$$k(w) = (1 - (\ln x/\pi Q_o))w/c \qquad \text{for large } x$$

$$\alpha(w) = w/2Q_o c$$

where Q_o = specific attenuation factor

$x = w/w_o$ where $w_o \ll 1.0$

$\simeq 10^{-4}$

c = non-dispersive wave velocity

The amplitude of the particle velocity may be then considered as:

$$U(w) = wA_o(w,0)\ \exp\ (-wT/2Q_o + i(wt - (wT - wT \ln x/\pi Q_o)))$$

where T = the travel time of the wave

t = 0 the arrival time of the wave

and t > 0 after the arrival time of the wave.

The phase lag decreases with increasing frequency suggesting that higher frequency components travel at higher velocity in the medium. The phase velocity variation for the upper mantle is, however, negligibly small (Wert et al., 1962). The attenuation coefficient has a large effect on the observed amplitude spectrum. The attenuation analysis of the Lake Superior Early Rise experiment (given in another chapter) suggests that Q_o lies in the range of 100 - 200 for the upper mantle.

Instrumentation Response

The manufacturer's geophone and amplifier responses along with measured verification of the responses are given in Chapter II. Since the attenuation response removes the higher frequencies, the most important portion of the instrumentation response is the low frequency response. Hence any change in filter settings for a high frequency cut-off greater than 10 hertz will not substantially change the signal response of the earth-model.

Combined Responses

The time domain and amplitude responses for the values of Q_o of 100, 150 and 200 and a travel time of T = 100 for the lab model are given in fig. 9-2.

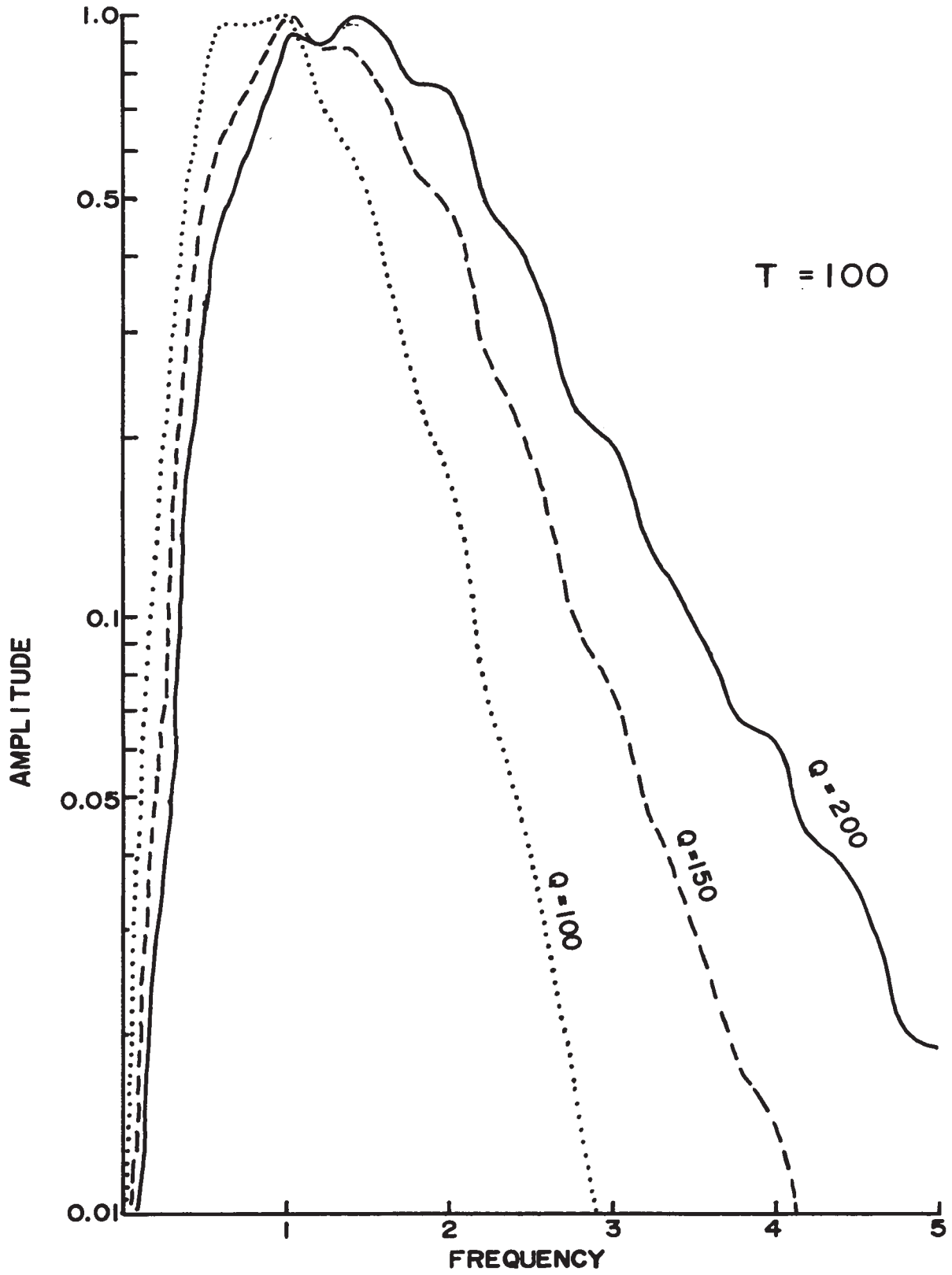

Fig. 9-2 (a) Amplitude spectrum of theoretical wavelets for Early Rise explosions showing the effect of attenuation Q.

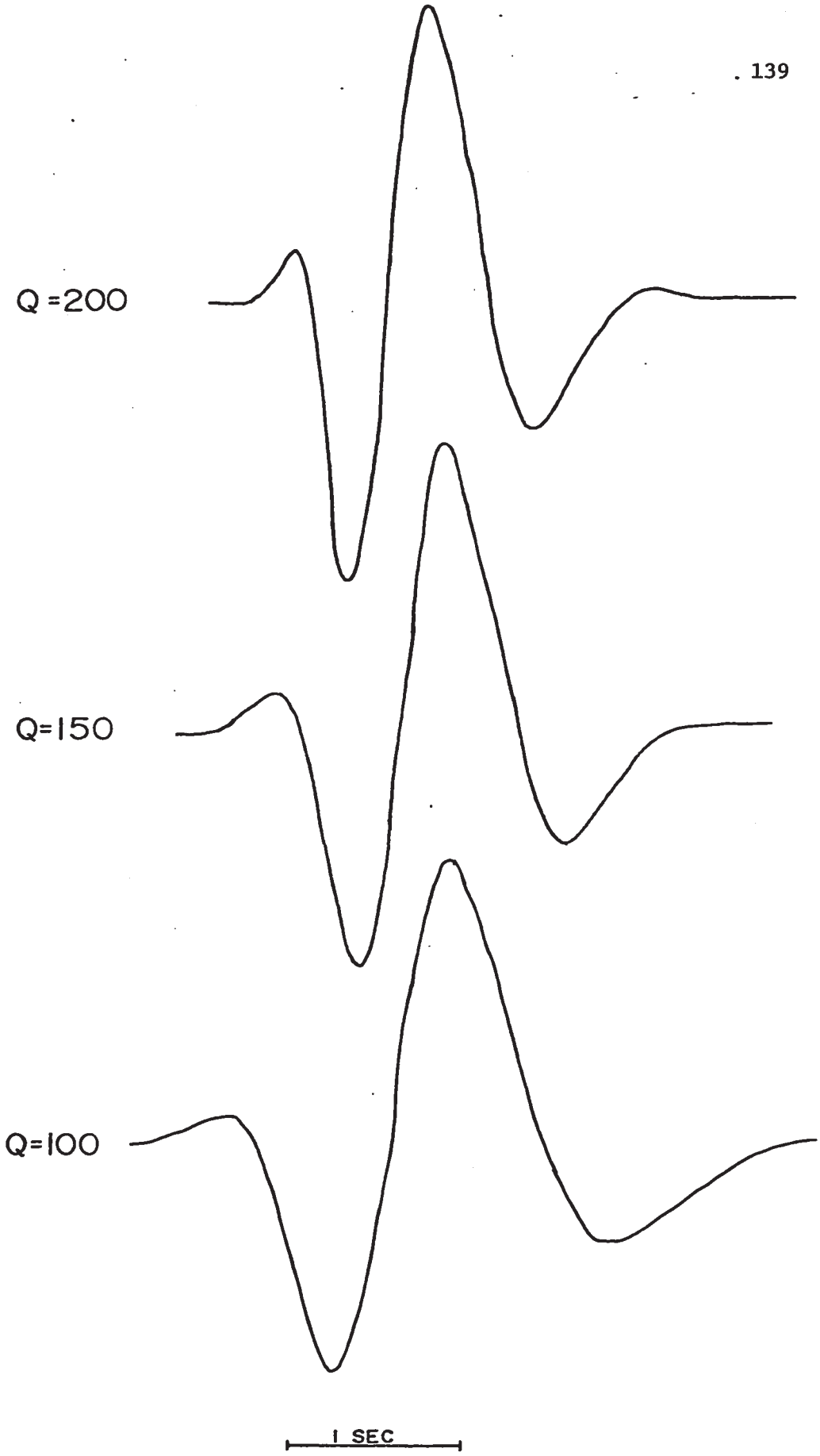

Fig. 9-2 (b) Pulse shapes of theoretical wavelets showing effects of attenuation Q.

b) Observed Wavelet Shapes

The high amplitude oscillary nature of the early portions of the Early Rise seismic records are considered to be the result of overlapping of many wavelets arriving within seconds of one another. The resultant "ringing" effect is a mask through which interpretation of wavelet arrivals must be made. To be interpretable a seismic event must contain a high amplitude and have a readily identifiable wavelet shape.

In an attempt to obtain some estimation of an individual wave packet, the unprocessed seismic records were searched for isolated arrivals. Some examples are shown in fig. 9-3. The wavelet onsets are, in general, low in amplitude which suggest that picking of onset times of later arrivals can easily be in error by at least one-half cycle or approximately 0.25 sec. The probable error involved in a wavelet pick decreases the usefulness of these events as indicators of fine structure. Indeed, in areas where overlapping of arrivals occur, the error in picking arrival times may be as much as 0.5 - 0.75 seconds.

From the examination of reflections from model studies it has been noted that phase shifts may be responsible for a change in wavelet characteristics within the wave packet. However, the packet length, and the number of cycles within the envelope remain unchanged.

Filtering processes applied to the Early Rise section, as described in the previous chapter, have attempted to amplify weak seismic events and to separate wave packets.

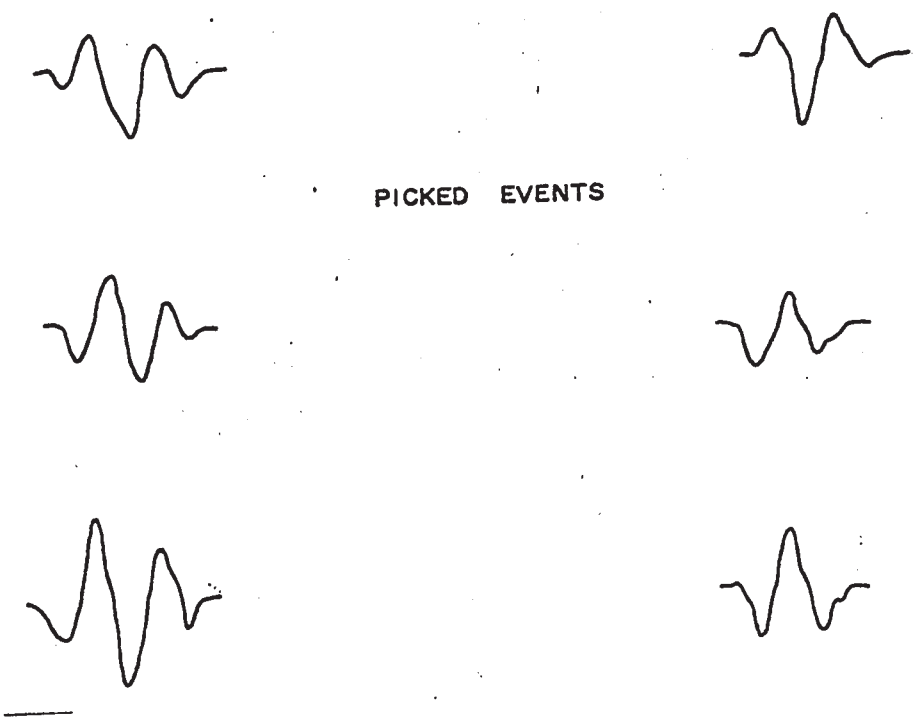

Fig. 9-3 Examples of wavelets picked from the Early Rise seismograms.

9.2 Picking of Later Events from the Early Rise Line

The events picked as prominent later arrivals on the Early Rise section were determined individually from each record. The "Picked" onset times for each of the filters are shown in sectional form for the Early Rise Line in fig. 9-4. Trend lines have been drawn through those events favouring such line-ups from either travel-time or amplitude characteristics as shown in fig. 9-5. In general, many later events are interpretable from the record sections. Correspondence between picked events on different sections is good. Often the "picked" events are separated in time by about one cycle, in comparing sections, suggesting that the onset time of an event is lost in the background noise.

Many high amplitude events occur as later arrivals in the near range out to 400 km. Wave packets follow one another closely and interpretation error is high. The earliest high amplitude event, corresponding to a reflection from the base of an upper crustal layer (11 wave code) is easily identifiable on most sections. The arrival times fit a model given by an average velocity of 6.15 km/sec and thickness of 15 km for the layer. This event is followed closely by several high amplitude events which are interpreted to be multiple reflections from the upper crustal layer (see fig. 9-6).

A weak amplitude later event is observed in the region of 250-400 km which has been interpreted to be the Moho reflection 1221. The event has a high picking uncertainty because of its low amplitude and the proximity to other high amplitude later arrivals. The travel times fit a model consisting of a lower crustal velocity of 6.68 km/sec and a layer thickness of 30 km. The low amplitudes associated with the

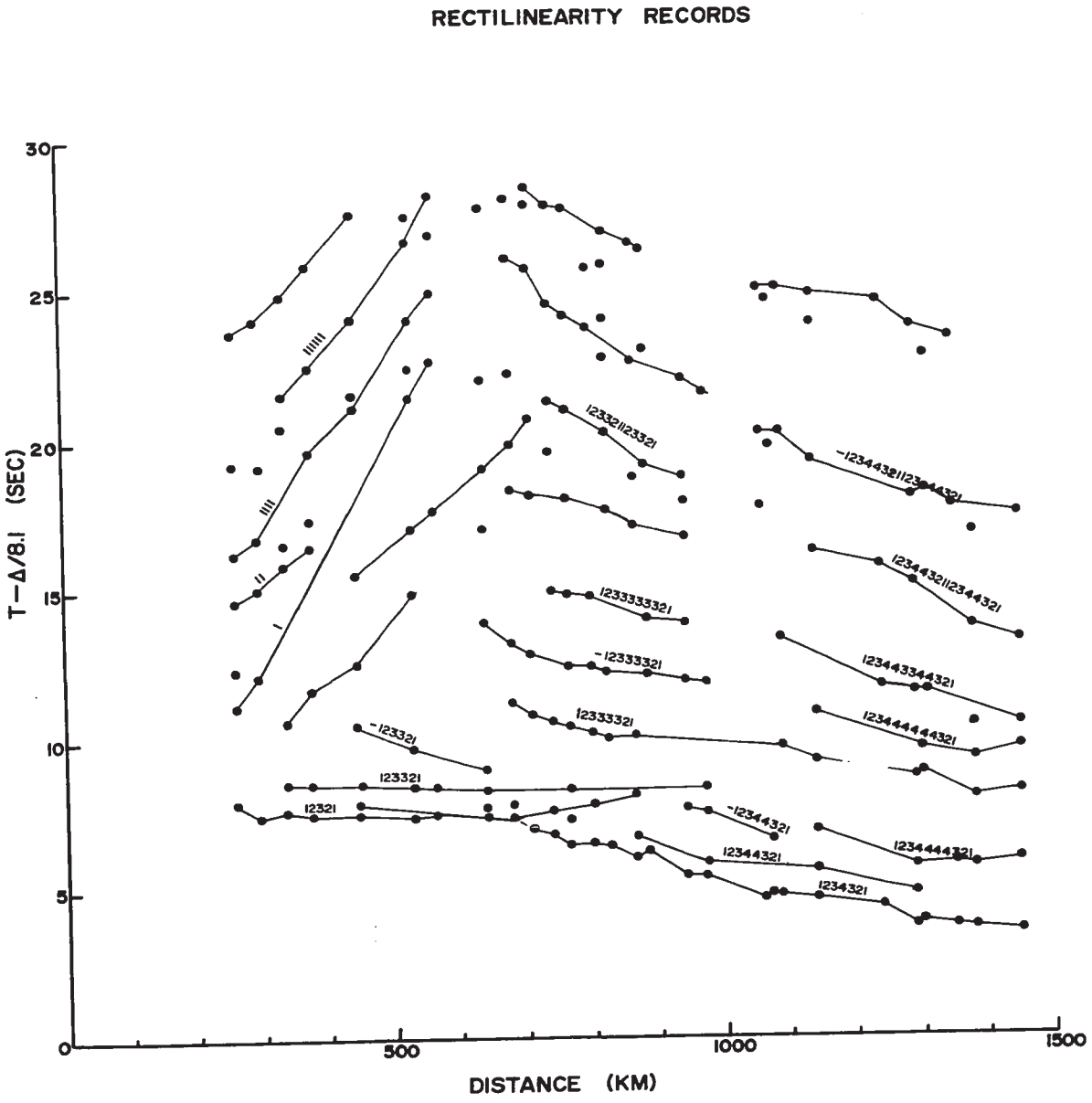

Fig. 9-4 (a) Picked events for the Early Rise line correlation records.

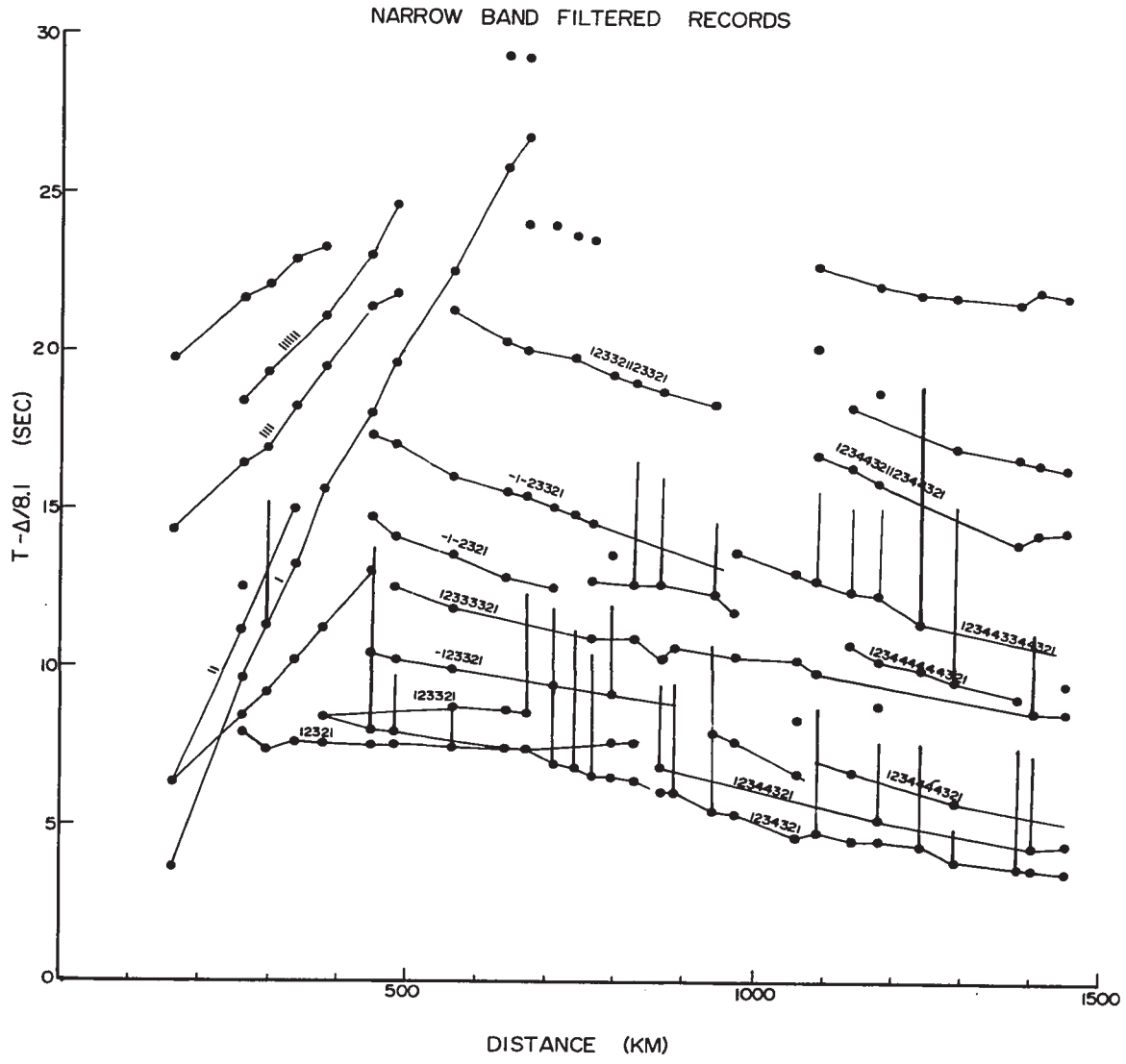

Fig. 9-4 (b) Picked events for the Early Rise line narrow-band filtered records.

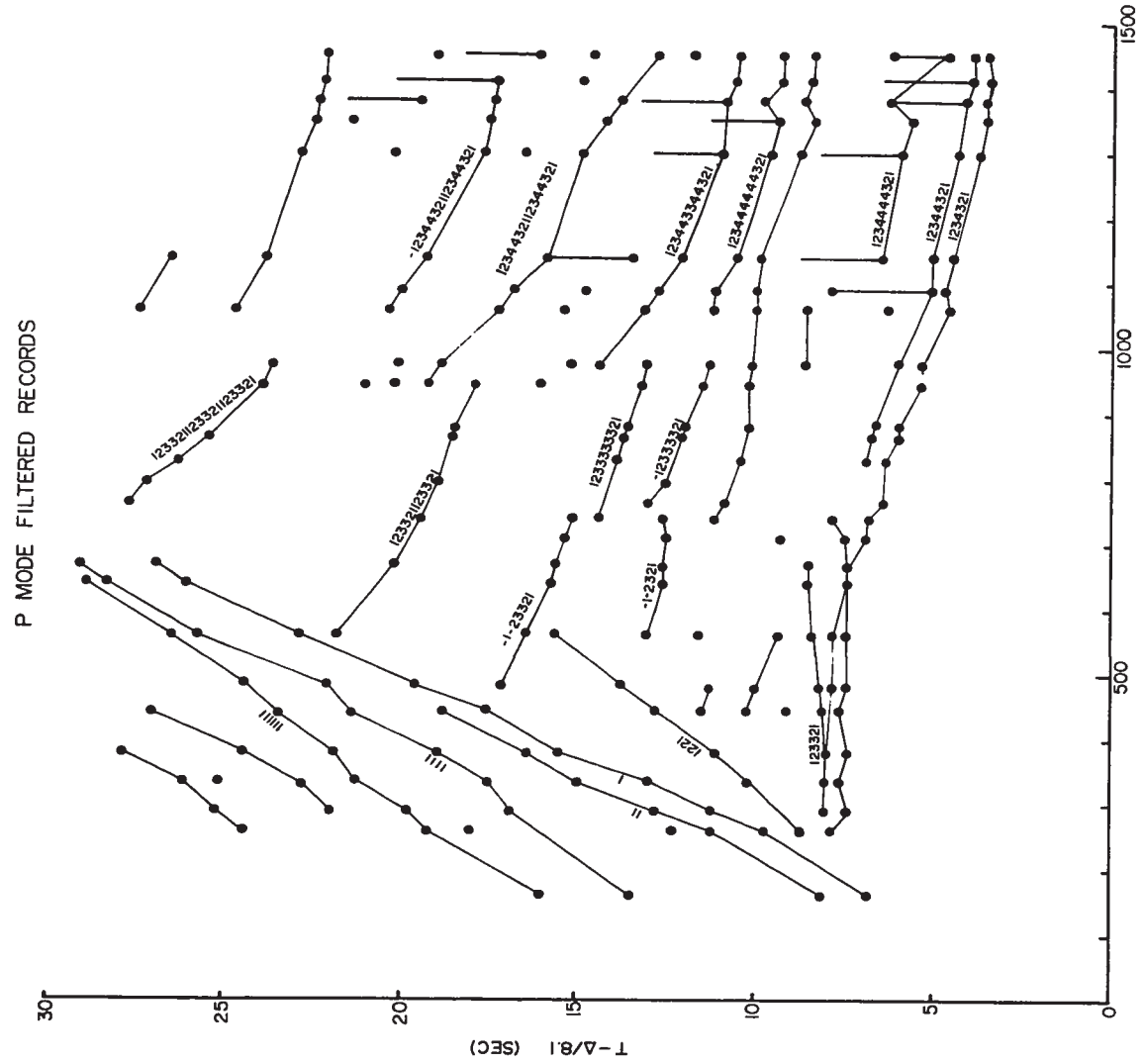

Fig. 9-4 (c) Picked events for the Early Rise line P mode filtered records.

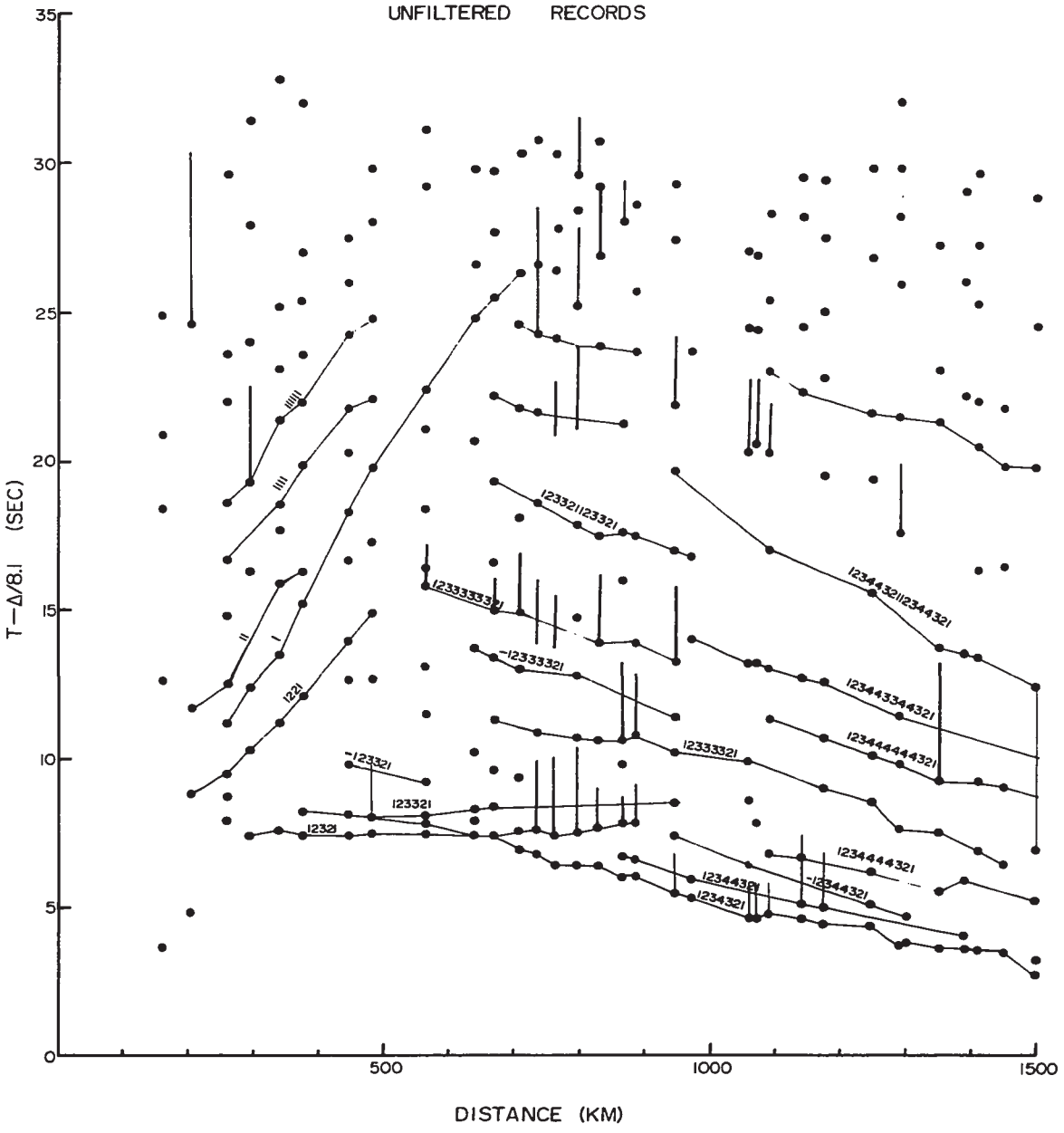

Fig. 9-4 (d) Picked events for the Early Rise line unfiltered records.

event may be explained by an interference phenomenon between this event and the phase-shifted refraction from this layer since the two arrival times are within 0.5 seconds of one another at these distances. As well, a small velocity gradient within this layer could also account for the low amplitudes yet causing only small changes in the travel time model.

A prominent event, closely following the first arrival, appears on the seismogram sections from 400 km outwards. This has been interpreted to be an event reflected from a sub-Moho interface (123321) denoted as the Hales discontinuity. Following this event outwards toward the break-over point to the 8.43 layer, it is lost in a grouping of large amplitude events in this area. A close investigation of the break-over point is shown in fig. 9-5. Events correlated with a travel time cusp have been interpreted in this area. The interpretation error is quite high since onsets are difficult to pick. Despite this difficulty, the occurrence of high amplitudes events in this region is in itself a good indication of cusping.

In the region of the seismic section from 400 - 1000 km, a series of later events have been picked from trace to trace correlation (see fig. 9-4). These events have been interpreted as multiple reflections from the Hales discontinuity and have been labelled using the standard wave coding. Comparison of arrival times from section to section often yield differences of 0.5 seconds or more.

Most of the reflected events from the Hales discontinuity cannot easily be traced beyond 1100 km because of interference phenomena from another set of waves. Hence reflected events from a sub-Hales discontinuity have been interpreted. The major reflection from this horizon is the primary compressional reflection (12344321) occurring within one

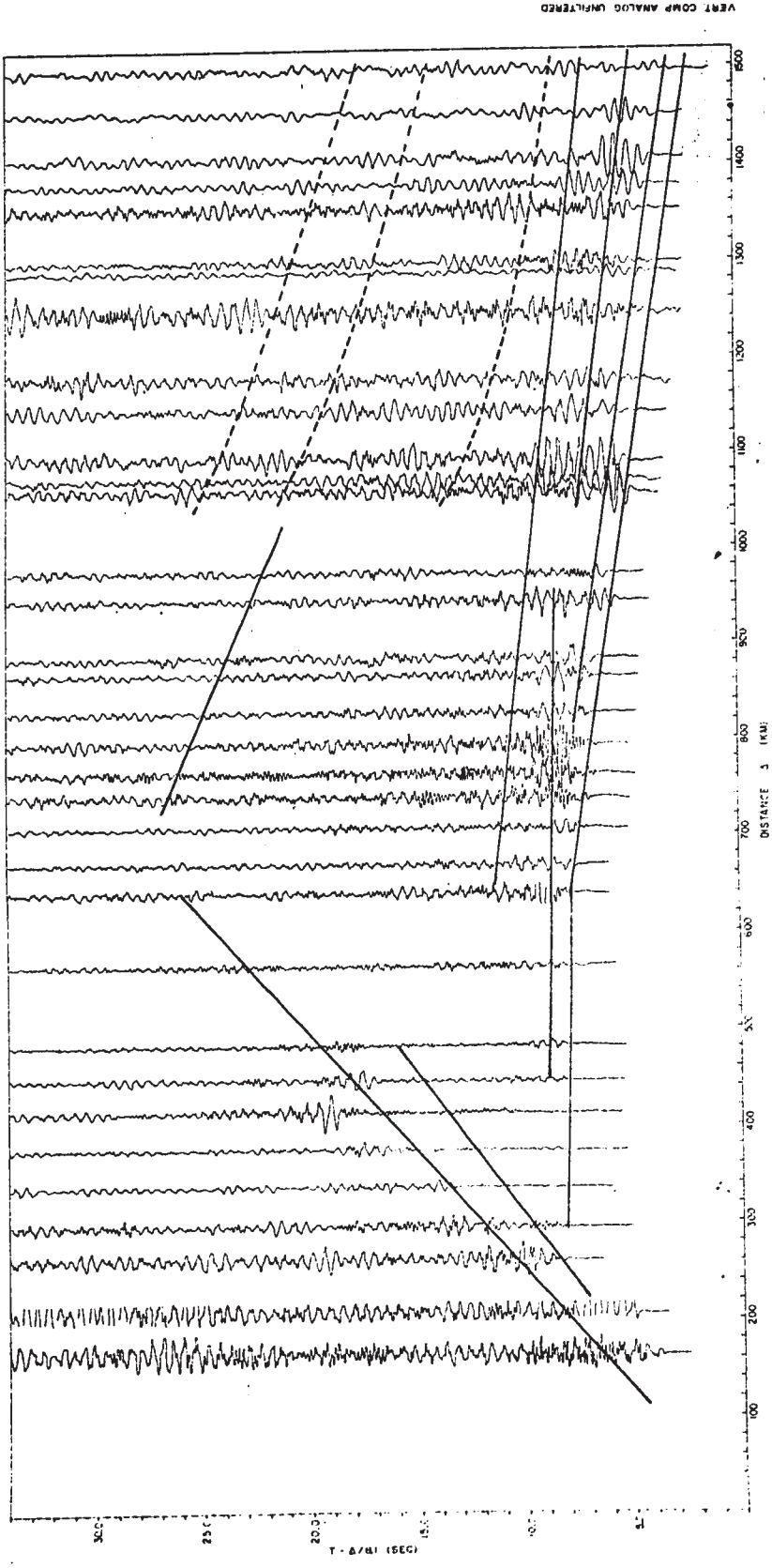

Fig. 9-5 (a) Trend lines through the Early Rise line unfiltered records.

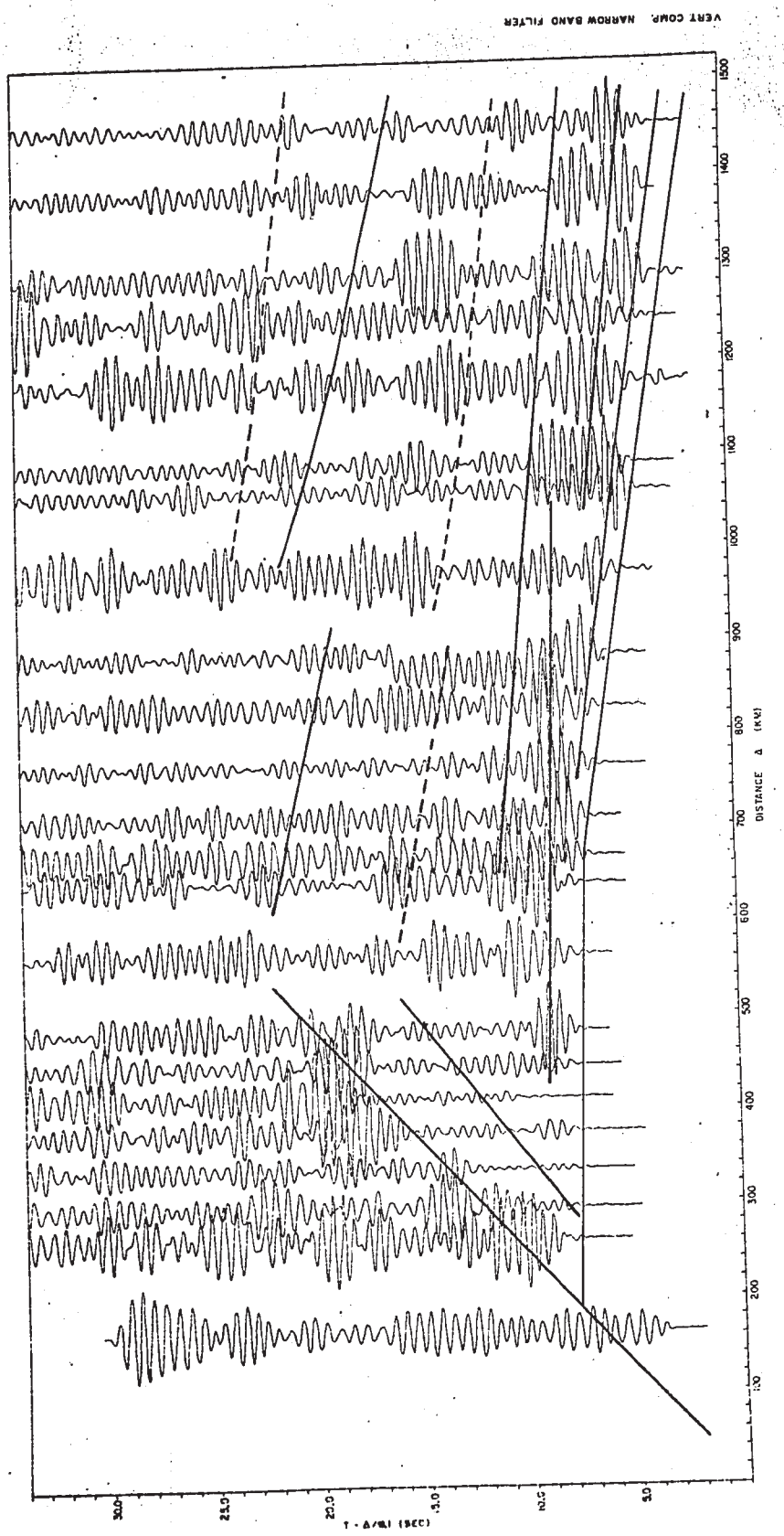

Fig. 9-5 (b) Trend lines through the Early Rise line narrow-band filtered records.

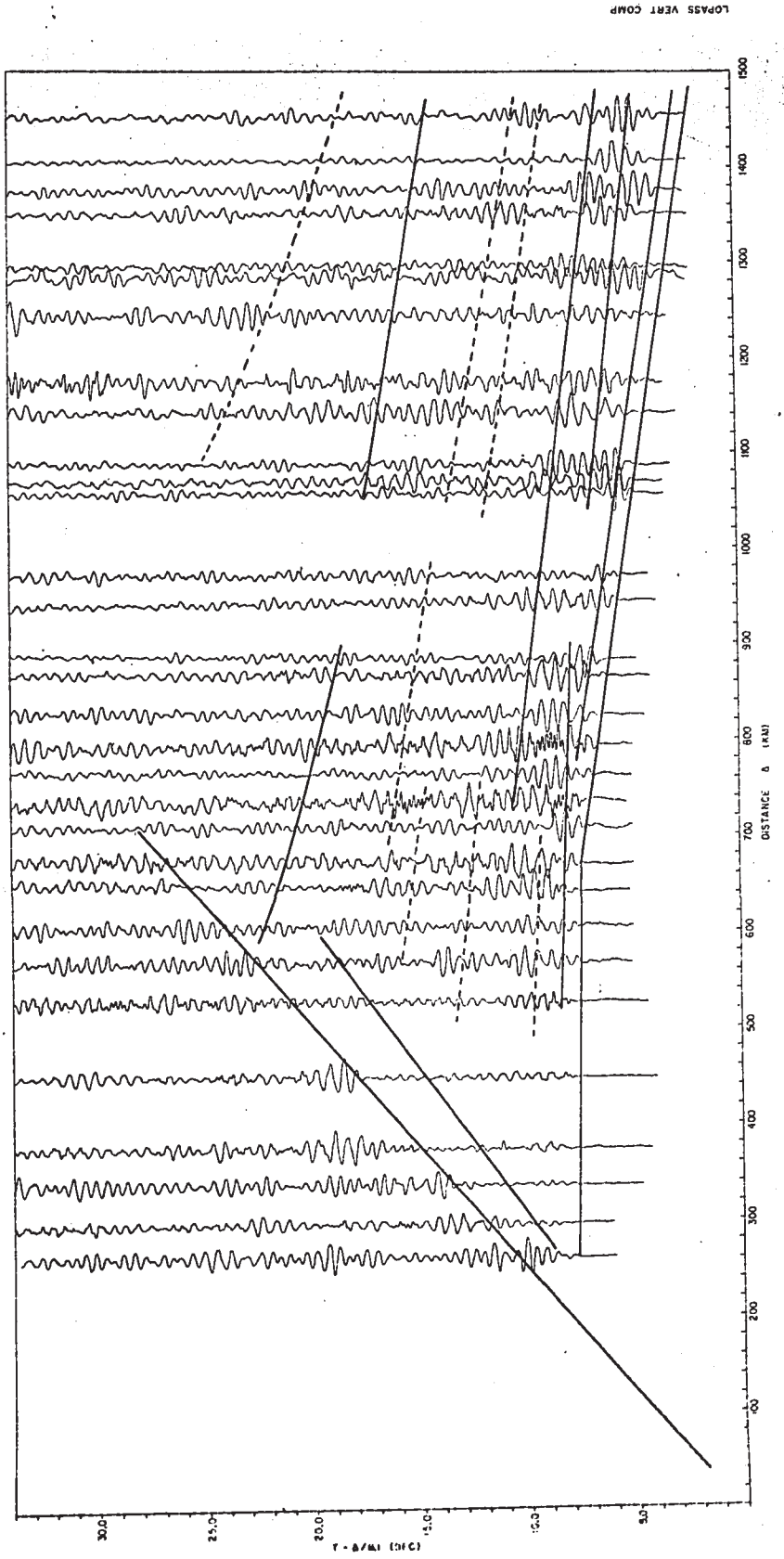

Fig. 9-5 (c) Trend lines through the Early Rise line low pass filtered records.

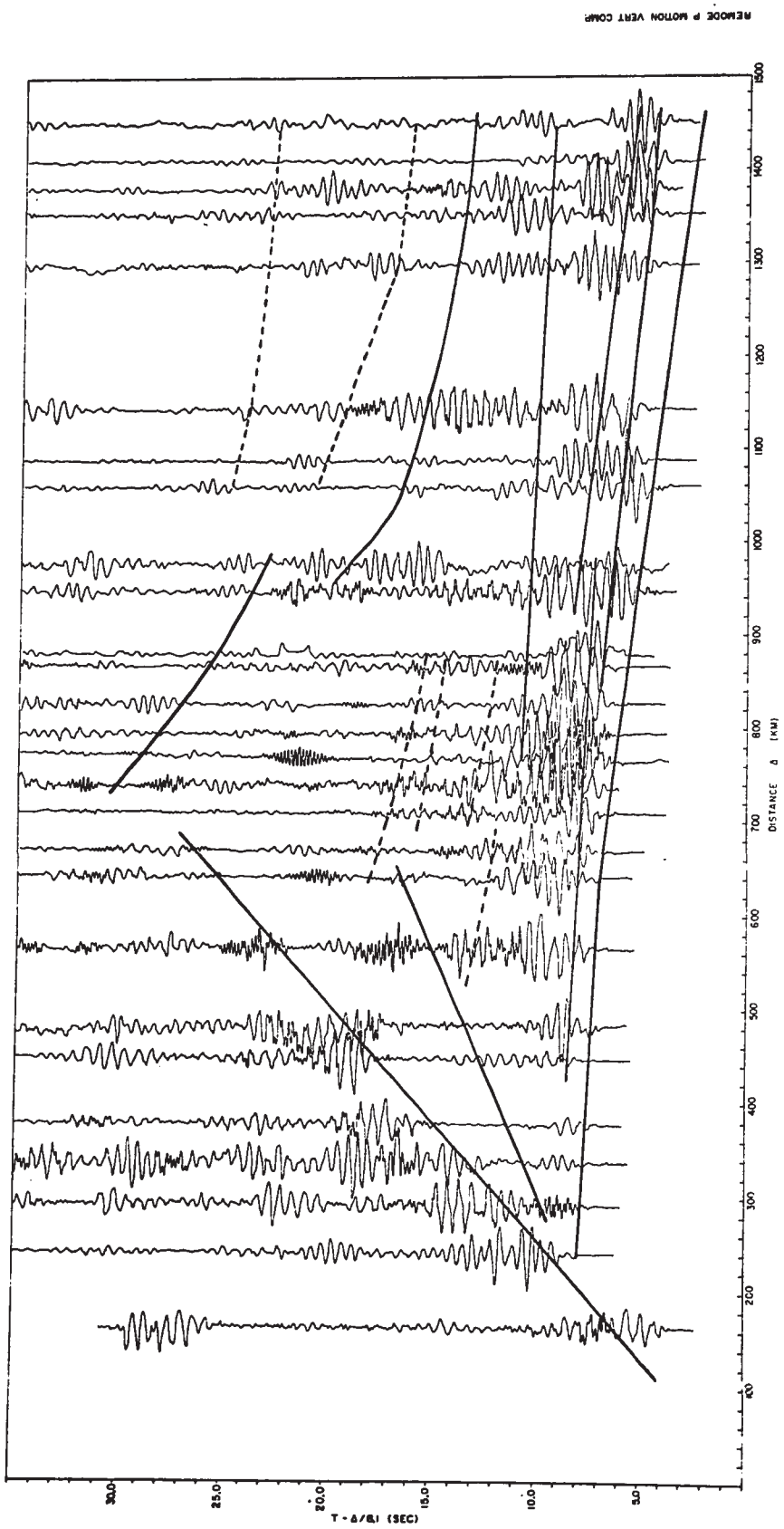

Fig. 9-5 (d) Trend lines through the Early Rise line P mode filtered records.

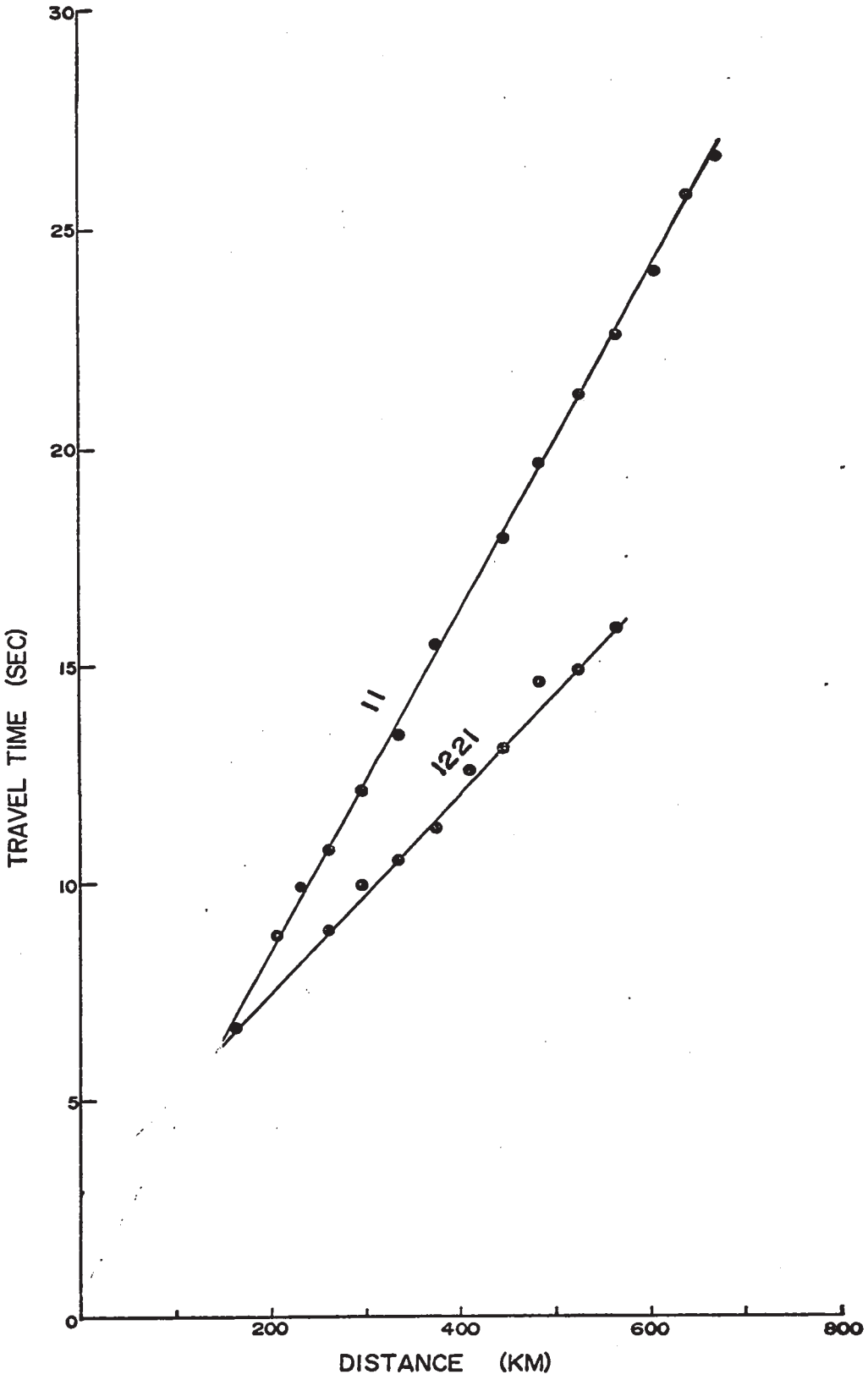

Fig. 9-6 Travel times of the upper crustal (11) and the Moho (1221) reflections.

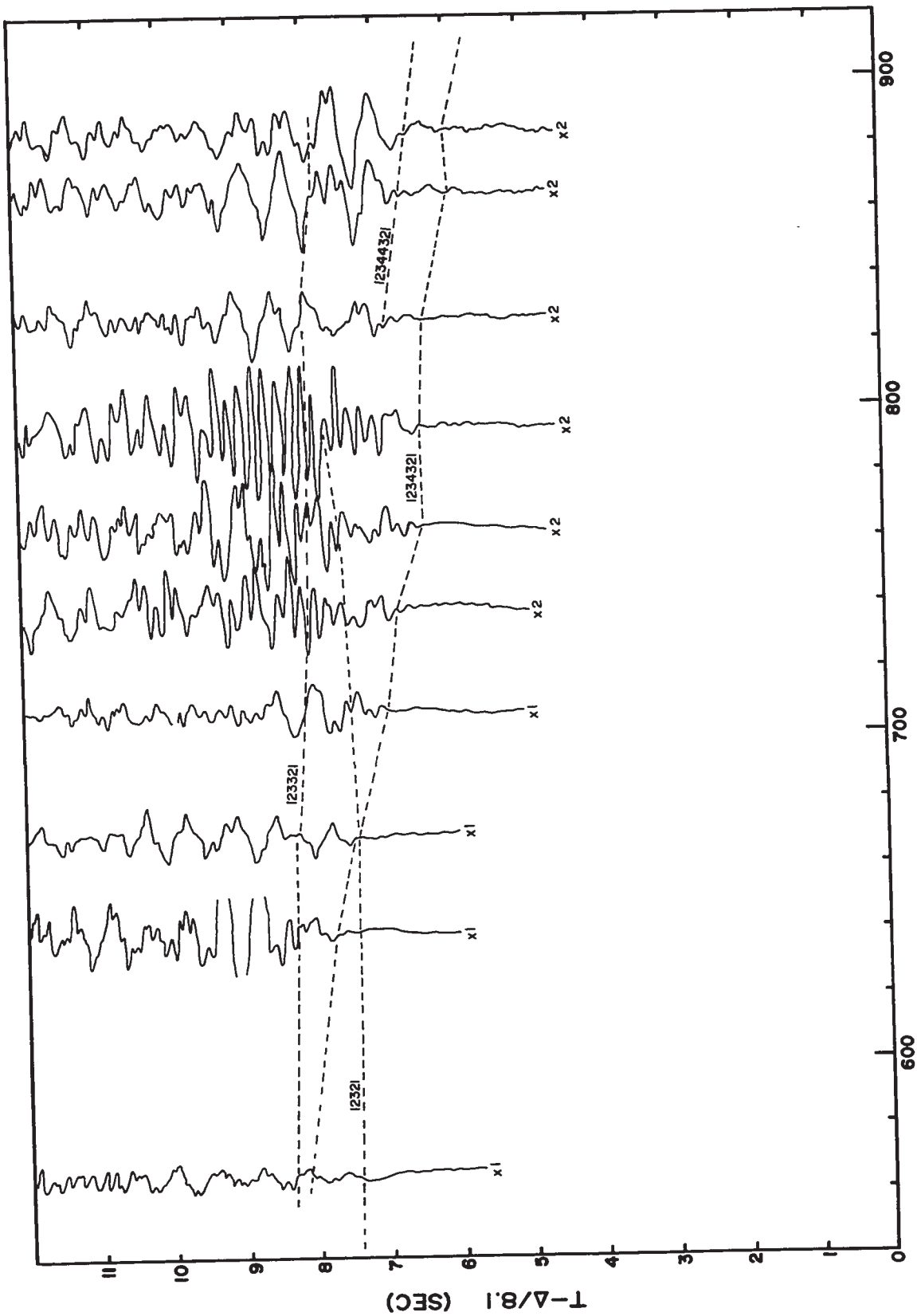

Fig. 9-7 Early Rise line record section in the vicinity of the travel time cusp.

second of the first arrival in the region of 800 - 1500 km along the line. Events corresponding to multiple reflections from this horizon have been interpreted in the region beyond 1100 km. The events are poorly defined with large arrival time and amplitude variation. The events are interpreted as being reflections from a discontinuous velocity increase, however, the nature of the velocity discontinuity is poorly defined from arrival times alone.

At the far end of the seismic line the records demonstrate "ringing" which is interpreted as being the result of reflections from both the Hales discontinuity and the sub-Hales discontinuity arriving with equal amplitudes.

9.3 Amplitudes of Later Arrivals from the Early Rise Line

Of the later events picked from the seismic sections the most prominent and most reliable are:

1) the crustal reflection 11
2) the reflection from the Hales discontinuity 123321
3) the multiple reflection from the Hales discontinuity 123321123321
4) the multiple reflection from the Hales discontinuity and the Moho 12333321
5) the reflection from the sub-Hales discontinuity 12344321
6) the multiple reflection from the sub-Hales discontinuity 1234432112344321
7) the multiple reflection from the sub-Hales discontinuity and the Hales discontinuity 1234444321

Amplitude measurements of the maximum peak-to-peak amplitude of the pulses were made for the events listed above and are plotted in fig. 9-6. All events exhibit decreasing amplitudes with distance, although a considerable scatter of points exist on some plots. In general, since measurement error may be large, comparison of amplitude curves with theoretical models depends more upon the first appearance of the wave as a prominent event than upon the detailed shape of the amplitude curve.

Shown on each plot of observed amplitudes of the waves are the theoretical amplitude curves based on a model following the observed arrival times. The model is given in Table 9-1. A quantitative estimate of ground motion was assigned to the theoretical amplitude curves following O'Brien (1960) for underwater explosion.

The amplitude plot for the 11 reflections show a large decrease with distance over the observable range. There is general agreement between observed and predicted amplitudes, however, one may interpret a high attenuation at greater distance resulting from either absorption or a small velocity gradient in the layer. Since the model velocity filtering the travel-time for this layer (6.15 km/sec) is in general slightly higher than that which is observed on surface from particle motion studies, it is suggested that the lower velocity is restricted to the upper few kilometres of the crust.

The amplitude results for the 123321 reflection from the Hales discontinuity demonstrate a detectable onset at about 300 km distance. No prominent peak amplitude is observed as predicted by the model, however reasonable correlation is obtained beyond 600 km. The lack of a definite amplitude peak may result from either attenuating

TABLE 9 - 1

AVERAGE CRUSTAL MODEL

EARLY RISE LINE

0		6.15
15		6.60
45	6.76	8.05
85		8.43
115		8. ?

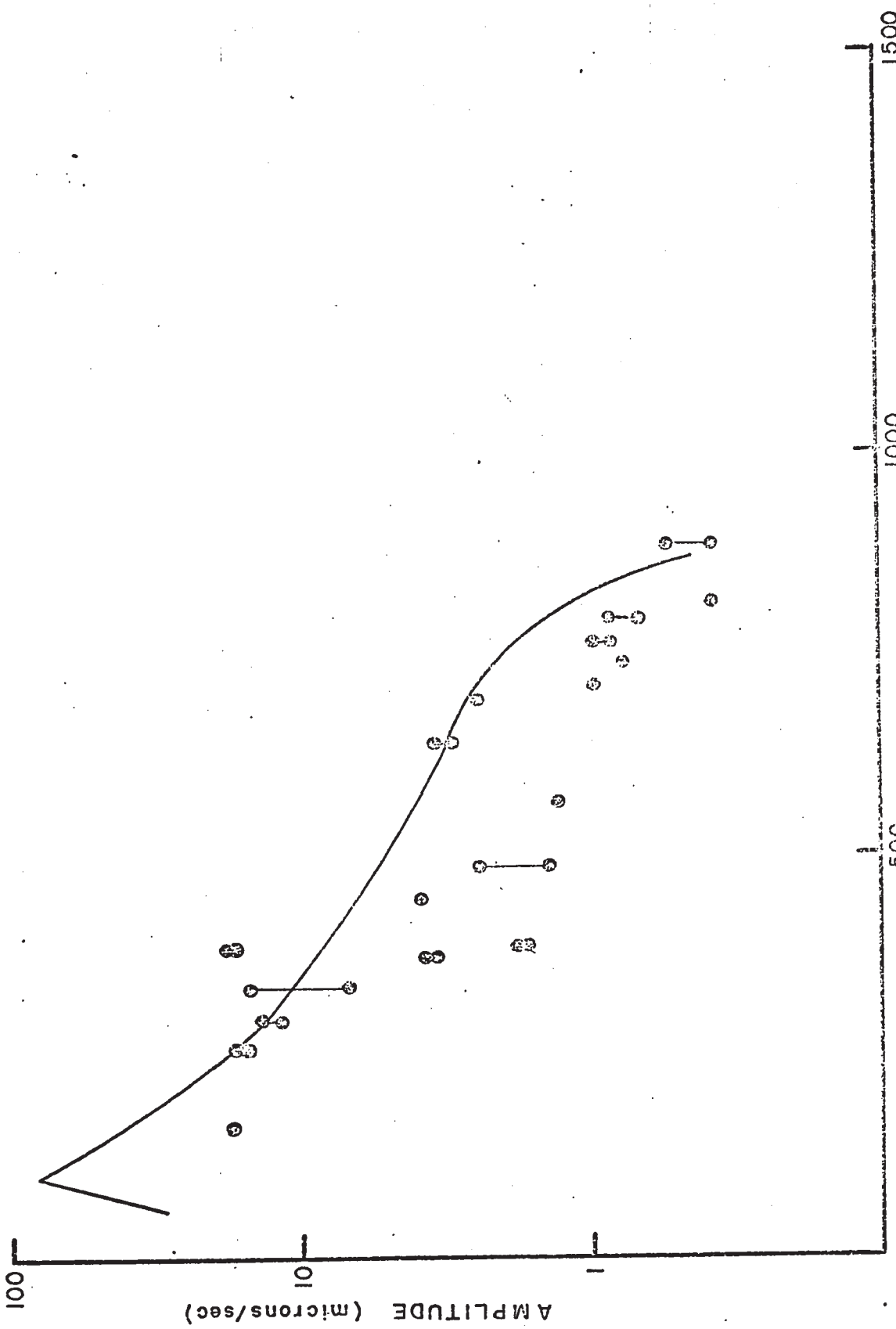

Fig. 9-8 (a) Early Rise line amplitude measurements for the upper crustal reflection 11.

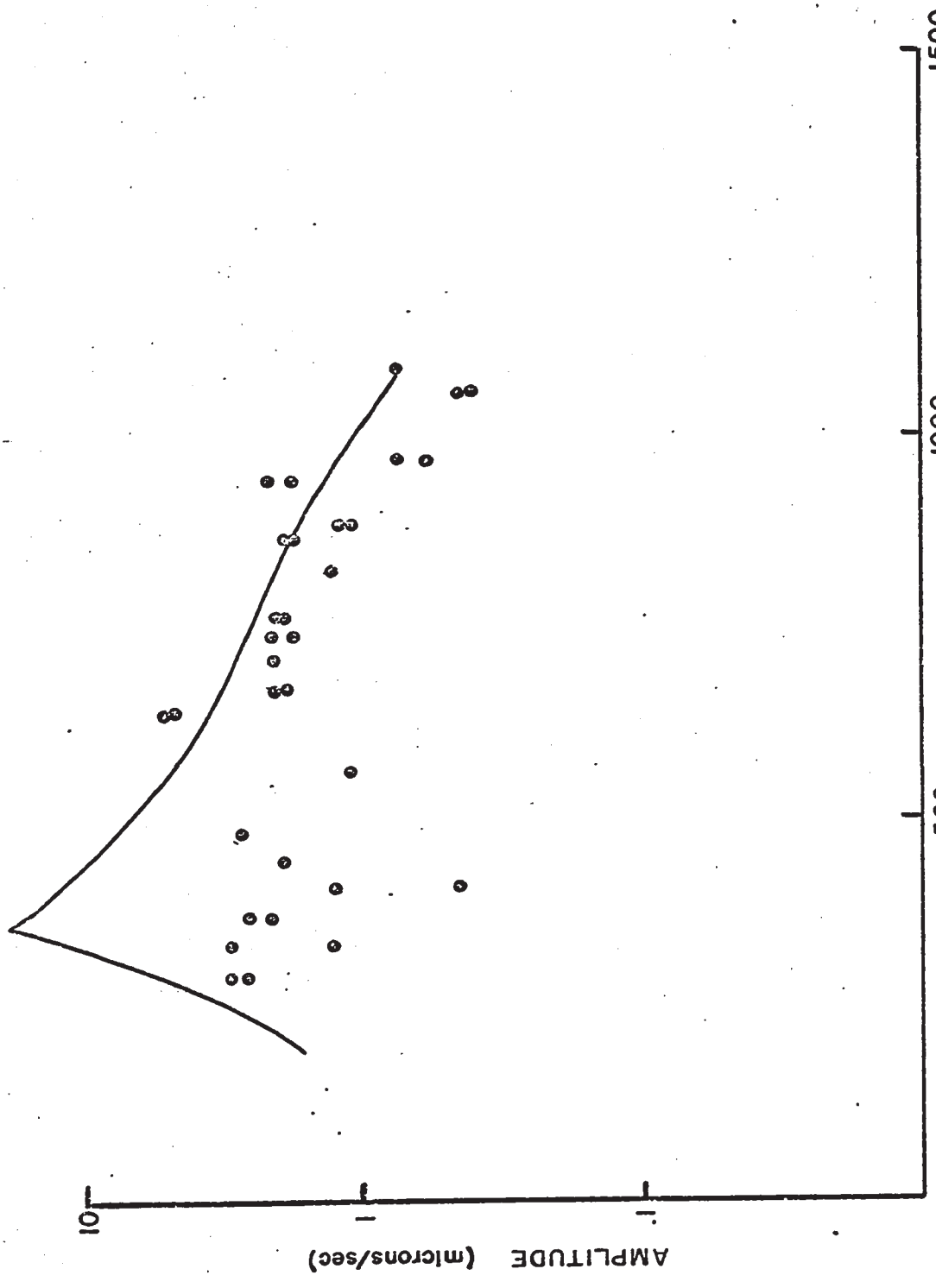

Fig. 9-8 (b) Early Rise line amplitude measurements for the 'Hales" discontinuity reflection 123321.

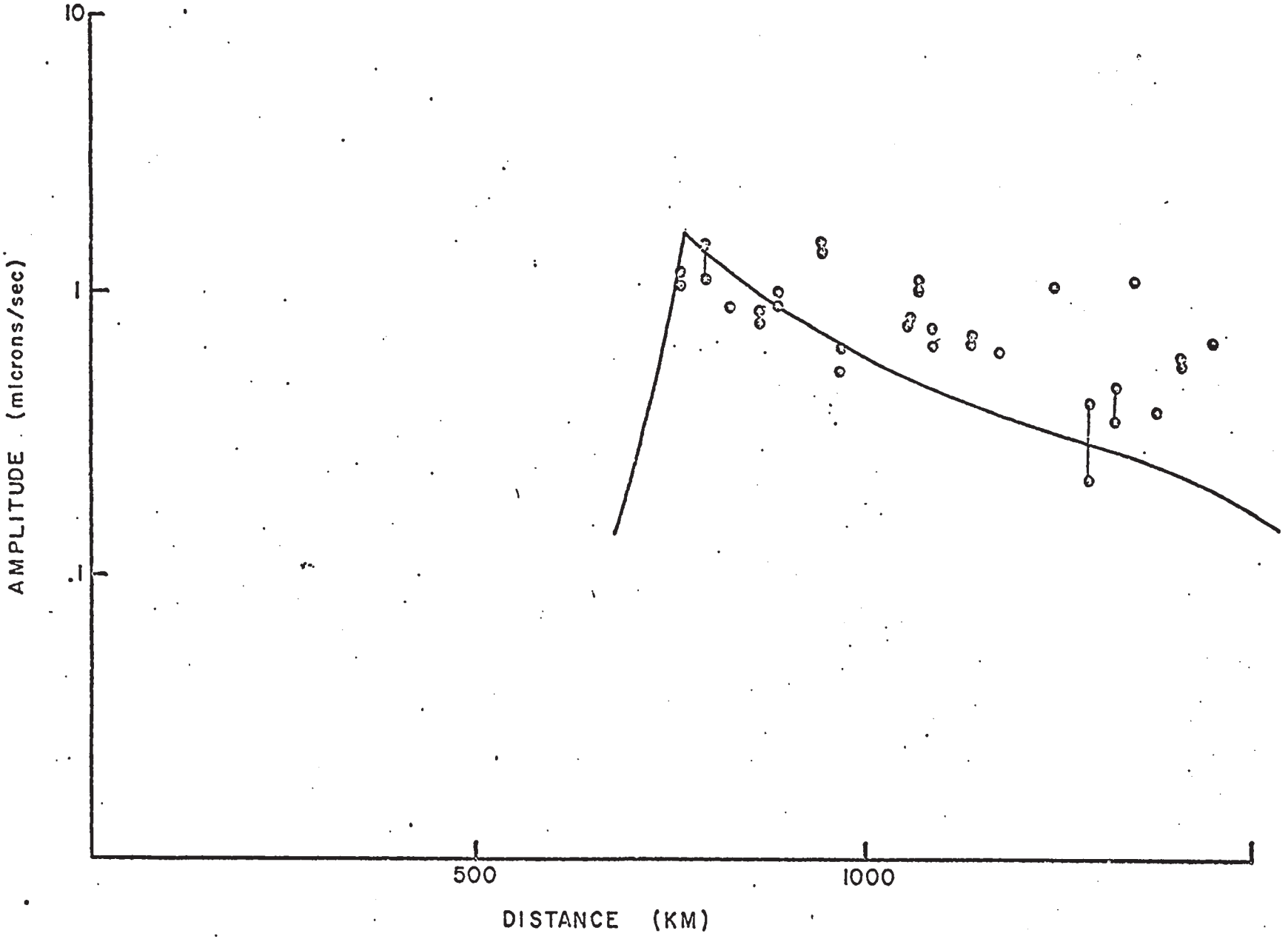

Fig. 9-8 (c) Early Rise line amplitude measurements for the 'Hales' discontinuity multiple reflection 123321123321.

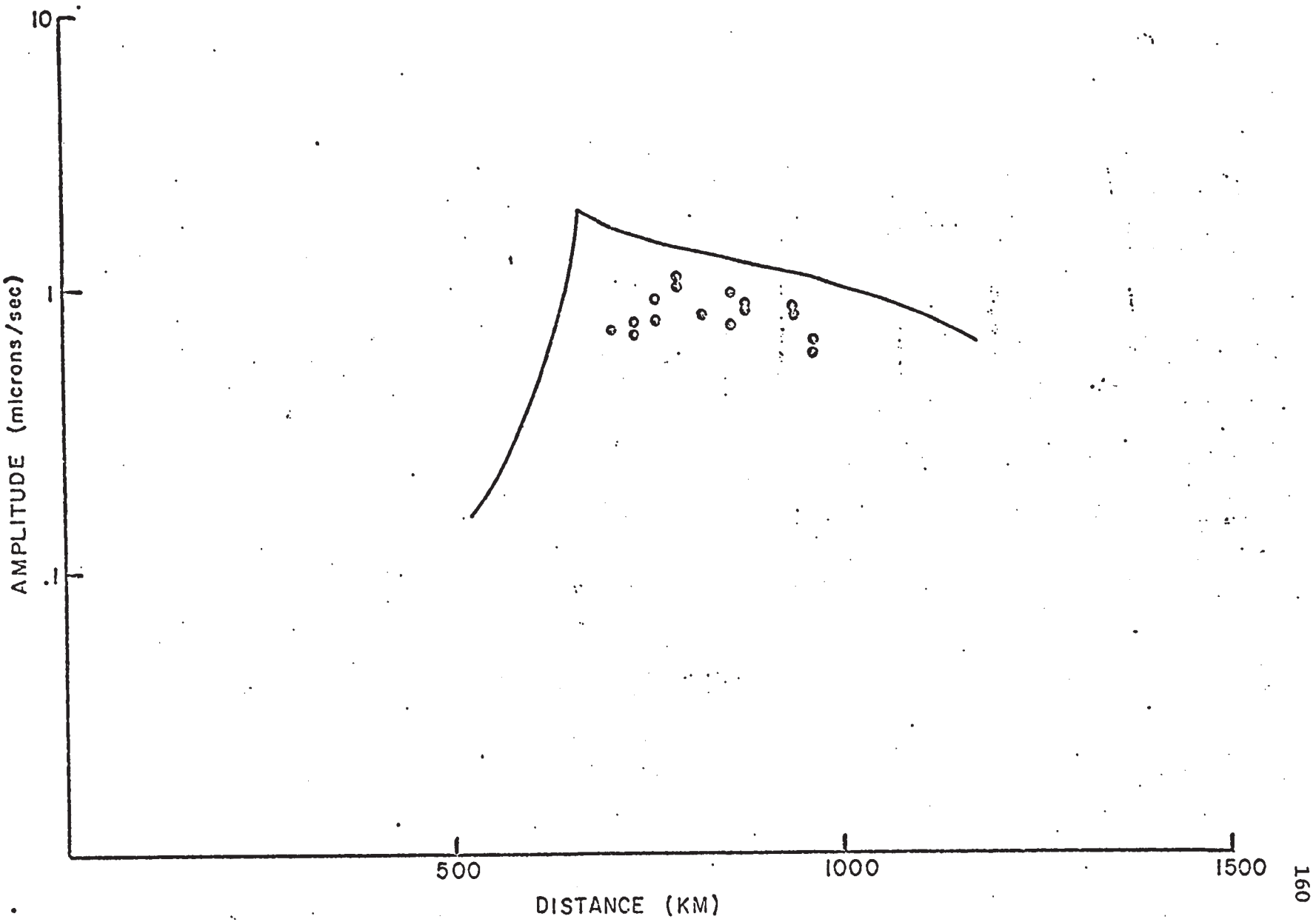

Fig. 9-8 (d) Early Rise line amplitude measurements for the 'Hales' discontinuity trapped multiple 12333321.

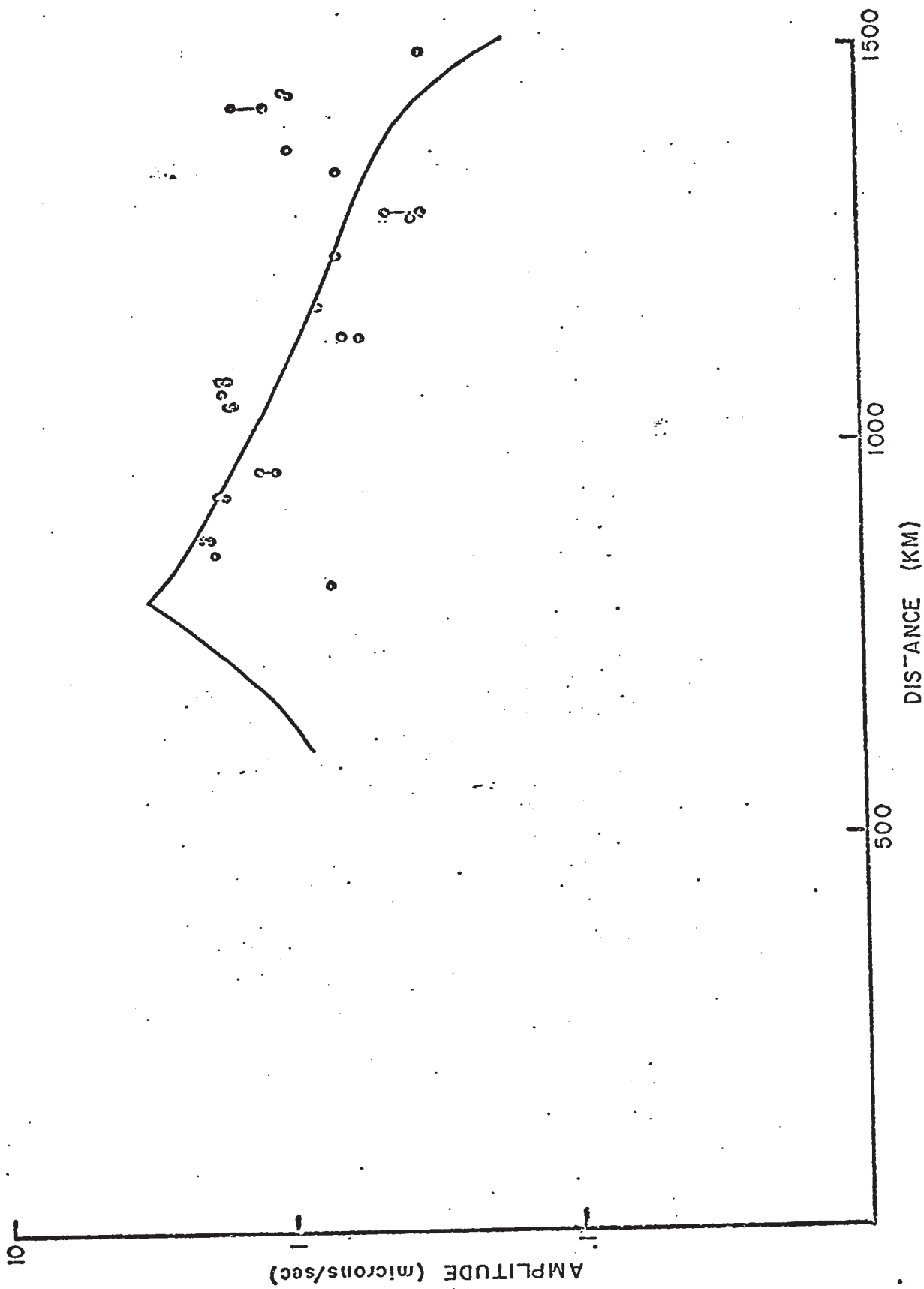

Fig. 9-8 (e) Early Rise line amplitude measurements for the sub-'Hales' reflector 12344321.

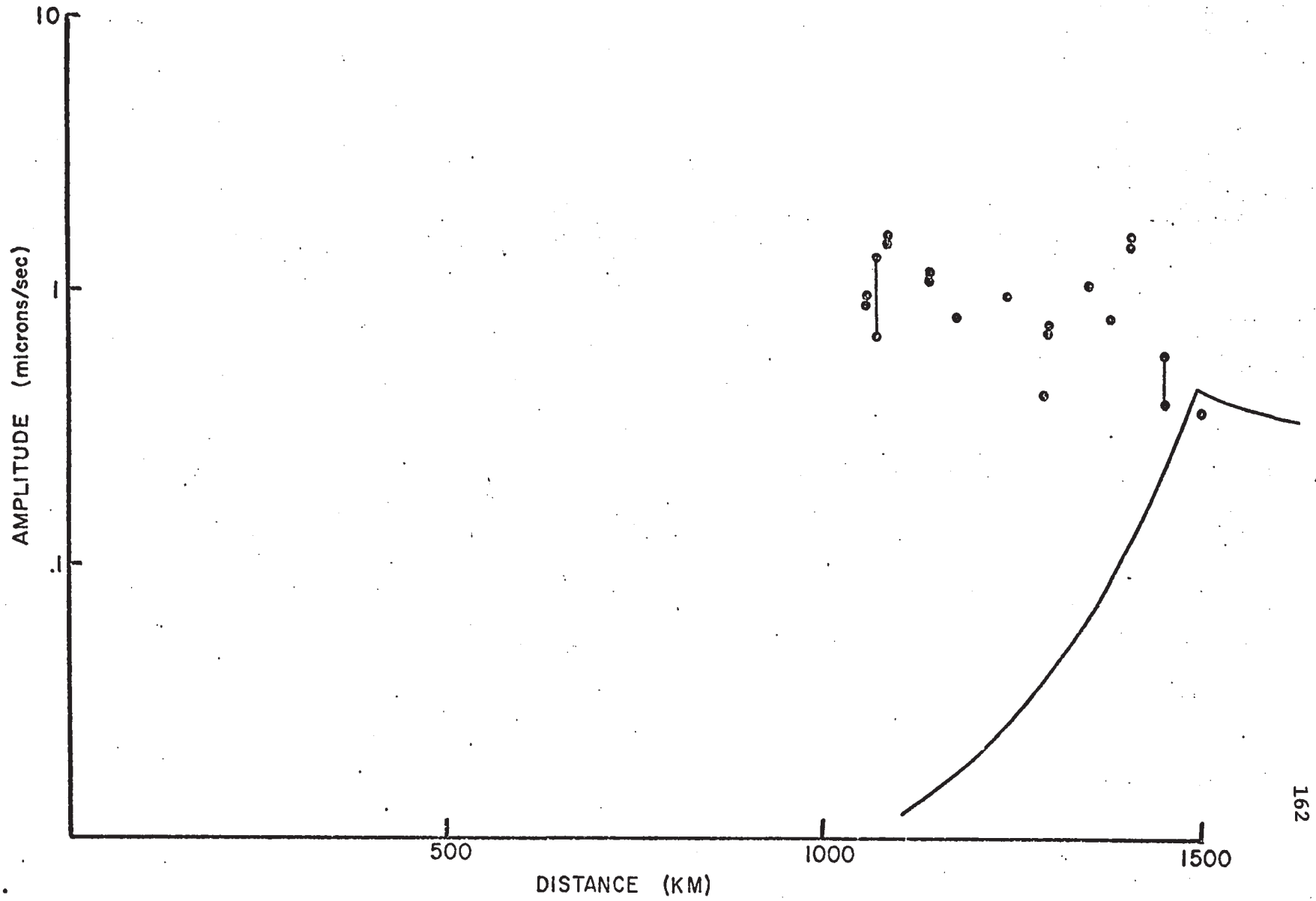

Fig. 9-8 (f) Early Rise line amplitude measurements for a possible sub-'Hales' multiple reflection 1234321123443 21.

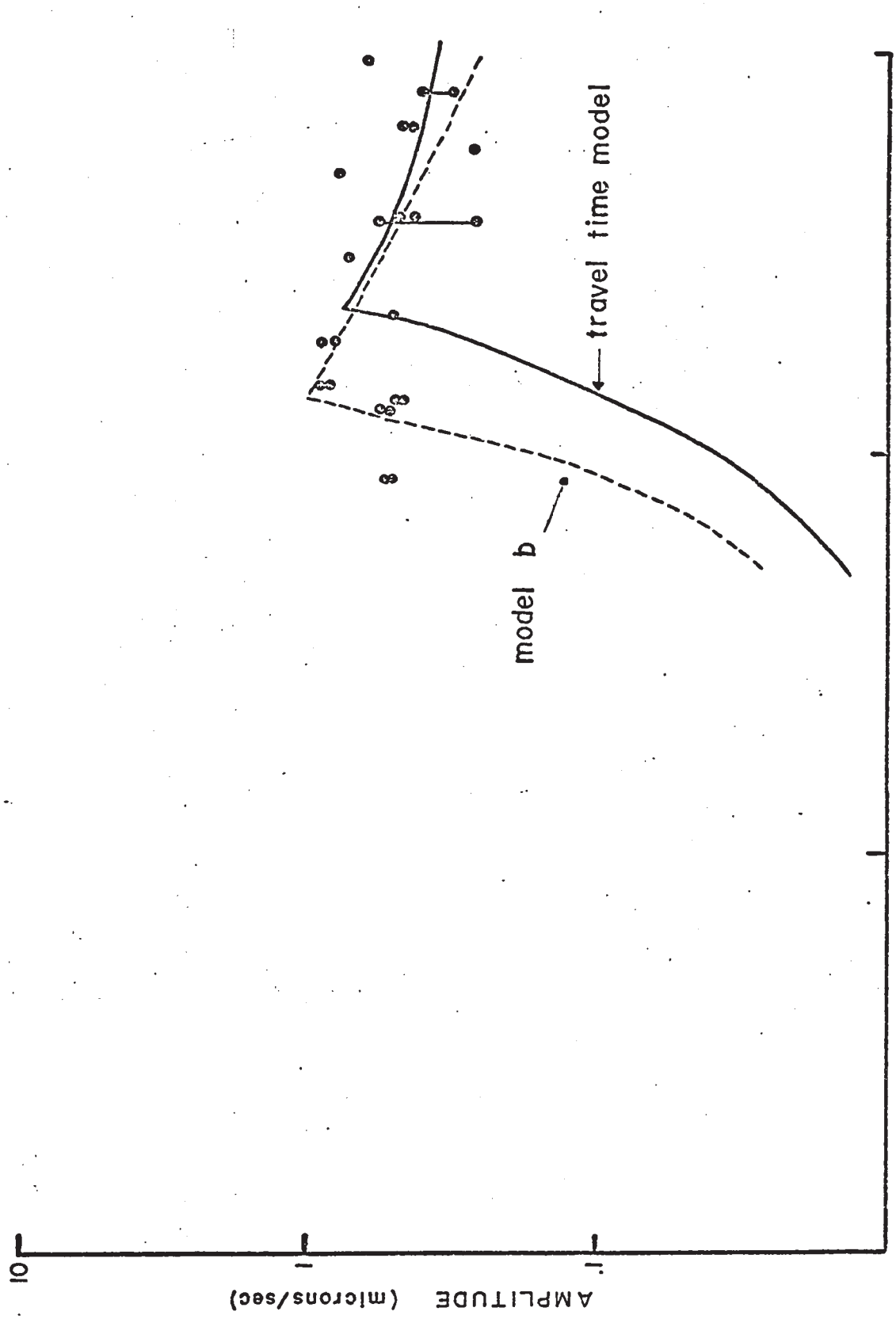

Fig. 9-8 (g) Early Rise line amplitude measurements for a possible sub'Hales" trapped multiple 1234444321.

effects of non-planar boundaries not taken into account by the model or it may result from a slight velocity gradient within the upper mantle.

The model fit with the amplitude plot for 12333321 shows some correlation with the first appearance of the event, however the predicted amplitudes are approximately 25% too high. If one assumes an undulatory boundary on the Moho these losses may be accounted for by scattering from a non-planar boundary.

The model fit with the 123321123321 amplitude plot is reasonable. First appearance of the wave coincides well with the model; however, the amplitude does not decrease with distance as sharply as predicted. This could result from a decrease in crustal thickness along the Early Rise line causing slightly larger amplitudes in the region of 1000 km.

In general there is reasonable correlation between the crustal model and major reflections from the Hales discontinuity with regard to first appearance of the wave and approximate amplitudes.

The model fit for waves belonging to a sub-Hales discontinuity is poor. Although there is reasonable agreement between predicted and observed amplitudes for the 12344321 wave, the multiple events 1234444321 and 1234432112344321 do not agree. The onset positions of these two waves are sensitive to depth to the discontinuity and thicknesses of layers above it, hence a change in crustal thickness in the region of 1000 km is suggested. The dotted lines shown in fig. 9-6 (f) and (g) are from model b consisting of a 30 km thick crust from sub-Hales model study of chapter 7. The closer set of this model for the 1234444321 wave suggests that crustal thinning from 45 km at the shot to 30 km along

the line may explain the early appearance of the wave on the section. As well, correcting the arrival times for the 12344321123 44321 wave results in close correlation of the travel time results. The appearance of 1234432112344321 can only be partially explained by a change in crustal thickness.

9.4 Interpretation of Later Events from the Nipigon-Smooth Rock Falls Section.

The unprocessed records of the vertical component of motion for the Nipigon-Smooth Rock Falls stations are shown in sectional form in fig. 9-9.

Later events picked from these records are shown in fig. 9-10 along with the best model fit of arrival times. The reflected event 11 fits a velocity model of 6.16 km/sec with a 15 km thick upper crust. This value is close to that obtained for the Early Rise Line. A fit of a model to the interpreted 121 refraction gave a velocity increase from 6.60 to 6.76 km/sec following $v = a\, r^{-b}$ law. The events from this layer are weak in amplitude and interpretation uncertainty is high. A best fit of arrivals for the P_n and Hales discontinuity 123321 events suggest an average depth to Moho of 43 km and a velocity increase from 8.10 to 8.16 km/sec at 73 km (Hales discontinuity). Assuming a velocity of 8.43 km/sec below the Hales discontinuity suggests that the break-over point for first arrivals is at approximately 500 km. This may explain the prominent amplitudes of some of the first arrivals observed at approximately 600 km on the section (see fig. 4-7).

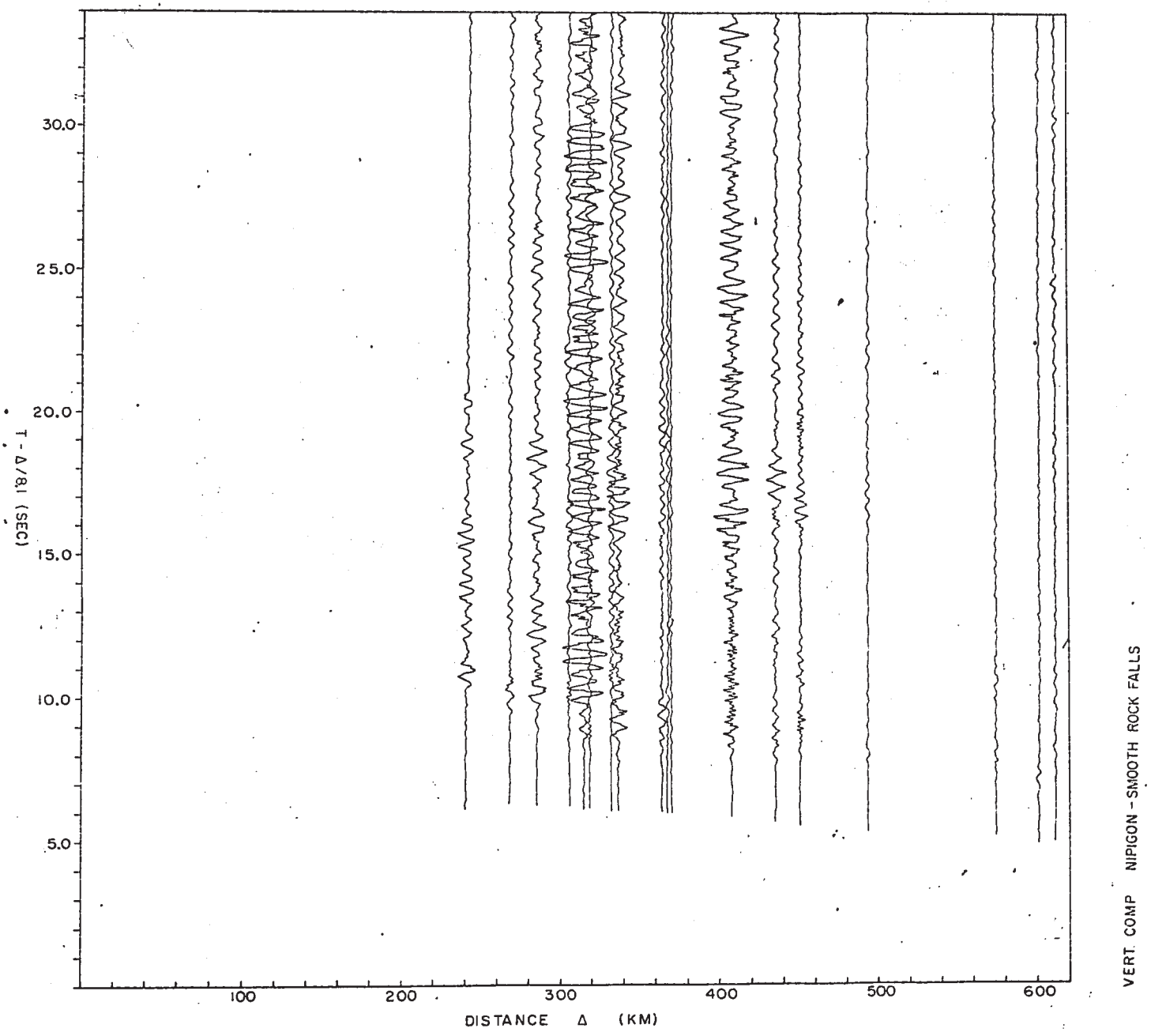

Fig. 9-9 Vertical component section for the Nipigon-Smooth Rock Falls records.

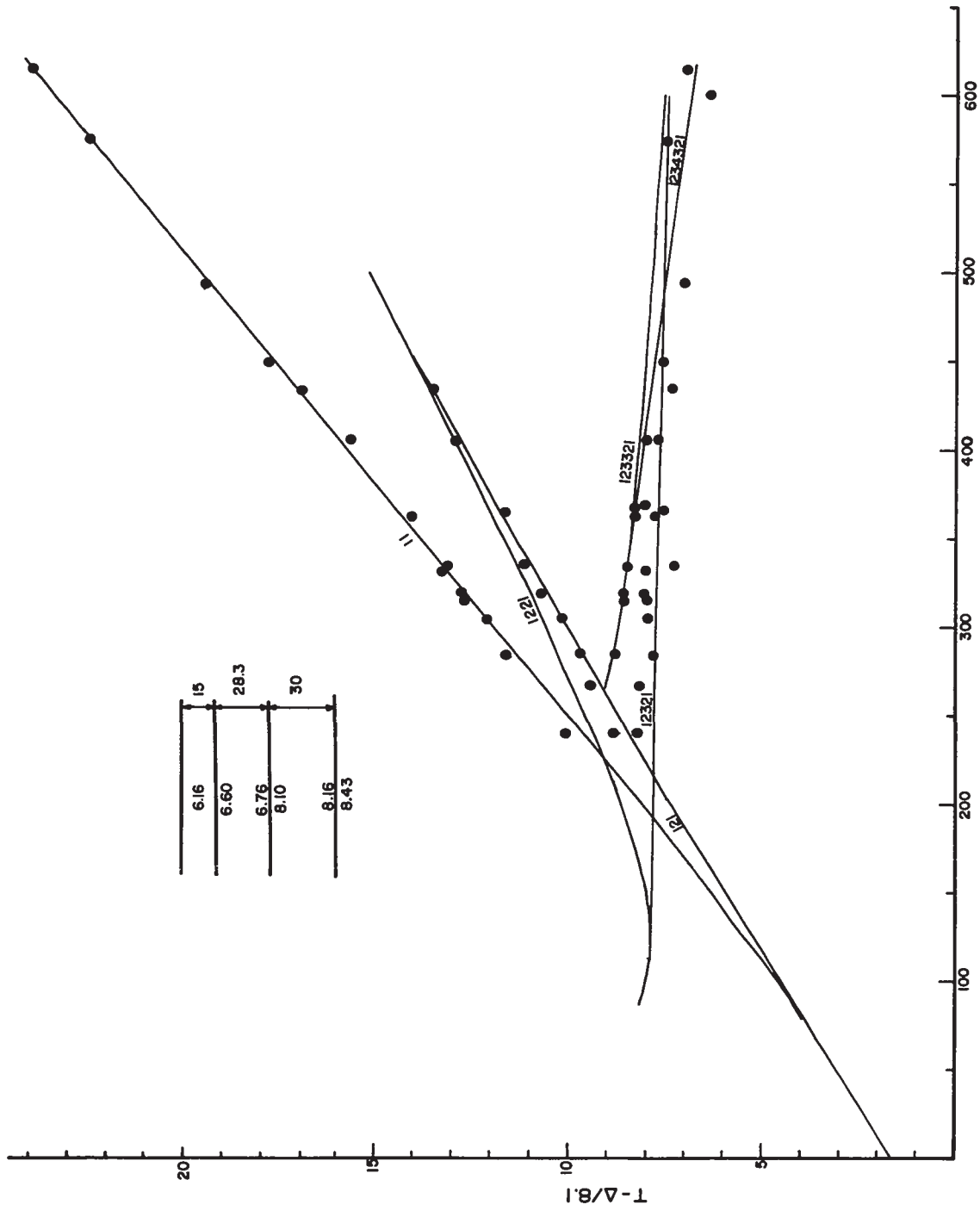

Fig. 9-10 Model fit for the Nipigon-Smooth Rock Falls events.

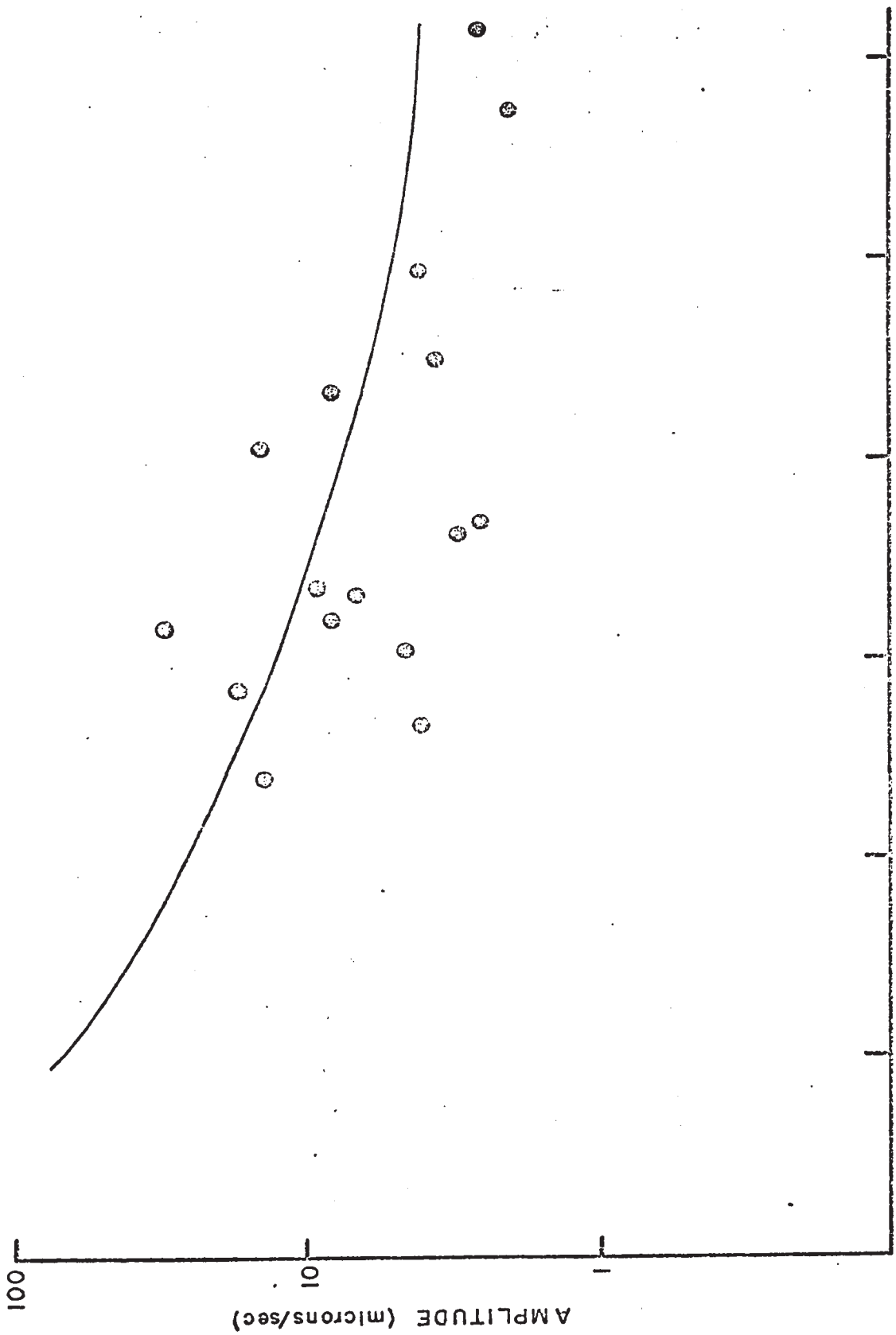

Fig. 9-11 (a) Nipigon-Smooth Rock Falls line amplitude measurements for the upper crustal reflection 11.

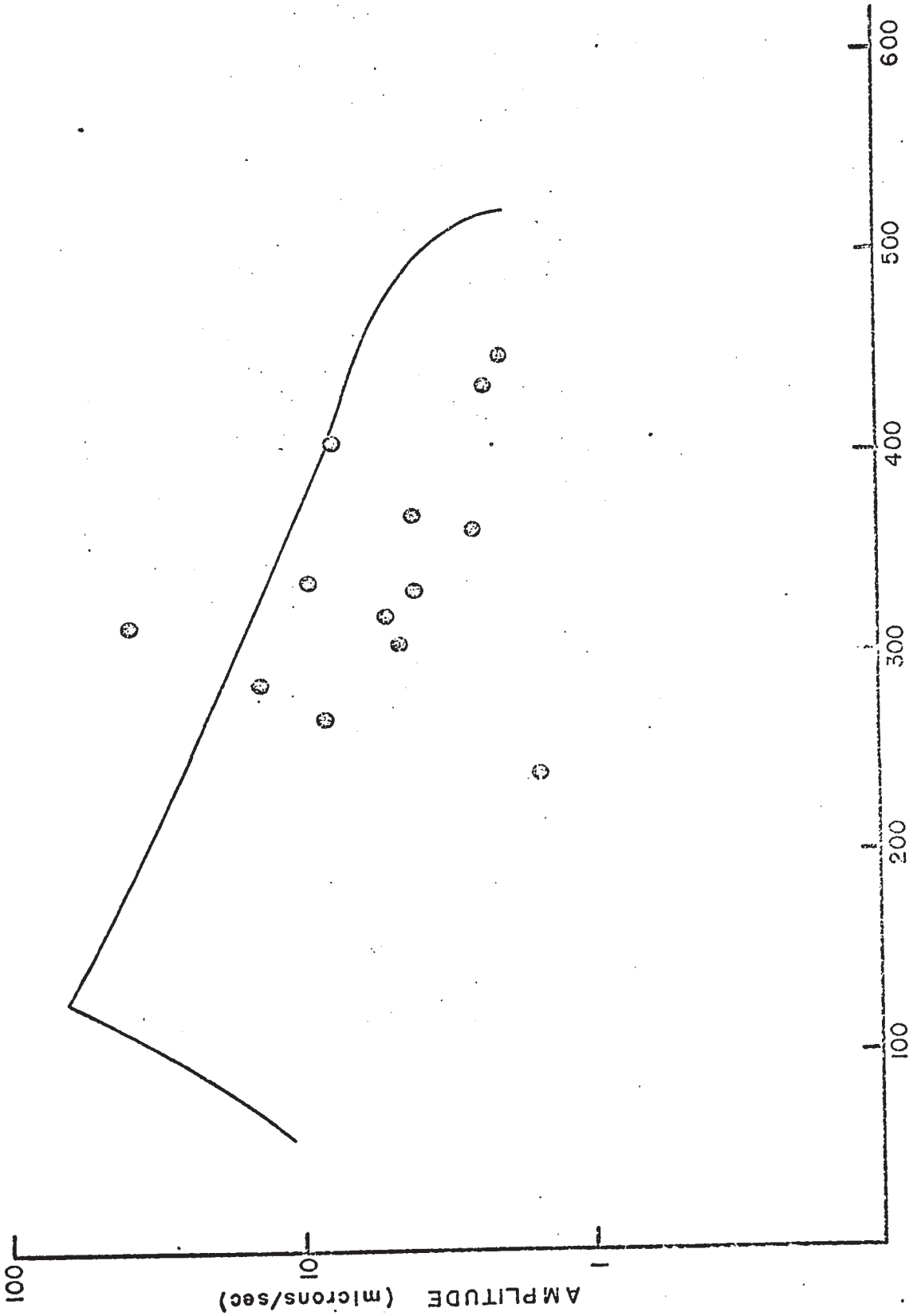

Fig. 9-11(b) Nipigon-Smooth Rock Falls line amplitude measurements for the Moho reflection 1221.

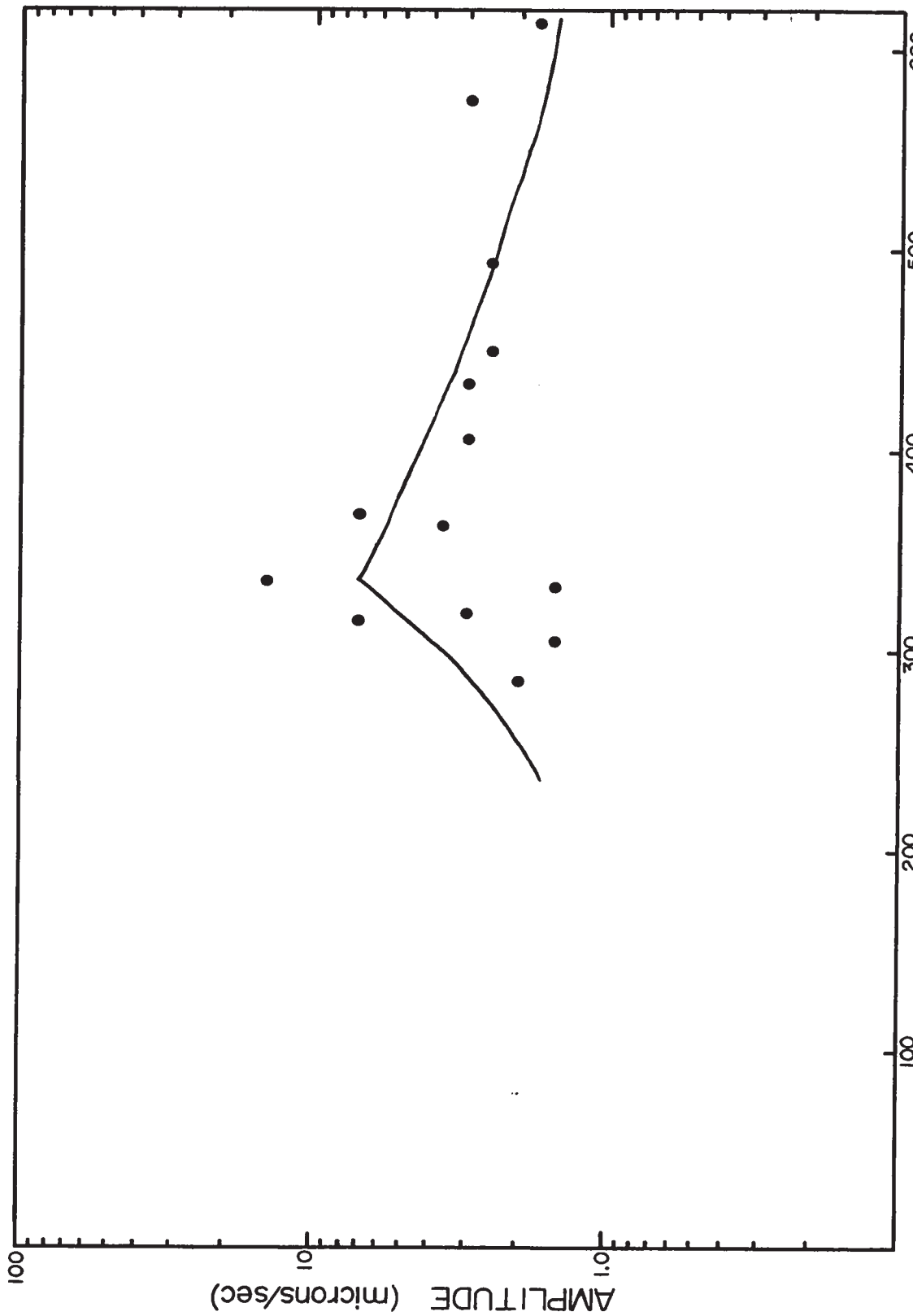

Fig. 9-11(c) Nipigon-Smooth Rock Falls line amplitude measurements for the 'Hales' reflection 123321.

The peak-to-peak amplitudes measured for the interpreted later events are shown in fig. 9-11. The measurements of all events demonstrate a large scatter limiting their effectiveness in refining the model fit. In general however, there is a correlation between measured amplitudes of the events and the predicted amplitude curves as computed from the arrival time model.

CHAPTER X

DISCUSSION AND SUMMARY

10.1 Conclusions Concerning the Earth's Crust in Northern Ontario and Manitoba

The average crustal velocities observed in Northern Ontario and Manitoba are typical of stable interior shield regions. From particle-motion studies the near-surface velocities measured along the Early Rise Line give values near 5.5 km/sec coinciding well with upper crustal velocities measured in Lake Superior.

Evidence for a two-layered crust comes from a weak later arrival which gives a velocity in the range 6.6-6.8 km/sec with a suggestion of a velocity gradient beneath this horizon. The average crustal velocity from direct waves for both the Early Rise and the Lake Nipigon-Smooth Rock Falls section is 6.15 km/sec suggesting a sialic composition. The exact thickness of the sialic upper crust cannot be determined from the results. However, the high velocities observed in the boundary zone between the Churchill and Superior Provinces, lead to the interpretation that the sialic upper crust is missing in that area.

Crustal thicknesses in the survey area vary between 55 km in Lake Superior and 50 km near the north end of the Early Rise line, to 30 km in the interior Superior Province. The thin crust determined under the oldest part of the Canadian Shield can be considered as evidence in favour of the hypothesis of uplift and erosion of the continental nucleus.

The thick crust observed in Lake Superior has been found to be confined to this area, forming a basin shaped depression in the Mohorovicic discontinuity horizon. Normal crustal thickness occurs immediately north of the lake.

Crustal velocity and thickness variations could not be correlated with divisions within structural provinces from the Early Rise data. Such structural belts as the English River, Cross Lake and Quetico, do not have structural expression on the Mohorovicic discontinuity associated with them and can be considered as near-surface phenomena.

10.2 Conclusions Concerning the Upper Mantle in Northern Ontario and Manitoba

Measurements of spectral components of the first arrival suggest that the average specific attenuation coefficient Q may be as low as 200; however, the statistical error involved in the analyses is high.

From first arrival times and first-break amplitude measurements a definite discontinuity in the seismic arrivals from the upper mantle has been noted. Through the use of digital filtering techniques later multiple reflected arrivals corresponding to this discontinuity model have been identified.

Hales (1969) has suggested a reasonable geological model corresponding to the above discontinuity to be the transition from spinel to garnet peridotite in the upper mantle. From experimental data this transition is postulated to be sharp but with a range of occurrence between 40 and 120 km depth. Since the earliest definition

of this horizon was due mainly to Hales this present author has denoted the discontinuity as the "Hales discontinuity" throughout this thesis. In view of the evidence accumulating for this discontinuity being at least continent-wide, it is suggested that the above terminology be adopted in seismological literature.

Beneath the Early Rise stations in Northern Ontario and Manitoba the best travel-time and amplitude fits suggest the Hales discontinuity from 8.05 km/sec to 8.43 km/sec to be at a depth of approximately 85 km.

The occurrence of later arrivals in the early portions of the Early Rise seismograms appearing as prominent events at distances near 1500 km has led to the model fit of a high velocity transition from 8.43 to a higher velocity at a depth of approximately 115 km giving rise to multiple reflected events.

10.3 Contributions to Knowledge

1. The portable three-component seismic station is a most efficient recording system for crustal refraction surveying.
2. Examination of particle-motion plots of first arrivals from three-component stations yields valuable information on the upper crustal velocities beneath the stations.
3. The boundary zone between the Superior and Churchill structural provinces is denoted by a velocity anomaly in the upper crust and by regional change in thickness of the crust.
4. Band pass filtering of crustal records has limited usefulness in enhancing later arrivals, however, some improvement was found. Particle-motion digital filtering of three-component records is a promising technique for enhancing later events.

6. A sub-Mohorovicic velocity discontinuity at a depth of approximately 85 km has been outlined from first arrival travel-time and amplitude discontinuities and has been substantiated by reflected events interpreted as later arrivals. This discontinuity has been denoted as the "Hales Discontinuity". Future crustal seismic studies should be designed to obtain more information on the nature of this discontinuity and to confirm its regional relationships. Amplitude measurements of reflected waves in conjunction with model studies may become a most powerful tool in the analysis of fine structure associated with this discontinuity.
7. The presence of a sub-Hales discontinuity at a depth of approximately 115 km. has been indicated from the interpretation of later reflected events, however the exact nature of this boundary is not well defined.

REFERENCES

Alsop, L.E., G.H. Sutton, and Maurice Ewing, (1961), 'Measurement of Q for Very Long Period Free Oscillations' Jour. Geophys. Res., Vol. 66, No. 9, pp. 2911-2916.

Anderson, D.L., (1967), 'Latest Information from Seismic Observations', Chapt. 12 in 'The Earth's Mantle', ed. by R. Gaskell, Academic Press, New York.

Anderson, D.L., and C.B. Archambeau, (1964), 'The anelasticity of the Earth', Jour. Geophys. Res., Vol. 69, No. 10, pp. 2071-2084.

Anderson, D.L., and M.N. Toksoz, (1963), 'Surface Waves on a Spherical Earth, 1. Upper Mantle Structure from Love Waves', Jour. Geophys. Res., Vol. 68, No. 11, pp. 3483-3500.

Archambeau, C.B. and E.A. Flinn, (1965), 'Automated Analysis of Seismic Radiation for Some Characteristics', Proc. of the I.E.E.E., pp. 1876-1877.

Arons, A.B., (1954), 'Underwater Explosion Shock Wave Parameters at Large Distances from the Charge', Jour. Acous. Soc. Am. Vol. 26, No. 3, pp. 343-346.

Asano, S., (1966), 'Reflection and Refraction of Elastic Waves at a Corrugated Interface', Bull. Seis. Soc. Am., Vol. 56, No. 1, pp. 201-222.

Barr, K.G., (1967), 'Upper Mantle Structure in Canada from Seismic Observations Using Chemical Explosions', Can. Jour. Earth Sci., Vol. 4, No. 5, pp. 961-976.

Basham, P.W., and R.M. Ellis, (1969), 'The Composition of P Codas Using Magnetic Tape Seismograms',Bull. Seis. Soc. Am., Vol. 59, No. 2, pp. 473-486.

Bath, Markus, and A.L. Arroyo, (1962), 'Attenuation and Dispersion of G Waves', Jour. Geophys. Res., Vol. 67, No. 5.

Bell, C.K., (1966), 'Churchill-Superior Province Boundary in Northern Manitoba', Geol. Surv. Can. Paper 66-1, pp. 133-136.

Berry, M.J. and G.F. West, (1966), 'A Time-Term Interpretation of the First-Arrival Data of the 1963 Lake Superior Experiment', in 'The Earth Beneath the Continents', ed. by J. S. Steinhart and T. J. Smith, A.G.U. Monograph No. 10, pp. 166-180.

Blackman, R.B. and J.W. Tukey, (1958), 'The Measurement of Power Spectra from the Point of View of Communications Engineering', Dover, New York.

Brune, J. and J. Dorman, (1963), 'Seismic Waves and Earth Structure in the Canadian Shield', Bull. Seis. Soc. Am., Vol. 53, pp. 167-209.

Bullen, K.E., (1963), 'An Introduction to the Theory of Seismology', Cambridge University Press, 3rd ed.

Cerveny, Vlastislav, (1966), 'On Dynamic Properties of Reflected and Head Waves in the n-layered Earth's Crust, Geoph. J. R. Astr. Soc., Vol. 11, pp. 139-147.

Cerveny, Vlastislav, (1967), 'On Some Kinematic and Dynamic Properties of Reflected and Head Waves in the Case of Layered Overburden', Geophysikalni Sbornik, No. 244, Ceskoslovenska Akademie Ved. 1966.

Costain, J.K., K.L. Cook, and S.T. Algermissen, (1963), 'Amplitude, Energy and Phase Angle of Plane SV Waves and Their Application to Earth Crustal Studies', Bull. Seis. Soc. Am., Vol. 53, No. 5, pp. 1039-1074.

Cole, R.H., (1948), 'Underwater Explosions', University Press, Princeton.

DeBraemaeker, J. Cl., (1968), 'Comment on Paper by Leroy M. Dorman, 'Anelasticity and the Spectra of Body Waves', Jour. Geophys. Res., Vol. 73, No. 22, pp. 7147-7148.

DeBremaeker, J.Cl., R.H. Godson, and J.S. Watkins, (1966), 'Attenuation Measurements in the Field', Geoph. Vol. 31, No. 3, pp. 562-569.

Dorman, L.M., (1968), 'Anelasticity and the Spectra of Body Waves', Vol. 73, No. 12, pp. 3877-3884.

Eaton, J.P., (1963), 'Crustal Structure from San Francisco, California, to Eureka, Nevada, from Seismic-Refraction Measurements', Jour. Geoph. Res. Vol. 68, No. 20, pp. 5789-5806.

Ellis, R.M. and P.W. Basham, (1968), 'Crustal Characteristics from Short Period P Waves', Bull. Seis. Soc. Am., Vol. 58, No. 5, pp. 1681-1700.

Ewing, W.M., W.S. Jardetzky, Frank Press, (1957), 'Elastic Waves in Layered Media', McGraw-Hill, Toronto.

Futterman, W.I., (1962), 'Dispersive Body Waves', Jour. Geophys. Res., Vol. 67, No. 13, pp. 5279-5211.

Gibb, R.A., (1968), 'A Geological Interpretation of the Bouger Anomalies Adjacent to the Churchill-Superior boundary in Northern Manitoba', Can. Jour. Earth Sci., Vol. 5, No. 3, Part 1, pp. 439-454.

Grant, F.S. and G.F. West,(1965), 'Interpretation Theory in Applied Geophysics', McGraw-Hill, Toronto.

Green, R.W.E., and A.L. Hales, (1968), 'The Travel Times of P Waves to 30° in the Central United States and Upper Mantle Structure', Bull. Seis. Soc. Am., Vol. 58, No. 1, pp. 267-289.

Hajnal, Z., (1969), 'A Two Layer Model for the Earth's Crust under Hudson Bay' in Earth Science Symposium on Hudson Bay, ed. by P. J. Hood, Geol. Surv. Can. Paper 68-53, pp. 326-336.

Hales, A.L., (1969), 'A Seismic Discontinuity in the Lithosphere', Earth and Plan. Sci. Let. Vol. 7, No. 1, pp. 44-46.

Hall, D.H. and W.C. Brisbin, (1965), 'Crustal Structure from Converted Head Waves in Central Western Manitoba', Geophysics, Vol. 30, No. 6.

Halls, H.C., (1966), 'A Review of the Keeweenawan Geology of the Lake Superior Region, in AGU Monograph No. 10, pp. 3-27.

Healey, J.H., (1963), 'Crustal Structure Along the Coast of California from Seismic-Refraction Measurements', Jour. Geophys. Res., Vol. 68, No. 20, pp. 5777-5787.

Healey, J.H., and D.H. Warren, (1969), 'Explosion Seismic Studies in North America', in The Earth's Crust and Upper Mantle, Geophysical Monograph No. 13, ed. P. J. Hart, American Geophysical Union, Washington, D.C., pp. 208-219.

Heelan, P.A., (1953), 'On the Theory of Head Waves', Geophysics, Vol. 18, No. 4, pp. 871-893.

Hill, D.P., and L.C. Pakiser, (1966), 'Crustal Structure Between the Nevada Test Site and Boise, Idaho from Seismic Refraction Measurements', in A.G.U. Monograph No. 10, pp. 391-419.

Hobson, G.D., A. Overton, D.N. Clay, and W. Thatcher, (1967), 'Crustal Structure under Hudson Bay', Can. Jour. Earth Sci. Vol. 4, No. 5, pp. 929-947

Hodgson, J.H., (1953), 'A Seismic Survey in the Canadian Shield', Dom. Obs. Pub., Vol. 16, No. 5 and No. 6.

Howell, B.F., (1966), 'Lake Superior Seismic Experiment: Frequency Spectra and Absorption' in A.G.U. Monograph No. 10, ed. by J. S. Steinhart and T. J. Smith, Washington, D.C. pp. 227-233.

Hunter, J.A., and R.F. Mereu, (1967), 'The Crust of the Earth under Hudson Bay', Can. Jour. Earth Sci., Vol. 4, No. 5, pp. 949-960.

Innes, M.J.S., (1960), 'Gravity and Isostasy in Northern Ontario and Manitoba', Publ. Dom. Obs. Vol. 21, No. 6, pp. 263-338.

Iyer, H.M., L.C. Pakiser, D.J. Stuart, and D.H. Warren, (1969), 'Project Early Rise: Seismic Probing of the Upper Mantle', Jour. Geophys. Res., Vol. 74, No. 17, pp. 4409-4441.

Kaila, K.L., (1970), 'Decay Rate of P-Wave Amplitudes from Nuclear Explosions and the Magnitude Relations in the Epicentral Range 1^{o} to 98^{o}, Bull. Seis. Soc. Am., Vol. 60, No. 2, pp. 447-460.

Knopoff, L., (1964), 'Q', Rev. of Geophysics, Vol. 2, No. 4.

_____, (1969), 'Attenuation of Seismic Waves in the Mantle', in A.G.U. Monograph 13, ed. by P.J. Hart, Washington, D.C. pp. 273-275.

Kornik, L.J. and A.S. MacLaren, (1966), 'Aeromagnetic Study of the Churchill-Superior Boundary in Northern Manitoba, Can. Jour. Earth Sci., Vol. 3, No. 4, pp. 547-557.

Lehmann, I., (1964), 'On the Travel Times of P as Determined from Nuclear Explosions', Bull. Seis. Soc. Am., Vol. 54, pp. 123-139.

Lewis, B.T.R., and R.P. Meyer, (1968), 'A Seismic Investigation of the Upper Mantle to the West of Lake Superior', Bull. Seis. Soc. Am., Vol. 58.

Lomnitz, C., (1962), 'Application of the Logarithmic Creep Law to Stress Wave Attenuation in the Solid Earth', Jour. Geophys. Res., Vol. 67, No. 1, pp. 365-368.

Long, L.T., and J.W. Berg, (1969), 'Transmission and Attenuation of the Primary Seismic Wave 100 to 600 km', Bull. Seis. Soc. Am., Vol. 59, No. 1, pp. 131-146.

Mansfield, R.H., and J.F. Evernden, (1966), 'Long Range Seismic Data from the Lake Superior Seismic Experiment 1963-1964', in A.G.U. Monograph No. 10, pp. 249-269.

McCamy, K., R.P. Meyer, and T. J. Smith, (1962), 'Generally Applicable Solutions of Zoepprity Amplitude Equation', Bull. Seis. Soc. Am., Vol. 52, No. 4, pp. 923-955.

McGarr, A.R.B. Hoffman, and G.D. Hair, (1964), 'A Moving-Window Signal-Spectra Process', Geophysics, Vol. 29, no. 2, pp. 212-220.

Mereu, R.F., (1965), 'A Study of the Apparent Angles of Emergence at Marathon, Ontario from the Lake Superior Data', Bull. Seis. Soc. Am., Vol. 55, No. 2, pp. 405-416.

Mereu, R.F., (1966), 'An Iterative Method for Solving the Time-Terms Equations' in A.G.U. Monograph No. 10, pp. 485-497.

Mereu, R.F. (1968), 'Curvature Corrections to Upper Mantle Seismic Refraction Surveys', Earth and Plan. Sci. Letters, Vol. 3, pp. 469-475.

Mereu, R.F., (1969), 'Effect of Mohorovicic Topography on the Amplitude of Seismic P Waves', Jour. Geophys Res., Vol. 74, No. 17, pp. 4371-4376.

Mereu, R.F. and J.A. Hunter, (1969), 'Crustal and Upper Mantle Structure Under the Canadian Shield from Project Early Rise Data', Bull. Seis. Soc. Am., Vol. 59, No. 1, pp. 147-165.

Nuttli, Otto, and J. D. Whitmore, (1961), 'An Observational Determination of the Variation of the Angle of Incidence of P Waves with Epicentral Distance', Vol. 51, No. 2, pp. 269-276.

O'Brien, P.N.S. (1960), "Seismic Energy from Explosions", Geophy. Jour. Roy. Astr. Soc., Vol. 3, pp. 29-39.

O'Brien, P.N.S. (1967), 'The Efficient Use of Large Charges', in Seismic Refraction Prospecting', ed. by A. W. Musgrove, S.E.G. Publication, pp. 152-170.

O'Brien, P.N.S., (1968), 'Lake Superior Crustal Structure - A Reinterpretation of the 1963 Seismic Experiment', Jour. Geophys. Res., Vol. 73, No. 8, pp. 2669-2689.

Overton, A., (1969), 'An Alternative Interpretation of the 1965 Hudson Bay Crustal Seismic Data', in Geol. Surv. of Can. Paper 68-53, pp. 292-306.

Pakiser, L.C. and D.P. Hill, (1963), 'Crustal Structure in Nevada from Nuclear Explosions', Jour. Geophys. Res., Vol. 68, No. 20, pp. 5757-5766.

Papazachos, Basil, (1964), 'Angle of Incidence and Amplitude Ratio of P and PP Waves', Bull. Seis. Soc. Am., Vol. 54, pp. 105-121.

Peacock, K.L., and Sven Treitel, (1969), 'Predictive Deconvolution Theory and Practice', Geophysics, Vol. 34, No. 2, pp. 155-169.

Press, Frank, (1964), 'Seismic Wave Attenuation in the Crust', Jour. Geophys. Res., Vol. 69, No. 20, pp. 4417-4418.

Robinson, E.A., (1967), 'Statistical Communication and Detection with Special Reference to Digital Data Processing of Radar and Seismic Signals, Griffin, London.

Roller, J.C.,(1965), 'Crustal Structure in the Eastern Colorado Plateaus Province from Seismic Refraction Measurements', Bull. Seis. Soc. Am., Vol. 55, No. 1, pp. 107-119.

Roller, J.C., and J.H. Healy, (1963), 'Seismic Refraction Measurements of Crustal Structure between Santa Monica Bay and Lake Mead', Jour. Geophys. Res., No. 20, pp. 5837-5849.

Roller, J.C., and W.H. Jackson, (1966), 'Seismic-Wave Propagation in the Upper Mantle Lake Superior, Wisconsin to Denver, Colorado', in the Earth Beneath the Continents, ed. by J.S. Steward and T.J. Smith, A.G.U. Monograph No. 10, Washington, pp. 270-275.

Romney, Carl, (1959), 'Amplitudes of Seismic Body Waves from Underground Nuclear Explosions', Jour. Geophys. Res., Vol. 64, No. 10, pp. 1489-1498.

Ruffman, A., (1969), 'Seismic Investigations of the Crust in the Hudson Bay Region', in Geol. Surv. Can. Paper 68-53, pp. 307-314.

Ruffman, Alan, and M.J. Keen, (1967), 'A Time-term Analysis of the First Arrival Data from the Seismic Experiment in Hudson Bay, 1965', Can. Jour. Earth Sci. Vol. 4, No. 5, pp. 901-928.

Ryall, Allan, And D.J. Stuart, (1963), 'Travel Times and Amplitudes from Nuclear Explosions, Nevada Test Site, to Ordway, Colorado', Journ. Geophys. Res. Vol. 68, No. 20, pp. 5821-5835.

Shimazu, Yasuo, (1962), 'A Study of the Geophysical and Geodetic Implications of Gravity Data for Canada', Dom. Obs. Pubs., Vol. 26, No. 7, pp. 323-354.

Slichter, L.B., (1951), 'Crustal Structure in the Wisconsin Area', Office Naval Res. Rept., N9onr 96200.

Smith, T.J., J.S. Steinhart and L.T. Aldrich, (1966), Lake Superior Crustal Structure,' Jour. Geophys. Res., Vol. 68, No. 20, pp. 5821-5835.

Spiegel, M.R., (1961), 'Statistics', Schaum, New York.

Steinhart, J.S., and R.P. Meyer, (1961), 'Explosion Studies of Continental Structure', Carnegie Inst. Wash. Pub. 622.

Stockwell, C.H., (1964), 'Geological Studies' in 'Age Determinations and Geological Studies', Geol. Surv. Can. Paper 64-17, Part II, 7-21.

Strick, E., (1967), 'The Determination of Q, Dynamic Viscosity and Transient Creep Curves from Wave Propagation Measurements', Geophys. J. R. Astr. Soc., Vol. 13, pp. 197-218.

Sutton, G.H., Walter Mitronovas, and P.W. Pomeroy, (1967), 'Short-Period Seismic Energy Radiation Patterns from Underground Nuclear Explosions and Small-Magnitude Earthquakes', Bull. Seis. Soc. Am., Vol. 57, No. 2, pp. 249-268.

Topping, J., (1962), 'Errors of Observation and their Treatment', Chapman and Hall, London.

Vanek, Jiri, (1968), 'Amplitude Curves of Seismic Body Waves between 5^{o} and 25^{o}', Bull. Seis. Soc. Am., Vol. 58, No. 3, pp. 1035-1039.

Vanek, Jiri, and Cornelius Radu, (1964), 'Amplitude Curves of Seismic Body Waves at Distances Smaller than 12^{o}, Stud. Geophys. et. Geod., Vol. 8, No. 4, pp. 319-325.

Walsh, J.B., (1966), 'Seismic Wave Attenuation in Rock Due to Friction', Jour. Geophys. Res., Vol. 71, No. 10, pp. 2591-2599.

Warren, D.H., J.H. Healy, J.C. Hoffmann, Reinis Kempe, S. Rauula, and D.J. Stuart, (1967), 'Project Early Rise: Travel Times and Amplitudes', U.S.G.S. Technical Letter, NCER-6.

Weber, J.R., and A.K. Goodacre, (1966), 'A Reconnaissance Underwater Gravity Survey of Lake Superior' in A.G.U. Monograph No. 10, pp. 56-65.

Werth, G.C., R.F. Herbst, and D. Springer, (1962), 'Amplitudes of Seismic Arrivals from the M Discontinuity', Jour. Geophys. Res., Vol. 67, pp. 1587-1610.

Weston, D.E., (1960), 'Underwater Explosions as Acoustic Sources', Proc. Phys. Soc. Vol. 76, No. 2, pp. 233-249.

Willis, D.E., and J.M. DeNoyer, (1966), 'Seismic Attenuation and Spectral Measurements from the Lake Superior Experiment', in A.G.U. Monograph No. 10, ed. by J.S. Steinhart and T.J. Smith, Washington, D.C., pp. 218-226.

Wilson, H.D.B., and W.C. Brisbin, (1962), 'Tectonics of the Canadian Shield in Northern Manitoba', Roy. Soc. Can. Special Pub. No. 4, pp. 60-75. The Tectonics of the Canadian Shield, ed. J. S. Stevenson.

Worthing, A.G., and J. Geffner, (1943), 'Treatment of Experimental Data', Wiley and Sons, New York.

APPENDIX A

1. Specifications for Instruments

CLOCK-SWITCH - PFN-LANDIS & GYR SHF 15.15
Spring-wound 3 day clock with 15 minute contact on-off sequence, programmable to 4 sequences per 24 hrs.

TIME-SIGNAL RADIO - DEVELCO MODEL 3202A

ELECTRICAL:

Antenna Inputs (Switchable):	Internal:	Built-in ferrite cored loop.
	External:	50 ohm input jack (BNC) for external antennal.
Carrier Frequency:	60 kHz.	
Intermediate Frequency:	2 kHz	
Bandwidths (Switchable):	100 Hz and 1 kHz.	

GEOTECH TAPE RECORDER (REMOTE STATION)

Heads	IRIG standard
Tracks	7
Tape, thickness	1.0 and 1.5 mil
type	Mylar instrumentation
reels	10.5 and 14 in.
width	0.5 in.
Speed, nominal	15/160 ips (2.38 mm/sec)
accuracy	±0.25%
Operating specifications	
Input, frequency	DC to 17 cps
impedance	50 kohm (minimum)
VCO, frequency	84.4 cps
deviation	±40%
sensitivity	1.0 to 5 V (rms) for full deviation
linearity error	±1% of full deviation
drift	variation does not exceed ±7% over the operating temperature range.
Signal-to-noise ratio	40 dB min (rms basis) 35 dB (p-p basis)
Power specifications	
Voltage, nominal	+12, 0, -12 Vdc
range	11 to 14 V both legs
Power, nominal	11 watts (7 channels record only) 13 watts (7 channels record and 1 channel reproduce)

SPRENGNETHER CHRONOMETER - MODEL TS-100

24 hour clock dial

Resettable sweep second hand
Minute switch - closure once per minute, 1 - 3 seconds (adjustable)
Hour switch - closure once per hour, 5 - 30 seconds (adjustable)
12 hour switch - closure once per 12 hours, 1-6 minutes (adjustable)
Contact rating - 2 Amps @ 115 V AC.

Sanborne Single Channel Recorder (Manned vertical component station)

Frequency Response:		Flat from d-c to 100 cycles within 3 db at 10 div. peak-to-peak amplitude.

Precision Instrument Tape Recorder (Manned 3-component station) Model PI-6104

Input Sensitivity:	(High Level)	1 to 20 volts peak-to-peak for ±40% deviation
	(Low Level)	0.030 to 1 volt peak-to-peak for ±40% deviation
Nominal Input Level:		2.8 volts peak-to-peak (1 vrms)
Input Impedance:	(High Level)	20 k ohms or greater, unbalanced to ground
	(Low Level)	50 k ohms or greater, unbalanced to ground

Carrier Frequency, Response, Signal-to-Noise Ratio:

High Level	Center Frequency	Response	S/N
.375 ips	500 cps	DC to 100 cps ±1 db	30 db
3.75 ips	5 k cps	DC to 1 kc ±1 db	35 db
37.5 ips	50 k cps	DC to 10 kc ±1 db	40 db
Low Level			
.375 ips	500 cps	5 to 100 cps ±1 db	30 db
3.75 ips	5 kc	5 cps to 1 kc ±1 db	35 db
37.5 ips	50 kc	5 cps to 10 kc ±1 db	40 db

Willmore Seismometer - Mark I model

Natural frequency = 1 hertz
Weight = 21 lbs
Size = 5 1/2" diam. x 11.5" high
Coil Resistance = 500 ohms.

Electrotech Seismometer - EV - 17

Mass - 2.2 kg.

Coil Resistance 500 ohms

Natural Frequency - 1.0 hertz.

AMPLIFIER - ELECTROTECH SPA-10

1.3.2 SPA-10 Amplifier Module

Gain:	5×10^5 voltage gain
Stability:	Within 3 db from -40° to 50° C.
	Within 1 db when voltage varies from -4 volts to +5 volts of nominal 24 volts.
Attenuation:	Two controls - one from 0 to -42 db in 6 db steps; second, from 0 to -6 db continuous between steps.
Noise:	Maximum equivalent input noise is 0.1 microvolts rms with a 500 ohm input at 12 cpts bandwidth.
Bandwidth:	0.1 to 350 cps between 70% response points - no filter bandwidth.
Filter:	1) Active type 18 db/octave low pass filter with cut-off frequencies of 5, 7, 10, 13, 17, 23 and 30 cps.
	2) Active 60 cps (or 50 cps if preferred) Notch filter also provided.
Input Impedance:	4000 ohms
	2200 ohms when mounted in the Control Unit.
Output:	Two - with one 30 db under the other.
	Output impedance less than 1000 ohms; all specifications are for 10,000 ohm resistive load.
Distortion:	Less than 1% with 1.0 volt rms output.
	Less than 5% with 4 volts rms.
Maximum Output Voltage:	1.0 volt (peak-to-peak) less than the supply voltage.
Power Requirements:	
Voltage:	Nominal 24 volts dc, -4 to +5 volts.
Current:	16 milliamperes.

2. Analog to Digital Conversion Technique

a) Analog Tape Search

To initiate A to D conversion the analog 1/4" tape was mounted on the P.I. tape recorder and the footage counter was reset to zero. The four channels from the P.I. were connected to the plug-board on the front panel of the digital system. A second set of plugs in parallel with these connected the P.I. tape recorder to the Sanborn 4-channel hot-wire monitor. Record searches were made in this manner from the P.I. to the hot-wire monitor through the digitizer input panel, with the digitizer on standby. By playing the P.I. tape at 37.5"/sec the beginning of a seismic record could be found with ease by observing the monitor. Exact positioning was made by playing the P.I. tape in both forward and reverse directions at standard speed of 3.75"/sec. Once the start point was determined , The P.I. speed was changed to 0.375"/sec with the 100 cps filter on and the tape was played in reverse while the digital system was being prepared. The above technique was developed when it was discovered that holding the P.I. tape recorder on standby caused high frequency signals to be generated in the input to the hot-wire monitor; this caused pen vibration and damage on the monitor.

b) Readying the Digital System

After allowing the digitizer component units one-half hour warm-up time, a digital grade 1/2" magnetic tape was mounted on the Kennedy incremental tape recorder. Mounting was done with the tape recorder

shut off to release the brakes. Care was taken to ensure that the silver strip begin-marker was not wound past the tape heads. With the Kennedy tape recorder turned on, and the system scanner set at manual, the tape wind advance button was depressed until a tone indicated automatic positioning had begun. At this point the tape heads were in the correct position past the silver strip beginning marker.

c) Writing the Experiment Identifier

Each digitized seismogram was assigned an identifying number between 0 and 99. This was done by scanning the channel having this number. The scanner was set to 100 measurements between I.R. gaps, and the left-hand channel scan switch was set to the channel number given by the seismogram identifier. The scan select panel was set to single channel and continuous measurement. This ensured that the number shown on the left-hand channel scan switch would be sampled continuously.

The scanner was set on automatic, the run button was depressed, and at least 20 measurements were allowed to be written on the tape before the re-set button was pressed to stop the recording. Since no connection had been made with the data channel belonging to this channel identifier, no information was measured. Since the seismogram identifier number (as the channel identification number) was less than 100, a subsequent computer editing program assigned the identifier number as this channel number in writing a binary tape.

d) Digitizing the Calibration Signal

To indicate the onset of the calibration oscillator signals on the three component channels, a series of channel measurements for channel 101 were put on the digital tape in a manner similar to that described above. This series of channel identifiers and blank data channels served as a spacer between the seismogram identifier channel and the onset of the test oscillator.

To record the test oscillator the channel scan was set to 195 on the left-hand side (minimum channel no. or start of scan) and 198 on the right-hand switch (Maximum channel no. or end of scan). The scanner I.R. gap control was set at 750 scans (750 x 4 channels = 3000 words), and the scanning mode was set at continuous scan. The analog tape was then played forward at 0.375"/sec until the test oscillator signal appeared on the hot-wire monitor. The digitizer was set at run position and several cycles of oscillator signal were recorded. The components of motion assigned to the data channels were as follows:

ch. 195	Vertical
ch. 196	North-South
ch. 197	East-West
ch. 198	Time

With the digitizer in scan mode, the channels were sampled sequentially starting with channel 195. The reset button was pressed to stop recording.

To indicate the end of the test oscillator recording and to act as a spacer, several measurements of single scan for channel 102 were put on the tape in a manner similar to that of the seismogram identifier

and the test oscillator onset identifier.

e) Digitizing the Seismic Traces

With the digitizer on stand-by, the analog tape was searched for the onset of the first arrival energy. The analog tape was then reversed to a start point approximately 6 seconds before the onset and returned to the 0.375"/sec speed and 100 hertz output filter. The digitizer was started on continuous scan between channel 195 and 198 with 750 scans between I.R. gaps. The digitizing continued until at least the onset of surface waves, when reset was pushed to terminate digitizing. If termination of a seismogram digitizing also coincided with the end of tape, a manual end-of-file signal was put on the tape by setting the scanner on manual and pushing the end-of-file mark button on the Kennedy incremental tape recorder. The system was not allowed to run out of tape while digitizing a record since it was found that the U.W.O. tape units did not recognize a silver strip end-of-file mark, and tape error messages resulted.

f) Tape Transfer Procedure

To transfer the 556 bits/inch B.C.D. tapes to 880 bits/inch binary tapes, more amenable to data processing, a program was written by Mrs. Iya Downing of the U.W.O. Computer Centre and is on file there. The control cards at the beginning of the program give the operator instructions for setting of tape densities prior to program execution. The program itself is written mainly in MAP language with a testing and printout subroutine in FORTRAN.

The resultant binary tape consists of data written in blocks of 20 words, ten of which are channel identifiers. The first word of each seismogram record is the channel identifier signifying the experimental number (0-99). The second number consists of an integer giving the numb er of measurements made in the experiment (recorded seismogram). Dividing this number by 4 yields the total number of measurements made on each trace plus 1/4 of the spacer measurements (channels 101 and 102). The remainder of this block and succeeding blocks consist of successive channel identifiers and measurements between channels 195 and 198. A value of 1000 added to the channel number signifies an inter-record gap (loss of seismic time) has occurred between this measurement and the following one. If an experiment ends before a block is filled, the remainder of the block is filled with zeros.

g) Condensed Tape Transfer

In an effort to put as much relevent seismic information as possible on a few magnetic tapes, a tape editing program was written to produce a new set of tapes. These tapes, in the binary format, were in many ways similar to the above-mentioned set, except that only the first 30 seconds of seismic record were written and all channel identifiers were absent. As well, the experiment identifier (the seismogram number) was converted to a floating point number multiplied by 10, and written 20 times (one block). The test oscillator recordings were not written on the condensed tape since gain calibration measurements had been made from the binary tape dump.

The resultant tapes (6 in all) contained all the information required to process the early portions of the seismograms in an efficient manner.

The experiment numbers assigned to each recording are given in Table A-7-I.

TABLE A - 7 - I

EARLYRISE STATION	RECORDING SHOT	EXPERIMENT NO.
2	1	1
4	2	2
4	3	3
7	4	4
6	5	5
8	6	6
8	7	7
10	8	8
12	10	9
12	11	10
13	13	11
16	15	12
18	16	13
18	17	14
20	19	15
22	20	16
22	21	17
24	22	18
24	23	19
26	24	20
26	25	21
28	26	22
28	27	23
30	29	24
32	30	25
34	32	26
34	33	27
36	35	28
38	36	29
38	37	30
40	38	31
40	39	32

EARLYRISE STATION	RECORDING SHOT	EXPERIMENT NO.
1	1	33
3	2	34
3	3	35
5	4	36
5	5	37
7	6	38
7	7	39
9	9	40
11	10	41
11	11	42
Earthquake		43
14	12	44
14	13	45
15	14	46
15	15	47
17	16	48
17	17	49
19	18	50
19	19	51
21	20	52
21	21	53
23	22	54
23	23	55
27	26	56
27	27	57
29	28	58
29	29	59
31	31	60
33	32	61
33	33	62
35	35	63
37	36	64
37	37	65
39	38	66
39	39	67

APPENDIX B

(a) DATA FOR SUPERIOR-CHURCHILL LINE

STATION NUMBER	STATION COORDINATES LATITUDE deg. min.	LONGITUDE deg. min.	SHOT NUMBER	DISTANCE (km)	(deg)	TRAVEL TIME (sec)	MOHO Time-term (sec)	MOHO DEPTH (km)
1	48 56.9	89 31.8	1	163.2	1.468	23.80		
2	49 19.8	89 38.0	1	206.0	1.854	30.25		
3	49 32.9	89 47.3	2	231.4	2.083	35.27		
3	49 32.9	89 47.3	3	231.4	2.083	35.26		
4	49 47.7	89 56.7	2	260.9	2.349	40.98	3.45	35
4	49 47.7	80 56.7	3	261.0	2.349	40.98	3.51	35
5	50 4.8	90 8.9	4	295.0	2.655	43.82	2.96	30
5	50 4.8	90 8.9	5	295.0	2.655	43.77	2.92	29
6	50 26.0	90 18.4	4	335.0	3.023	49.10	3.25	33
6	50 26.0	90 18.4	5	335.9	3.023	49.09	3.24	33
7	50 45.0	90 31.2	6	374.0	3.366	53.56	3.00	30
7	50 45.0	90 31.2	7	374.0	3.366	53.77	3.22	33
8	51 4.0	90 44.4	6	412.4	3.711			
8	51 4.0	90 44.4	7	412.4	3.711			
9	51 20.0	90 59.1	8	446.1	4.015			
9	51 20.0	90 59.1	9	446.2	4.016	62.57	3.13	32
10	51 40.3	91 3.9	8	483.4	4.351	67.14	3.10	31
10	51 40.3	91 3.9	9	483.5	4.351			
11	51 59.5	91 24.2	10	524.6	4.721	72.10	2.97	30
11	51 59.5	91 24.2	11	525.2	4.727	72.20	3.02	30
12	52 19.2	91 36.7	10	563.8	5.074	77.22	3.28	33
12	52 19.2	91 36.7	11	564.5	5.080	77.10	3.07	31
13	52 37.6	91 56.4	12	605.0	5.445	82.16	3.12	31
13	52 37.6	91 56.4	13	605.2	5.447	82.16	3.10	31
14	52 56.0	92 2.7	12	639.3	5.755	86.33	3.06	31
14	52 56.0	92 2.7	13	639.5	5.756	86.37	3.07	31
15	53 8.0	92 27.2	14	669.0	6.021	89.98	3.05	31
15	53 8.0	92 27.2	15	669.6	6.027	90.01	2.98	30
16	53 26.4	92 44.0	14	707.7	6.370			

STATION NUMBER	STATION COORDINATES LATITUDE deg. min.	LONGITUDE deg. min.	SHOT NUMBER	DISTANCE (km)	(deg)	TRAVEL TIME (sec)	MOHO Time-term (sec)	MOHO DEPTH (km)
16	53 26.4	92 44.0	15	708.4	6.376	94.40	3.00	30
17	53 39.5	93 2.6	16	738.4	6.646	97.93	3.04	31
17	53 39.5	93 2.6	17	738.7	6.649	98.00	3.08	31
18	53 51.8	93 15.2	16	764.9	6.885	100.92	2.87	29
18	53 51.8	93 15.2	17	765.2	6.888	100.91	2.79	28
19	54 7.7	93 21.9	19	795.1	7.157	104.60	3.14	32
19	54 7.7	93 21.9	18	795.2	7.158	104.65	3.10	31
20	54 24.7	93 30.4	19	827.6	7.450	108.52	3.28	33
20	54 24.7	93 30.4	18	827.7	7.450			
21	54 42.8	93 50.5	20	866.8	7.802	112.99	3.09	31
21	54 42.8	93 50.5	21	867.2	7.805	113.04	3.10	31
22	54 51.7	93 56.9	20	884.7	7.963	115.24	3.33	34
22	54 51.7	93 56.9	21	885.0	7.966	115.46	3.59	36
23	55 20.0	94 22.8	22	944.5	8.502	122.03	3.02	30
23	55 20.0	94 22.8	23	944.6	8.503	121.96	2.91	29
24	55 32.1	94 40.3	22	972.8	8.757	125.44	3.18	32
24	55 32.1	94 40.3	23	972.9	8.758	125.41	3.12	31
25	56 4.4	94 55.1	25	1032.6	9.205			
25	56 4.4	94 55.1	24	1032.7	9.296			
26	56 12.8	95 20.3	25	1058.2	9.526	135.20	2.78	28
26	56 12.8	95 20.3	24	1058.3	9.527	135.24	2.83	28
27	56 20.0	95 22.6	26	1071.3	9.643	135.89	3.02	30
27	56 20.0	95 22.6	27	1071.3	9.644	136.93	3.08	31
28	56 31.1	95 19.2	26	1088.1	9.795	139.09	3.38	34
28	56 31.1	95 19.2	27	1088.2	9.795	139.09	3.39	34
29	56 56.2	95 45.6	28	1142.3	10.283	145.57	3.65	37
29	56 56.2	95 45.6	29	1142.4	10.284	145.56	3.63	37
30	57 9.6	96 10.5	29	1176.0	10.586	149.68	3.91	39
30	57 9.6	96 10.5		1176.1	10.587			
31	57 23.6	96 23.8	31	1204.8	10.845	153.20	4.16	42
31	57 23.6	96 23.8	30	1204.9	10.846	153.19	4.13	42
32	57 43.6	96 38.7	31	1244.5	11.203	157.70	3.88	39
32	57 43.6	96 38.7	30	1244.6	11.204	157.70	4.31	43
33	57 54.9	96 50.8	32	1268.6	11.420	160.48		

STATION NUMBER	STATION COORDINATES LATITUDE deg. min.	LONGITUDE deg. min.	SHOT NUMBER	DISTANCE (km)		TRAVEL TIME (sec)	MOHO Time-term (sec)	MOHO DEPTH (km)
33	57 54.9	96 50.8	33	1269.0	11.424	160.30	3.56	36
40	58 45.8	93 52.0	38	1290.1	11.614	162.99	3.86	39
40	58 45.8	93 52.0	39	1290.4	11.616	162.99	3.81	38
34	58 8.9	97 4.1	32	1297.7	11.682	164.01	4.05	41
34	58 8.9	97 4.1	33	1298.1	11.686	164.10	4.11	41
35	58 33.2	97 35.3	35	1352.6	12.177	170.56	4.27	43
36	58 45.7	97 48.9	35	1379.3	12.417	173.94	4.67	47
37	59 0.5	98 1.8	36	1408.3	12.678	177.52	4.98	50
37	59 0.5	98 1.8	37	1408.7	12.681	177.44	4.81	48
38	59 19.5	98 28.4	36	1451.5	13.067	182.68	5.17	52
38	59 19.5	98 28.4	37	1451.9	13.070	182.78	5.27	53
39	59 40.8	98 39.7	38	1492.2	13.434	186.93	4.44	45
39	59 40.8	98 39.7	39	1492.5	13.436	187.00	4.49	45
40	58 45.8	93 52.0	38	1290.1	11.614	162.99	3.86	39
40	58 45.8	93 52.0	39	1290.4	11.616	162.99	3.81	38

(b) DATA FOR LAKE NIPIGON TO SMOOTH ROCK FALLS ONTARIO

46	49 38.2	88 5.6	8	240.0	2.160	37.90	3.94	40
46	49 38.2	88 5.6	9	240.1	2.161	36.52		
48	49 42.2	87 21.1	12	267.6	2.408	41.38	4.02	41
48	49 42.2	87 21.1	13	267.6	2.409	41.25	3.88	39
45	49 44.6	86 56.2	7	284.9	2.564	43.01	3.47	35
45	49 44.6	86 56.2	6	284.9	2.564	42.92	3.38	34
47	50 12.4	87 54.3	10	304.7	2.742	45.04	3.02	30
47	50 12.4	87 54.3	11	305.3	2.748	45.67	3.67	37
50	49 25.1	85 49.5	17	309.7	2.788	46.52	3.92	40
50	49 25.1	85 49.5	16	309.9	2.789	46.66	4.09	41
49	49 47.7	86 19.2	14	315.2	2.837	46.88	3.63	37
49	49 47.7	86 19.2	15	315.8	2.842	46.82	3.47	35
44	50 2.2	86 46.6	4	318.9	2.870	47.89	4.20	42
44	50 2.2	86 46.6	5	319.0	2.871	47.47	3.75	38
51	49 47.3	85 57.1	18	332.1	2.989	48.97	3.62	37
51	49 47.3	85 57.1	19	332.4	2.991	48.80	3.43	35

STATION NUMBER	STATION COORDINATES LATITUDE deg. min	STATION COORDINATES LONGITUDE deg. min.	SHOT NUMBER	DISTANCE (km)	DISTANCE (deg)	TRAVEL TIME	MOHO time-term (sec)	MOHO DEPTH (km)
43	50 13.0	86 53.4	3	333.0	2.997	48.74	3.26	33
42	50 11.1	86 43.5	2	335.8	3.022	48.72	2.85	29
53	49 16.7	84 46.2	23	363.2	3.269	52.62	3.43	36
41	50 35.2	86 57.6	1	366.9	3.302	52.83	3.15	32
52	49 45.8	85 13.2	20	368.6	3.317	53.69	3.87	39
52	49 45.8	85 13.2	21	368.8	3.319	53.61	3.75	38
54	49 46.7	84 33.4	25	406.5	3.659	57.94	3.39	34
54	49 46.7	84 33.4	24	406.8	3.661	57.95	3.37	34
56	49 30.9	83 50.8	29	434.6	3.911	61.00	2.97	30
56	49 30.9	83 50.8	28	434.7	3.912	61.02	2.98	30
55	50 5.5	84 9.9	26	449.8	4.048	63.12	3.23	33
55	50 5.5	84 9.9	27	449.9	4.049	63.12	3.23	33
57	49 32.8	82 57.3	31	494.4	4.450	68.08	2.63	27
57	49 32.8	82 57.3	30	494.6	4.451	67.93	2.45	25
58	49 23.2	82 17.6	33	531.4	4.783	72.60	2.59	26
58	49 23.2	82 17.6	32	532.0	4.788	72.80	2.73	28
59	49 16.7	81 37.1	35	574.7	5.172	78.50	3.21	32
60	49 53.3	81 33.8	36	601.9	5.417	80.67		
61	49 17.2	81 4.2	38	613.1	5.518	82.64	2.61	26
61	49 17.2	81 4.2	39	613.2	5.519	82.64	2.53	27

APPENDIX C

1. Computer Printout of First Arrivals

High gain three-component computer printer-plots were obtained for the first arrival portions of all records. The three-component voltage values were written on the left hand side of the plot and the three traces were plotted using representative symbols. A continuous trace representation made by connecting the symbols with a pen. For choosing the onset of the arrival, the plot was matched with the pick obtained from the analog records. As well the time trace plot was often useful for orienting the plot with respect to the analog trace. Voltage measurements were made for the first-break and peak-to-peak measurements from the printed values. Gain settings for the printer-plot were based on maximum amplitudes of the first few seconds of record.

2. Amplitude Measurements

The amplitude measurements made on the first peak and first peak-to-peak amplitudes of the digitized records for the Early Rise Line are given in Table C-2-1. Voltage measurements (seismometer output) were converted to microns/sec ground velocity from the manufacturer's seismometer specifications.

The amplitude measurements made on the first few angles of the Nipigon-Smooth Rock Falls profile are given in Table C-2-II. Since these records were not digitized, all measurements were made from the original analog records and can be considered as having a high measurement error.

TABLE C - 2 - I

FIRST ARRIVAL

AMPLITUDE MEASUREMENTS FOR EARLY RISE LINE

(millicrons/ SEC)

EXPERIMENT NO.	DISTANCE (km)	FIRST BREAK	PEAK TO PEAK
2	260.92	167.	508.
3	261.00	195.	418.
4	336.01	118.	236.
5	335.94	95.0	202.
6	412.27	74.8	78.6
7	412.28	59.6	108.0
8	483.41	42.0	70.8
9	563.74	15.8	--
10	564.22	14.9	49.7
12	708.42	44.4	173.0
13	764.97	50.0	104.5
14	765.33	36.4	89.5
15	827.57	24.4	68.0
16	884.69	27.6	65.2
17	885.04	18.9	51.2
18	972.85	33.9	53.0
19	972.92	47.8	54.9
20	1058.40	31.3	105.5
21	1058.34	32.9	80.0
22	1088.17	37.3	82.2
23	1088.16	17.9	86.9
24	1176.02	17.5	29.8
25	1244.64	11.9	23.9
26	1297.72	23.0	20.9
27	1298.11	14.4	24.3
28	1379.34	30.7	28.4
29	1451.57	19.3	50.4
30	1451.87	19.8	35.7
31	1290.10	12.2	39.2
32	1290.37	18.6	23.1
33	163.22	356.0	885.0
37	295.07	90.5	151.0

EXPERIMENT NO.	DISTANCE (km)	FIRST BREAK	PEAK TO PEAK
38	373.93	37.1	87.9
39	374.04	35.5	90.5
40	446.11	25.9	40.9
41	524.53	25.1	23.3
44	639.37	20.4	59.0
45	639.50	26.2	86.5
46	668.96	56.3	158.0
47	669.67	38.7	114.0
48	738.44	59.0	83.1
49	738.80	43.2	90.0
50	795.22	28.8	92.5
51	795.06	24.8	85.2
52	866.83	17.2	36.1
53	867.18	25.9	55.5
54	944.56	20.5	47.9
55	944.63	34.1	59.7
56	1071.32	22.2	104.0
57	1071.31	19.7	103.0
58	1142.30	20.2	50.0
59	1142.37	14.9	23.3
60	1204.78	11.8	--
63	1352.66	15.5	18.6
64	1408.39	23.7	50.4
65	1408.68	30.4	66.3
66	1492.23	12.1	24.2
67	1492.49	18.1	18.1

TABLE C - 2 - II

FIRST ARRIVAL

AMPLITUDE MEASUREMENTS FOR NIPIGON - SMOOTH ROCK FALLS

(millimicrons/SEC)

RECORD	DISTANCE	PEAK TO PEAK
8-46	240.0	91.8
9-46	240.1	52.5
12-48	267.6	157.0
13-48	267.6	144.0
7-45	284.9	91.8
6-45	284.9	72.0
10-47	304.7	13.1
11-47	305.3	91.8
17-50	309.7	210.0
16-50	309.9	197.0
14-49	315.2	328.0
15-49	315.8	380.0
4-44	318.9	157.0
5-44	319.0	144.0
18-51	332.1	65.5
19-51	332.4	91.8
3-43	333.0	237.0
2-42	335.8	328.0
23-53	363.2	170.0
1-41	366.9	275.0
20-52	368.6	236.0
21-52	368.8	197.0
25-54	406.5	288.0
24-54	406.8	237.0
29-56	434.6	144.0
28-56	434.7	118.0
26-55	449.8	118.0
27-55	449.9	118.0
31-57	494.4	118.0
30-57	494.6	118.0
33-58	531.4	65.5

RECORD	DISTANCE	PEAK TO PEAK
32-58	532.0	91.8
35-59	574.7	288.0
36-60	601.1	262.0
38-61	613.1	91.8
39-61	613.2	78.6

APPENDIX D

1. Spectral Analysis

The method of spectral analysis followed was that given by McGarr, Hoffman, and Hair (1964). The Fourier transform computed over a time window is:

$$F(\omega) = \sum_{n=-(p-1)/2}^{n=(p-1)/2} \cos(\omega n\Delta) f(n\Delta t) \quad -i \sum_{n=-(p-1)/2}^{n=(p-1)/2} \sin(\omega n\Delta t) f(n\Delta t)$$

where,

p = no. of digital increments in the time window

ω = angular frequency

Δt = digital time increment

$f(n\Delta t)$ = the seismic trace at time $n\Delta t$

Measurement over a time window introdces side lobes in the frequency domain which are reduced by 'hanning'. The 'hanned' transform is given by:

$$L(\omega) = 0.25\ F(\omega - \frac{2\pi}{\Delta tp}) + 0.50\ F(\omega) + 0.25\ F(\omega + \frac{2\pi}{\Delta tp})$$

The amplitude component is given by:

$$A(\omega) = L(\omega - \frac{2\pi}{\Delta tp} + 0.50\ F(\omega) + 0.25\ F(\omega + \frac{2\pi}{\Delta tp})$$

The amplitude component is given by:

$$A(\omega) = L(\omega)L(\omega)^*$$

where $L(\omega)^*$ is the complex conjugate of $L(\omega)$.

The computer program for the spectral analysis is given in Fig. D-1-1 in the form of a subroutine SPCTRM.

FORTRAN SOURCE LIST

SOURCE STATEMENT

FIG. D-1-1

```
TC SPCTRM
      SUBROUTINE SPCTRM(IPRINT,INUM,ICNTER,DELTAT,X,AMP,PHASE)
      DIMENSION X(401),AMP(401),PHASE(401),REL(401),AMAG(401)
      ANUM=INUM-1.
      RNUM=INUM
      DELTAF=1./(RNUM*DELTAT)
      IRW=ANUM/2.
      DO 5 I=1,IRW
      AMP(I)=0.0
    5 PHASE(I)=0.0
      STEPF=0.0
      DO 2 I=1,IRW
      STEPF=STEPF+DELTAF*DELTAT*2.*3.14159265
      ALEFT=-ICNTER
      DO 3 J=1,INUM
      ALEFT=ALEFT+1.0
      AMP(I)=AMP(I)+X(J)*COS(STEPF*ALEFT)
    3 PHASE(I)=PHASE(I)+X(J)*SIN(STEPF*ALEFT)
      IC=IRW-2
      DO 4 I=1,IC
      K=I+1
      L=I+2
      REL(K)=0.25*AMP(I)+0.5*AMP(K)+0.25*AMP(L)
    4 AMAG(K)=0.25*PHASE(I)+0.5*PHASE(K)+0.25*PHASE(L)
      REL(1)=0.667*AMP(1)+0.333*AMP(2)
      AMAG(1)=1.667*PHASE(1)+0.333*PHASE(2)
      IR=IRW-1
      REL(IRW)=0.333*AMP(IR)+0.667*AMP(IRW)
      AMAG(IRW)=0.333*PHASE(IR)+0.667*PHASE(IRW)
      DO 6 I=1,IRW
      AMP(I)=SQRT(REL(I)*REL(I)+AMAG(I)*AMAG(I))
    6 PHASE(I)=ATAN(AMAG(I)/REL(I))
      IF(IPRINT.EQ.1)GO TO 45
      WRITE(6,1)
    1 FORMAT(1H ,19HAMPLITUDE SPECTRUM)
      WRITE(6,2)(AMP(I),I=1,IRW)
    2 FORMAT(1H ,1P E12.5)
      WRITE(6,3)
    3 FORMAT(1H ,19HPHASE SPECTRUM)
      WRITE(6,2)(PHASE(I),I=1,IRW)
   45 CONTINUE
      RETURN
      END
```

2. Spectral and Trace Diagrams

The frequency spectra and the vertical component of ground velocity for some examples are given in the following figs. D-2-1. Since the analysis involves the low end of the frequency spectrum, only the components between 0 and 5 hertz are shown. The amplitude units denoted by the vertical axes are proportional to ground velocity and are identical for all diagrams.

The three second trace of the vertical component of the first arrival recording is shown below each spectrum. The purpose of these diagrams is to demonstrate the form of the first arrival hence no attempt was made to maintain a standard gain.

3. Least Squares Technique

The least-squares technique used in the analysis was the familiar one for a straight-line fit (Topping, 1962). A definition of Chauvenet's Rejection Criterion has been given by Worthing and Geffner (1943) to be:

"Any reading of a series of n readings shall be rejected when the magnitude of its deviation from the mean of a series is such that the probability of occurrence of all deviations that large or larger does not exceed 1/2n."

4. Justification of Reproducible Source Conditions

An attempt was made to justify the assumption that the shots fired in the same location produced the same frequency and amplitude conditions.

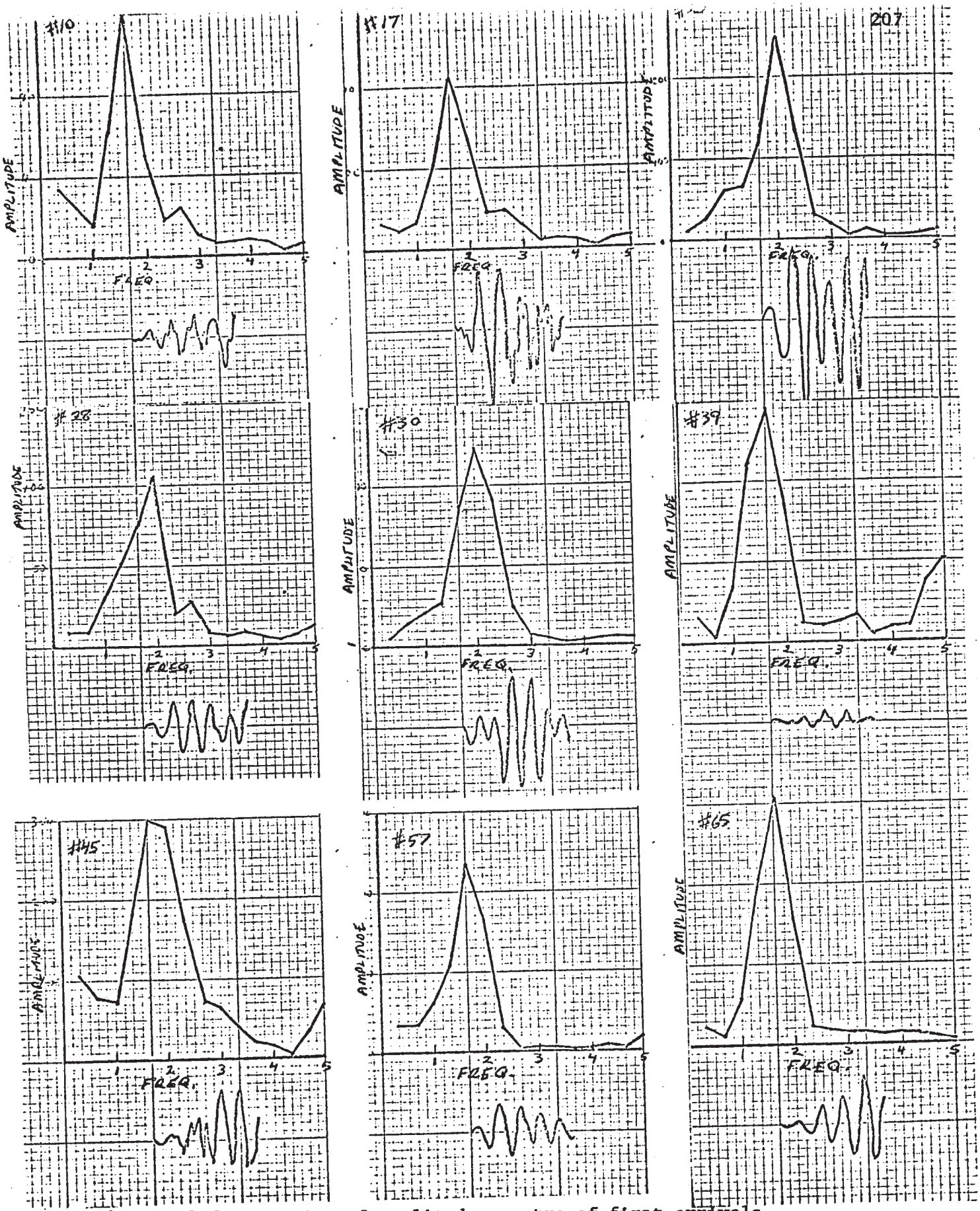

Fig. D-2-1 Examples of amplitude spectra of first arrivals.

Since many stations recorded two shots at the same location it was decided to examine these sets for similarities, hence, the recording pairs were reproduced analoguely with matching gain settings. All record pairs displayed wave forms which could be matched in shape easily, suggesting that the signal from two different shots had matching spectral forms.

To investigate the reproducibility of amplitudes, ten wavelets were picked, for each record pair, which were of high amplitude, of matching form, and apparently free of noise. Peak-to-peak amplitude ratios were computed for each wavelet for comparison between records, and the average ratio of the ten wavelets was computed. The resulting average ratios of all station pairs used are shown in Table D-4-1. Most ratios are close to 1.0 suggesting that the amplitude of the input signal was constant throughout the Early Rise experiment.

TABLE D-4-I

RECORD PAIR	AVERAGE AMPLITUDE RATIO	
2-3	1.08	
4-5	0.90	
6-7	1.07	
9-10	1.08	
13-14	0.96	
16-17	0.97	
18-19	0.92	
20-21	0.99	
22-23	1.04	
26-27	1.00	
29-30	1.01	
31-32	1.66	(probably gain was adjusted)
34-35	0.96	
36-37	1.09	
38-39	1.04	
41-42	1.00	
44-45	1.01	
46-47	1.03	
48-49	1.00	
50-51	0.99	
52-53	1.01	
54-55	0.98	
56-57	0.98	
58-59	1.00	
64-65	1.00	

APPENDIX E

Particle-Motion Plot Program

This computer program as shown in fig. E-1-1 was written utilizing a number of general-purpose subroutines written by the author. The main program is used as an entry point and to call subroutines. A brief description of the subroutines follows:

LOPASS - generates the filter coefficients for a low-pass filter

FINDIT - searches the data tape for the correct record and shifts the total record to storage

READCH - compiles one component of motion, gain adjust, centres the trace, and rotates the axis of motion when necessary

CORREL - performs the correlation of the filter coefficients with the trace.

Input Variables

ISHOT - shot number

ZEROCH (I) - trace centering values for each of the traces

CORR (I)- Gain adjustment to equalize gains on all traces

U12 - input tape mounted on Utility 12.

```
134307 J HUNTER                                    FORTRAN SOURCE LIST
  ISN       SOURCE STATEMENT

      C $IBFTC
        C
        C              ER-61
        C
        C       HORIZONTAL AND VERTICAL PARTICLE MOTION PLOT VERSION TWO
        C
        C       CONTIAINS ROUTINE TO INTERPOLATE ALONG THE DIGITAL TRACES
    1         COMMON TR
    2         DIMENSION TR(1200),ZEROCH(4),CORR(4),V(1200),SN(1200),EW(1200),WTS
             1(401)
    3         REWIND 12
    4         CALL LOPASS(1,5.0,0.022222,1,INUM,IXNTER,INTSPL,SUMWTS,WTS)
    5      20 READ(5,1)ISHOT,(ZEROCH(I),I=1,4),(CORR(J),J=1,4)
   17         IF(ISHOT.EQ.0)GOTO99
   22       1 FORMAT(I2,29X,4F5.2,4F4.2)
   23         READ(5,2)ANGLE
   24         ANGLE=(-ANGLE)
   25       2 FORMAT(6X,F5.2)
   26         CALL FINDIT(ISHOT)
   27         CALL READCH(ISHOT,25,1,ZEROCH,CORR)
   30         CALL CORREL(INUM,WTS,25)
   31         DO21 I=1,999
   32         K=I+1
   33      21 V(I)=TR(K)
   35         REWIND 12
   36         CALL FINDIT(ISHOT)
   37         CALL READCH(ISHOT,25,2,ZEROCH,CORR)
   40         CALL CORREL(INUM,WTS,25)
   41         DO22 I=1,999
   42         K=I+1
   43      22 SN(I)=0.75*TR(K)+0.25*TR(I)
   45         REWIND 12
   46         CALL FINDIT(ISHOT)
   47         CALL READCH(ISHOT,25,3,ZEROCH,CORR)
   50         CALL CORREL(INUM,WTS,25)
   51         DO23 I=1,999
   52         K=I+1
   53      23 EW(I)=0.50*TR(K)+0.50*TR(I)
   55         ANGLE=ANGLE*3.14159265/180.
   56         AMAX=0.0
   57         DO24 I=1,999
   60         XX=EW(I)
   61         YY=SN(I)
   62         EW(I)=XX*COS(ANGLE)+YY*SIN(ANGLE)
   63         SN(I)=YY*COS(ANGLE)-XX*SIN(ANGLE)
   64         AV=ABS(V(I))
   65         ASN=ABS(SN(I))
   66         AEW=ABS(EW(I))
   67         IF(AV.GT.AMAX)AMAX=AV
   72         IF(ASN.GT.AMAX)AMAX=ASN
   75         IF(AEW.GT.AMAX)AMAX=AEW
  100      24 CONTINUE
  102         WRITE(6,8)AMAX
  103       8 FORMAT(1H ,F12.4)
  104         DO25 I=1,999
```

UWO 250566

Fig. E-1-1 Particle-motion plot program and examples.

```
134307 J HUNTER                                          FORTRAN SOURCE LIST
       ISN        SOURCE STATEMENT

       105           V(I)=V(I)*2.0/AMAX
       106           SN(I)=SN(I)*2.0/AMAX
       107        25 EW(I)=EW(I)*2.0/AMAX
       111           IK=0
       112           DO73 KL=1,2
       113           CALL PLOTS(30,60.0,10.75,1)
       114           CALL PLOT(0.0,8.0,-3)
       115           DO72 LK=1,11
       116           CALL PLOT(5.0,-4.5,-3)
       117           CALL PLOT(0.00,-2.0,3)
       120           CALL PLOT(0.0,2.0,2)
       121           CALL PLOT(-2.0,0.0,3)
       122           CALL PLOT(2.0,0.0,2)
       123           CALL PLOT(0.0,0.0,3)
       124           DO71 I=1,40
       125           IK=IK+1
       126           H=SN(IK)*SQRT(SN(IK)*SN(IK)+EW(IK)*EW(IK))/ABS(SN(IK))
       127           VEE=-V(IK)
       130           IF(I.EQ.1)CALL SYMBOL(H,VEE,0.14,1H+,0.0,1)
       133           IF(I.EQ.1)GOTO71
       136           CALL PLOT(H,VEE,2)
       137        71 CONTINUE
       141           IK=IK-40
       142           CALL PLOT(0.0,4.5,-3)
       143           CALL PLOT(0.00,-2.0,3)
       144           CALL PLOT(0.0,2.0,2)
       145           CALL PLOT(-2.0,0.0,3)
       146           CALL PLOT(2.0,0.0,2)
       147           CALL PLOT(0.0,0.0,3)
       150           DO70 I=1,40
       151           IK=IK+1
       152           SAN=SN(IK)
       153           IF(I.EQ.1)CALL SYMBOL(EW(IK),SAN,0.14,1H+,0.0,1)
       156           IF(I.EQ.1)GOTO70
       161           CALL PLOT(EW(IK),SAN,2)
       162        70 CONTINUE
       164           WRITE(6,9)
       165         9 FORMAT(1H ,5HCHECK)
       166        72 CONTINUE
       170           CALL ENDPLT
       171        73 CONTINUE
       173           GOTO20
       174        99 STOP
       175           END
```

134307 J HUNTER FORTRAN SOURCE LIST

ISN SOURCE STATEMENT

```
C $IBFTC READCH
      SUBROUTINE READCH(ISHOT,ISEC,ICH,ZEROCH,CORR)
      COMMON TR
      DIMENSION TR(9999),ZEROCH(4),CORR(4),A(20),X(4,225),XSUM(4)
      WRITE(6,1)ISHOT
    1 FORMAT(1H ,21HNOW READING SHOT NO. ,I2)
      IMAX=ISEC*9/45
      III=-225
      DO40 I=1,IMAX
      III=III+225
      DO45 J=1,4
   45 XSUM(J)=0.0
      DO50 J=1,45
      READ(12)(A(K),K=1,20)
      DO50 K=1,5
      DO50 L=1,4
      M=L+(K-1)*4
      N=J*5+K-5
      IF(A(M).GT.3.0)WRITE(6,7)
    7 FORMAT(1H ,10HBIG NUMBER)
      IF(A(M).GT.3.0)A(M)=0.001
      IF(A(M).LT.(-3.0))WRITE(6,7)
      IF(A(M).LT.(-3.0))A(M)=0.001
      X(L,N)=(A(M)-ZEROCH(L))*CORR(L)
   50 XSUM(L)=XSUM(L)+X(L,N)
      DO51 J=1,4
   51 XSUM(J)=XSUM(J)/225.
      DO52 K=1,4
      DO52 J=1,225
      X(K,J)=X(K,J)-XSUM(K)
   52 CONTINUE
      DO60 MM=1,225
      LL=III+MM
      SYNE=1.0
      IF(ICH.GT.4)GOTO65
      TR(LL)=X(ICH,MM)
      GOTO60
   65 CONTINUE
      IF(X(3,MM).LT.0.0)SYNE=-1.0
      H=SYNE*SQRT(X(2,MM)*X(2,MM)+X(3,MM)*X(3,MM))
      IF(ICH.GT.5)GOTO67
      TR(LL)=H
      GOTO60
   67 CONTINUE
      IF(X(1,MM).LT.0.0)SYNE=-1.0
      TR(LL)=SYNE*SQRT(X(1,MM)*X(1,MM)+H*H)
   60 CONTINUE
   40 CONTINUE
      WRITE(6,2)ISHOT
    2 FORMAT(1H ,26HFINISHED TRANSFERING SHOT ,I2)
      RETURN
      END
```

134307 J HUNTER FORTRAN SOURCE LIST

```
ISN       SOURCE STATEMENT

  C $IBFTC FINDIT
  1        SUBROUTINE FINDIT(ISHOT)
  2        DIMENSION A(20)
  3     20 READ(12)(A(I),I=1,20)
 10        IF(A(1).GT.9.9.AND.A(10).GT.9.9.AND.A(20).GT.9.9)GOTO30
 13        GOTO20
 14     30 CONTINUE
 15        AA=A(10)/10.0
 16        IA=AA
 17        IF(IA.EQ.ISHOT)GOTO40
 22        GOTO20
 23     40 CONTINUE
 24        WRITE(6,1)ISHOT
 25      1 FORMAT(1HO,22HHAVE LOCATED SHOT NO. ,I3)
 26        RETURN
 27        END
```

134307 J HUNTER — FORTRAN SOURCE LIST

```
ISN     SOURCE STATEMENT

C $IBFTC LCPASS
1       SUBROUTINE LCPASS(IPRINT,FREQ,DELTAT,IPICK,INUM,ICNTER,INTSPL,SUMW
       1TS,WTS)
2       DIMENSION WTS(401)
C       WHEN IPRINT IS ZERO DATA IS WRITTEN, IF IPRINT=1, NO DATA IS
C       WRITTEN
C       WHEN IPICK IS 1, HANNING IS APPLIED
C        WHEN IPICK IS 2, HAMMING IS APPLIED
C       FREQ IS THE CUTOFF FREQUENCY READ IN
C       DELTAT IS THE DIGITAL INCREMENT READ IN
C       INUM IS THE TOTAL NUMBER OF WEIGHTS PRODUCED-AN ODD NUMBER
C       ICNTER IS THE NUMBER OF THE CENTRAL WEIGHT, COUNTING FROM THE LEFT
C       INTSPL IS THE OPTIMUM NUMBER OF DIGITAL INTERVALS TO BE SKIPPED
C        BETWEEN SUCCESSIVE APPLICATION OF THE WEIGHTING FN,BASED ON FREQ
C        BEING THE NYQUIST FREQUENCY.
C       THE ARRAY WTS(I) IS THE SET OF WEIGHTS PRODUCED, STARTING AT THE
C        LEFT HAND SIDE OF THE SYMMETRICAL FUNCTION, THE CENTRE OF THE FN
C        IS GIVEN BY WTS(ICNTER)
C       THE BASIC WEIGHTING FN IS THE SINC FN TYPE SIN(X)/X
C       SUMWTS IS THE SUM OF ALL THE WEIGHTS
3         A=0.54
4         B=0.46
5         IF(IPICK.EQ.1)A=0.50
10        IF(IPICK.EQ.1)B=0.50
13        ISIDE=3.0/(FREQ*DELTAT)
14        INUM=ISIDE*2+1
15        ICNTER=ISIDE+1
16        INTSPL=1./(DELTAT*2.*FREQ)
17        SUMWTS=0.0
20        T=0.0
21        W=3.14159265*FREQ*2.
22        WD=W/10.0
23        DO20 I=1,ISIDE
24        K=ICNTER-I
25        L=ICNTER+I
26        T=T+DELTAT
27        WTS(K)=SIN(W*T)*(A+B*COS(WD*T))/(W*T)
30        WTS(L)=WTS(K)
31        SUMWTS=SUMWTS+2.*WTS(K)
32      20 CONTINUE
34        WTS(ICNTER)=1.0
35        SUMWTS=SUMWTS+WTS(ICNTER)
36        IF(IPRINT.EQ.1)GOTO45
41        WRITE(6,1)FREQ,DELTAT,IPICK,INUM,ICNTER,INTSPL
42      1 FORMAT(1H1,16HLOW PASS CUTOFF=,F5.1,12H DIG. INCR.=,F5.3,15H LAG W
         1INDOW NO.=,I2,12H NO. OF ETS=,I4,15H CENTRE WT NO.=,I4,,23H OPTIMUM
         2 SKIP INTERVAL=,I4)
43        WRITE(6,2)
44      2 FORMAT(1HC,23HLOW PASS FILTER WEIGHTS)
45        WRITE(6,3)(WTS(I),I=1,INUM)
52      3 FORMAT(1H ,15F8.3)
53        WRITE(6,4)SUMWTS
54      4 FORMAT(1HO,5HSUM =,F8.3)
55     45 CONTINUE
56        RETURN
```

134307 J HUNTER FORTRAN SOURCE LIST

```
ISN     SOURCE STATEMENT

C $IBFTC CORREL
      1       SUBROUTINE CORREL(INUM,WTS,ISEC)
      2       COMMON TR
      3       DIMENSION TR(1200),WTS(401)
      4       IMAX=ISEC*45
      5       DO20 I=1,IMAX
      6       TR(I)=0.0
      7       DO2C J=1,INUM
     1C       K=I+J
     11    20 TR(I)=TR(I)+WTS(J)*TR(K)
     14       IJ=IMAX+INUM/2
     15       DO3C I=1,IMAX
     16       IK=IJ+1-I
     17       IL=IMAX+1-I
     2C    30 TR(IK)=TR(IL)
     22       MLM=INUM/2
     23       DO35 I=1,MLM
     24    35 TR(I)=0.0
     26       WRITE(6,1)
     27     1 FORMAT(1H ,36HFINISHED LOPASS FILTERING THE RECORD)
     3C       RETURN
     31       END
```

UWO 250566

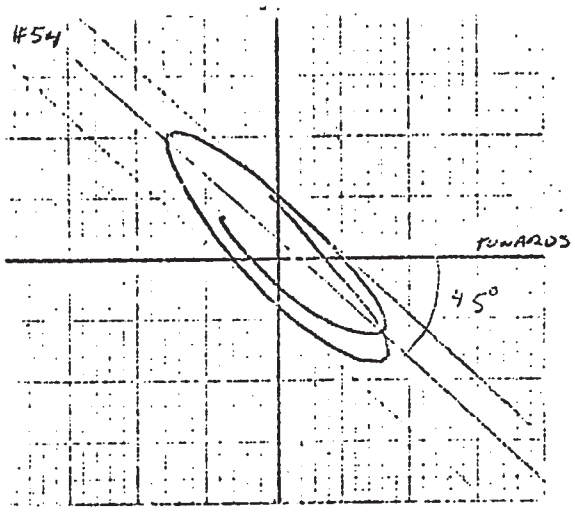
#54
TOWARDS
45°

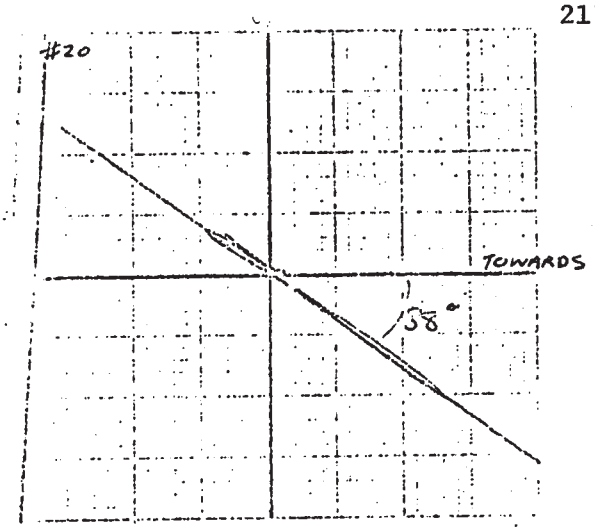
#20
TOWARDS
58°

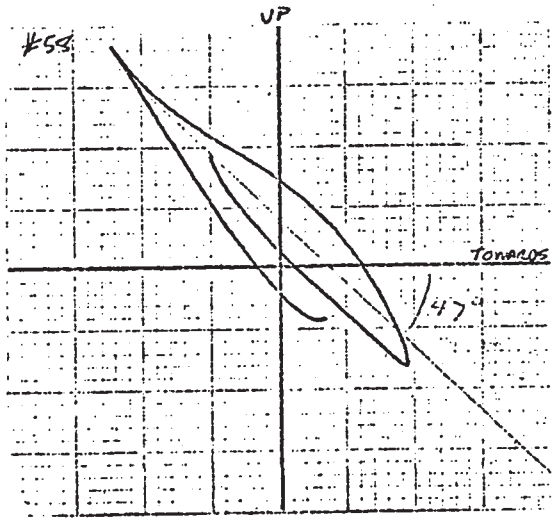
#58
VP
TOWARDS
47°

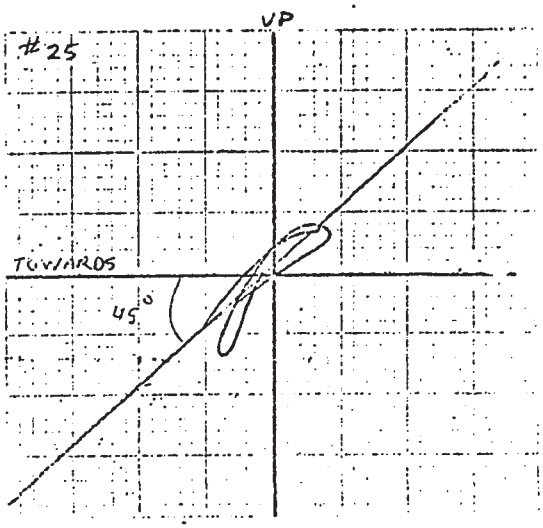
#25
VP
TOWARDS
45°

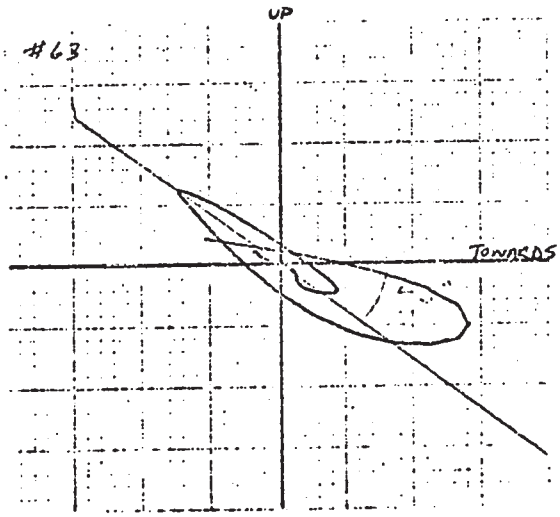
#63
VP
TOWARDS

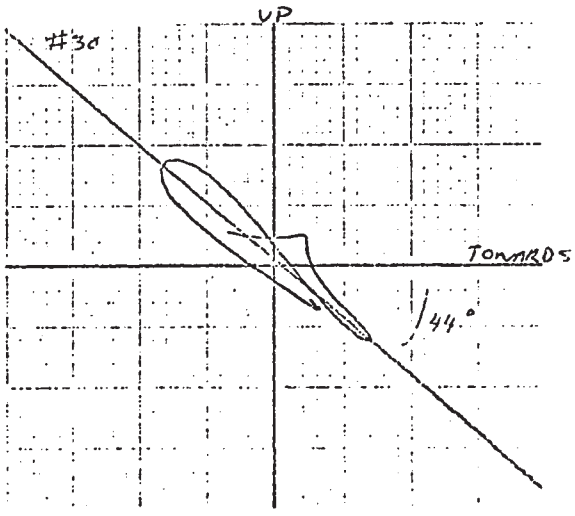
#30
VP
TOWARDS
44°

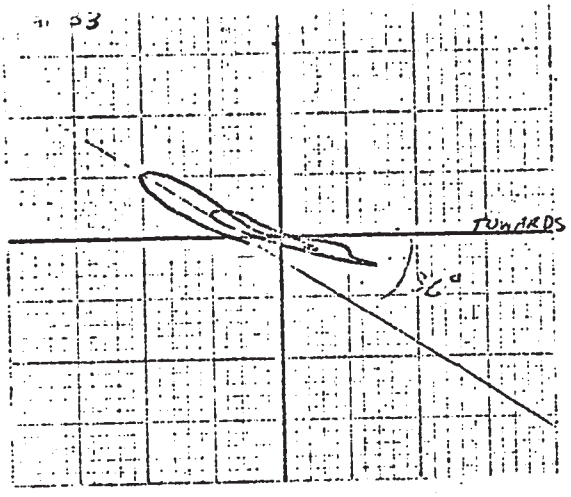
#3
TOWARDS
26°

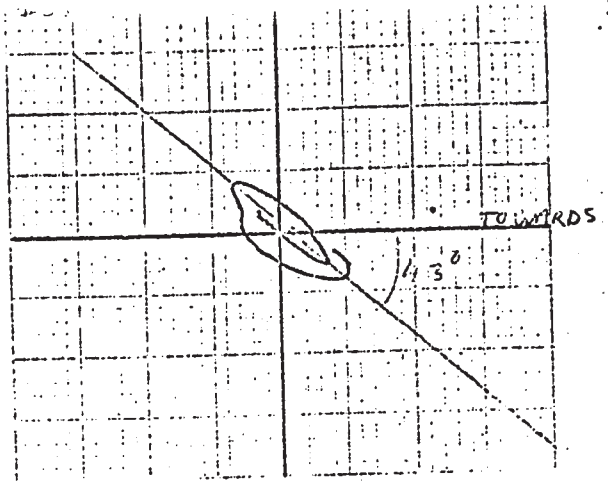
TOWARDS
43°

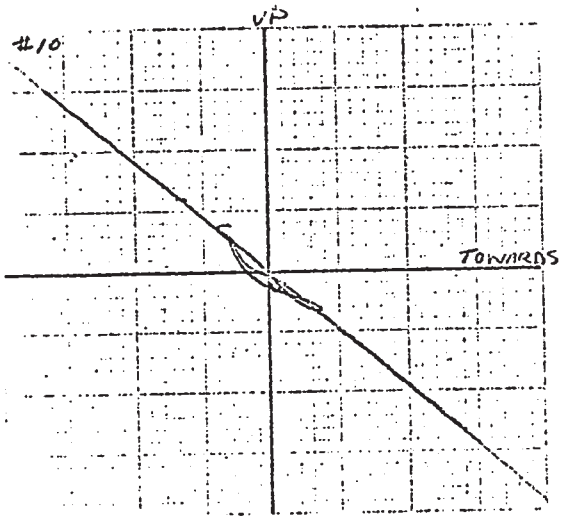
#10
UP
TOWARDS

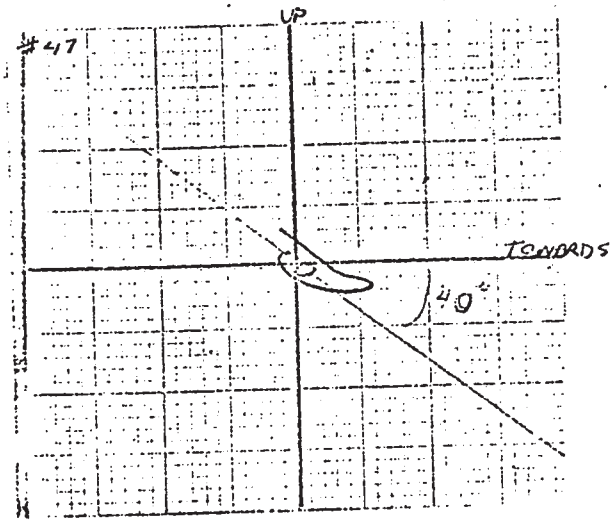
#47
UP
TOWARDS
40°

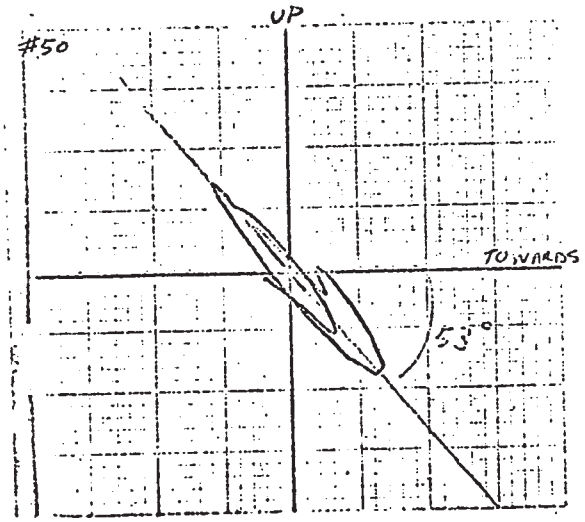
#50
UP
TOWARDS
53°

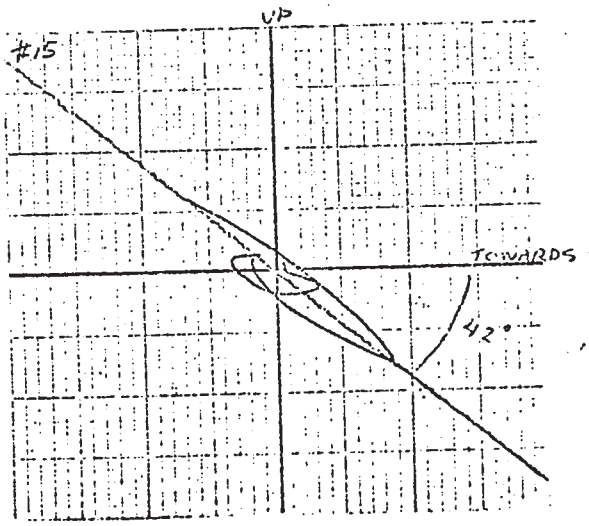
#15
UP
TOWARDS
42°

APPENDIX F

1. AMPLITUDE PROGRAM

A program was written to produce the resultant vertical and horizontal ground amplitude recorded at the surface of a curved D-layered earth for any specified wave.

The amplitude program is shown in fig. F-1-1. The velocity information describing the layered earth is read in as input. If a velocity variation exists in a layer it is assumed to be in the form $v = ar^{-b}$. Thus only upper and lower limits of velocity in that layer need to be read in. The subroutine GNGBNG computes the ray parameter computed previously. The subroutine AMP computes the amplitude positioning at each interface including the effect of the free surface for the up-going portion of the wave. The subroutine ZOEP (kindly supplied by Dr. R. F. Mereu) computes the solutions to the Zoeppritz equations for a wave incident at any interface.

INPUT VARIABLES

R - radius of the earth (in km)

POISSN - Poissons ratio (constant for the model)

LAYERS - Number of layers in the model

VP(1,I), VP(2,I) - compressional velocity (km/sec) at top and bottom respectively of layer I. Model assumes a $N = a\, r^{-b}$ gradient.

Z(I) - thickness of layer I (km).

OUTPUT VARIABLES

DEL - shot station distance in degrees

DELTA - shot-station distance in km

MODE(L)- wave code

P - ray parameter

T - travel time (sec)

V - vertical amplitude

PHZV - vertical phase change

H - horizontal amplitude

PHZH - horizontal phase change

APEM - apparent angle of emergence

ENERG - total energy (source = 1)

AMPTOT - total amplitude

TR - reduced travel-time $T - \Delta/8.1$

```
                                3200  FORTRAN    (2.1)          13/10/70
      PROGRAM CONGERER
C                ER-68
C
C
C       GENERAL AMPLITUDE ANALYSIS FOR CURVED EARTH
C
      DIMENSION VP(2,9),VS(2,9),DN(2,9),Z(9),B(9),ETA(2,40),MODE(40)
      READ(60,3)R,POISSN,LAYERS
    3 FORMAT(F6.1,F5.2,I2)
   17 READ(60,1)(VP(1,I),VP(2,I),Z(I),I=1,9)
    1 FORMAT(16F5.2)
      IF(VP(1,1).EQ.0.0)99,401
  401 CONTINUE
      DO19 I=1,LAYERS
      IF(VP(1,I).EQ.VP(2,I))601,602
  602 CONTINUE
      B(I)=ALOG(VP(1,I)/VP(2,I))/ALOG((R-Z(I))/R)
  601 CONTINUE
      DN(1,I)=1.15+0.27*VP(1,I)
   19 DN(2,I)=1.15+0.27*VP(2,I)
      WRITE(61,2)(VP(1,I),DN(1,I),VP(2,I),DN(2,I),B(I),Z(I),I=1,9)
    2 FORMAT(1H ,20F6.2)
      WRITE(61,523)
  523 FORMAT(1H0,131HDELTA  DIST   WAVE CODE NUMBER
     1      P       T        V AMP  V PHASE H AMP H PHASE E ANGLE  ENERGY
     2TOT.AMP RED. T)
      RATIO=(1.0-POISSN)/(0.5-POISSN)
      RATIO=SQRT(RATIO)
      DO20 I=1,LAYERS
      VS(1,I)=VP(1,I)/RATIO
   20 VS(2,I)=VP(2,I)/RATIO
   21 READ(60,4)(MODE(I),I=1,40)
    4 FORMAT(40I2)
      IF(MODE(1).EQ.0)98,91
   91 CONTINUE
      IP=0
      DO22 I=1,40
      K=41-I
      IF(MODE(K).EQ.0)29,22
   29 IP=K
   22 CONTINUE
      IP=IP-1
      DEL=0.0
      DELTA=0.0
      DO23 I=1,30
      DELTA=DELTA+50.
      DEL=DELTA*180./(3.14159265*R)
      DIST=DEL
      CALL GNGBNG(DIST,LAYERS,MODE,ETA,IP,VP,VS,B,Z,R,DPDDEL,P)
      IF(P.EQ.0.0)23,28
   28 CONTINUE
      CALL TYME(P,B,MODE,ETA,IP,LAYERS,T)
      CALL AMP(MODE,IP,LAYERS,VP,VS,DN,R,Z,DPDDEL,DEL,P,ENERGY,AMPTOT,V,
     1H,PHZV,PHZH,APEM)
      TR=T-DELTA/8.1
      WRITE(61,5)DEL,DELTA,(MODE(L),L=1,20),P,T,V,PHZV,H,PHZH,APEM,ENERG
     1Y,AMPTOT,TR
      WRITE(61,6)(MODE(L),L=21,40)
    5 FORMAT(1H0,F4.1,F8.2,20I2,F9.3,F6.2,F9.4,F5.0,F9.4,F5.0,F6.2,2F10.
     15,F7.2)
    6 FORMAT(1H ,12X,20I2)
```

Fig. F-1-1 Ampltude program for curved earth models.

```
      23 CONTINUE
         GOTO21
      98 CONTINUE
         GOTO17
      99 CONTINUE
         STOP
         END
```

3200 FORTRAN DIAGNOSTIC RESULTS - FOR CONGERER

NO ERRORS

```
                                    3200  FORTRAN     (2.1)          13/10/
      SUBROUTINE GNGRNG(DIST,LAYERS,MODE,ETA,IP,VP,VS,B,Z,R,DPDDEL,P)
      DIMENSION MODE(40),ETA(2,40),VP(2,9),VS(2,9),B(9),Z(9)
      P=9999.0
      ISIG=0
      B(9)=0.0
      Z(9)=0.0
      SMZ=0.0
      DO22 K=1,LAYERS
   22 SMZ=SMZ+Z(K)
    7 FORMAT(1H ,F10.4)
      DO20 I=1,IP
      ID=IABS(MODE(I))
      BOT=0.0
      DO21 J=1,ID
   21 BOT=BOT+Z(J)
      TOP=BOT-Z(ID)
      ETA(1,I)=(R-TOP)/VP(1,ID)
      ETA(2,I)=(R-BOT)/VP(2,ID)
      IF(MODE(I).LT.0)101,102
  101 ETA(1,I)=(R-TOP)/VS(1,ID)
  102 CONTINUE
      IF(MODE(I).LT.0)103,104
  103 ETA(2,I)=(R-BOT)/VS(2,ID)
  104 CONTINUE
      IF(ID.EQ.LAYERS)105,106
  105 ETA(2,I)=0.0
  106 CONTINUE
      LLL=LAYERS-1
      IF(ID.EQ.LAYERS)91,107
  107 CONTINUE
      IF(ID.EQ.LLL)92,108
  108 CONTINUE
      GOTO93
   91 Q=ETA(1,I)
      IF(Q.LT.P)109,110
  109 P=Q
  110 CONTINUE
      GOTO93
   92 Q=ETA(2,I)
      IF(Q.LT.P)111,112
  111 P=Q
  112 CONTINUE
   93 CONTINUE
   20 CONTINUE
      DIST=DIST*3.14159265/180.
      DDEL=DIST
      Q=P
      P=P-0.00001
      EP=P
   40 DELNEW=0.0
      IF(P.GT.Q)113,114
  113 P=0.0
  114 CONTINUE
      IF(P.EQ.0.0)99,115
  115 CONTINUE
      IF(P.GT.EP)402,403
  402 WRITE(61,1)
  403 CONTINUE
      IF(P.GT.EP)99,404
  404 CONTINUE
```

```
    1 FORMAT(1H ,31HP IS TOO NEAR TO ETA TO ITERATE)
      DO41 I=1,IP
      ID=IABS(MODE(I))
      BBB=B(ID)
      FCTR=1.0/(1.0+BBB)
      IF(ETA(2,I).EQ.0.0)42,116
  116 CONTINUE
      DELNEW=DELNEW+FCTR*(ARSIN(P/ETA(2,I))-ARSIN(P/ETA(1,I)))
      GOTO41
   42 CONTINUE
      DELNEW=DELNEW+FCTR*(3.14159265-2.0*ARSIN(P/ETA(1,I)))
   41 CONTINUE
      AC=ABS(DDEL)
      DDEL=DELNEW-DIST
      AD=ABS(DDEL)
   88 CONTINUE
      DDELDP=0.0
      DO45 I=1,IP
      ID=IABS(MODE(I))
      BBB=B(ID)
      FCTR=1.0/(1.0+BBB)
      IF(ETA(2,I).EQ.0.0)47,117
  117 CONTINUE
      DDELDP=DDELDP+FCTR*((1.0/SQRT(ETA(2,I)**2-P*P))-(1.0/SQRT(ETA(1,I)
     1**2-P*P)))
      GOTO45
   47 CONTINUE
      IF(ETA(1,I).EQ.P)45,118
  118 CONTINUE
      DDELDP=DDELDP-2.0*FCTR*(1.0/SQRT(ETA(1,I)**2-P*P))
   45 CONTINUE
      DPDDEL=1.0/DDELDP
      DP=DPDDEL*DDEL
      IF(DP.EQ.0.0)119,120
  119 P=0.0
  120 CONTINUE
      P=P-DP
      DR=R*ABS(DDEL)
      IF(DR.LT.0.1)99,121
  121 CONTINUE
      GOTO40
   99 CONTINUE
      RETURN
      END
```

3200 FORTRAN DIAGNOSTIC RESULTS - FOR GNGBNG

NULL STATEMENT NUMBERS
11 7

```
                                        3200  FORTRAN     (2.1)          13/10/70
      SUBROUTINE AMP(MODE,IP,LAYERS,VP,VS,DN,R,Z,DPDDEL,DEL,P,ENERGY,AMP
     1TOT,V,H,PHZV,PHZH,APEM)
      DIMENSION MODE(40),Z(9),DN(2,9),VS(2,9),VP(2,9)
      ERGCOF=1.0
      FAZCOF=0.0
      DO21 I=1,LAYERS
      DIRECT=1.0
      IK=IP-1
      DO21 J=1,IP
      IF(LAYERS.EQ.1)70,101
  101 CONTINUE
      JJ=J+1
      IQQ=IABS(MODE(JJ))
      IPP=IABS(MODE(J))
      IF(IPP.NE.I)21,102
  102 CONTINUE
      DIRECT=DIRECT*(-1.0)
      K=I+1
      L=I-1
      IF(DIRECT.LT.0.0)22,103
  103 CONTINUE
      IF(I.EQ.1)70,104
  104 CONTINUE
      P2=VP(2,L)
      S2=VS(2,L)
      D2=DN(2,L)
      GOTO71
   70 P2=0.0
      S2=0.0
      D2=0.0
   71 P1=VP(1,I)
      S1=VS(1,I)
      D1=DN(1,I)
      GOTO23
   22 P2=VP(1,K)
      S2=VS(1,K)
      D2=DN(1,K)
      IF(I.EQ.LAYERS)105,106
  105 P2=VP(2,L)
  106 CONTINUE
      IF(I.EQ.LAYERS)107,108
  107 S2=VS(2,L)
  108 CONTINUE
      IF(I.EQ.LAYERS)109,110
  109 D2=DN(2,L)
  110 CONTINUE
      P1=VP(2,I)
      S1=VS(2,I)
      D1=DN(2,I)
      IF(I.EQ.LAYERS)111,112
  111 P1=VP(1,I)
  112 CONTINUE
      IF(I.EQ.LAYERS)113,114
  113 S1=VS(1,I)
  114 CONTINUE
      IF(I.EQ.LAYERS)115,116
  115 D1=DN(1,I)
  116 CONTINUE
   23 IF(MODE(J).LT.0)24,117
  117 CONTINUE
```

```
                                        3200  FORTRAN     (2.1)

      SUBROUTINE TYME(P,B,MODE,ETA,IP,LAYERS,T)
      DIMENSION B(9),MODE(40),ETA(2,40)
      T=0.0
      DO20 I=1,IP
      ICK=IABS(MODE(I))
      BBB=B(ICK)
      FCTR=1.0/(1.0+BBB)
      IF(ICK.EQ.LAYERS)21,101
  101 CONTINUE
      T=T+FCTR*(SQRT(ETA(1,I)**2-P*P)-SQRT(ETA(2,I)**2-P*P))
      GOTO20
   21 T=T+FCTR*2.0*SQRT(ETA(1,I)**2-P*P)
   20 CONTINUE
      RETURN
      END
```

3200 FORTRAN DIAGNOSTIC RESULTS - FOR TYME

NO ERRORS

```
 78 IF(MODE(IP).LT.0)147,148
147 THETAU=ARCOS(P*VS(1,1)/R)
148 CONTINUE
    VEE=VP(1,1)
    IF(MODE(1).LT.0)149,150
149 VEE=VS(1,1)
150 CONTINUE
    DOL=DEL*3.14159265/180.
    AK=ABS(VEE*COS(THETAD)*DPDDEL/(R*SIN(THETAD)*SIN(THETAU)*SIN(DOL))
   1)
 21 CONTINUE
    ENERGY=AK*ERGCOF
    AMPTOT=SQRT(ENERGY)
    SS=SS*AMPTOT
    V=V*AMPTOT
    PHZV=PHZV+FAZCOF
    PHZH=PHZH+FAZCOF
    APEM=EMERG
    H=SS
    RETURN
    END
```

3200 FORTRAN DIAGNOSTIC RESULTS - FOR AMP

NULL STATEMENT NUMBERS
7

APPENDIX G

TABLE G- 1 - 1

AMPLITUDES OF LATER EVENTS ON EARLY RISE LINE (MICRONS/SEC)

SHOT	DIST	123321	SHOT	DIST	123321
4)	336.01	2.97	39	374.04	2.12
5)	335.94	1.27	40	446.11	1.91
6)	412.27	1.27	44	639.37	4.77
7	412.28	0.425	45	639.50	4.98
8	483.41	2.76	46	668.96	2.02
9	563.74	1.06	47	669.67	1.80
10	564.22	1.06	48	738.44	2.07
12	708.42	2.02	49	738.80	1.75
13	764.97	1.91	52	866.83	1.80
14	765.33	1.91	53	867.18	1.75
15.	827.57	1.27	54	944.56	2.12
16	884.69	1.06	55	944.63	1.75
17	885.04	1.17			
18	972.85	0.583			
19	972.92	0.742			
20	1058.40	0.452			
21	1058.34	0.398			
22	1088.17	0.744			
36	295.14	2.54			
37	295.07	2.97			
38	373.93	2.54			

SHOT	DIST	12333321	SHOT	DIST	12333321
13	764.97	1.17	30	1451.87	0.648
14	765.33	1.06	31	1290.10	0.405
15	827.57	0.799	32	1290.37	0.216
16	884.69	1.01	50	795.22	1.11
17	885.04	0.90	51	795.06	1.49
18	972.85	0.53	52	866.83	0.849
19	972.92	0.637	53	867.18	0.795
20	1058.40	0.783	54	944.56	1.48
21	1058.34	0.810	55	1071.32	1.05
22	1088.17	0.755	57	1071.32	1.05
23	1088.16	0.648	58	1142.30	0.675
24	1176.02	0.621	59	1142.37	0.675
25	1244.64	1.05	63	1352.66	1.11
26	1297.72	0.351	64	1408.68	0.567
27	1298.11	0.459	65	1408.68	0.567
28	1379.34	0.378	66	1492.23	0.567
29	1451.57	0.675			

SHOT	DIST	123321123321
12	708.42	0.705
13	764.97	0.900
14	765.33	0.743
15	827.57	0.795
16	884.69	0.848
17	885.04	0.848
18	972.85	0.583
19	972.92	0.637
48	738.44	0.68
49	738.80	0.74
50	795.22	1.01
51	795.06	1.06
52	866.83	0.795
53	867.18	0.741
54	944.56	0.848
55	944.63	0.795

SHOT	DIST	12344321
15	827.57	0.689
16	884.69	1.910
17	885.04	1.855
18	972.85	1.06
19	972.92	1.22
20	1058.40	1.51
21	1058.34	1.51
22	1088.17	1.62
23	1088.16	1.62
24	1176.02	0.755
25	1244.64	0.648
26	1297.72	0.324
27	1298.11	0.432
28	1379.34	0.945
29	1451.57	0.945
30	1451.87	0.945
32	1290.37	0.351
52	866.83	1.75
53	867.18	1.75
54	944.56	1.64
55	944.63	1.69
56	1071.32	1.62
57	1071.31	1.59
58	1142.30	0.540
59	1142.37	0.621
63	1352.66	0.648
64	1408.39	1.16
65	1408.68	1.51
66	1492.23	0.324

SHOT	DIST	1234444321
20	1058.40	0.890
21	1058.34	0.916
22	1088.17	1.510
23	1088.16	1.485
24	1176.02	0.782
25	1244.64	0.945
26	1297.72	0.728
27	1298.11	0.702
28	1379.34	0.785
29	1451.57	0.378
30	1451.87	0.567
32	1290.37	0.405
56	1071.32	0.675
57	1071.31	1.32
58	1142.30	1.08
59	1142.37	1.11
63	1352.66	1.03
64	1408.39	1.43
65	1408.68	1.51
66	1492.23	0.351

SHOT	DIST	1234432112344321
18	972.85	0.53
19	972.92	0.53
20	1058.40	0.54
21	1058.34	0.54
22	1088.17	0.835
23	1088.16	0.890
24	1176.02	0.515
25	1244.64	0.730
26	1297.72	0.486
27	1298.11	0.432
28	1379.34	0.270
29	1451.57	0.405
30	1451.87	0.324
31	1290.10	0.568
32	1290.37	0.270
56	1071.32	0.485
57	1071.31	0.485
58	1142.30	0.810
59	1142.37	0.891
63	1352.66	0.782
64	1408.39	0.458
65	1408.68	0.458
66	1492.23	0.620